

Figure 311.23: Comparison of obtained motion at the surface using frequency independent and frequency dependent Caughey 4th order damping.

periods of the motions are used and comparison is made. Different shear wave velocities and input motion frequencies are used which is mentioned for each case. The input motion considered for simulation is Ricker wavelet considering different dominant frequencies.  $V_s$  is the soil profile shear wave velocity and  $f_r$  is the frequency of the Ricker wavelet, and  $\xi_i$  is the Rayleigh damping ratio at considered frequencies.

The height of the finite element model is 60m and boundary conditions are introduced in order to model 1C wave propagation. The motion is imposed at one side of the model and Rayleigh damping is applied to couple of the elements on the other side of the model in order to damp out the waves. Results are recorded at the boundary of damped and undamped zones.

Figure (311.24) shows the comparison of time histories for the soil column with shear wave velocity of 100m/s and input motion frequency of 8Hz. Frequencies used to calculate Rayleigh damping coefficients in this case are natural frequencies of the soil column. The same damping ratio is used for all the damping zone elements. It can be observed that the one with constant damping ratio of 0.5 has done better job in terms of damping out the reflected motions.

Same analysis is done by using frequencies of 6Hz and 12Hz for the Rayleigh damping. As shown in Figure (311.25), in this case the reflected waves are damped out more comparing to previous case where natural frequencies of the soil were used for Rayleigh damping. This fact shows that the frequencies to be used for calculating the Rayleigh damping coefficients, do not have to be the natural frequencies of the soil which sometimes used in practice and depends on the frequency range of the input motion as

well. Since the Ricker wavelet used here has a peak frequency of  $8\text{Hz}$ , the higher values of frequencies should be used for Rayleigh damping coefficients. Figure (311.26) shows the results of the same case except that linear increasing pattern is used for damping ratio of the 5 elements in damping zone. It seems that using the linear pattern starting from 0.3 to 1.1 results in less reflected motions.

The reason could be because of the nature of Rayleigh damping which is frequency dependent. So different damping ratios are observed at different frequencies. In deed by changing the damping ratio at each element, five different patterns of Rayleigh damping are being used which has more capability of absorbing motions with different frequencies and amplitudes.

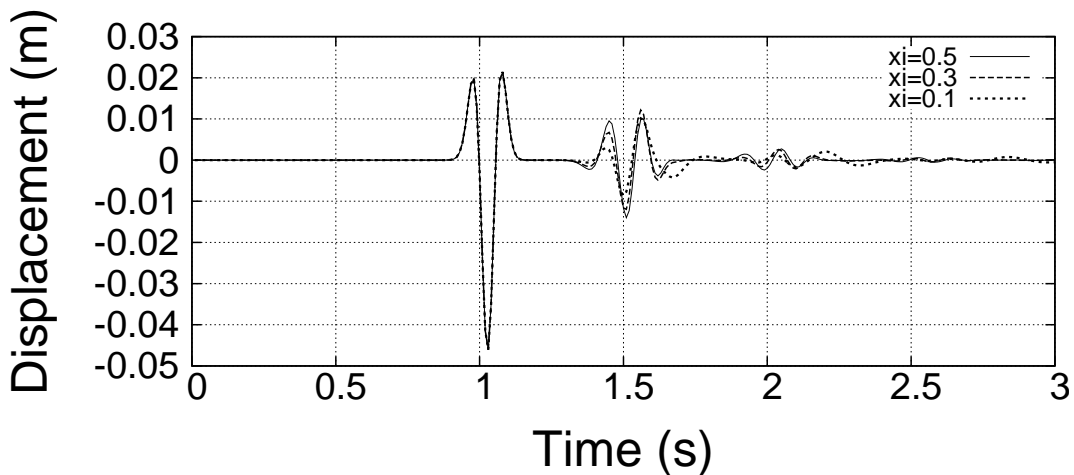


Figure 311.24: Displacement time history considering Rayleigh damping using natural frequencies of the soil,  $V_s=100\text{m/s}$ ,  $f_r=8\text{Hz}$

Figures (311.27) and (311.28) show the displacement time histories for same patterns of constant damping ratio for all elements in the damping zone and linearly increasing damping ratios respectively but for shear wave velocity of  $V_s = 300\text{m/s}$  and input motion frequency of  $5\text{Hz}$ . Same conclusion can be made here as previous case regarding the pattern of damping ratios and frequencies to be used for Rayleigh damping.

Figures (311.29) and (311.30) are comparisons of recorded displacement time histories between patterns of same damping ratio for damping zone elements, damping ratio changes along the length of damping zone, and case of with out damping. Figure (311.29) is the case which shear wave velocity of the soil column is  $100\text{m/s}$  and frequency of input Ricker motion is  $1\text{Hz}$  while soil profile used in Figure (311.30) has shear wave velocity of  $300\text{m/s}$  with input motion frequency of  $8\text{Hz}$ .

It can be observed that in case of having no physical damping, waves are getting trapped in the model and are reflecting back from the boundaries. Displacement time histories obtained from mentioned

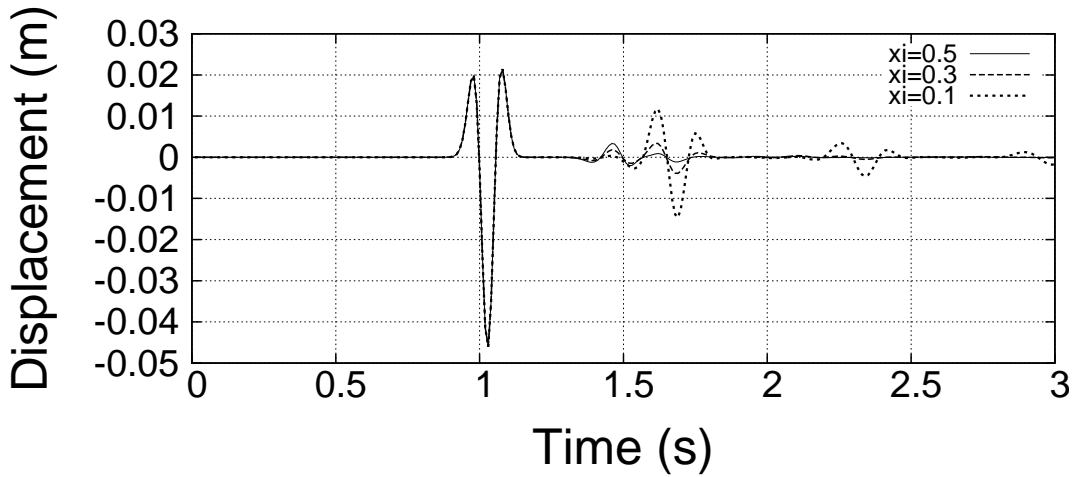


Figure 311.25: Displacement time history considering Rayleigh damping using  $f_1, f_2 = 6, 12 \text{ Hz}$ ,  $V_s = 100 \text{ m/s}$ ,  $f_r = 8 \text{ Hz}$

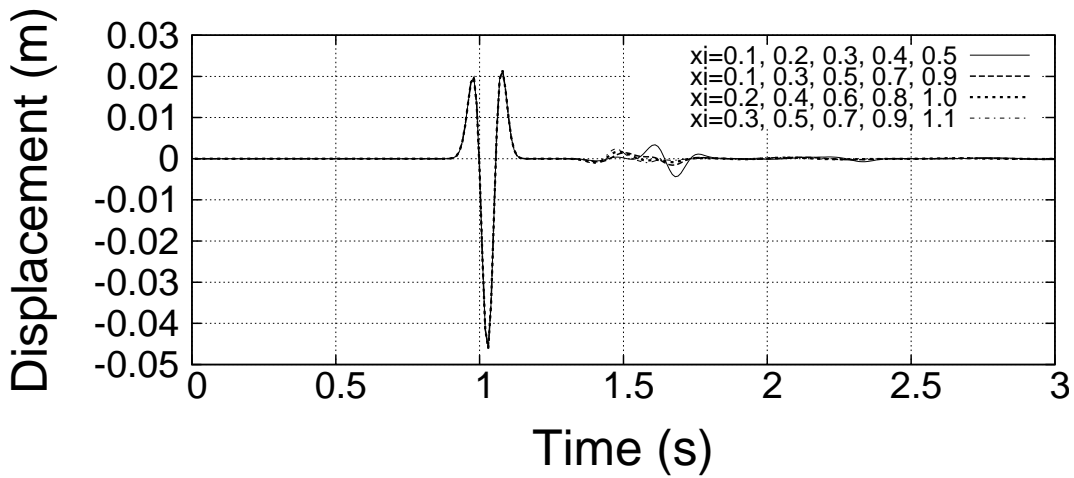


Figure 311.26: Displacement time history considering Rayleigh damping using  $f_1, f_2 = 6, 12 \text{ Hz}$ ,  $V_s = 100 \text{ m/s}$ ,  $f_r = 8 \text{ Hz}$

patterns of damping ratios have minor differences which does not mean always will be this close but still the pattern of using linearly increasing of damping ratio seems to do a better job for damping the reflecting waves.

In order to have a better understanding of these patterns of damping, wave propagation through the depth of model is recorded for case of shear wave velocity of  $100 \text{ m/s}$  and input motion frequency of  $8 \text{ Hz}$ . Displacement time histories in Figures (311.31) to (311.33) show wave propagation through the model for cases of using uniform damping ratios, linearly increasing damping ratios, and with out damping

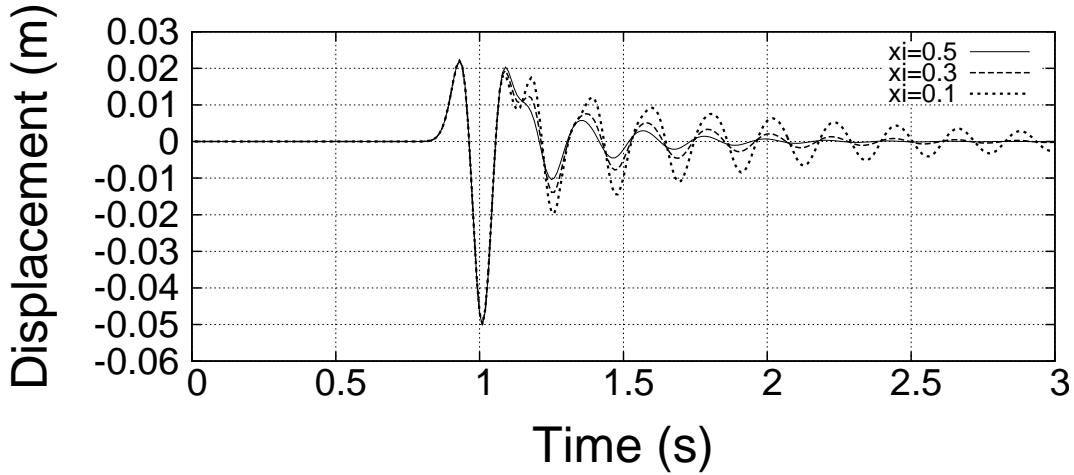


Figure 311.27: Displacement time history considering Rayleigh damping using  $f_1, f_2 = 5, 8 \text{ Hz}$ ,  $V_s = 300 \text{ m/s}$ ,  $f_r = 5 \text{ Hz}$

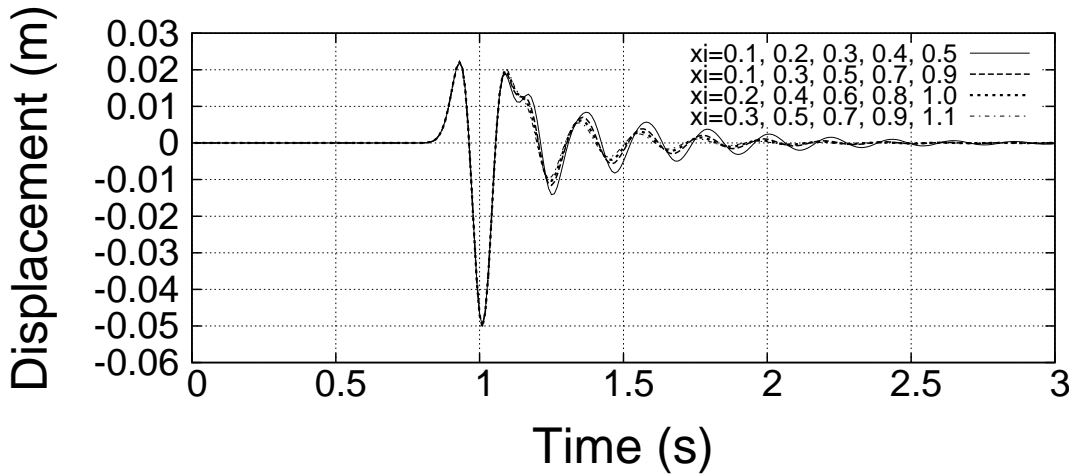


Figure 311.28: Displacement time history considering Rayleigh damping using  $f_1, f_2 = 5, 8 \text{ Hz}$ ,  $V_s = 300 \text{ m/s}$ ,  $f_r = 5 \text{ Hz}$

respectively. By looking at the wave propagation through the whole soil profile it can be concluded that for this soil profile using the linearly increasing of damping ratios does a better job for damping the reflected motions at different depths.

Figure (311.34) shows the comparison of cumulative total energy time histories for the soil profile with shear wave velocity of  $100 \text{ m/s}$  and input motion frequency of  $8 \text{ Hz}$  for different Rayleigh damping patterns of uniform, increasing linearly, and case of no damping. What is expected to be observed is that total energy keeps increasing until the input motion gets to zero in time which energy should remain

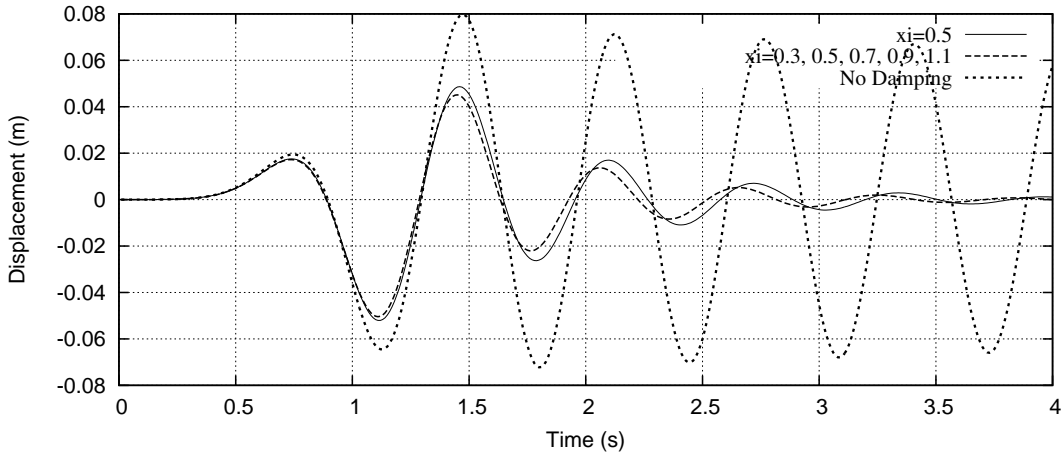


Figure 311.29: Displacement time history considering Rayleigh damping using  $f_1, f_2 = 0.5, 2 \text{ Hz}$ ,  $V_s = 100 \text{ m/s}$ ,  $f_r = 1 \text{ Hz}$

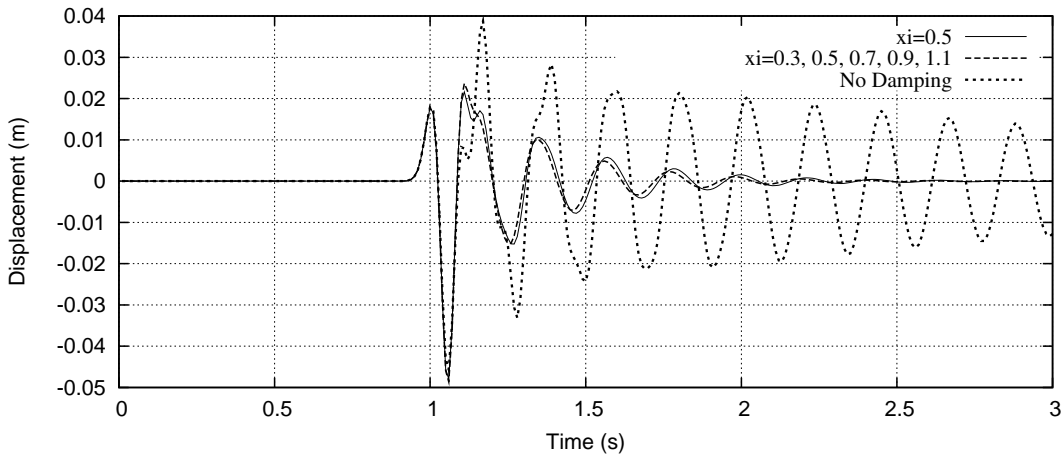


Figure 311.30: Displacement time history considering Rayleigh damping using  $f_1, f_2 = 6, 12 \text{ Hz}$ ,  $V_s = 300 \text{ m/s}$ ,  $f_r = 8 \text{ Hz}$

constant unless there are waves reflecting back from boundaries. As it is shown, total energy slightly increase by time due to the reflected motions. This difference is much higher for case of no physical damping used since higher portion of the motions will get trapped in the model.

In order to be able to see the effect of size of damping zone on reflected motions, analysis is done on the soil profile with shear wave velocity of  $100 \text{ m/s}$  and frequency of  $8 \text{ Hz}$  for input motion. Comparison of displacement time histories for different size of the damping zones is shown in Figure (311.35). As expected, by reducing the size of damping zone, more waves are reflecting back from model boundaries.

The effect of number of elements to be used in damping zone is also studied here. Comparison is

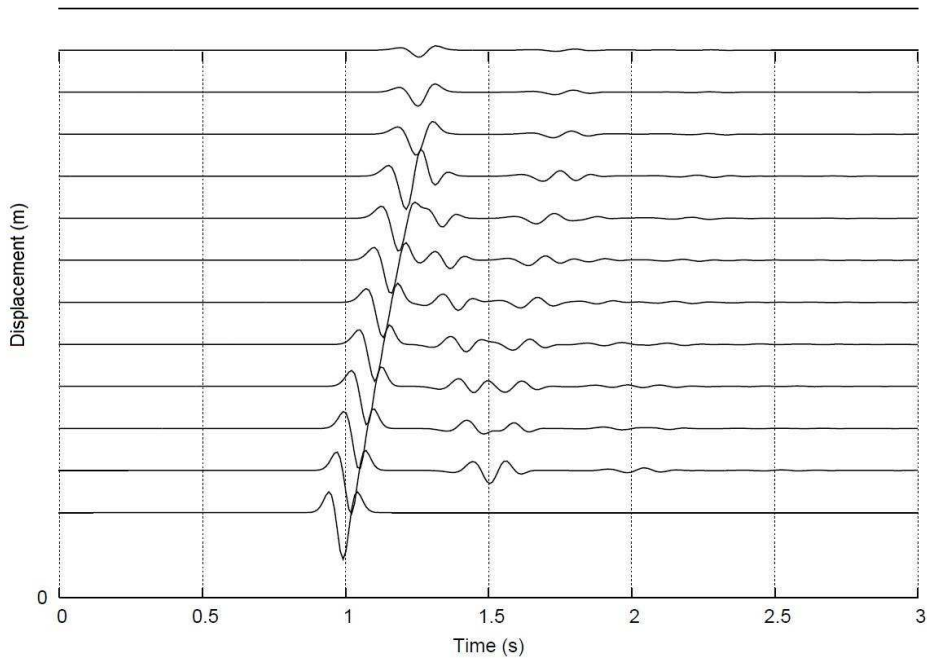


Figure 311.31: Displacement time history in depth considering homogeneous damping (15m),  $\xi=0.5$ ,  $V_s=100\text{m/s}$ ,  $f_r=8\text{Hz}$

made for cases which the size of the damping zone is the same but the size of the elements (and therefore number of the elements) in that zone is changed. The size of the damping zone assumed to be 15m while the number of the elements used in that zone is considered to be 3, 5, and 15. The comparison for this change of number of the elements is shown in Figure (311.36). Rayleigh damping ratio with pattern of increasing linearly from 0.3 to 1.1 is used. As it is observed, by reducing number of elements in the damping zone, the amount of reflected waves are getting higher.

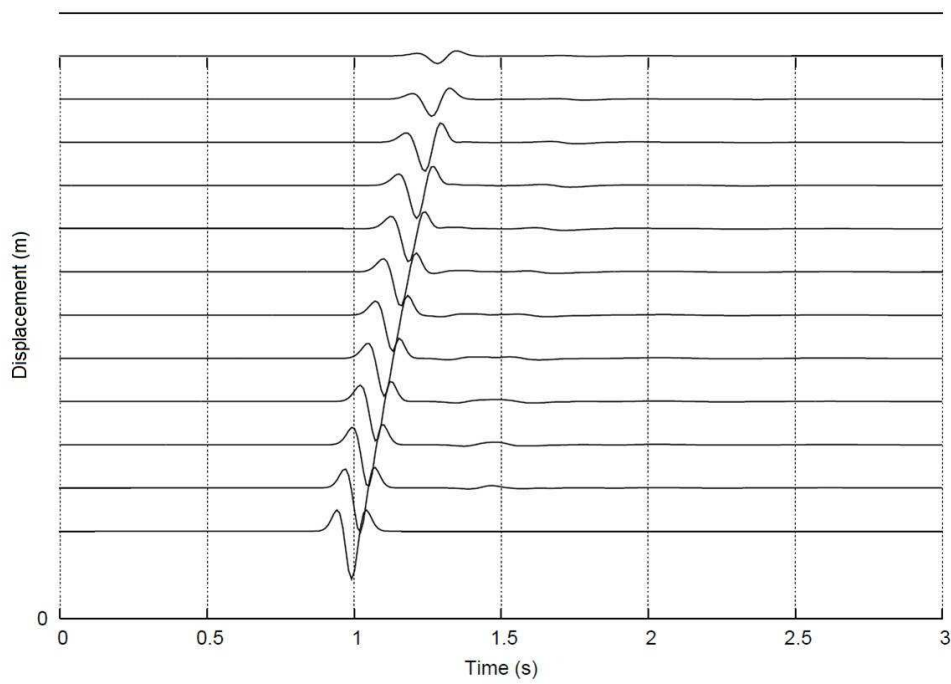


Figure 311.32: Displacement time history in depth considering linear increasing of  $\xi$  in Rayleigh damping (every 3m),  $\xi_i = 0.3, 0.5, 0.7, 0.9, 1.1$ ,  $V_s = 100\text{m/s}$ ,  $f_r = 8\text{Hz}$

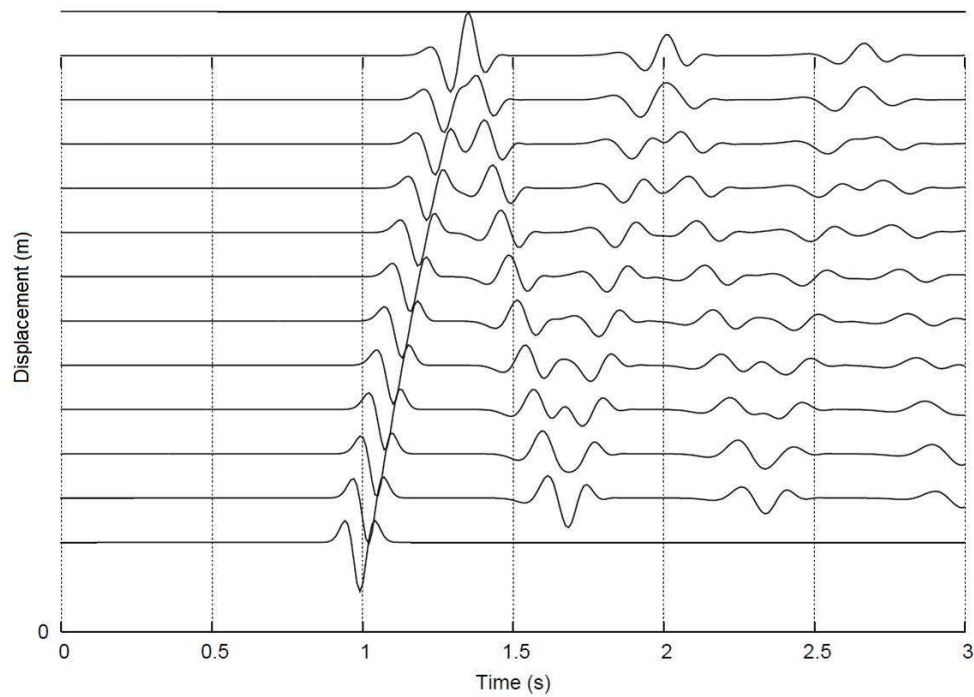


Figure 311.33: Displacement time history in depth with out considering damping,  $V_s=100\text{m/s}$ ,  $f_r=8\text{Hz}$

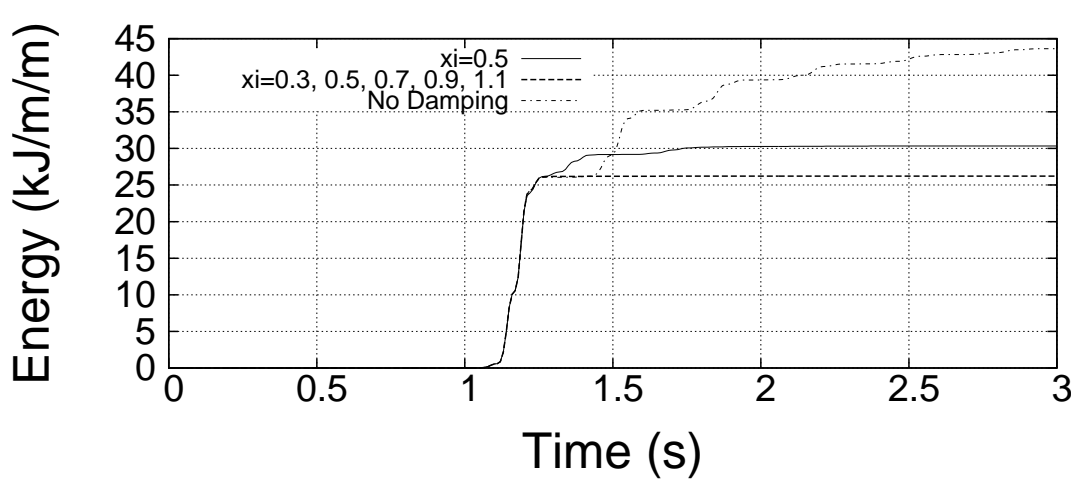


Figure 311.34: Comparison of energy time history by considering different Rayleigh damping patterns (in the non-damping zone at the middle of model),  $V_s=100\text{m/s}$ ,  $f_r=8\text{Hz}$

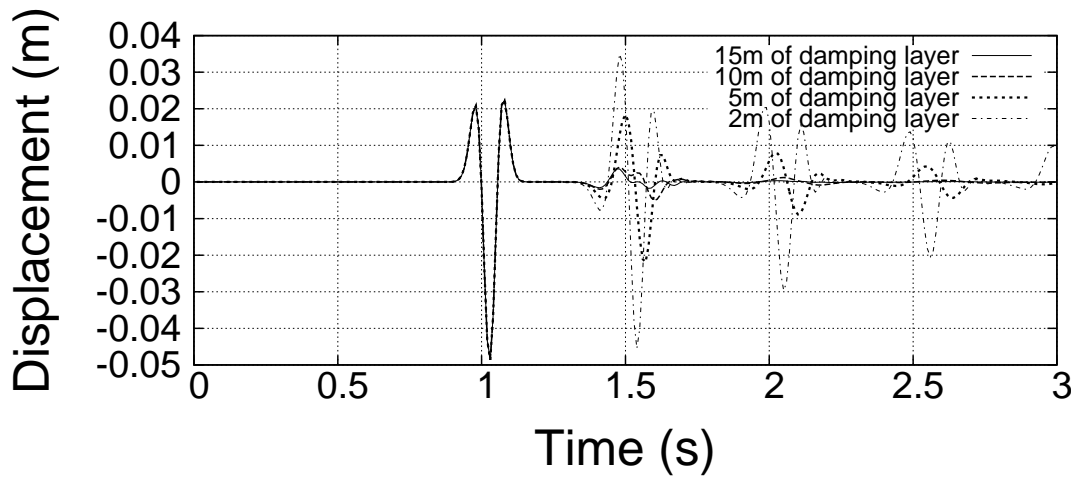


Figure 311.35: Comparison of displacement time histories for different size of damping zones

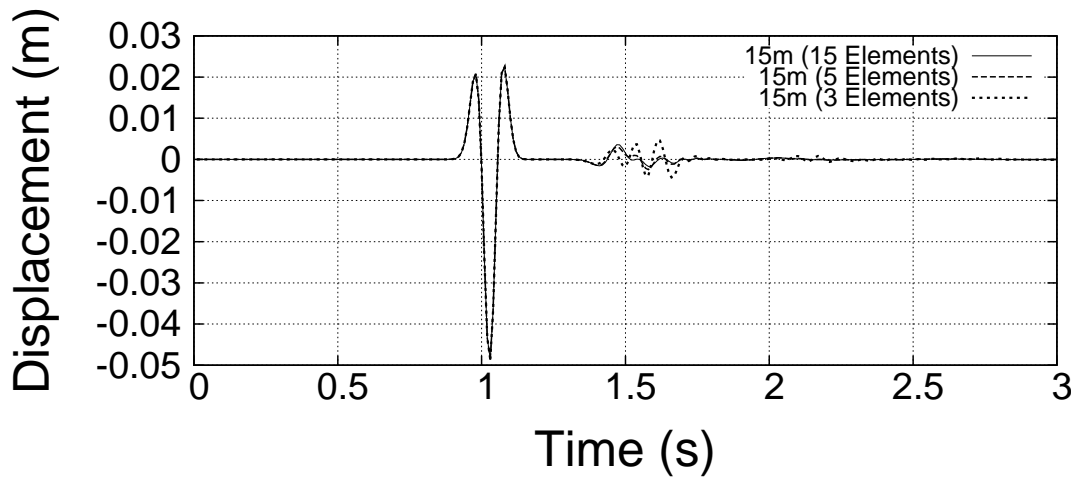


Figure 311.36: Displacement time history at a point in the non-damping zone close to the boundary of imposing motion

## 311.5 Mesh Size Effects for Linear (8 Node Brick) and Quadratic (27 Node Brick) Finite Elements on Wave Propagation

Generally, the results of numerical analysis using finite element method technique for the dynamic problem are affected by size of mesh (grid spacing). According to [Argyris and Mlejnek \(1991\)](#), about 10 nodes per wavelengths are required to simulate accurately for the given frequency and fewer than 10 nodes may induce an artificial damping due to the numerical reason.

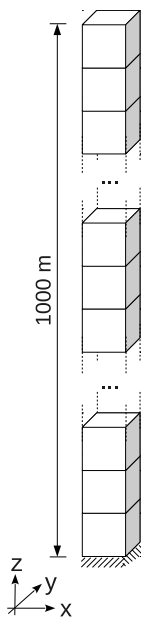


Figure 311.37: One dimensional column test model to inspect the mesh size effect

In this section, mesh size effect is inspected to decide an appropriate size of the mesh to build finite element model for verification. One dimensional column model is built as shown in figure [311.37](#). Total height of the model is 1000 m. Two models are built with element height of 20 m and 50 m, and each model have two different shear wave velocities (100 m/s and 1000 m/s). Density is set as  $2000 \text{ kg/m}^3$ , and Poisson's ratio is set as 0.3, for all test models. Various cases are set and tested as shown in table [311.1](#). Both 8 node and 27 node brick elements are used for all models. Thus, total 24 parametric study cases are inspected. Linear elastic elements are used for all analyses. All analyses are performed in time domain with Newmark dynamic integrator without any numerical damping ( $\gamma = 0.5$ , and  $\beta = 0.25$ , no numerical damping, unconditionally stable).

Ormsby wavelet ([Ryan, 1994](#)) is used as an input motion and imposed at the bottom of the model.

Table 311.1: Analysis cases to determine a mesh size

Case number	Vs (m/s)	Cutoff freq. (Hz)	Element height (m)	Max. propagation freq. (Hz)
1	1000	3	10	10
2	1000	8	10	10
3	1000	15	10	10
4	100	3	10	1
5	100	8	10	1
6	100	15	10	1
7	1000	3	20	5
8	1000	8	20	5
9	1000	15	20	5
10	100	3	20	0.5
11	100	8	20	0.5
12	100	15	20	0.5

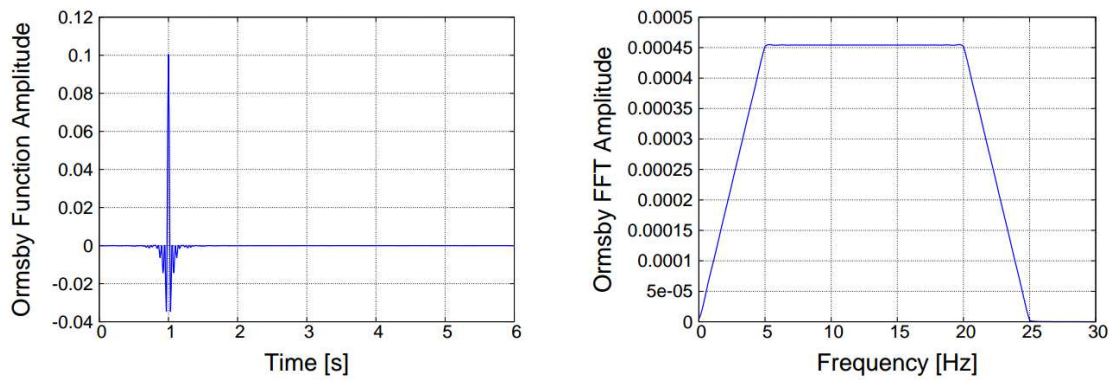


Figure 311.38: Ormsby wavelet in time and frequency domain with flat frequency content from 5 Hz to 20 Hz

Ormsby wavelet features a controllable flat frequency content with formulation shown in equation 311.3.

$$f(t) = A \left( \left( \frac{\pi f_4^2}{f_4 - f_3} \text{sinc}(\pi f_4(t - t_s))^2 - \frac{\pi f_3^2}{f_4 - f_3} \text{sinc}(\pi f_3(t - t_s))^2 \right) - \left( \frac{\pi f_2^2}{f_2 - f_1} \text{sinc}(\pi f_2(t - t_s))^2 - \frac{\pi f_1^2}{f_2 - f_1} \text{sinc}(\pi f_1(t - t_s))^2 \right) \right) \quad (311.3)$$

where  $f_1$  and  $f_2$  define the lower range frequency band,  $f_3$  and  $f_4$  define the higher range frequency band,  $A$  is the amplitude of the function, and  $t_s$  is the time that maximum amplitude is happening, and

$\text{sinc}(x) = \sin(x)/x$ . Figure 311.38 shows an example of Ormsby wavelet with flat frequency content from 5 Hz to 20 Hz.

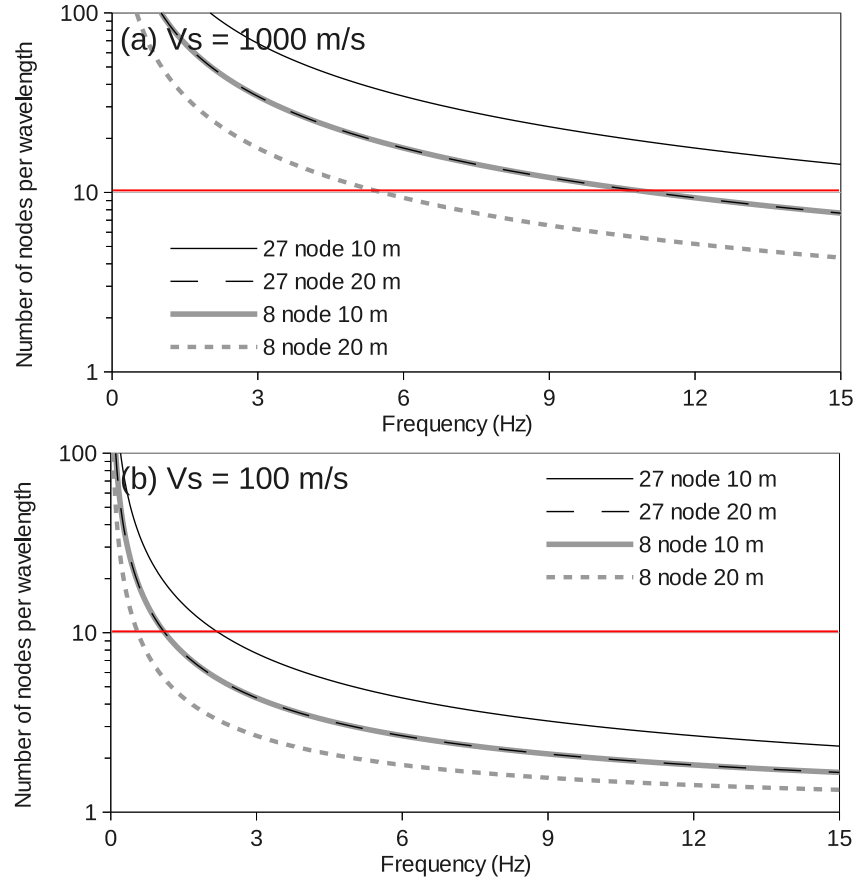


Figure 311.39: Number of nodes per wavelength along frequencies, and element sizes (a)  $V_s = 1000$  m/s (b)  $V_s = 100$  m/s

For this example, cutoff frequencies of Ormsby wavelets are set as 3, 8, and 15 Hz (table 311.1). Figure 311.39 shows number of nodes per wavelength along frequencies and figure 311.40 – 311.46 show comparison of analysis results. As shown in figure 311.40, case 1 and 7 (analysis using Ormsby wavelet with 3 Hz cutoff frequency) predict exactly identical results to the analytic solution in both time and frequency domain. Since, number of nodes per wavelength for both cases are over 10 (see figure 311.39(a) and table 311.1, all cases under 3 Hz shows more than 10 nodes per wavelength), those exact results are expected.

Increasing cutoff frequency from 3 Hz to 8 Hz induces numerical errors as shown in figure 311.41. In frequency domain, both 10 m and 20 m element height model with 27 node brick element predict exactly same results with the analytic one. However, in time domain, asymmetric shape of time history

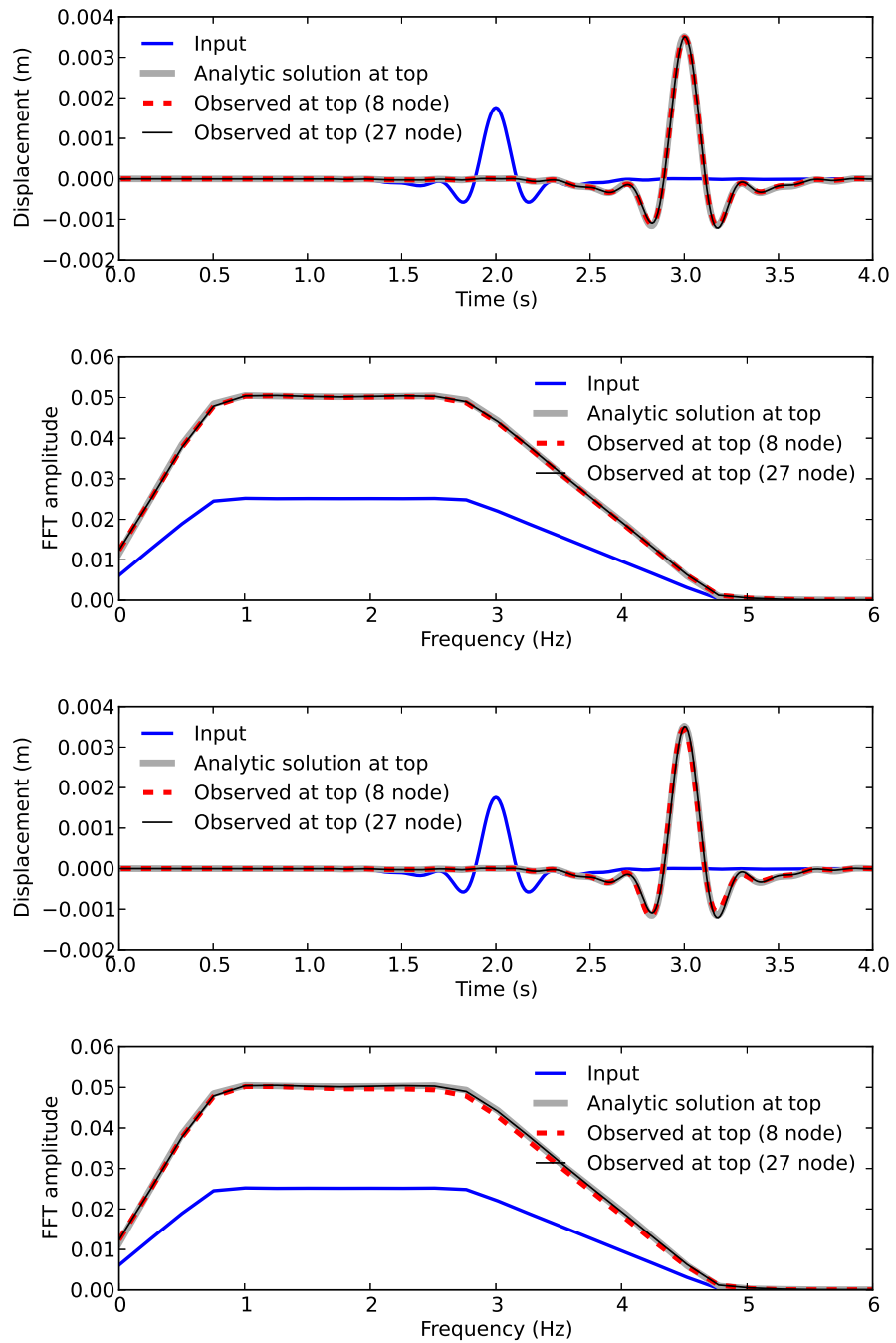


Figure 311.40: Comparison between (a) case 1 (top,  $V_s = 1000$  m/s, 3 Hz, element size = 10m) and (b) case 7 (bottom,  $V_s = 1000$  m/s, 3 Hz, element size = 20m)

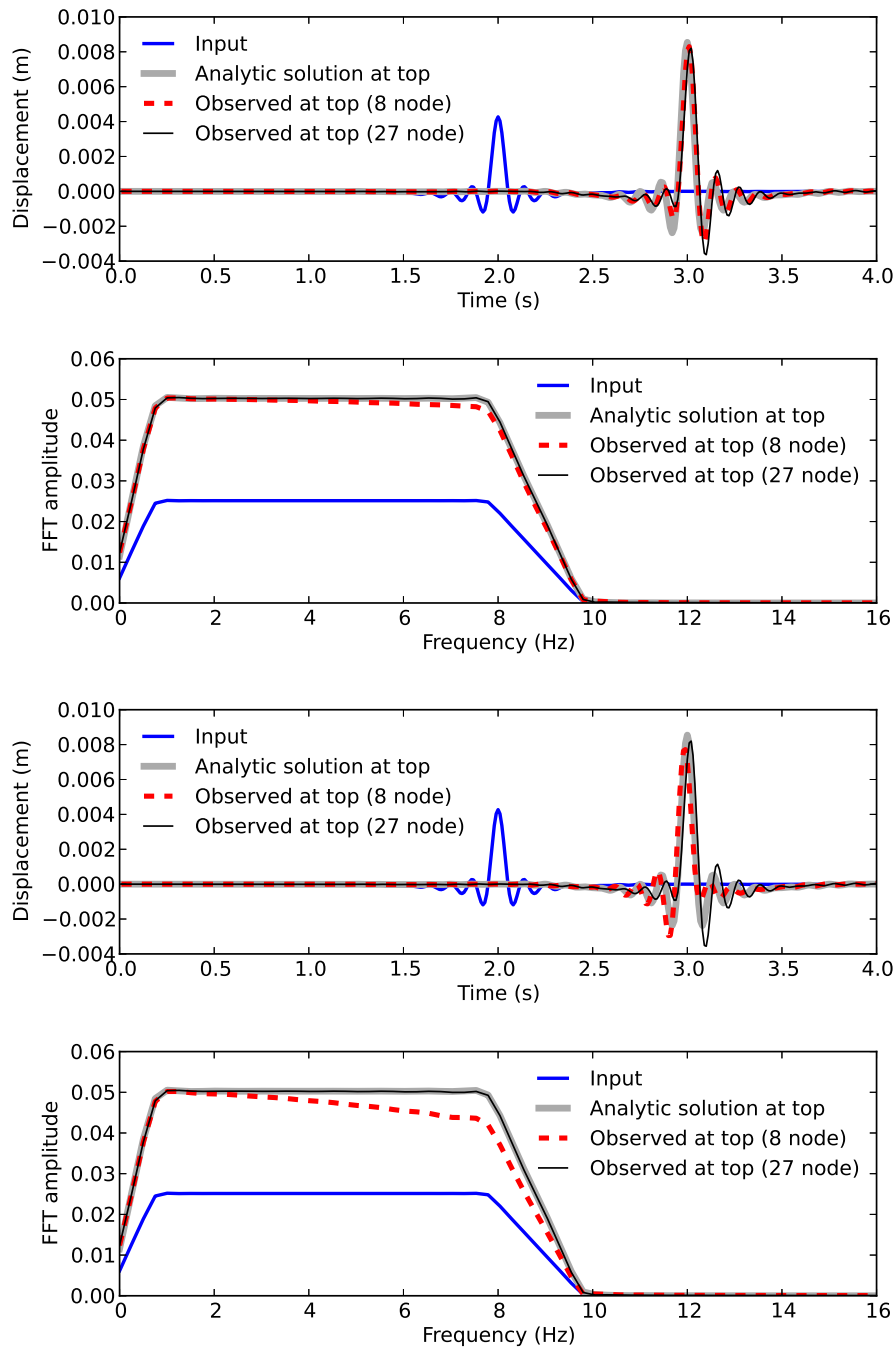


Figure 311.41: Comparison between (a) case 2 (top,  $V_s = 1000$  m/s, 8 Hz, element size = 10m) and (b) case 8 (bottom,  $V_s = 1000$  m/s, 8 Hz, element size = 20m)

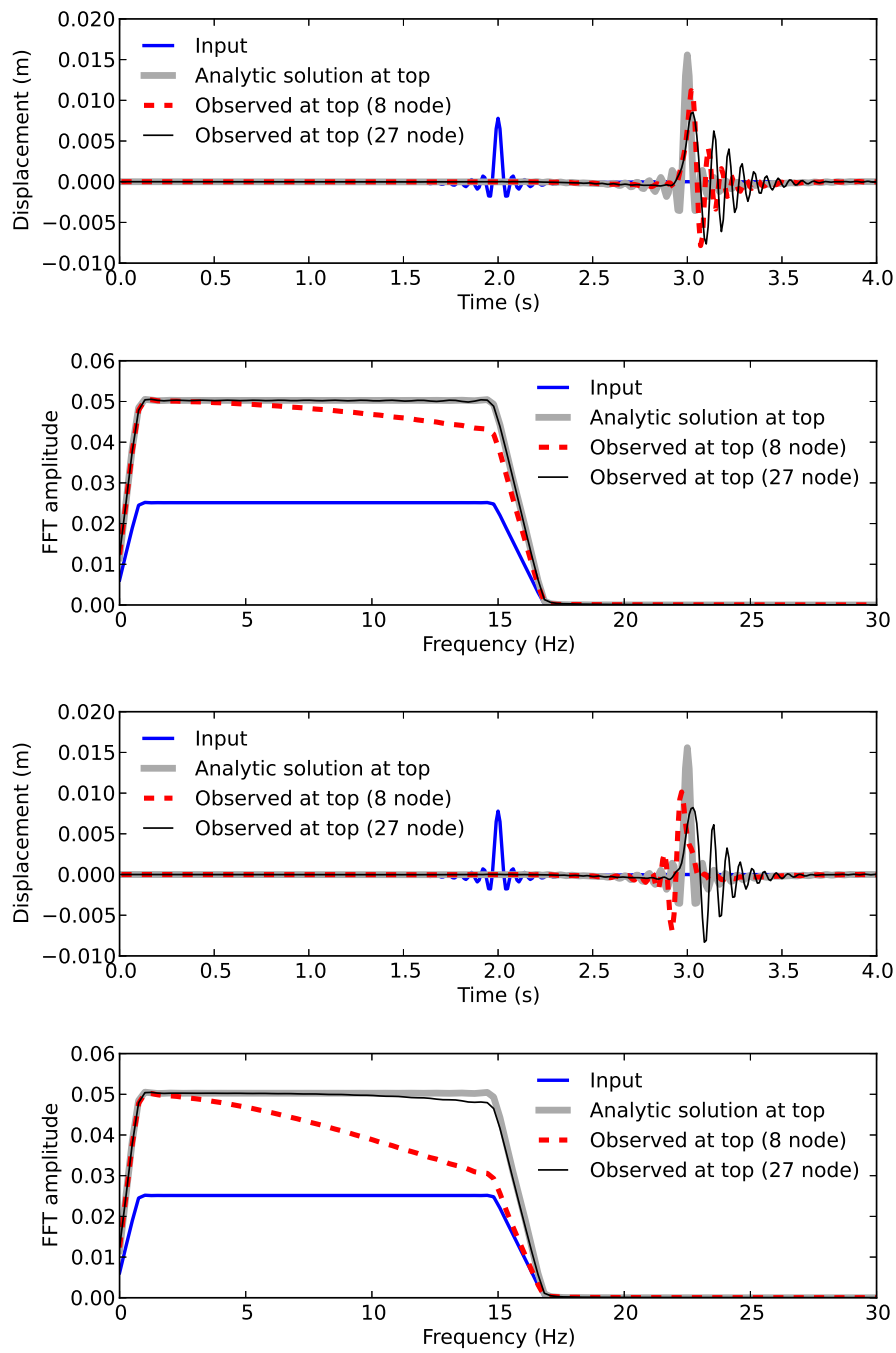


Figure 311.42: Comparison between (a) case 3 (top,  $V_s = 1000$  m/s, 15 Hz, element size = 10m) and (b) case 9 (bottom,  $V_s = 1000$  m/s, 15 Hz, element size = 20m)

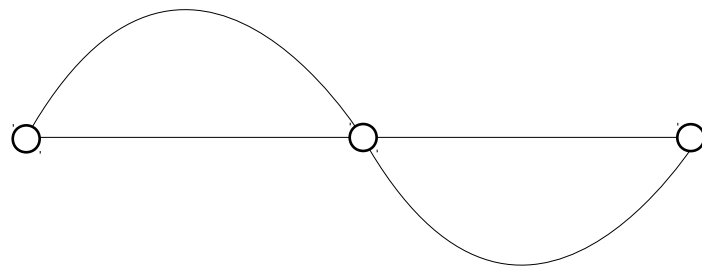


Figure 311.43: Schematic cartoon to show that nodes can behave like frequency contents filter

displacements are observed. Observations from top of 8 node brick element models show more numerical error in both time and frequency domain due to the decreasing number of nodes per wavelength (figure 311.39). Figure 311.42 shows analysis results with 15 Hz cutoff frequency. Results from 27 node brick elements are almost same in frequency domain but asymmetric shapes are also observed in time domain. Decreasing amplitudes in frequency domain along increasing frequencies are observed from 8 node brick element cases.

Figure 311.44 – 311.46 show results predicted from  $V_s = 100$  m/s cases. Similar as  $V_s = 1000$  m/s cases, decreasing amplitude along increasing frequencies are observed in all cases. One interesting observation is bumps in frequency domain which can be seen at natural frequencies (natural modes) of the elements ( $n$  th mode of elements,  $f = (2n - 1)V_s/4H$ , 2.5 Hz, 5.0 Hz, and so on). This observation may mean that if certain condition is satisfied between modes and size of the element, it will behave like frequency contents filter. Figure 311.43 shows possible explanation of this observation. As in the case of figure 311.43, nodes (circle in the figure) cannot capture harmonic oscillation of the frequency since amplitude of the oscillation is always zero. As a result, the frequency contents at the frequency cannot be predicted by the analysis.

The results shown here are used as a reference to determine mesh size and frequency range of input motions for the verification.

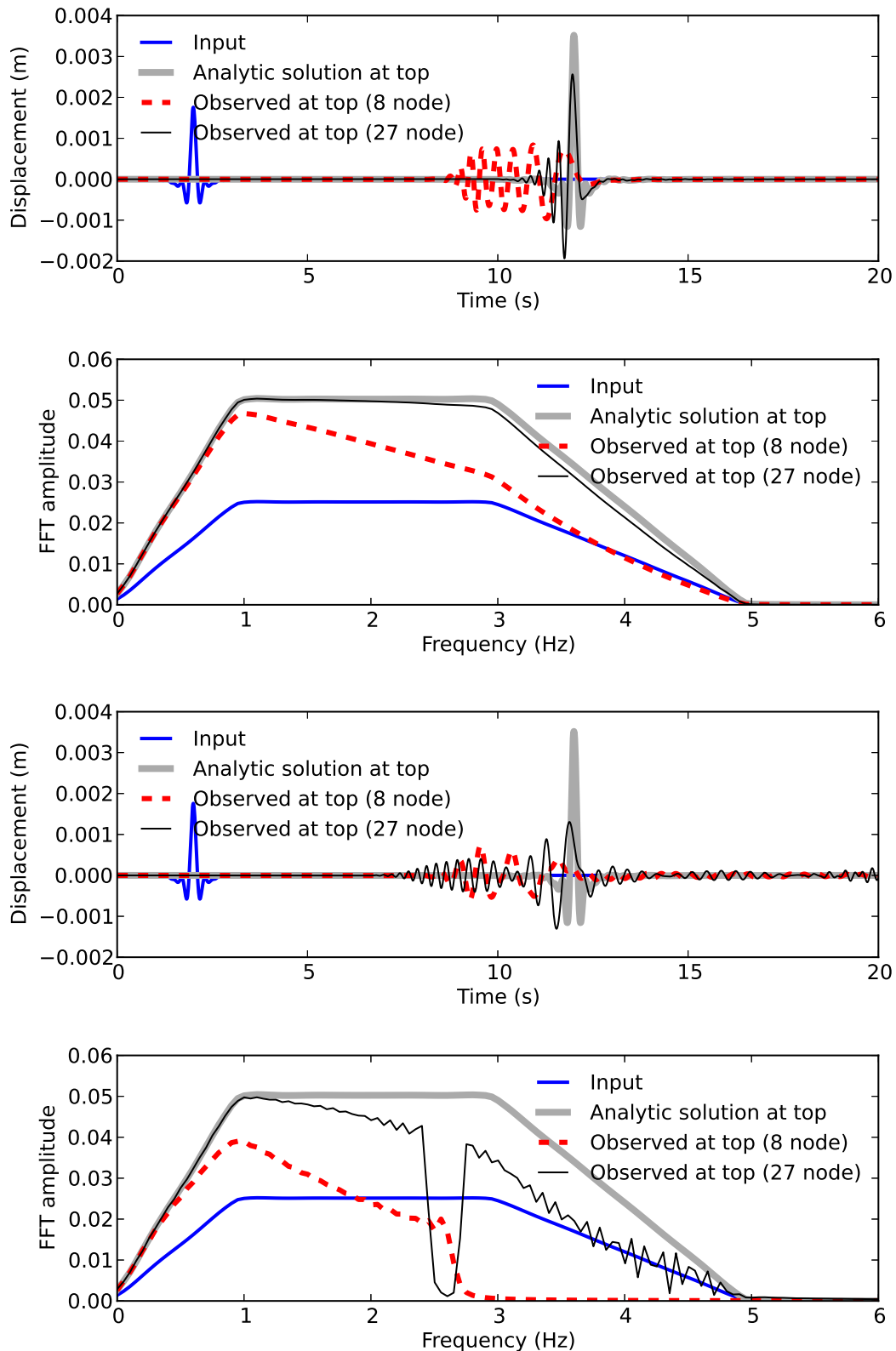


Figure 311.44: Comparison between (a) case 4 (top,  $V_s = 100 \text{ m/s}$ , 3 Hz, element size = 10m) and (b) case 10 (bottom,  $V_s = 100 \text{ m/s}$ , 3 Hz, element size = 20m)

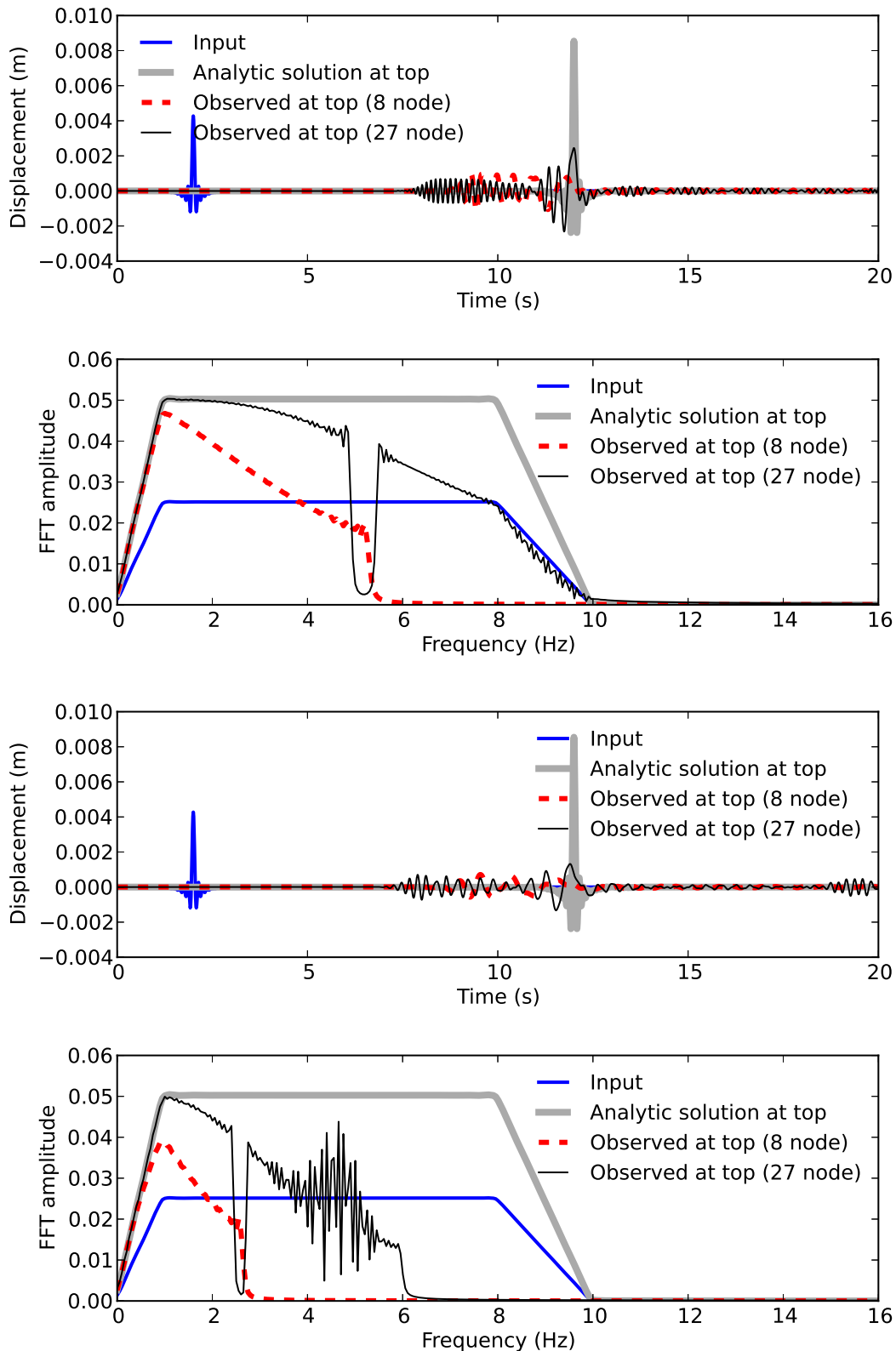


Figure 311.45: Comparison between (a) case 5 (top,  $V_s = 100 \text{ m/s}$ , 8 Hz, element size = 10m) and (b) case 11 (bottom,  $V_s = 100 \text{ m/s}$ , 8 Hz, element size = 20m)

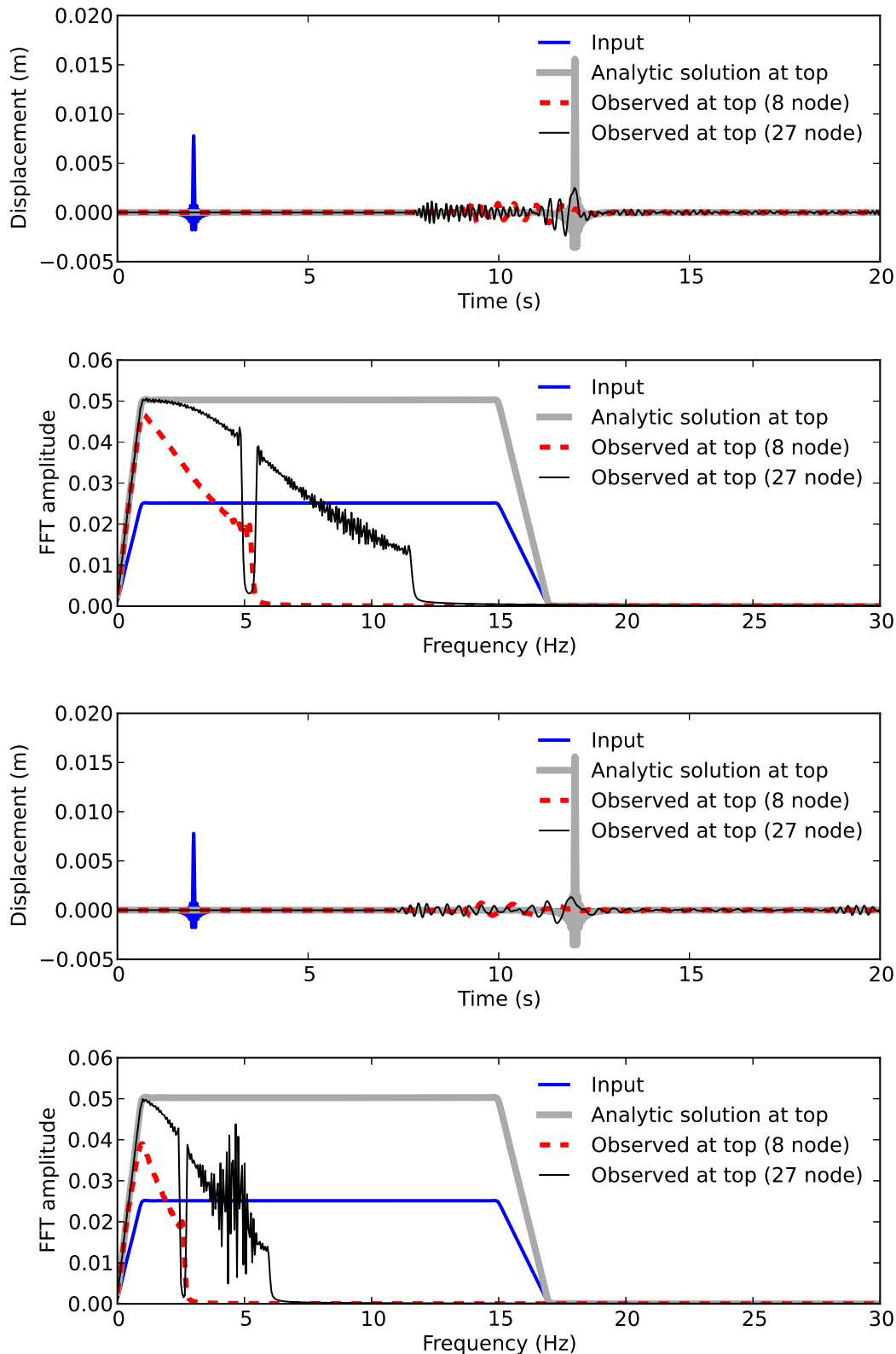


Figure 311.46: Comparison between (a) case 6 (top,  $V_s = 100 \text{ m/s}$ , 15 Hz, element size = 10m) and (b) case 12 (bottom,  $V_s = 100 \text{ m/s}$ , 15 Hz, element size = 20m)

## 311.6 Verification of the Seismic Input (Domain Reduction Method) for 3C, Inclined Seismic Wave Fields

### 311.6.1 Inclined, 3C Seismic Waves in a Free Field

In this section verification of the 3C wave propagation problem using Domain Reduction Method will be studied. In order to do so, a finite element model with dimensions of  $10000m \times 50m \times 5000m$  is considered. Two cases are studied here with the source of motion (fault) to be located at  $(x = 3000m, y = 0, z = 3000m)$  and  $(x = 3000m, y = 0, z = 3000m)$ . Figures (311.47) and (311.48) show these two models respectively.

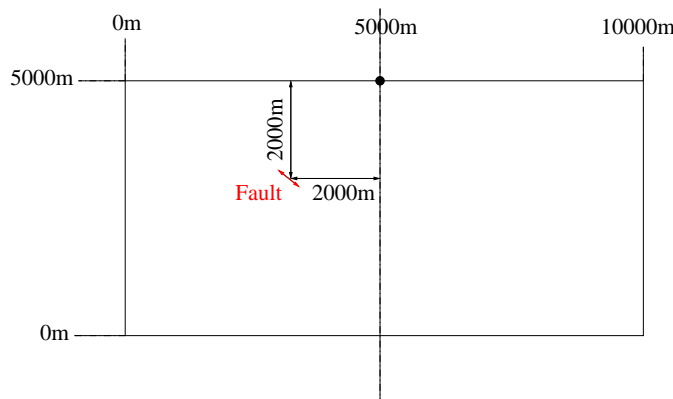


Figure 311.47: Domain to be analyzed for the 1<sup>st</sup> stage of DRM with fault located at an angle of  $45^\circ$  with respect to the top middle point of the model

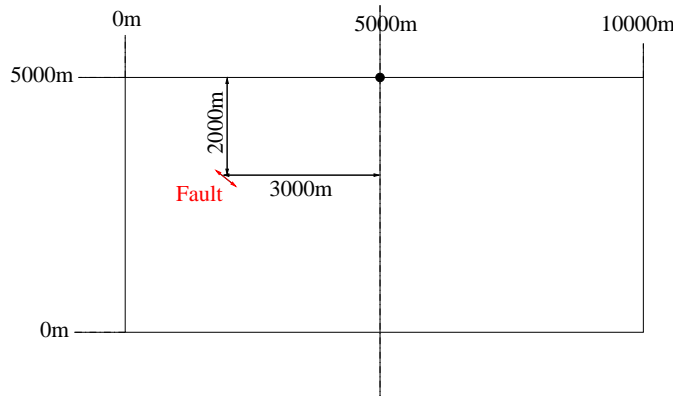


Figure 311.48: Domain to be analyzed for the 1<sup>st</sup> stage of DRM with fault located at an angle of  $34^\circ$  with respect to the top middle point of the model

The size of the elements is chosen to be  $50m$  in all directions for both cases in order to reduce the computational time. The soil parameters are: shear wave velocity of  $700m/s$ , density of  $1800kg/m^3$ , and Poisson's ratio of 0.1. Analyses for the fault slip model are done by applying the motion at the nodes of one element. This is done in order to represent the wave propagation starting from the fault using Multiple Support Excitation. This is representing the first stage of analysis of DRM in which a big model including the fault is considered for free field case in order to obtain the required motions for DRM layer. For simulating the second stage of DRM, a smaller model with dimensions of  $240m \times 5m \times 70m$  is considered as shown in Figure (311.49). The size of the plastic bowl is  $200m \times 5m \times 50m$ . Size of the elements for this model is chosen to be  $5m$ .

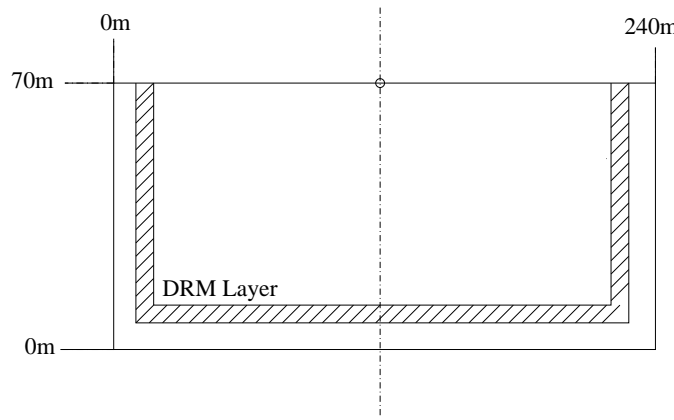


Figure 311.49: Domain to be analyzed for the  $2^{nd}$  analysis stage of DRM with smaller size comparing to the original model

Displacement and acceleration time histories of corresponding nodes of DRM layer are obtained by interpolating between the results obtained from the first model. These displacement and accelerations are used to calculate the effective forces as an input for DRM analysis. Input motions to be used here are Ricker wave, Morgan Hill, and Kocaeli earthquakes. The maximum allowable frequency to be propagated through this model can be calculated based on Equation (311.4):

$$\Delta h \leq \lambda/10 = V_s/(10f_{max}) \quad (311.4)$$

Based on the shear wave velocity of  $700m/s$  and element size of  $50m$ , maximum allowable frequency to be propagated through this model would be  $1.4Hz$  for the original model and based on element size of  $5m$  would be  $14Hz$  for the DRM model.

### 311.6.1.1 Ricker Wavelets

Figure (311.50) show the displacement time history and FFT of Ricker wave of 2<sup>nd</sup> order with dominant frequency of 1Hz and maximum amplitude occurring at 1 second.

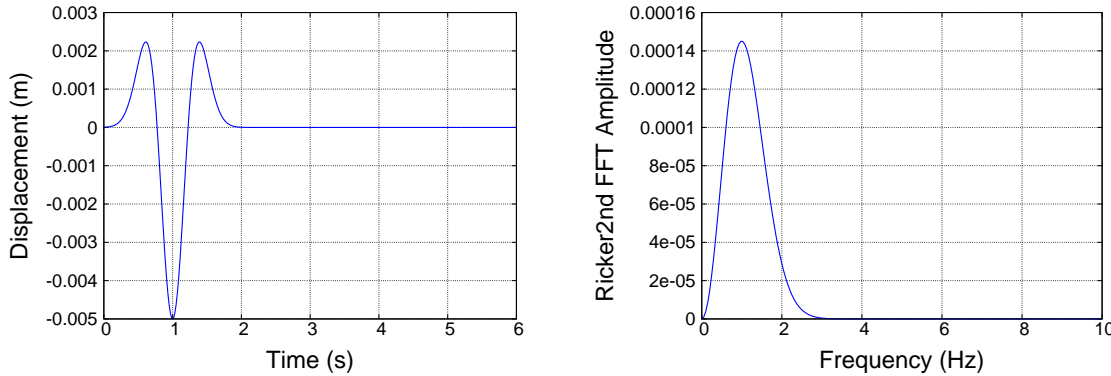


Figure 311.50: Displacement time history and FFT of Ricker wave with dominant frequency of 1Hz

The first case to be studied here is the one with the fault source located at ( $x = 3000m, y = 0, z = 3000m$ ) which has the angle of 45° with respect to the top middle point of the model. Results to be discussed here are comparison of displacement and acceleration time histories at the top middle point of the model ( $x = 5000m, y = 0, z = 5000m$ ) between the fault slip and DRM models. Comparison of displacement time histories in X and Z directions are shown in Figure (311.51). As it can be observed, the results of DRM model matches perfectly with the ones obtained from the fault slip model.

Figure (311.53) is the displacement and acceleration time history of a point located outside of DRM layer in X direction ( $x = 10m, y = 0, z = 40m$ ). As mentioned before in definition of DRM, no motion should come out of the DRM layer in case of free field. As shown in these figures, displacement and acceleration time histories at this point are zero which verifies this fact.

The same motion is applied to the model with fault source located at ( $x = 2000m, y = 0, z = 3000m$ ) which has the angle of 34° with respect to the top middle point of the model. Displacement time histories of the top middle point show the perfect match between results obtained from fault slip model with the ones obtained from DRM mode.

As shown in Figure (311.55), the second motion to be used for analysis is Ricker wave with frequency of 0.5Hz and maximum amplitude occurring at 3 seconds. Figure (311.56) shows the displacement time histories of X and Z directions for the same point as before ( $x = 5000m, y = 0, z = 5000m$ ). As it is shown, results of the fault slip and DRM model are the same which verifies the solution from DRM formulation for this motion as well.

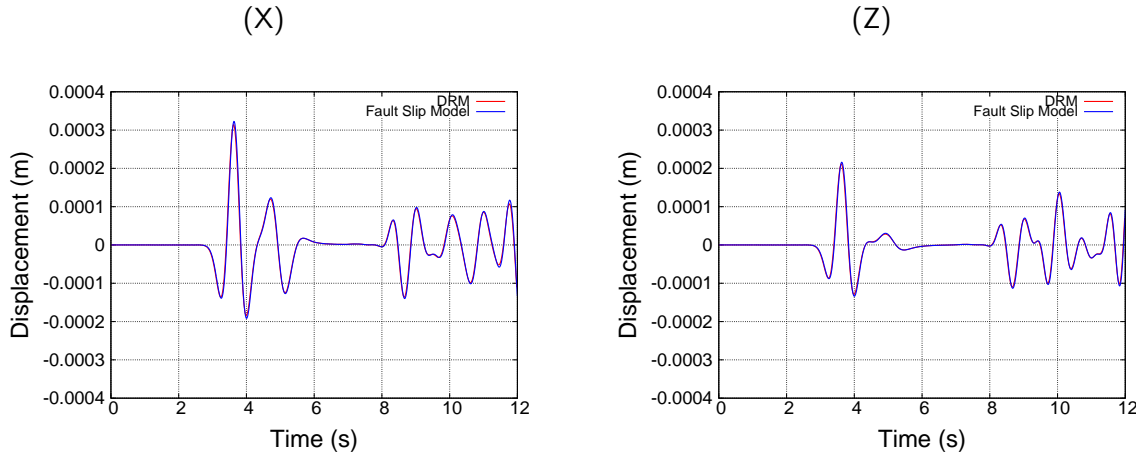


Figure 311.51: Comparison of displacements for top middle point using Ricker wave ( $f = 1\text{Hz}$ ) as an input motion

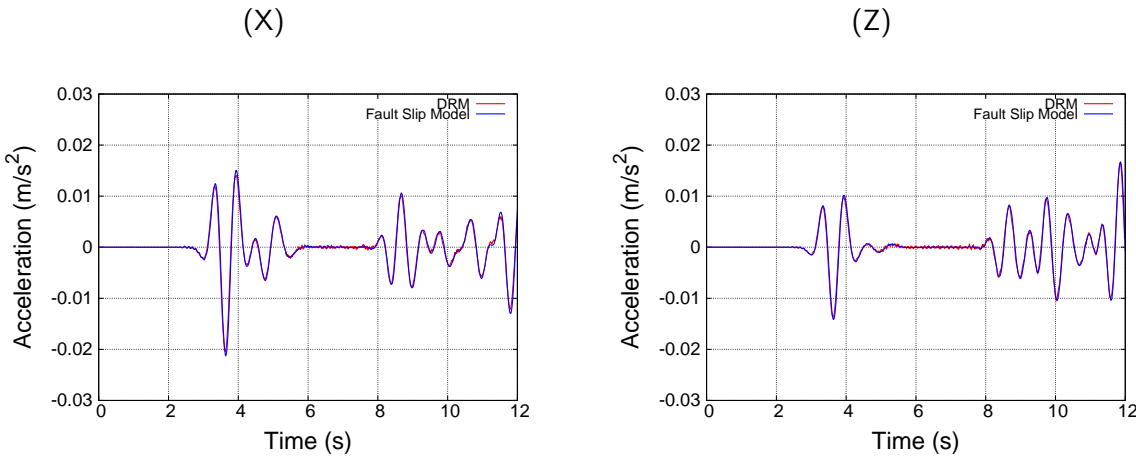


Figure 311.52: Comparison of accelerations for top middle point using Ricker wave ( $f = 1\text{Hz}$ ) as an input motion

The third motion to be used is Ricker wave with frequency of  $2\text{Hz}$  and maximum amplitude happening at 1 second as shown in Figure (311.57). Comparison of displacement time histories between the fault slip and DRM model has been done and shown in Figure (311.58) along X and Z directions respectively.

In this case, results do not match for the top middle point of the model. The main reason is due to the frequency of the motion. The maximum allowable frequency to be propagated in the fault slip model is  $1.4\text{Hz}$  while it is  $14\text{Hz}$  in DRM model. Dominant frequency of the Ricker wave as input motion is  $2\text{Hz}$ . Frequencies above the  $1.4\text{Hz}$  can not be propagated in the fault slip model while they will propagate in

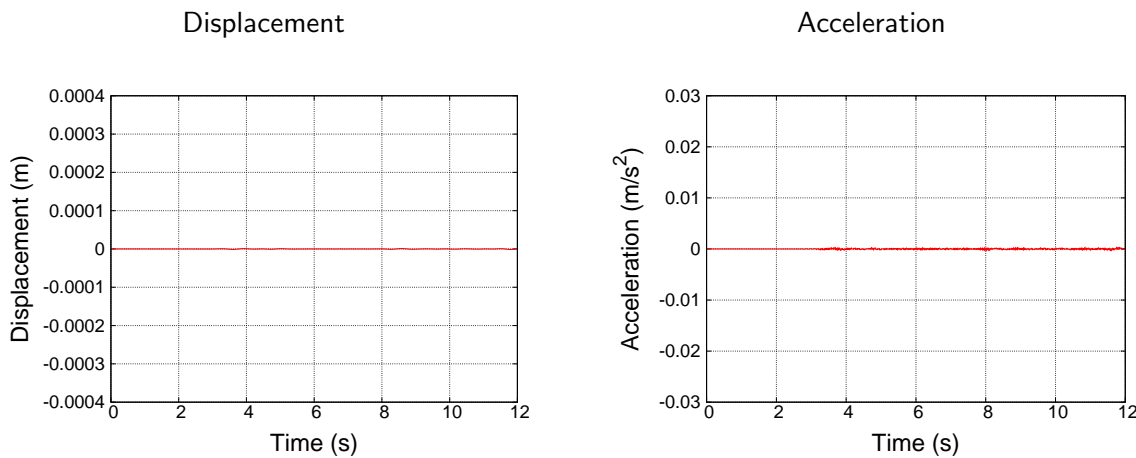


Figure 311.53: Displacement and acceleration time history for a point outside of DRM layer in (x) direction

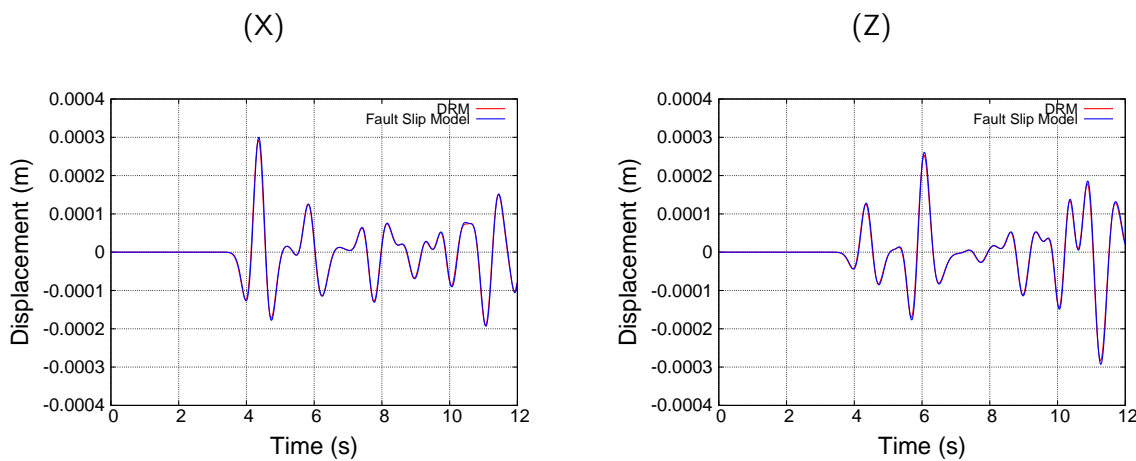


Figure 311.54: Comparison of displacements for top middle point using Ricker wave ( $f = 1\text{Hz}$ ) as an input motion

the DRM model. this can change the characteristics of the motion propagating through the model and is the main reason of differences between the obtained results.

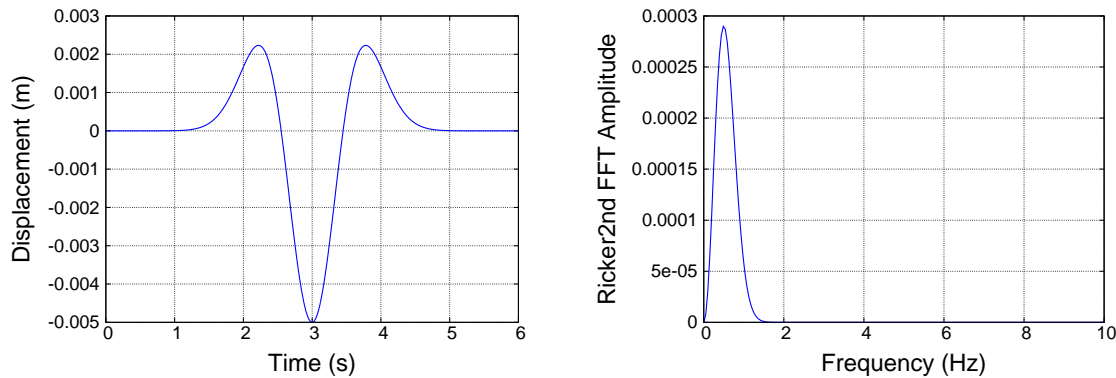


Figure 311.55: Displacement time history and FFT of Ricker wave with dominant frequency of  $0.5\text{Hz}$

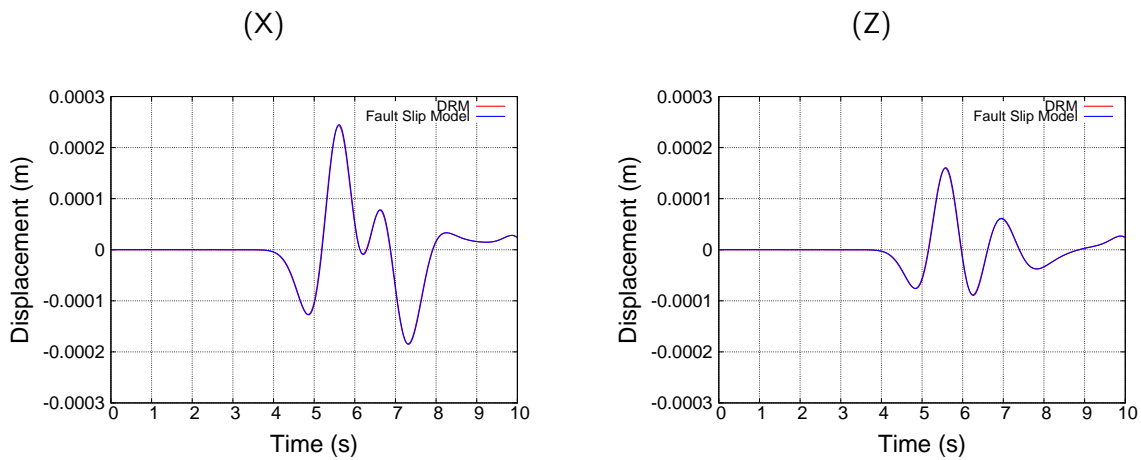


Figure 311.56: Comparison of displacements for top middle point using Ricker wave ( $f = 0.5\text{Hz}$ ) as an input motion

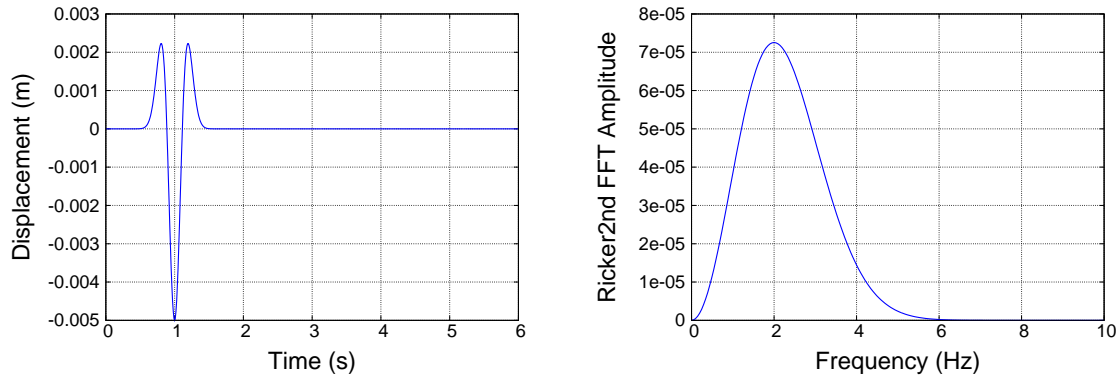


Figure 311.57: Displacement time history and FFT of Ricker wave with dominant frequency of 2Hz

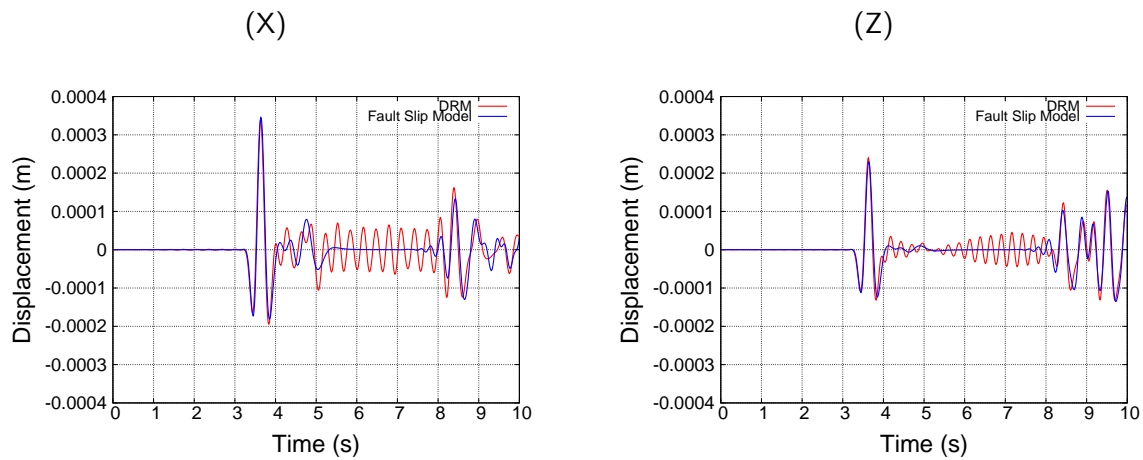


Figure 311.58: Comparison of displacements for top middle point using Ricker wave ( $f = 2\text{Hz}$ ) as an input motion

### 311.6.2 Vertical (1C) Seismic Waves in a Free Field

#### 311.6.2.1 Morgan Hill and Kocaeli Earthquakes

In order to investigate more, Morgan Hill and Kocaeli earthquakes are used as an input motions for the same models as before. These earthquakes were recorded during the ground shaking and obtained from PEER motion database. Figure (311.59) shows the acceleration time history and FFT of Morgan Hill earthquake with major frequency range of up to 4Hz. Acceleration time history and FFT of Kocaeli earthquake are shown in Figure (311.60). Major part of the frequency range for Kocaeli earthquake is up to frequency of 4Hz.

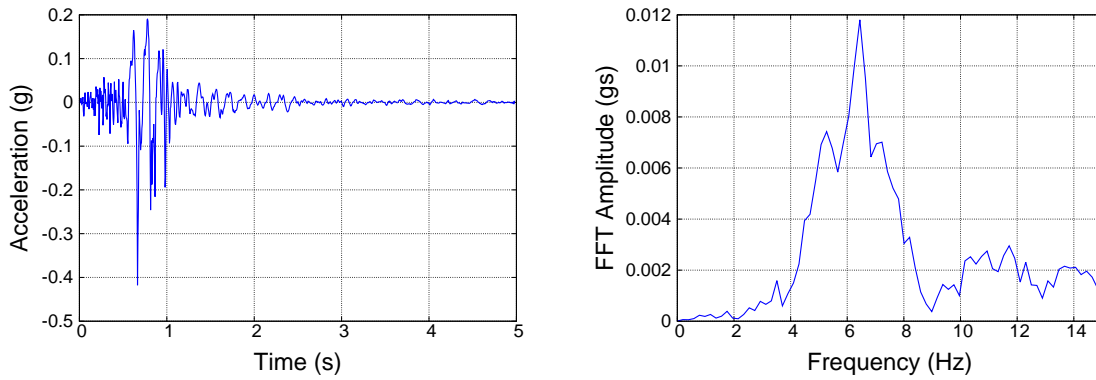


Figure 311.59: Acceleration time history and FFT of Morgan Hill earthquake

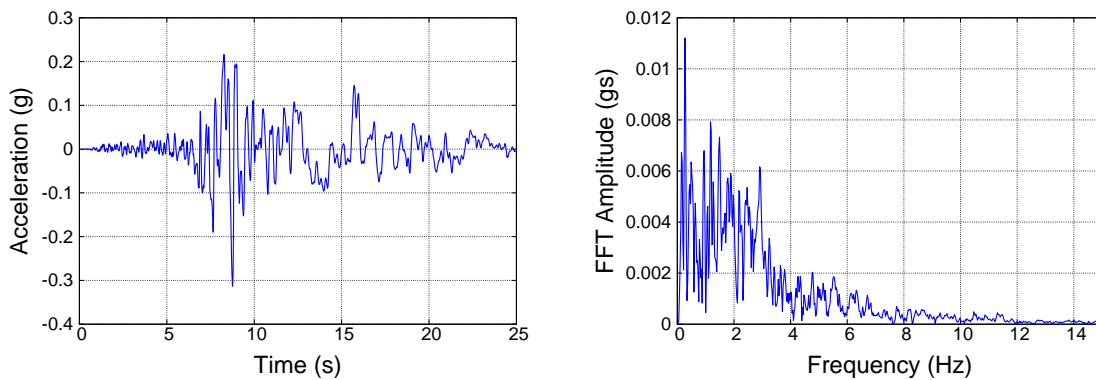


Figure 311.60: Acceleration time history and FFT of Kocaeli earthquake

Figure (311.61) shows the displacement time histories of the top middle point of the model for

Morgan Hill earthquake while the ones from Kocaeli earthquake are shown in Figure (311.62). As it is observed, results of fault slip model and DRM model do not match since the majority of the energy in the earthquake is in the range of up to  $4\text{Hz}$  which is higher than the maximum allowable frequency to be propagated in the original model ( $1.4\text{Hz}$ ).

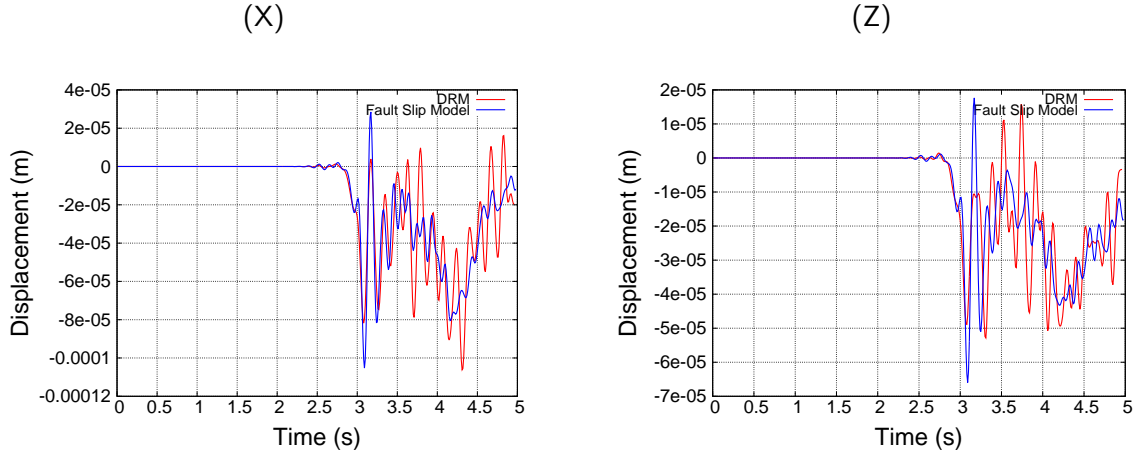


Figure 311.61: Comparison of displacements for top middle point using Morgan Hill earthquake as an input motion

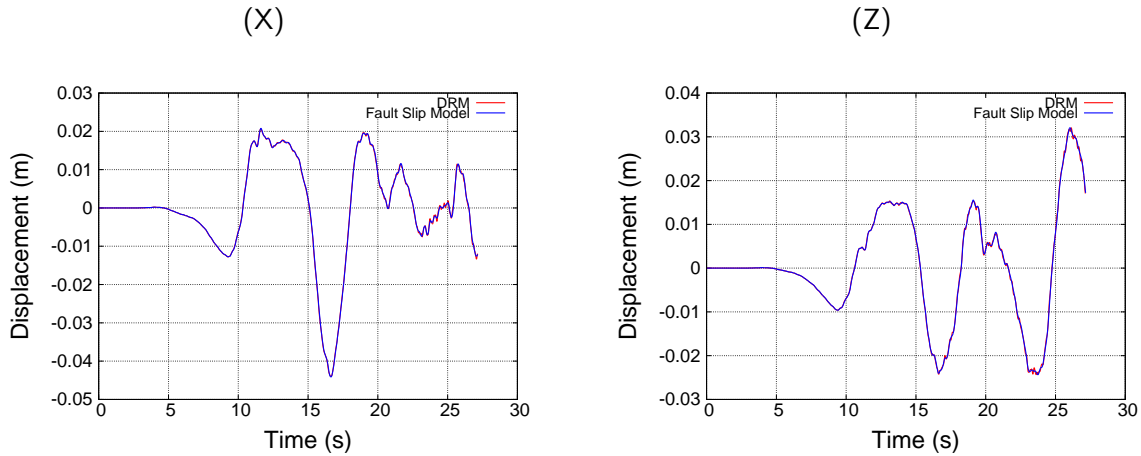


Figure 311.62: Comparison of displacements for top middle point using Kocaeli earthquake as an input motion

In order to investigate more regarding the frequency content issue, Kocaeli acceleration time history is considered and frequencies above  $1.4\text{Hz}$  are filtered out of the record. Acceleration time history and

FFT of the filtered record are shown in Figure (311.63). The majority of the energy is in the frequency range of below  $1.4\text{Hz}$  while still there are frequencies up to  $2\text{Hz}$  in the motion as can be observed in FFT of the filtered motion.

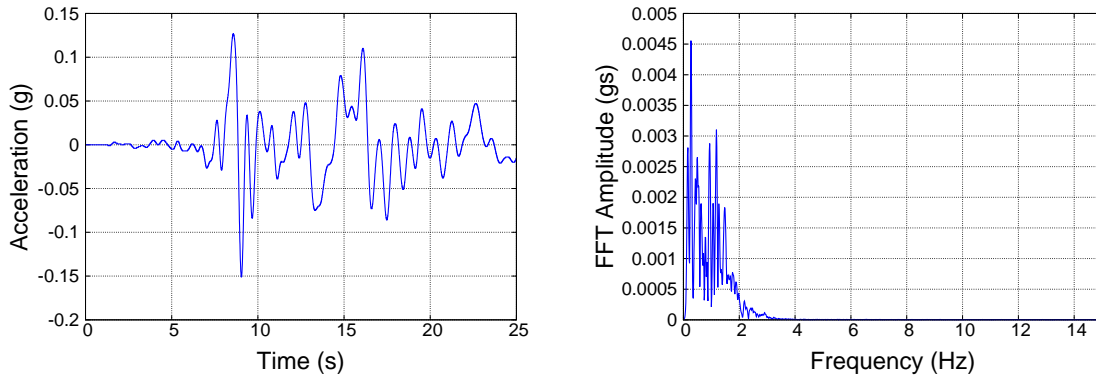


Figure 311.63: Acceleration time history and FFT of filtered Kocaeli earthquake

Figure (311.64) shows the displacement time histories for the same point as the one studied for the actual record. As it is observed, the obtained time histories match perfectly between the case of fault slip and DRM models. Figure (311.65) shows the acceleration time histories. Comparing the time histories shows an acceptable match between the results. There are tiny differences in acceleration time histories (specially at the peaks) which can be due to the fact that there are still frequencies above  $1.4\text{Hz}$  in the input motion but with much less impact in terms of amplitude.

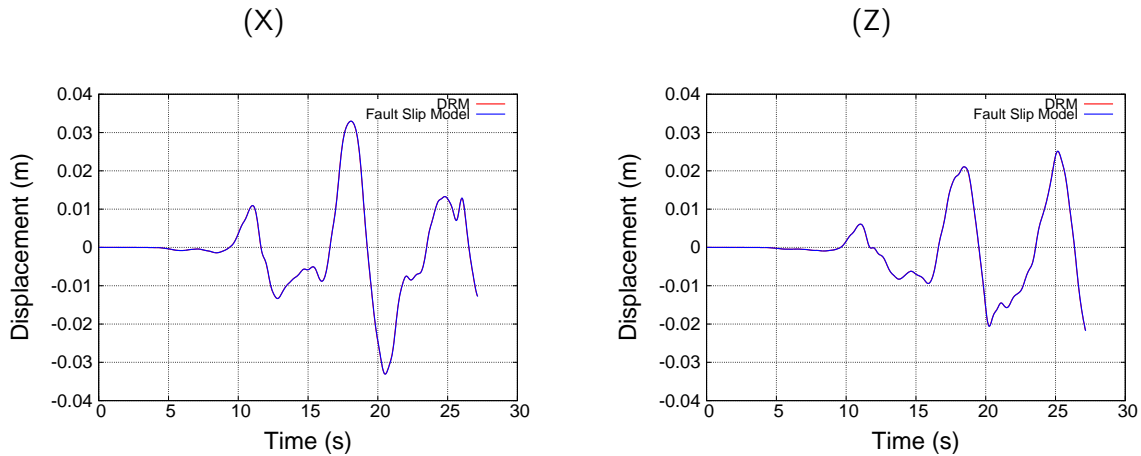


Figure 311.64: Comparison of displacements for top middle point using filtered Kocaeli earthquake as an input motion

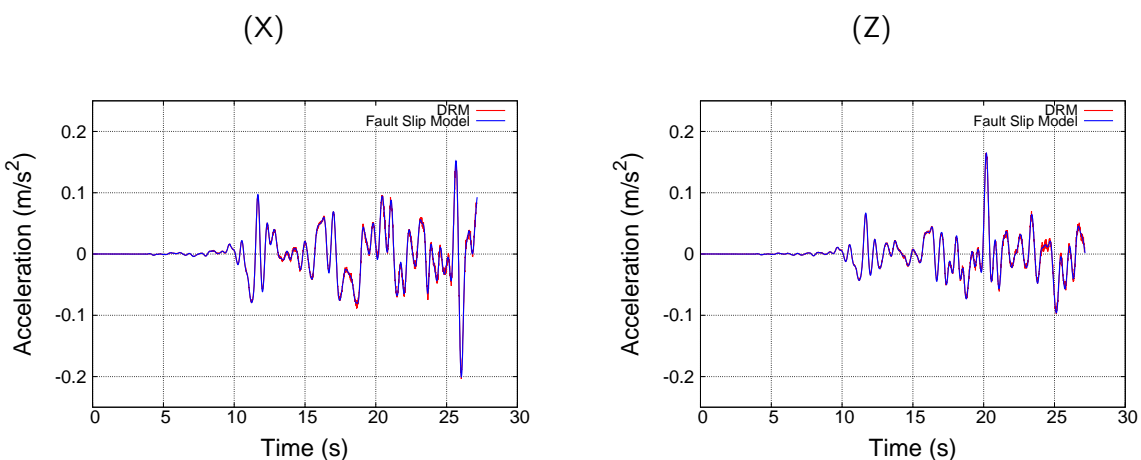


Figure 311.65: Comparison of accelerations for top middle point using filtered Kocaeli earthquake as an input motion

### 311.6.3 Earthquake-Soil-Structure Interaction Verification for Simulated Northridge Seismic Motions

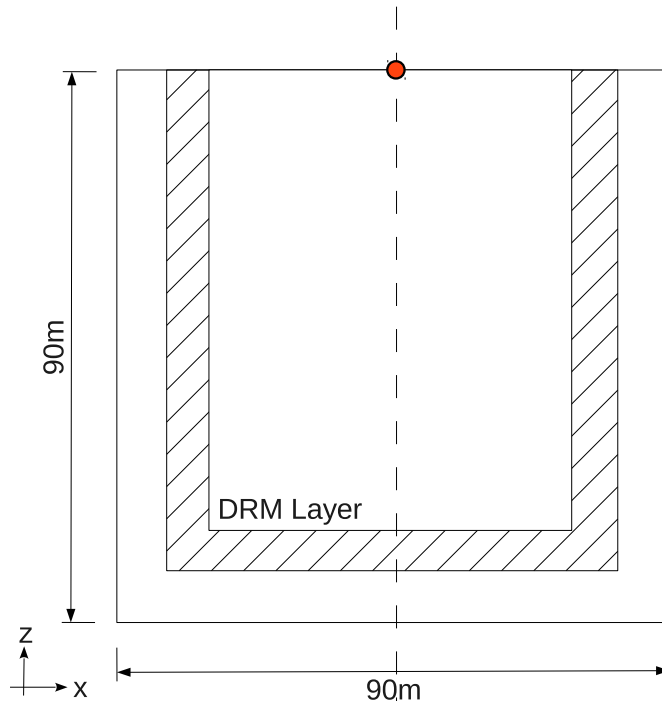


Figure 311.66: Finite element model to be used on analyses with input motions computed by integration equation (x-z plane view)

More realistic example is shown here. Seismic wave fields of Northridge earthquake simulated by program fk are applied as an input motion for this example. Figure 311.66 shows x-z plane view of three dimensional model. Similar as analytic case, using fk program, acceleration and displacement fields are generated at all nodes in DRM layer.

Figure 311.67 shows analysis results observed at the top-midpoint of the finite element model. As shown in figure 311.67, both results show perfect match.

### 311.6.4 Curious Case of 1C versus 3C modeling

To inspect more, artificial downhole array is prepared as shown in figure 311.68. Total 2 observation points are set on 0 m, and 50 m depth from the ground surface. one dimensional site response analyses are performed along artificial downhole array usind DEEPSOIL v5.0 (Hashash and Park, 2002). 1D soil column model is built to run DEEPSOIL with identical soil properties to finite element model. Linear time domain site response analyses are performed. Displacements recorded at 200 m depth are used as an input motion. Site response analyses results on the observation points are compared with fk, and

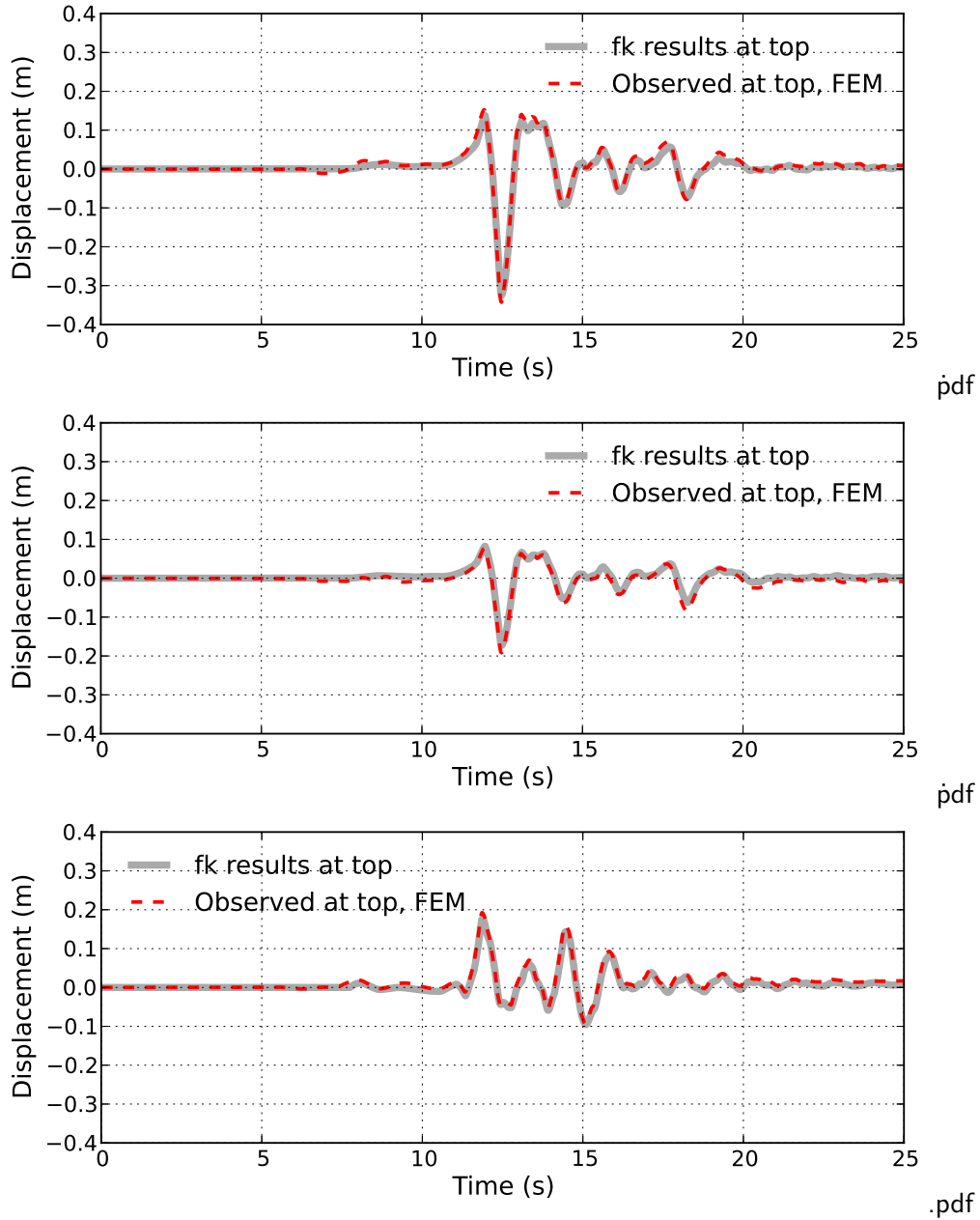


Figure 311.67: Comparison between results computed from program fk and finite element analysis, observed at the top middle point of the finite element model

finite element analyses results.

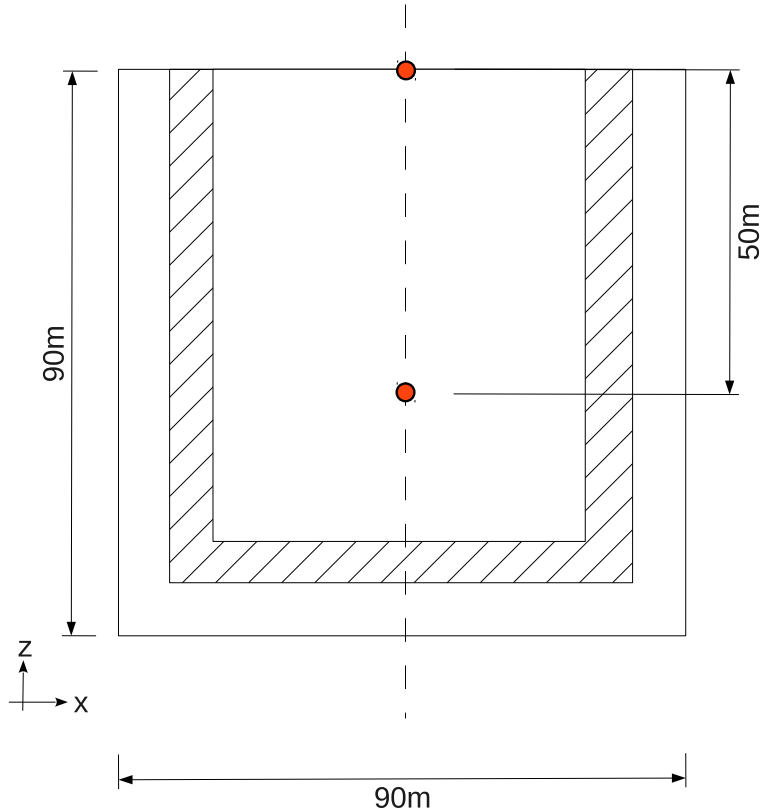


Figure 311.68: Comparison between analytic solution and FEM analysis result observed at top, middle point of the model (SV (imposed on x direction) Ricker wave input with  $0^\circ$ , x component)

Figure 311.69 – 311.74 are analyses results. Figure 311.69, 311.70, and 311.71 show comparison of results observed at the ground surface, EW, NS, and UD components, respectively. For the case of EW and NS components, 1C site response analyses results predict similar response as fk and FEM results compared to UD case. For all cases, 1C analyses results shows larger amplitude especially on UD case, 1Hz frequency contents show unrealistic response amplification. The same trend can be observed at 50 m depth cases (figure 311.72 – 311.74).

Possible explanation are as follows. fk results includes all components of waves (body and surface) and interaction between them. However, 1C wave propagation analyses cannot incorporate such effect. Also, 1C analyses is very sensitive to material properties (stiffness, damping ratio, and so on) and frequency contents of input waves.

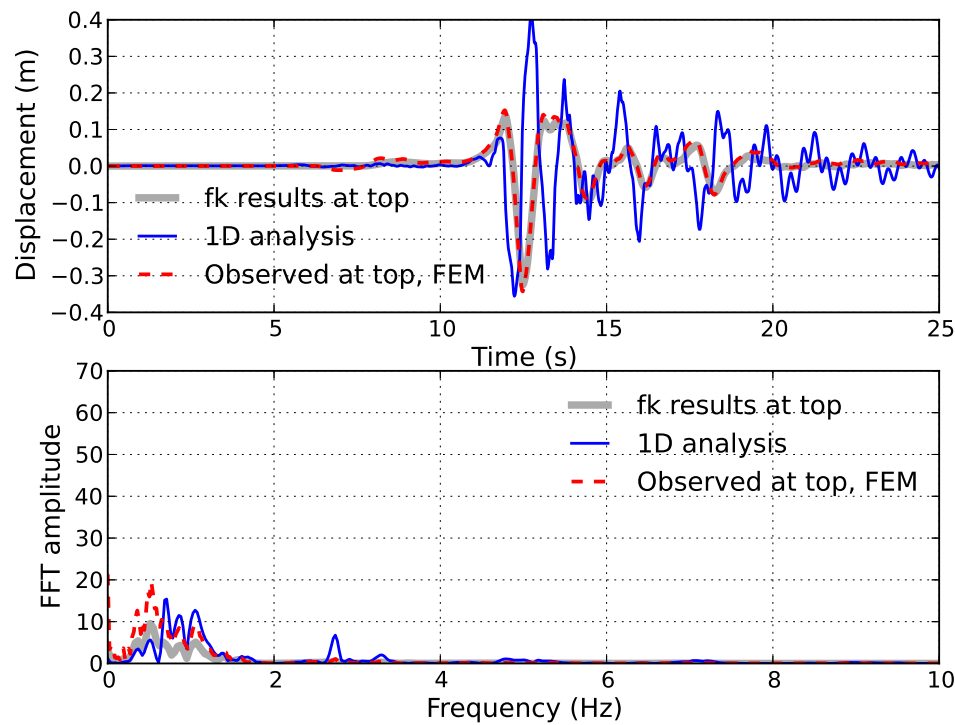


Figure 311.69: Comparison between results computed from program fk, finite element analysis, and 1C analysis, observed at the top middle point, EW component

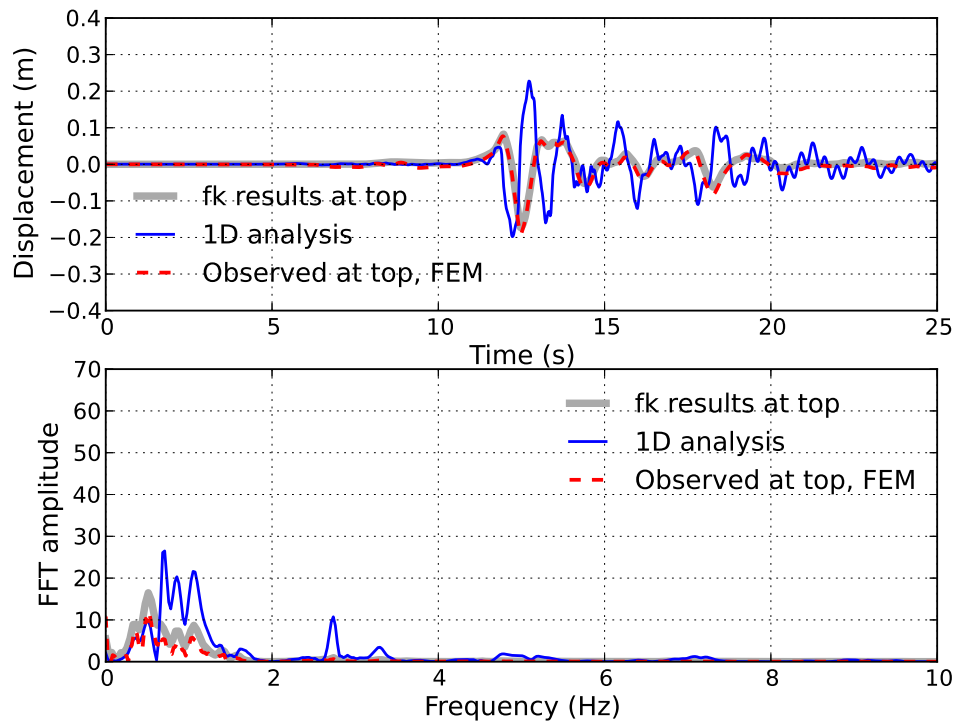


Figure 311.70: Comparison between results computed from program fk, finite element analysis, and 1D analysis, observed at the top middle point, NS component

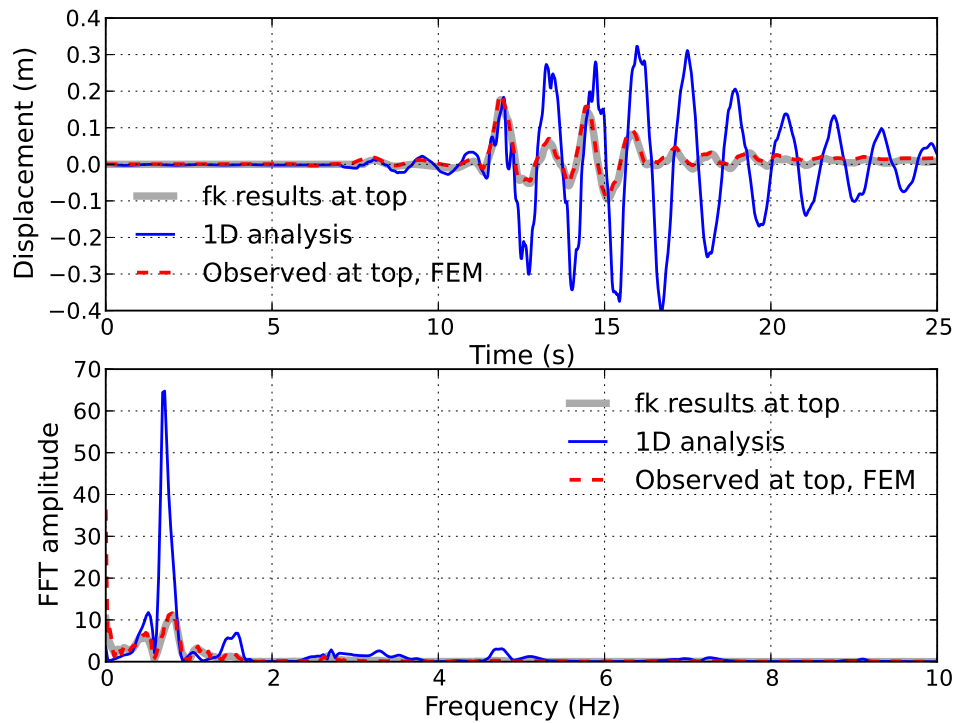


Figure 311.71: Comparison between results computed from program fk, finite element analysis, and 1D analysis, observed at the top middle point, UD component

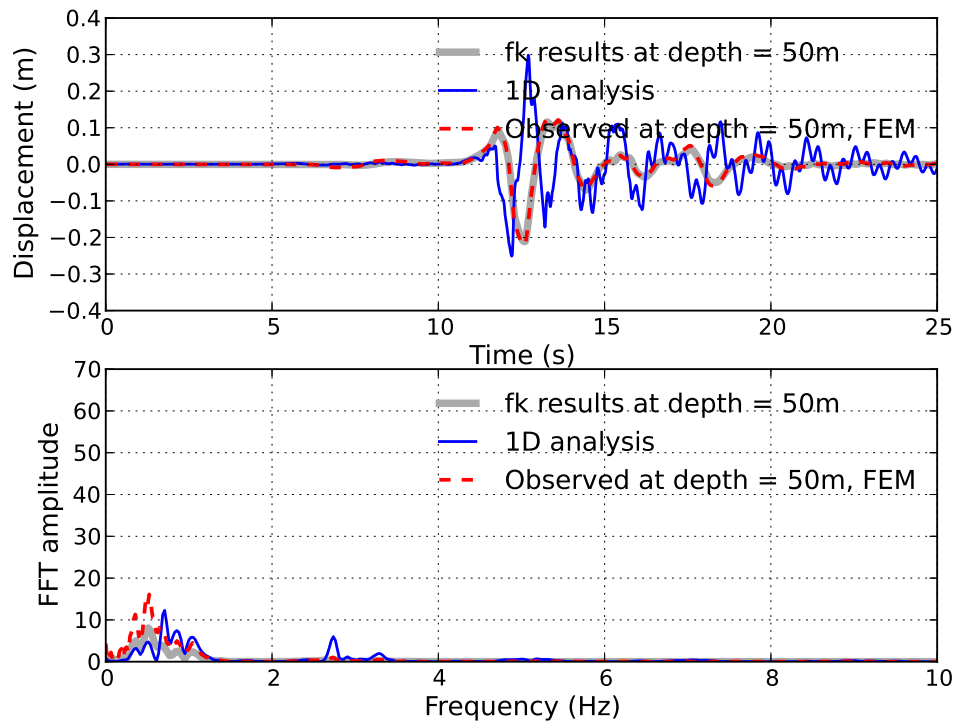


Figure 311.72: Comparison between results computed from program fk, finite element analysis, and 1D analysis, observed at the depth = 50m, EW component

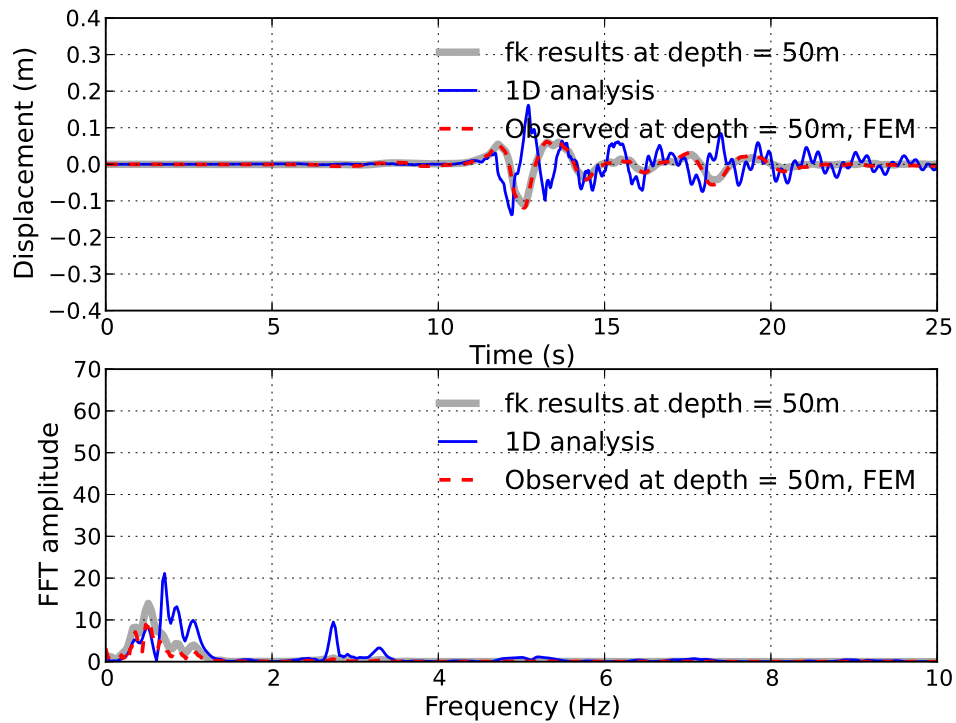


Figure 311.73: Comparison between results computed from program fk, finite element analysis, and 1D analysis, observed at the depth = 50m, NS component

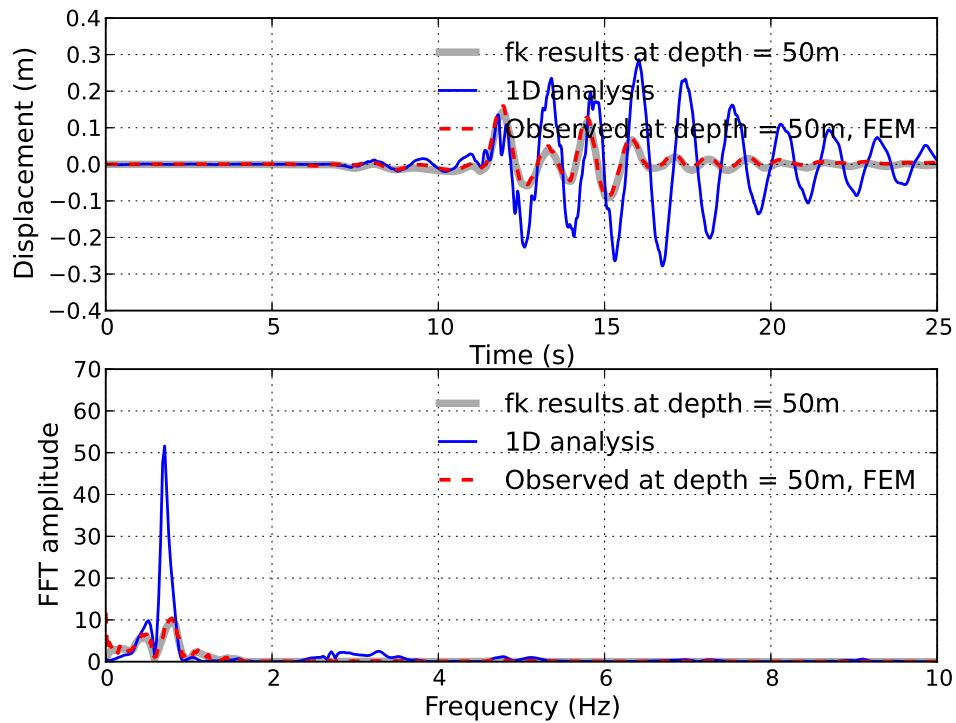


Figure 311.74: Comparison between results computed from program fk, finite element analysis, and 1D analysis, observed at the depth = 50m, UD component

### 311.6.5 Earthquake-Soil-Structure Interaction for Surface and Embedded Structures

Luco (1974) Gazetas and Roessel (1979) Wong and Luco (1978) Iguchi and Luco (1981) Kausel and Roessel (1975) Wong and Luco (1985) Day (1977) Zhang and Chopra (1991) Papageorgiou and Pei (1998) Luco et al. (1990) Pais and Kausel (1989) Apsel and Luco (1987) Gazetas and Roessel (1979) Kausel and Roessel (1975)

311.6.5.1 Uniform half-space

311.6.5.2 Layered half-space

311.6.5.3 Layered over rigid lower boundary

## 311.7 Case History: Simple Structure on Nonlinear Soil

### 311.7.1 Simplified Models for Verification

Due to the complexity of full scale finite element models it is helpful to perform preliminary tests on simplified models in order to verify the adequacy of the time and mesh discretization with respect to the input motion. It also provides good insight in the performance of the nonlinear material model. To achieve this a series of tests on a one-dimensional soil column have been proposed:

- Static pushover test on nonlinear soil column

Through the static pushover test the behavior of the nonlinear material model can be verified.

- Dynamic test of elastic soil column

By applying an earthquake motion to the elastic soil column it can be tested whether the selected grid spacing is capable of representing the motion correctly without filtering out any relevant frequencies. This test also allows to choose appropriate damping parameters. It should be noted that this is additional (small) damping that is used for stability of the numerical scheme and should not be relied upon to provide major energy dissipation. Major energy dissipation should be coming from inelastic deformations of the SFS system.

- Dynamic test of nonlinear soil column

Finally the stability and the accuracy of the numerical method can be examined by applying the earthquake motion to the nonlinear column of soil. A second analysis with a time step reduced by 50% should not give a significantly different result.

Furthermore it will be examined how propagation through an elastic-plastic material will change the frequency content of the motion.

#### 311.7.1.1 Model Description

The one-dimensional soil column used for verification has the same depth and element sizes as the 2d and 3d models that will be addressed later. Its total depth is 10.5 meters and it consists of a single stack of 8-node brick elements of 1.5 meters side length. In order to achieve one-dimensional wave propagation in vertical direction the movement of four nodes at each level of depth is constrained to be equal. The input motion is applied to the four nodes at the base of the model. As input motions four time histories from the Northridge Earthquake are selected (Figure 311.75).

The material properties of the soil are given in Table 311.7.1.1.

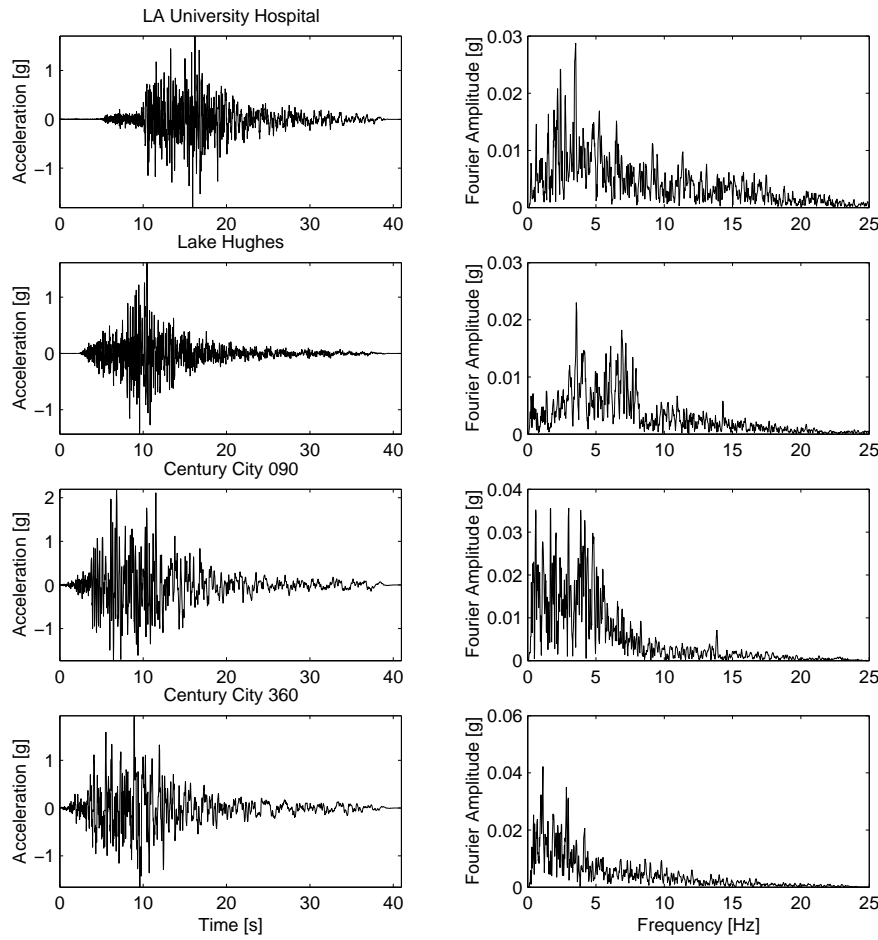


Figure 311.75: Acceleration time histories and Fourier amplitude spectra's of the selected ground motions

Friction angle $\phi'$	$37^\circ$
Undrained shear strength $c_u$	10 kPa
Mass density $\rho$	$1800 \text{ kg/m}^3$
Shear wave velocity $v_s$	200 m/s

The discretization parameters, the time step  $\Delta t$  and the maximum grid spacing  $\Delta h$ , are determined following the guidelines outlined in Section 502.3.3. This yields a maximum grid spacing of

$$\Delta h \leq \frac{v_s}{10f_{max}} = \frac{200}{10 \cdot 10} = 2 \text{ m} \quad (311.5)$$

For the following analysis  $\Delta h = 1.5 \text{ m}$  is selected. The maximum time step is

$$\Delta t \leq \frac{\Delta h}{v_s} = \frac{1.5}{200} = 0.0075 \text{ s} \quad (311.6)$$

Taking into account a further reduction of the time step by about 60% due to the use of nonlinear material models  $\Delta t = 0.002 \text{ s}$  is chosen.

### 311.7.1.2 Static Pushover Test on Elastic-Plastic Soil Column

For the static pushover test, an elastic perfectly plastic Drucker-Prager material model as specified in Table 311.7.1.1 is used.

After applying self weight a horizontal load of 100 kN is applied to a surface node in increments of 0.1 kN. The system of equations is solved using a full Newton-Raphson algorithm. The predicted shear strength of the first element that is expected to fail, the one at the surface, is:

$$\begin{aligned}\tau_f &= c_u + z \rho g \tan \phi' \\ &= 10 + 0.75 \times 1.8 \times 9.81 \tan 37^\circ \\ &= 19.98 \text{ kPa}\end{aligned}\tag{311.7}$$

where  $z$  is the depth of the center of the first element.

Self weight produces the following stresses in the element at the surface:

$$\begin{aligned}\sigma_x = \sigma_y &= 8.83 \text{ kPa} \\ \sigma_z &= 13.24 \text{ kPa}\end{aligned}$$

The maximum shear stress is

$$\tau_{max} = \sqrt{\left(\frac{\sigma_z - \sigma_x}{2}\right)^2 + \tau_{xz}^2}\tag{311.8}$$

The theoretical failure load can be obtained as follows:

$$\begin{aligned}P_f &= \tau_{xz} A \\ &= \sqrt{\tau_f^2 - \left(\frac{\sigma_z - \sigma_x}{2}\right)^2} A \\ &= 44.7 \text{ kN}\end{aligned}\tag{311.9}$$

The static failure load is underestimated by about 6%. This accuracy is acceptable for the given model because the boundary conditions cannot assure constant stresses at a given depth (no shear stress is applied to the lateral surfaces).

### 311.7.1.3 Dynamic Test on Elastic Soil Column

In order to test the spatial discretization of the model an earthquake motion is propagated through an elastic soil column. The grid spacing of the finite element mesh can be considered sufficiently fine if frequencies up to  $f_{max} = 10$  Hz are represented accurately in the numerical analysis. A good way to verify this is to calculate transfer functions between the base and the surface of the soil column.

Because transfer functions don't depend on the input motion they can easily be compared with closed form solutions.

The transfer function of a soil deposit describes the amplification between the frequencies of the motion at the base and at the soil surface:

$$TF(\omega) = \frac{u(z=0, \omega)}{u(z=H, \omega)} \quad (311.10)$$

where  $z$  is the depth measured from the surface and  $H$  is the thickness of the soil deposit above the bedrock.  $\omega = 2\pi f$  is the circular frequency.

For elastic soil with viscous damping the wave equation can be written as (Kramer, 1996a)

$$\rho \frac{\partial^2 u}{\partial t^2} = G \frac{\partial^2 u}{\partial z^2} + \eta \frac{\partial^3 u}{\partial z^2 \partial t} \quad (311.11)$$

$\eta$  is the damping coefficient, defined as

$$\eta = \frac{2G}{\omega} \xi \quad (311.12)$$

where  $\xi$  is the frequency independent hysteretic material damping.

After solving the wave equation the transfer function can be written as

$$TF(\omega) = \frac{1}{\cos \omega H/v_s^*} \quad (311.13)$$

where  $v_s^*$  is the complex shear wave velocity

$$v_s^* = \sqrt{\frac{G^*}{\rho}} = \sqrt{\frac{G(1 + i2\xi)}{\rho}} \quad (311.14)$$

In a finite element model with mass- and stiffness proportional Rayleigh damping the damping coefficient  $\eta$  is constant. Therefore the hysteretic material damping ratio  $\xi$  needs to be frequency dependent in order to satisfy Equation 311.12. Solving Equation 311.12 for  $\xi$  and substituting it into Equation 311.14 and then into Equation 311.13 yields a new transfer function:

$$TF(\omega) = \frac{1}{\cos \left( \omega H \sqrt{\frac{\rho}{G + i\omega\eta}} \right)} \quad (311.15)$$

Figure 311.76 shows a comparison between the closed form solution and the numerical transfer functions obtained from the finite element analysis. Rayleigh damping is used to obtain the damping matrix  $\mathbf{C}$ :

$$\mathbf{C} = \alpha \mathbf{M} + \beta \mathbf{K} \quad (311.16)$$

The analysis are performed using stiffness proportional Rayleigh damping of  $\beta = 0.001$  and  $\beta = 0.01$ . No mass proportional damping is applied ( $\alpha = 0$ ). The damping coefficients of the closed form solution are chosen to be  $\eta = \beta G$ .

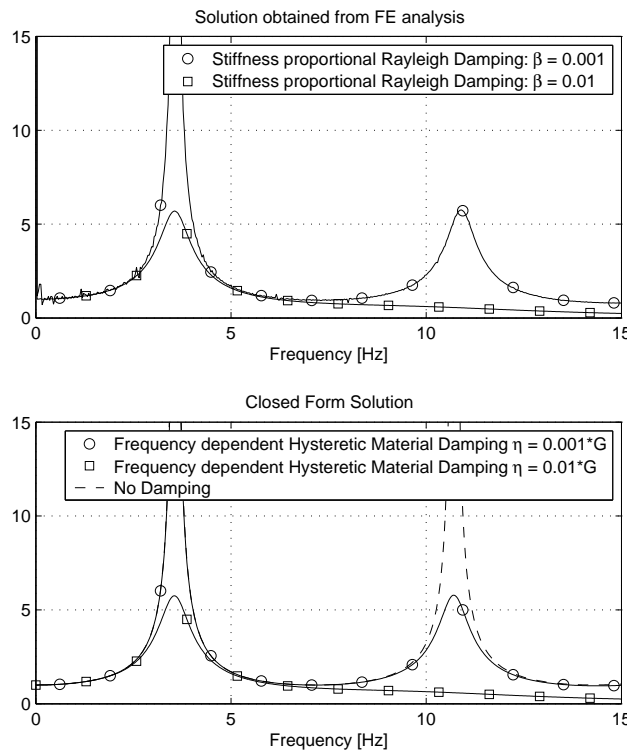


Figure 311.76: Transfer Function between Surface and Base of Soil Layer

It can be seen that the numerical transfer functions are very close to the closed form solutions for  $\eta = \beta G$ . The peak corresponding to the second natural frequency of the soil layer is slightly shifted to the right in the result of the FE analysis. For the FE analysis the Rayleigh damping cannot be reduced any further as the solution would become unstable. This result proves that a FE analysis involving Rayleigh damping with  $\alpha = 0$  and  $\beta = \eta/G$  is equivalent to the closed form solution of the wave equation with frequency-dependent hysteretic material damping.

Based on the above observations a stiffness proportional Rayleigh damping of  $\beta = 0.01$  is selected for the finite element analysis. This choice damps frequencies above 10 Hz appropriately.

#### 311.7.1.4 Dynamic Test on Elastic-Plastic Soil Column

As the next step an elastic-plastic material model of Drucker-Prager type with kinematic strain hardening has been selected. Previous analysis involving material with isotropic hardening have proved to be unsuitable because energy can only be dissipated as the yield surface expands. For dynamic problems this can lead to an unreasonably large extension of the yield surface, especially if resonance frequencies are present. Therefore only kinematic hardening has been selected in this analysis.

The analysis were performed with four different ground motions using time steps of  $\Delta t = 0.002s$  and

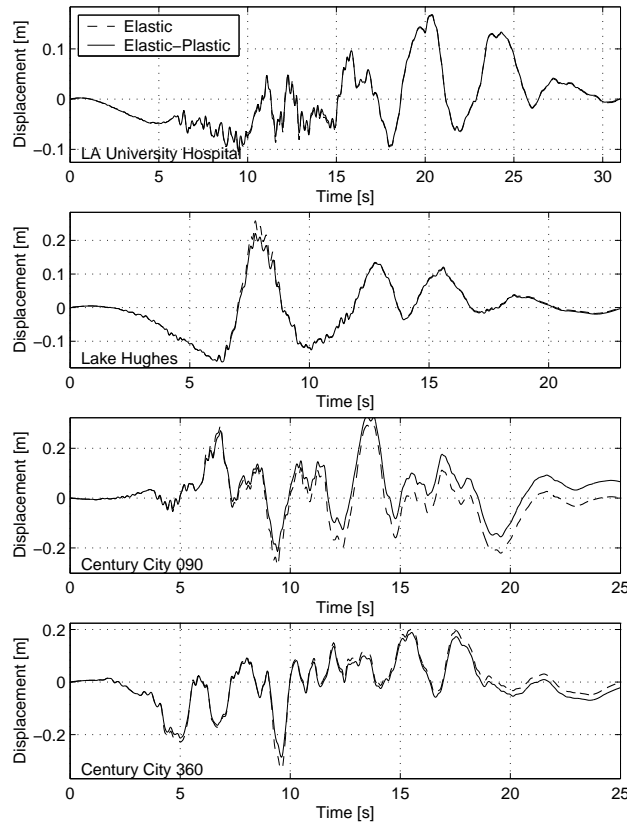


Figure 311.77: Displacement Time-Histories at surface of 1d Soil Column, elastic and elastic-plastic material

$\Delta t = 0.001\text{s}$ . A linear integrator without iterations within a time step was used. All ground motions were scaled to a maximum acceleration of  $1\text{g}$ . For comparison the analysis were also performed on elastic material. Figure 311.77 shows the displacement time histories at the surface for all four ground motions. While the overall shapes of the displacements are the same as for the elastic case there is some residual plastic displacement resulting in the time histories of the Century City motions.

The Fourier amplitude spectra's of the acceleration recorded at the surface (Figure 311.78) have the same general shape for the case of elastic and elastic-plastic material. The amplification at the first resonance frequency ( $f = 4.75\text{Hz}$ ) is bigger in the elastic analysis. Higher frequencies resulting from plastic slip are damped out effectively in the nonlinear analysis.

Figure 311.79 shows the acceleration time history at the upper node of the lowest element, that is the first free node above the base. The record shows large peaks of the order of about  $6\text{ g}$ . These peaks are caused by plastic slip and counter balancing of the resulting plastic deformation. The periods of the peaks are of the order of a few time steps, they add a very high frequency component to the

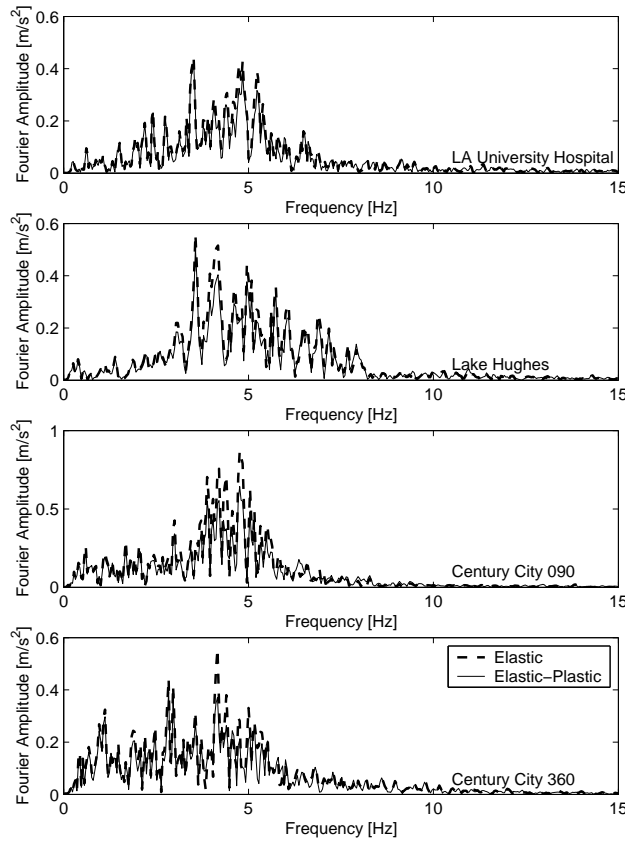


Figure 311.78: Fourier Amplitudes at surface of 1d Soil Column

acceleration. Because these frequencies are due to a purely numerical phenomenon, they should not be allowed to propagate through the model. This can be achieved easily by specifying an appropriate numerical procedure (Newmark with appropriate combination of  $\gamma$  and  $\beta$ ) or with Rayleigh Damping.

As for the elastic model transfer functions were also computed for the nonlinear model. In Figure 311.80 the transfer functions between the acceleration at the soil surface and the base are compared. The functions for the nonlinear model are not smooth anymore but the general shape is the same as for the linear elastic model, i.e. the first natural frequency of the layer is clearly visible. The peaks that are present in the range of 25 Hz are purely numerical as they appear due to the division by a very small value.

A second set of analysis performed with half the time step of the previous analysis gives an idea of the accuracy of the numerical method. In Figure 311.81 the difference between the displacement (or acceleration) of the analysis with  $\Delta t = 0.002s$  and  $\Delta t = 0.001s$ , divided by the corresponding maximum

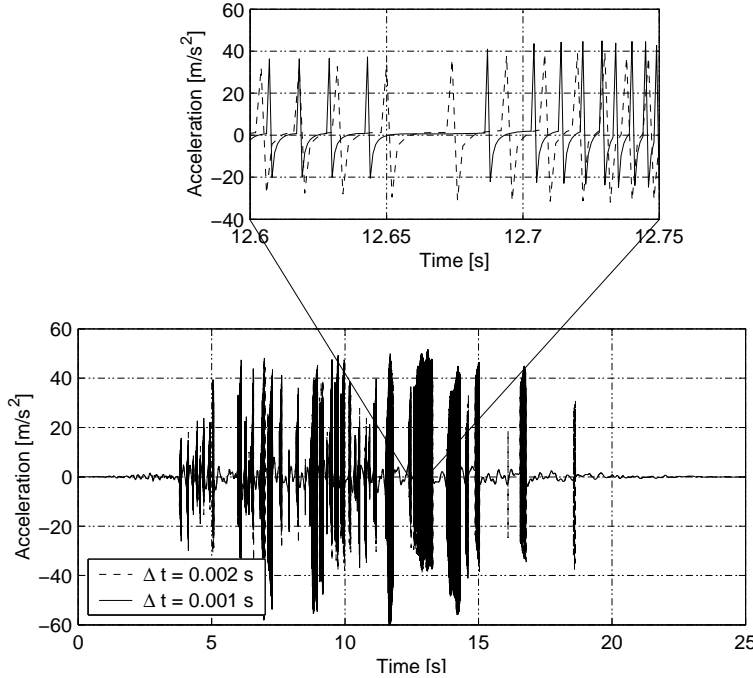


Figure 311.79: Acceleration time history at lowest free node

value is given for the entire time history:

$$\Delta d = \frac{d_{0.002}(t) - d_{0.001}(t)}{\max d_{0.001}} \quad \text{and} \quad \Delta a = \frac{a_{0.002}(t) - a_{0.001}(t)}{\max a_{0.001}} \quad (311.17)$$

In Figure 311.82 an integral measure for the difference in displacements and accelerations between the two analysis is given for all depths. The integral measures are defined as

$$diff_d = \frac{1}{\max |d|} \frac{1}{T} \sum_0^T |d_{0.002}(t) - d_{0.001}(t)| dt \quad (311.18)$$

$$diff_a = \frac{1}{\max |a|} \frac{1}{T} \sum_0^T |a_{0.002}(t) - a_{0.001}(t)| dt \quad (311.19)$$

$$(311.20)$$

The integral differences in accelerations are quite large in the elements that are close to the base, that is where the motion is applied. Toward the surface the difference becomes smaller than 1%. This is a result of the fact that most of the plastic deformation occurs near the base which represents an undesired boundary effect. Again this result underlines the importance of an appropriate choice of the size of the computational domain.

With a point wise difference not exceeding 5% for accelerations and 2% for displacements the time step  $\Delta t = 0.002s$  is sufficiently small to ensure stable and accurate results.

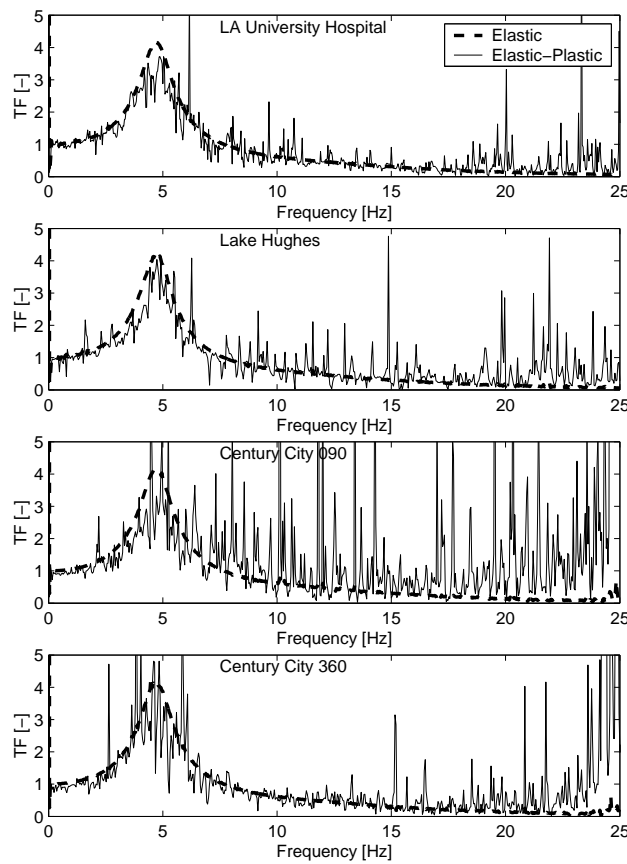


Figure 311.80: Transfer functions between acceleration at the soil surface and the base

### 311.7.1.5 2d Model

A 2d-model is proposed as a simplification of the full 3d-model. Representing a cross section of the full model it is expected to provide insight into its dynamic behavior while requiring considerably less computational resources. The 2d-model consists of one slice of eight-node brick elements as shown in Figure 311.83. The nodes of the two lateral faces are constrained to move together in x- and z-direction, the out-of-plane displacement in y-direction is fixed. The model approximates a plane strain situation.

The earthquake motion is applied to the model by the DRM method.

### 311.7.1.6 Input Motions

As input for the 2d model the motion from the Northridge earthquake recorded at LA University Hotel (Figure 311.75) is used. The acceleration time history is scaled to a peak ground acceleration of 1 g. Motion is applied in x-direction only, that is, this is a 1-D wave propagation.

Acceleration time histories at all the nodes of the boundary layer are obtained by vertically propagating

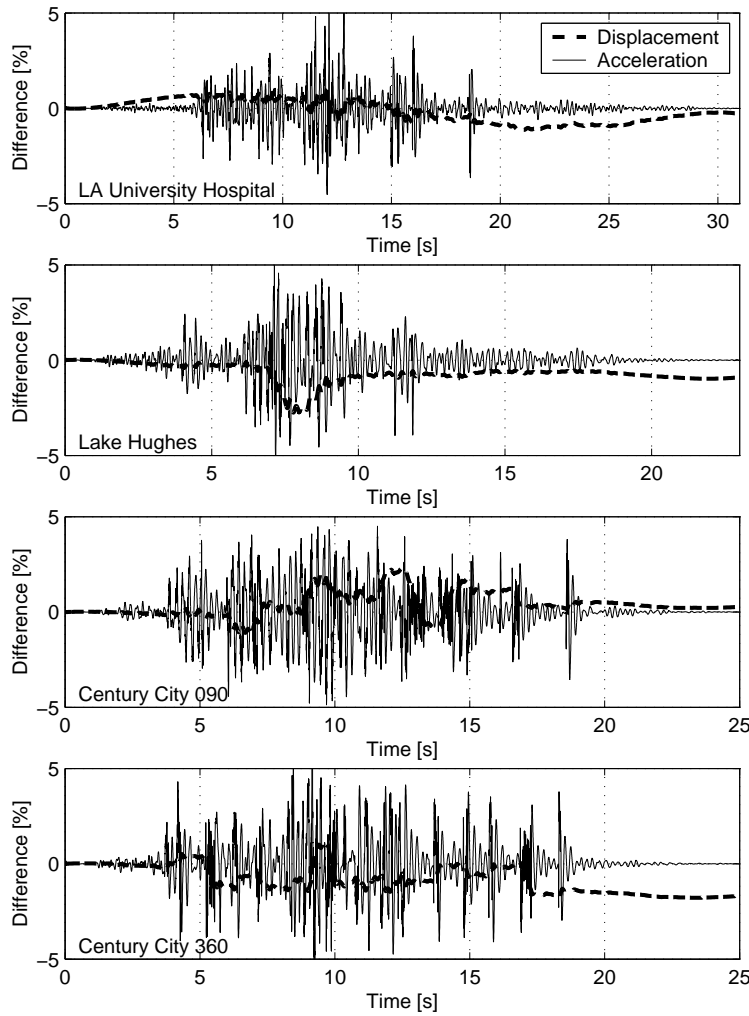


Figure 311.81: Difference between results of analysis with different time steps, in percent of the maximum value

a plane wave using the program SHAKE91 ([Idriss and Sun, 1992](#)). Because the free-field model has to match the properties of the free field as represented by the finite element model for the reduced domain, only linear elastic material without strain dependent reduction of shear modulus and a constant amount of hysteretic material damping is used in the SHAKE91-analysis. The earthquake motion obtained in this way corresponds to a shear wave propagating upward through a homogeneous linearly elastic half space.

The acceleration time histories from the SHAKE91-analysis are then integrated twice to obtain displacements. Before integration the acceleration and velocity time histories are transformed into Fourier space, multiplied with a high pass filter and transformed back into time domain. Then a simple parabolic baseline correction is performed in order to obtain zero initial, final and mean values.

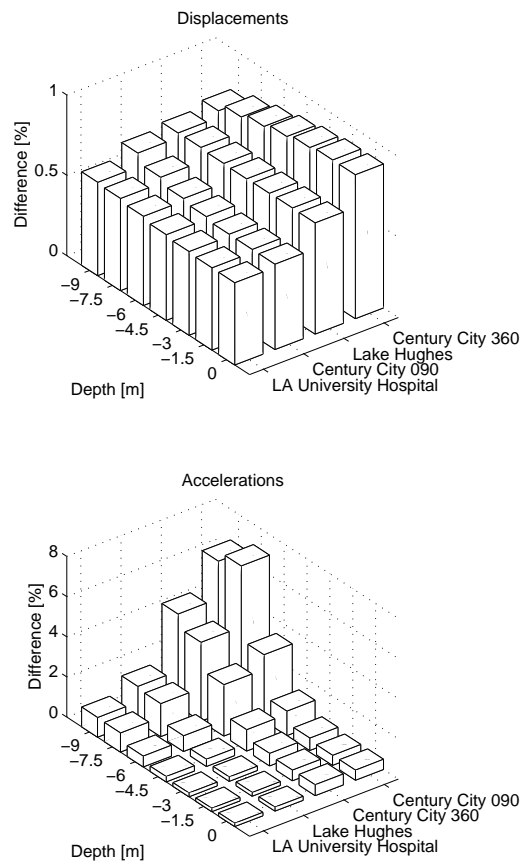


Figure 311.82: Averaged differences between results of analysis with different time steps

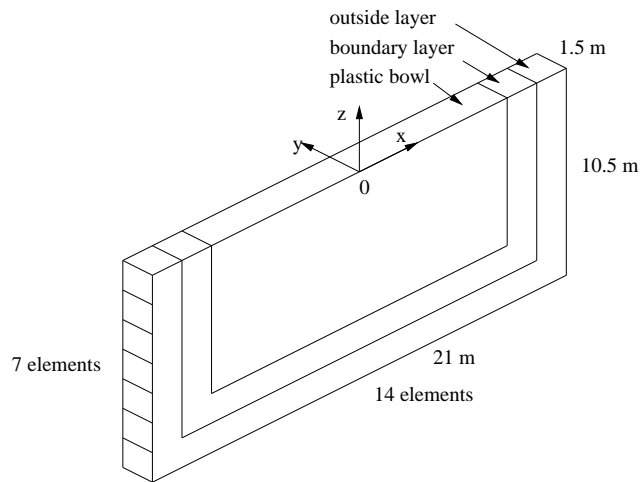


Figure 311.83: Two-dimensional quasi-plane-strain model

### 311.7.1.7 Boundary Conditions

Different boundary conditions are tested on the free-field model. First all outside boundary nodes are fully fixed as shown in Figure 311.84 a). Then they are released and attached to dash pots that are

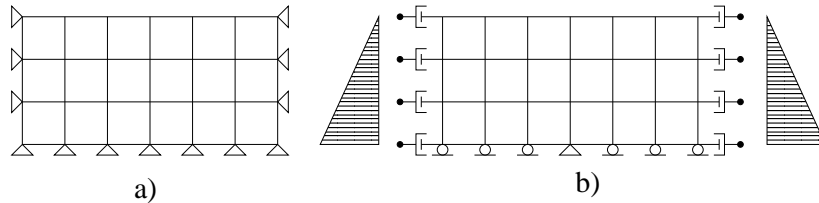


Figure 311.84: The boundary conditions of the 2d model

both perpendicular and tangential to the boundary (schematically shown in Figure 311.84 b)). The dash pots perpendicular to the boundary are specified to absorb p-waves, those tangential to the boundary to absorb s-waves. Because in this configuration no displacement constraint is imposed to the model on the faces at  $x = \pm 10.5$  meter the horizontal at-rest soil pressure has to be applied to the corresponding nodes manually. This is done by recording the reaction forces in the model with fixed boundaries and applying them with opposite sign to the model with absorbing boundaries. The horizontal displacements after applying self weight should be very small.

This configuration of boundary conditions has no fixed point in x-direction. Because the dash pots only provide resistance to high velocity motions the model is very sensitive to low frequency components of the motion. The slightest imbalance in acceleration causes the entire model to move as a rigid body in x-direction. To avoid this to happen the node at the center of the base ( $x = 0.0$  m,  $z = -10.5$  m) is fully fixed in the following analysis.

Figure 311.85 shows results from a free-field analysis on a homogeneous elastic model. Displacements on an exterior boundary node as well as transfer functions between a point at the surface and a point on the exterior boundary of the plastic bowl are presented for the two configurations of boundary conditions shown in Figure 311.84. It can be seen that the displacements outside the plastic bowl in the model using absorbing boundary conditions are much larger compared to the model with fixed boundaries. This result is as expected considering the immediate proximity of the boundary. It also gives an idea about the constraints the fixed boundary imposes on the motions. The transfer function in Figure 311.85 b) is defined as the ratio between the Fourier amplitude spectra of a point at the surface and a point on the exterior boundary:

$$TF(\omega) = \frac{A_1(\omega)}{A_2(\omega)} \quad (311.21)$$

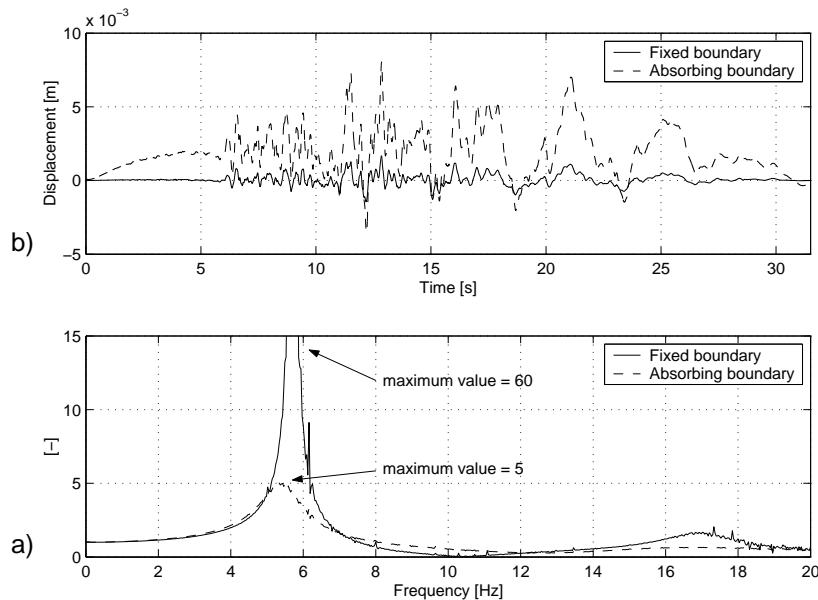


Figure 311.85: Elastic homogeneous free-field model: a) Displacements of an exterior boundary node  $(x,z) = (9.0,0.0)$  m, b) Acceleration transfer function between surface and depth  $\frac{A(\omega)_1}{A(\omega)_2}$

where  $A_1(\omega)$  is the Fourier amplitude spectrum of the acceleration time history at the point  $(x,z) = (0,0)$  m and  $A_2(\omega)$  the corresponding spectrum at the point  $(x,z) = (9.0,-7.5)$  m. The figure shows that the large peak representing the first natural frequency of the system, corresponding to a standing shear wave in a soil layer of 10.5 meter depth, gets reduced considerably by the absorbing boundary. An energy build-up in the model due to reflection of waves on the model boundaries can be reduced effectively with the configuration of boundary conditions shown in Figure 311.84 b). By releasing the fixed node at  $(x,z) = (0,-10.5)$  m the resonance peak could be reduced by another 10% approximately, however at the cost of remaining permanent displacements at the end of the analysis.

Alternatively to imposing a rigid constraint to a single node at the base the model can be prevented to move horizontally as a rigid body through uniaxial springs. This gives the possibility to adjust the frequency of the eigenmode that corresponds to a vertically propagating plane shear wave. By appropriately choosing the spring constants the model can therefore be adjusted in such a way that it represents the natural frequency of a soil deposit on bedrock.

### 311.7.1.8 Structure

Four very simple structures are chosen to illustrate the effects of dynamic SFSI. A beam-column element of length  $L$  and moment of inertia  $I_y$  is fixed to a footing. A lumped mass of  $M = 100,000$  kg is added to

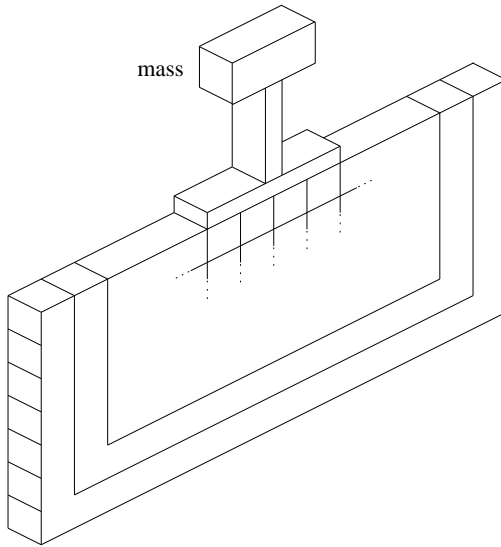


Figure 311.86: The 2d SFSI-model

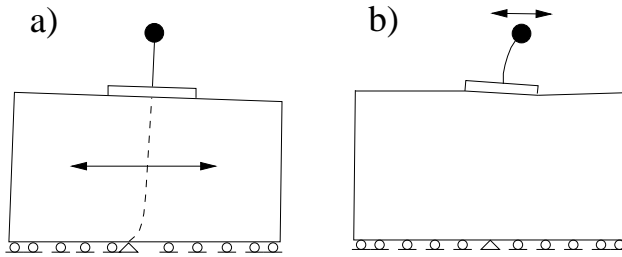


Figure 311.87: a) First eigenmode, b) second eigenmode of SFSI-system

the translational degrees of freedom of the top of the structure. The footing is 0.5 m deep, spans over four soil elements and is rigidly connected to the adjacent soil nodes. Its Young's modulus is chosen large enough so that the footing can be considered rigid. The mass density of the footing is  $\rho = 2400 \text{ kg/m}^3$ , the column is considered massless. The moment connection between the nodes of the footing, having 3 (translational) degrees of freedom, and the 6 degrees of freedom of the nodes of the column is assured by a very stiff beam element that is connected to a node at the bottom and a node at the top of the footing. The column is then simply connected to the upper node of this auxiliary beam element.

The parameters of the four columns are chosen such that the second natural frequency, that is the natural frequency attributed to bending of the column (Figure 311.87 b)), is evenly distributed over the frequency range of the input motion (Figure 311.88). Structure 4 is designed such that it's second natural frequency matches the largest spike in the input motion. Table 311.2 lists the properties of the structures used in the analysis. For the nonlinear columns a strain hardening material is chosen

Structure	Length [m]	Stiffness $E I_y$ [ $MN m^2$ ]	Mass [kg]	Yield Moment [kNm]
1	5.5	1680	100,000	800
2	3.5	5670	100,000	1,800
3	2.5	13440	100,000	320
4	5.0	5670	100,000	1,800

Table 311.2: Properties of the analyzed structures

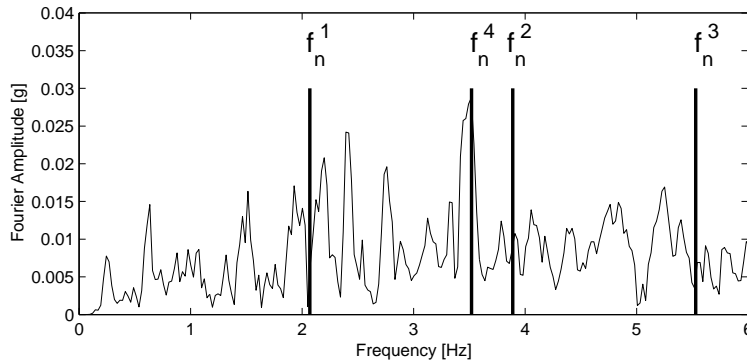


Figure 311.88: Fourier amplitude spectrum of input motion with second natural frequencies of the 4 SFSI-systems

that consists of an initial elastic branch with tangent modulus  $E$  and a post-yield branch with tangent modulus  $0.2E$ . The Young's modulus for all four structures is  $E = 210$  GPa. The yield stress  $f_y$  for structures 1, 2 and 4 is 20 MPa and for structure 3 it is 2 MPa.

### 311.7.1.9 Structure with Fixed Base

To begin with a parametric study of a series of structures with varying stiffnesses is analyzed. The stiffness is varied by changing the width of the column section. The different structures are expected to respond specifically to the frequency range of the input motion that is in the neighborhood of the natural frequency of the column. The input motion that is applied at the base of the structure has been recorded in a previous free-field analysis of the 2d-model.

The results of this parametric study are shown in Figures 311.89 and 311.90 for linear and nonlinear structures, respectively. The Fourier amplitudes spectra's of the acceleration at the top of the structure are plotted for 15 structures with variable natural frequency  $f_n$ . A line of equal frequency is also provided. The input motion is plotted in the background of the figure. It can be seen that the maxima of the

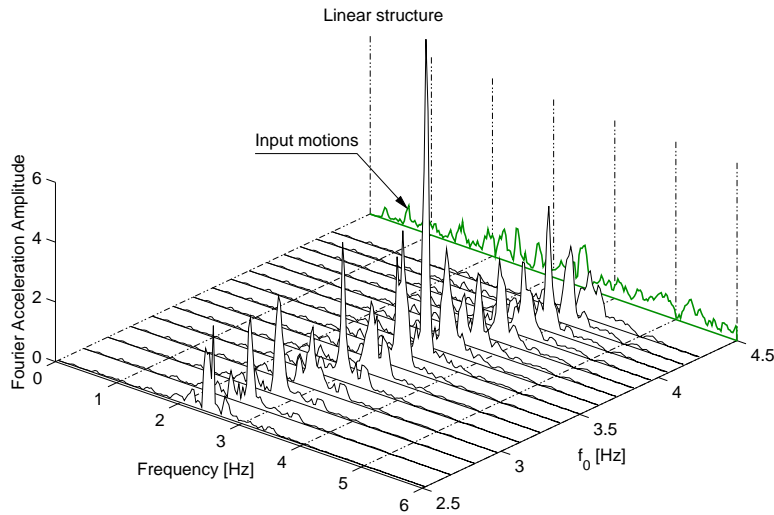


Figure 311.89: Parametric study of 15 *linear* structures with varying natural frequency.

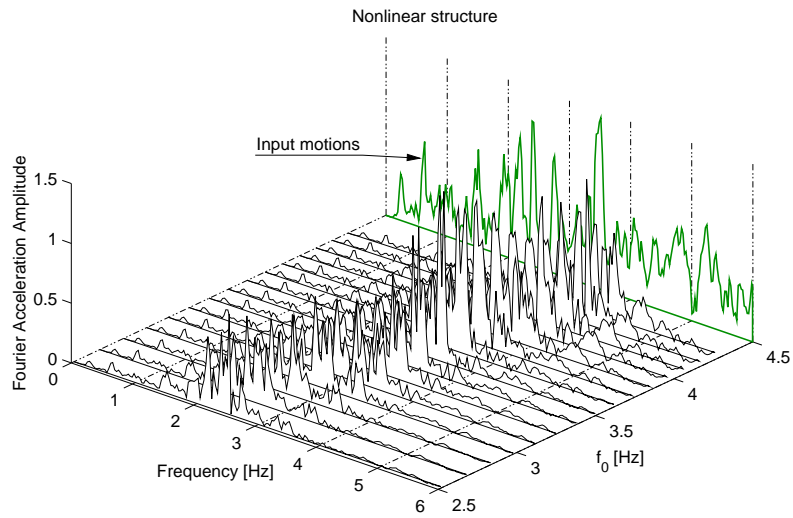


Figure 311.90: Parametric study of 15 *nonlinear* structures with varying natural frequency

frequency spectra's are almost perfectly aligned along the line of equal frequency. This is even more obvious in the case of a linear structure. In that case the responses of the structures are very narrow banded. As the structure remains elastic the top of the structure oscillates mainly in its initial natural frequency. Lower and higher frequencies are eliminated to a great extent.

In the case of the inelastic structure there is clearly more damping and reduction of the responses at some (most) frequencies. The nonlinearity in structure is producing a longer effective period for the structure, and that effective period changes during shaking. This in turn widens the frequency range of structural response. That is, the response is lower, but the frequency characteristic is (much) wider.

A series of fixed-base analysis is also performed on the four structures mentioned in Section 311.7.1.8. The first natural frequencies of the four structures with its base fixed, corresponding to the second mode of vibration of the SFSI-model, are given in Table 311.3. It can be seen that the influence of the soil on the natural frequency of the SFSI-system increases as the overall stiffness of the structure increases.

Structure	1 <sup>st</sup> natural frequency of fixed-base system [Hz]	2 <sup>nd</sup> natural frequency of SFSI-system [Hz]
1	2.71	2.07
2	9.82	3.89
3	25.1	5.53
4	5.75	3.52

Table 311.3: Eigenfrequencies of the analyzed models

### 311.7.1.10 Results

The results of the SFSI- as well as the fixed-base analysis are presented in the following. The displacements at the top of the nonlinear structures are recorded and plotted in Figure 311.91. It can be seen that the results from the SFSI- and the fixed-base-model differ considerably in terms of maximum as well as permanent displacement. In contrast to this the displacements at the base of the column are almost identical for the two models (results not plotted). Figure 311.92 displays the displacements at the top of structures 1 and 2 for all the combinations of linear and nonlinear soil and structures that have been analyzed. Due to the low yield moment the permanent displacement for structure 1 is relatively large in the analysis involving nonlinear columns. The results involving nonlinear columns on linear and on nonlinear soil are very similar in their overall shape, however permanent deformations are very different. It seems that the forces that trigger plastic deformations in the column strongly depend on the behavior of the soil beneath the foundation.

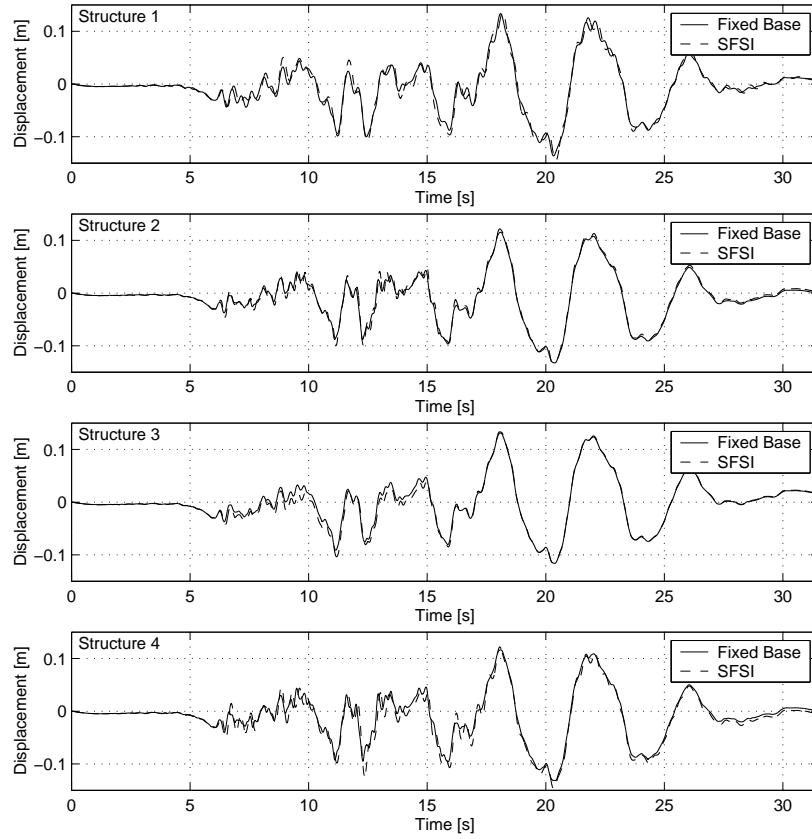


Figure 311.91: Displacements in x-direction at the top of the *nonlinear* structures

In order to investigate the forces causing plastic deformations in the structures we look at the base moments between foundation and column. In Figure 311.93 the moments at the base of the linear structures are plotted.

For structures 1 and 4 the moments for the fixed-base model are higher than for the SFSI-model. This means that in this case neglecting the effects of SFSI leads to a conservative design. Structures 2 and 3 however have to resist higher moments when SFSI is taken into account. Because the SFSI-system is more flexible than the fixed-base structure its modes of vibration are excited by a different range of frequencies contained in the input motion. For a particular motion this can lead to resonance of the SFSI-system. This result is in contradiction with current engineering practice suggesting that neglecting SFSI in general leads to a more conservative design.

Figure 311.94 shows the moments at the base of structures 1 to 4, this time for the analysis involving nonlinear column elements. The evolution of the second natural frequency of the SFSI-system is also provided as a qualitative indication for when plastic deformations occur. The base moments for structures 1 and 3 in the fixed-base- and the SFSI-analysis are very similar. Due to the low yield moment of the

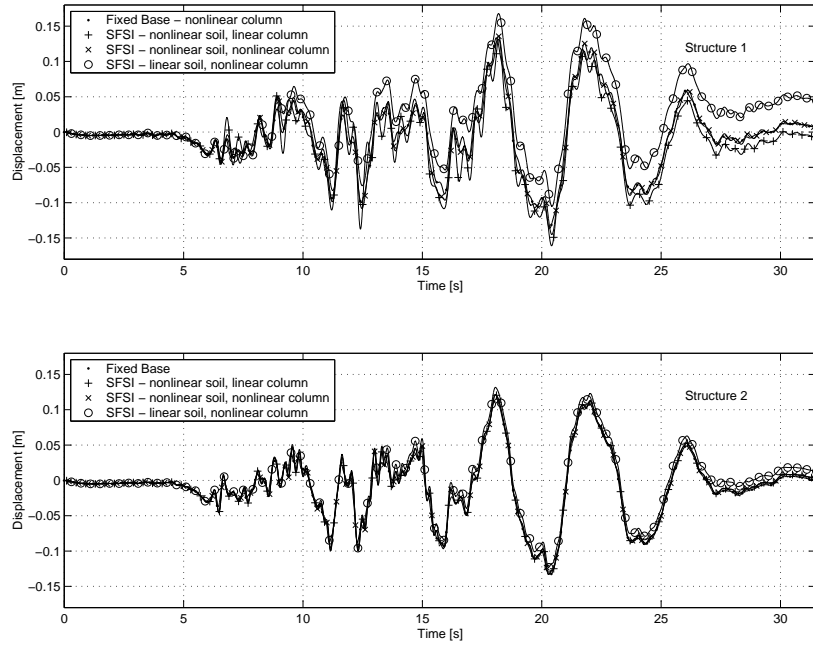


Figure 311.92: Displacements in x-direction at the top of structures 1 and 2

structure no resonance with the input motion occurs as a lot of energy is dissipated through plastic deformation.

Figure 311.95 shows an interesting aspect of nonlinear SFSI. In the analysis involving elastic-plastic soil the Fourier amplitudes of the moment at the base of the structure are reduced in the neighborhood of the natural frequency of the system. This is most likely due to dissipation of energy caused by elastic-plastic deformations in the soil that, in their turn, are a result of large loads provoked by resonance between the SFSI-system and the input motion.

As a measure of the plastic strain occurring beneath the footing the equivalent plastic strains averaged over all the Gauss points are calculated. The results are given at  $t = 12\text{ s}$  and at  $t = 14\text{ s}$ , that is shortly before and after the largest plastic deformation occurs (Figures 311.96 and 311.97).

Plastic strains are larger in the analysis involving an elastic structure. This reflects the fact that elastic structures don't dissipate any energy by themselves. For structure 2 no significant difference can be observed because of its high yield moment. Structure 4 is characterized by the same yield moment, its slightly smaller natural frequency however causes resonance with the input motion which leads to larger plastic strains beneath the footing. The largest plastic strains develop in the layer of elements adjacent to the boundary layer. This can be due to an input motion that isn't fully compatible with the elastic properties of the DRM-model. It should be possible to reduce these undesired plastic strains by either increasing the size of the soil model or by selecting a method to obtain the free-field motions that

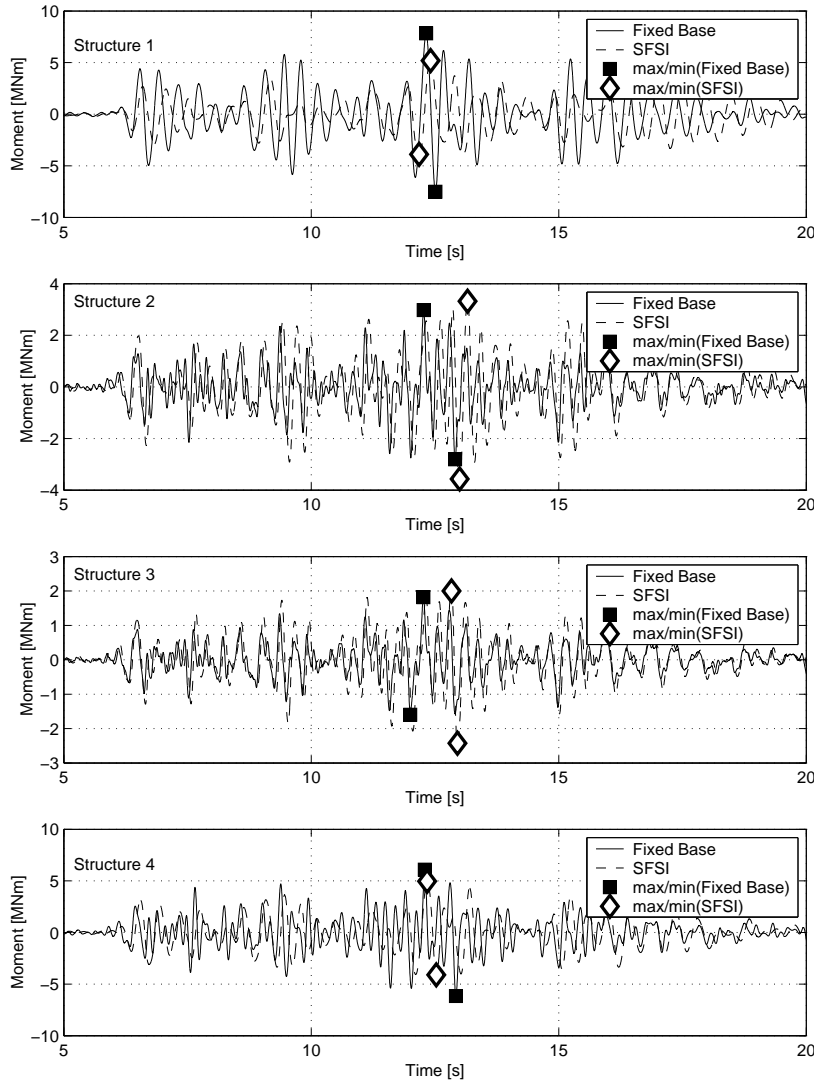


Figure 311.93: Moments at the base of the *linear* column

represents the soil properties of the DRM-model more closely.

### 311.7.2 Full nonlinear 3d Model

The 2d SFSI-model presented in the previous section is extended to a 3d model in the following. The goal is to show that the considerations for accuracy and stability of the numerical method obtained from the 1d-model remain valid for the 3d-model. Even if the simplicity of the analyzed problem doesn't necessarily justify the additional computational effort it is important to show that it is possible to obtain reliable results for a problem that involves the following elements:

- 3d model with about 700 elements, 960 nodes and 2700 equations

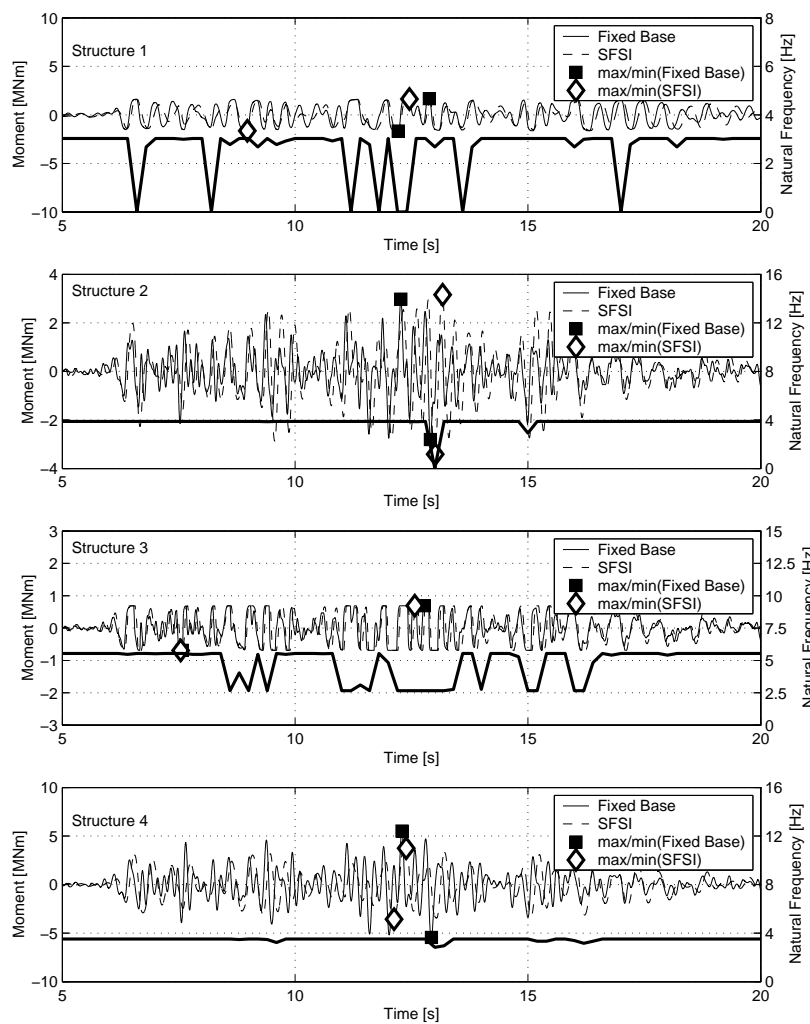


Figure 311.94: Moments at the base of the *nonlinear column*

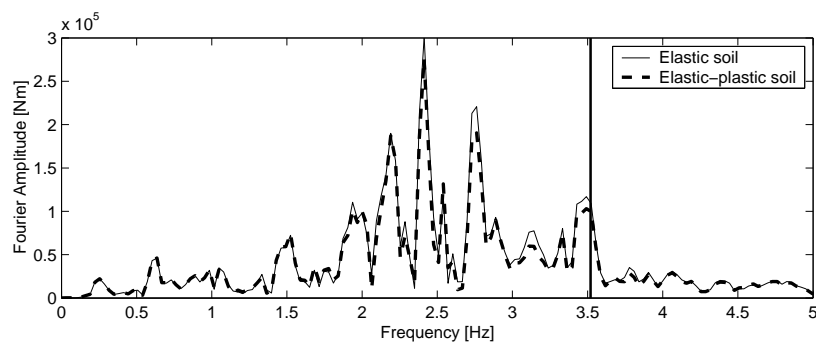
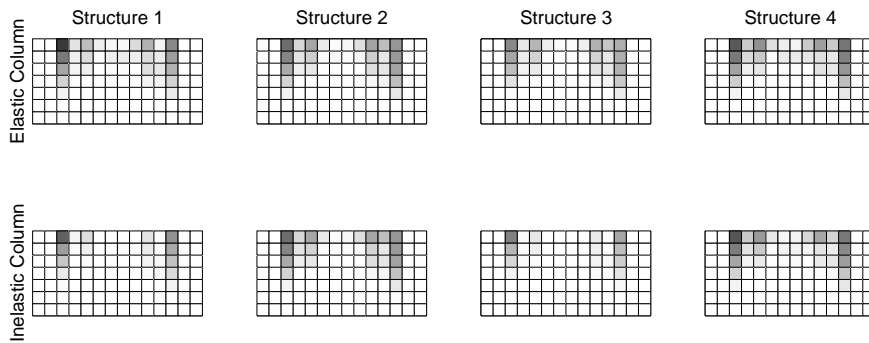
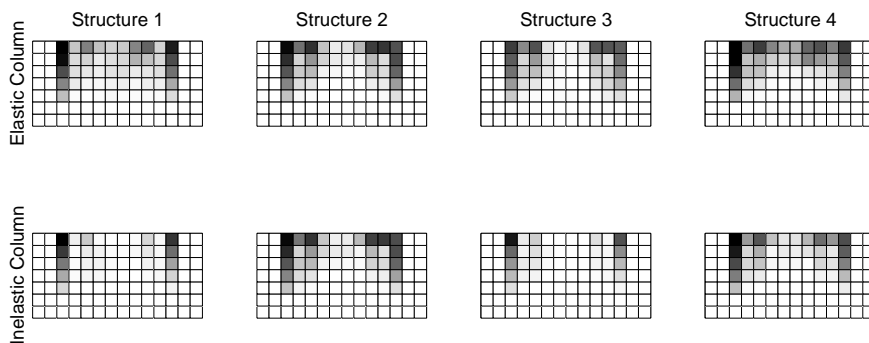


Figure 311.95: Fourier amplitude spectra of moments at the base of *nonlinear column*, SFSI-analysis

Figure 311.96: Average equivalent plastic strain at time  $t = 12$  sFigure 311.97: Average equivalent plastic strain at time  $t = 14$  s

- Elastic-plastic soil (Drucker-Prager with kinematic hardening)
- Nonlinear structure (bilinear material model)
- Ground motion applied through the Domain Reduction Method (DRM)
- Absorbing boundary of Lysmer type

### 311.7.2.1 Description of Model

The 3d model is based on the 2d model shown in Figure 311.86. In y-direction 6 more slices of  $7 \times 14$  elements are added (Figure 311.98). The x-z plane at  $y = 0$  represents a plane of symmetry. Lysmer boundaries are attached to all outside boundaries with the exception of the plane of symmetry and the soil surface. The main difference to the 2d model is that 3d wave propagation is possible which leads to higher radiation damping.

The structure was chosen to have the same geometric and material properties as Structure 4 in the previous section.

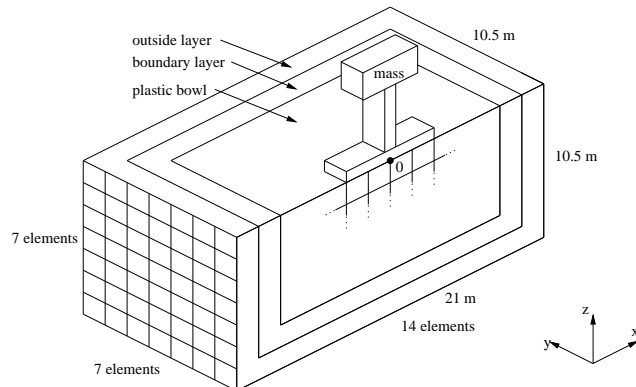


Figure 311.98: The full 3d-model

### 311.7.2.2 Results

Some results of the 3d-analysis together with the corresponding data of the 2d analysis are presented in Figure 311.99. Due to limited memory only the first 20 seconds of the time history were processed. A more efficient implementation of the application of effective forces for the DRM-method inside the finite element code should solve this problem. The analysis took 66 hours to finish.

The displacements obtained at the top of the structure as well as the moments at its base are very close to the results of the 2d-analysis. This shows that the analysis provides reliable results for a full 3d nonlinear SFSI problem. The amplitude of the base moment is at several instances larger for the 3d-model than for the 2d-model. This can be explained with the fact that more energy is present in the 3d-model whereas the energy the structure can absorb is the same as in the 2d-model. Also it is obvious that the natural frequencies of the 3d-model are not exactly the same as for the 2d-model and therefore changes the dynamic behavior in a way that is almost impossible to predict beforehand.

Because of the simple geometry of the problem the 2d-model is absolutely sufficient for analyzing the forces acting on the structure. If one is interested in the stress history in the soil surrounding the footing then the 3d-model can provide valuable additional information.

. . .

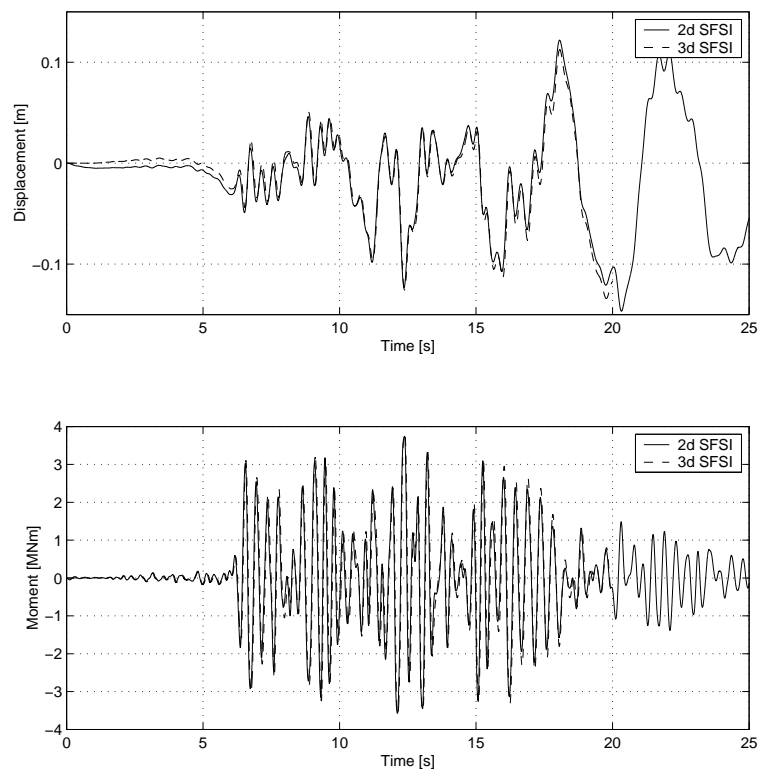


Figure 311.99: Top: Displacements at the top of Structure 4, Bottom: Moments at the base of Structure 4

## 311.8 Lotung Large Scale Seismic Test (LLSST) Earthquake 07

### 311.8.1 Introduction

Figure 311.100 shows the G/Gmax and Damping data used for Pisano model.

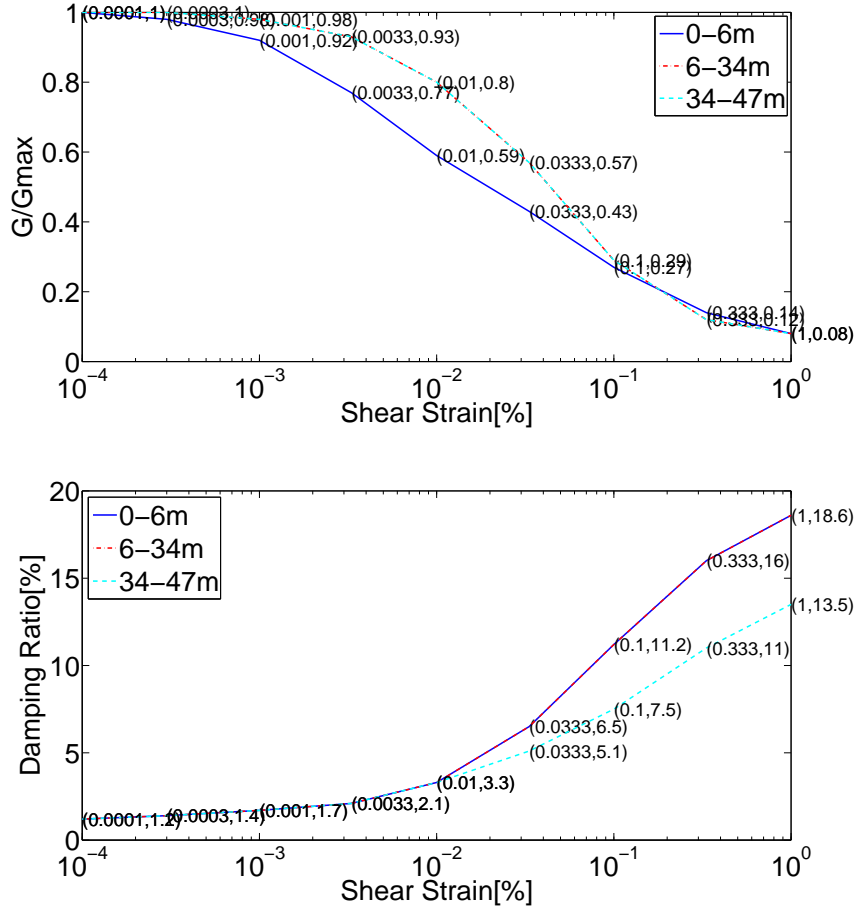


Figure 311.100: G/Gmax and Damping Curves

### 311.8.2 Input motion and input method

We use the data from Lotung Large Scale Seismic Test (LLSST) which is operated by TaiPower and IES during the period from 1985 to 1990. We choose event 07 to verify our modeling. Seismic motion data is available for download [HERE](#).

### 311.8.3 Results

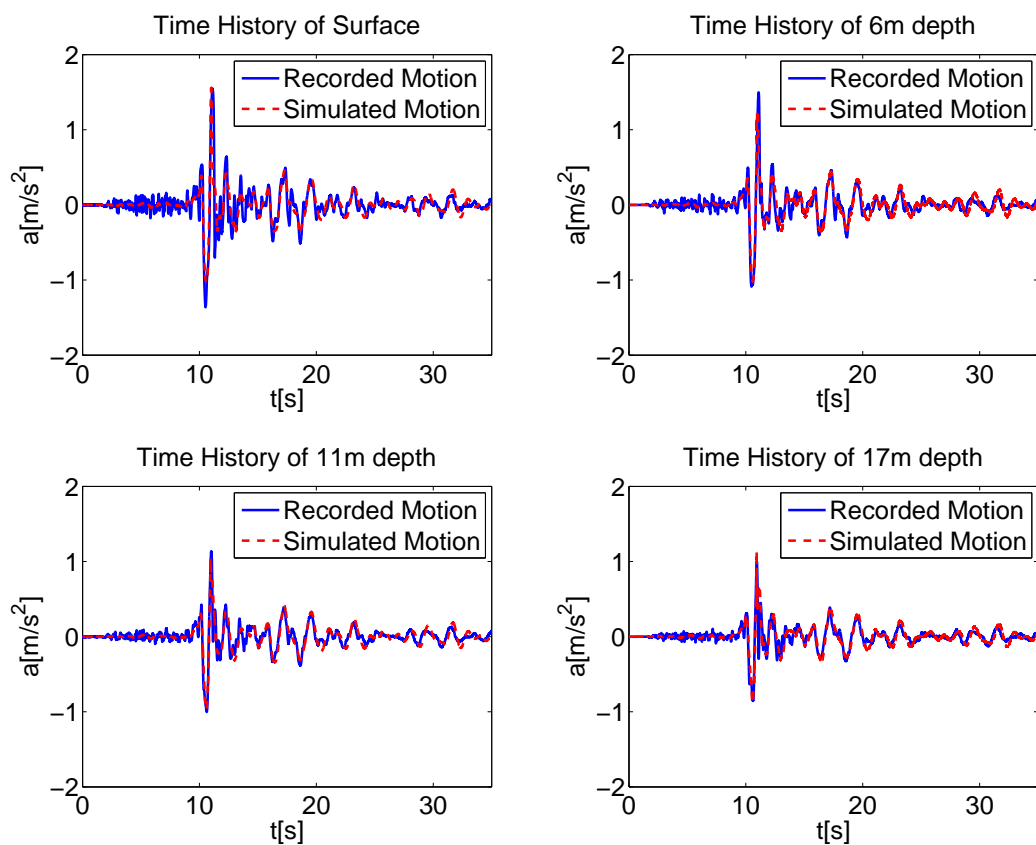


Figure 311.101: Time history comparison at different depths

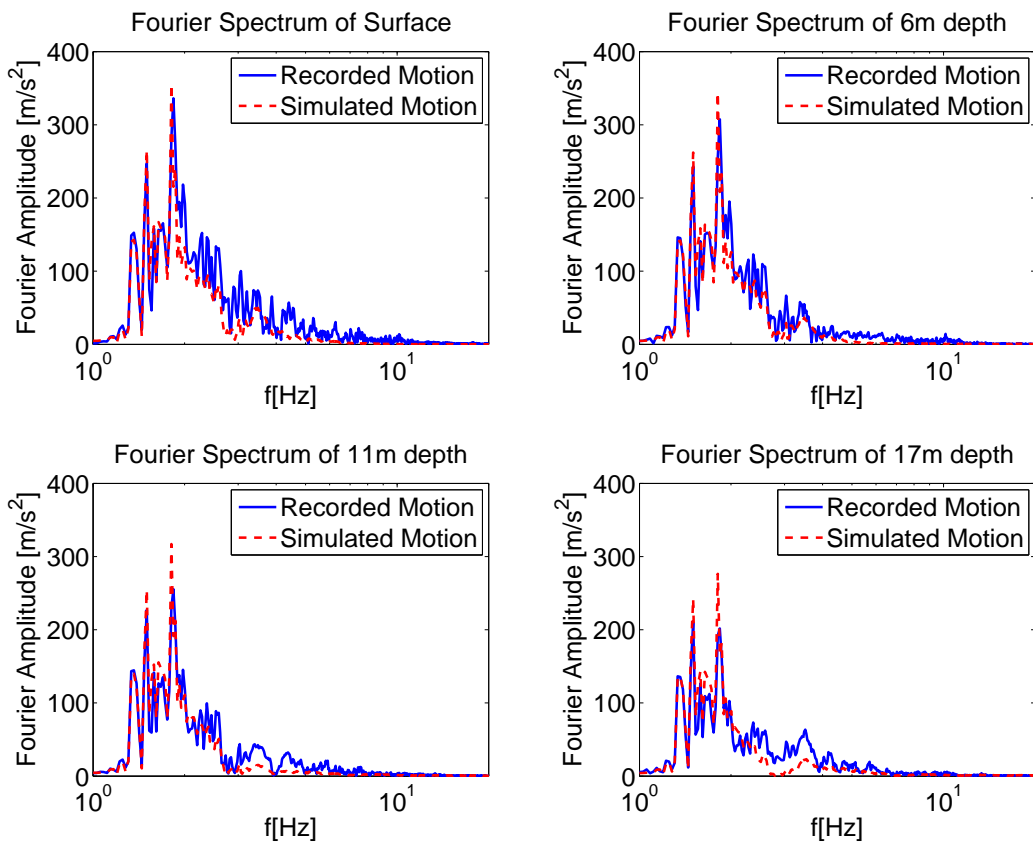


Figure 311.102: Fourier spectrum comparison at different depths

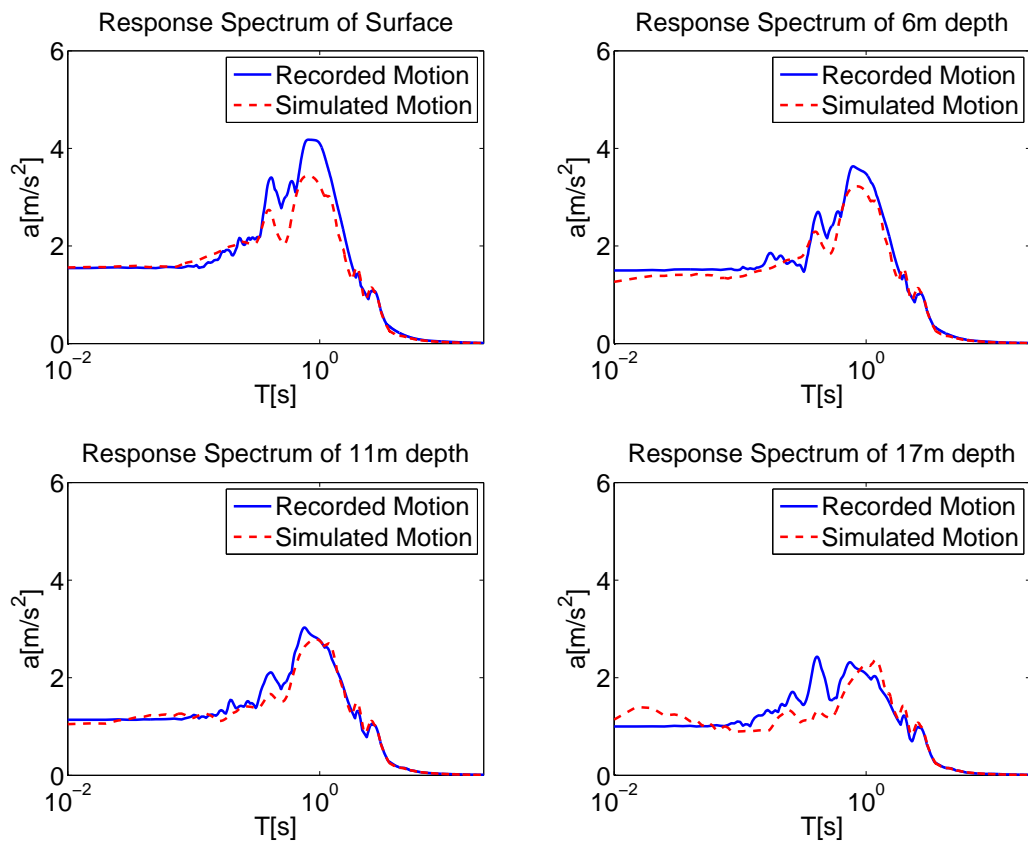


Figure 311.103: Response spectrum comparison at different depths (damping ratio 5%)

## Chapter 312

# Verification and Validation for Static and Dynamic Behavior of Soil-Structure-Interaction

(2012-2017-2018-2019-2021-)

(In collaboration with Dr. Nima Tafazzoli, Dr. Yuan Feng, Prof. Han Yang, and Dr. Hexiang Wang)

## 312.1 Chapter Summary and Highlights

## 312.2 Solid-Beam Model-Comparison of Real-ESSI eigen frequencies with ANSYS and Sofistik

Figure 312.1 and Table 312.1

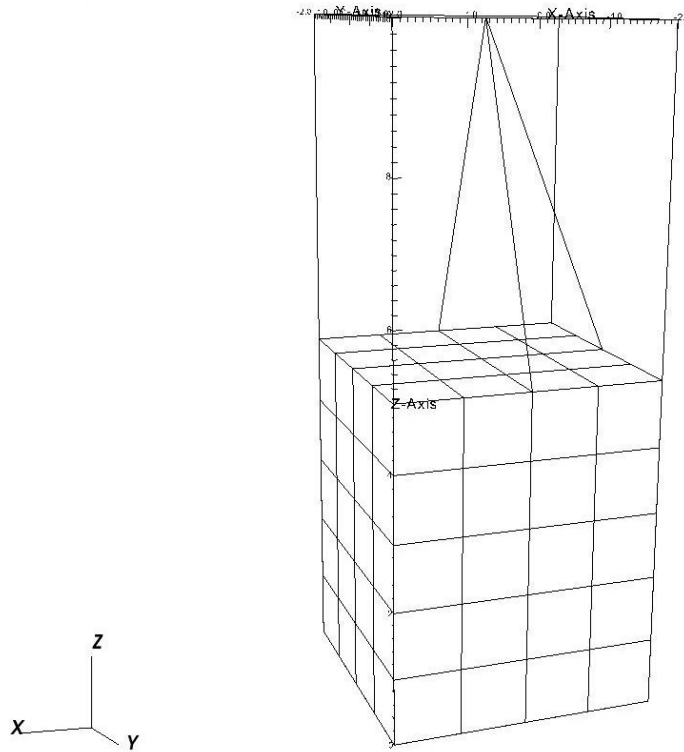


Figure 312.1: Finite element model

Table 312.1: Comparison of eigen frequencies obtained from Real-ESSI, ANSYS, and Sofistik

Mode	Real-ESSI (Hz)	ANSYS (Hz)	Sofistik (Hz)
1	5.4887	5.3868	5.439
2	7.1729	7.0711	7.311
3	12.6907	12.4670	12.751
4	13.197	13.1137	15.688

### 312.3 Solid-Beam Model-Comparison of model responses using elastic beams with 12dofs and 9dofs

#### 312.3.1 FEM Model

Figure 312.2

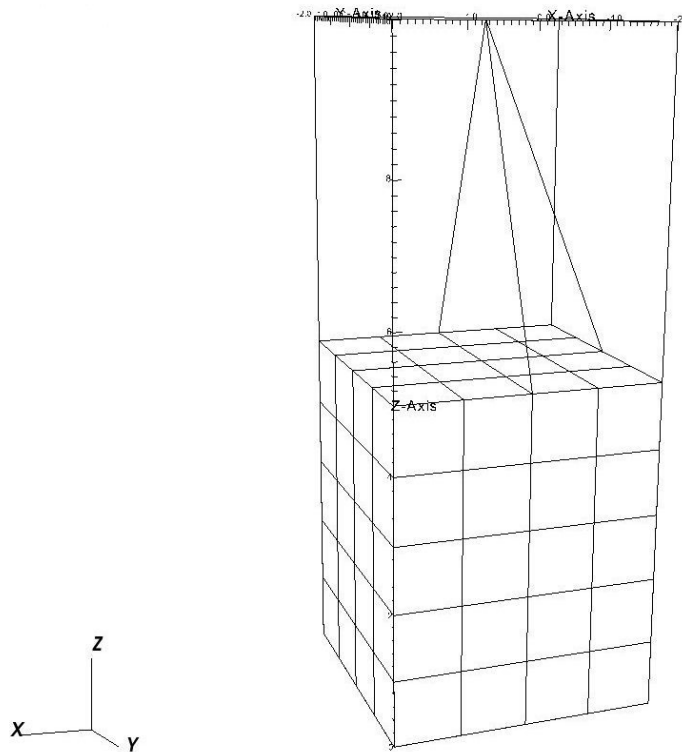


Figure 312.2: Finite element model

#### 312.3.2 Static Analysis

Figure 312.3

#### 312.3.3 Dynamic Analysis-Applying Force

Figures 312.4 and 312.5

#### 312.3.4 Dynamic Analysis-Applying Displacement

Figures 312.6 and 312.7 and 312.8

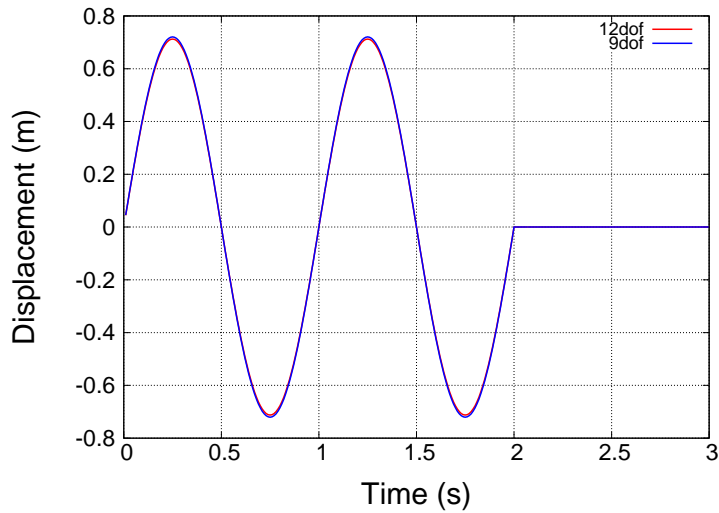


Figure 312.3: Comparison of static displacements (pseudo time) of the top nodes, Force time history applied to the top node

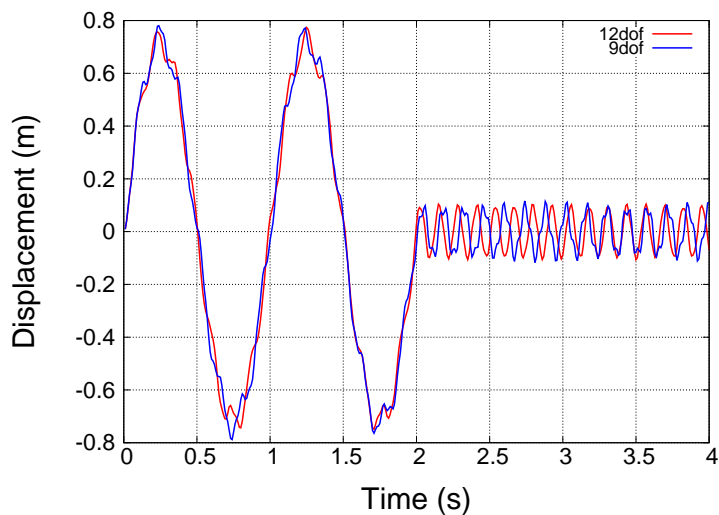


Figure 312.4: Comparison of displacement time histories of top node, Force time history applied to the top node, mass comes from the lumped mass added to the top node as well as the beams density

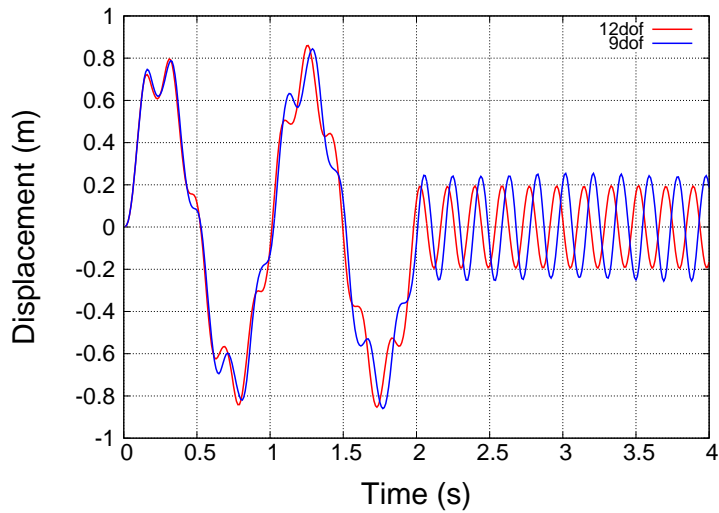


Figure 312.5: Comparison of displacement time histories of top node, Force time history applied to the top node, mass comes only from the beams density

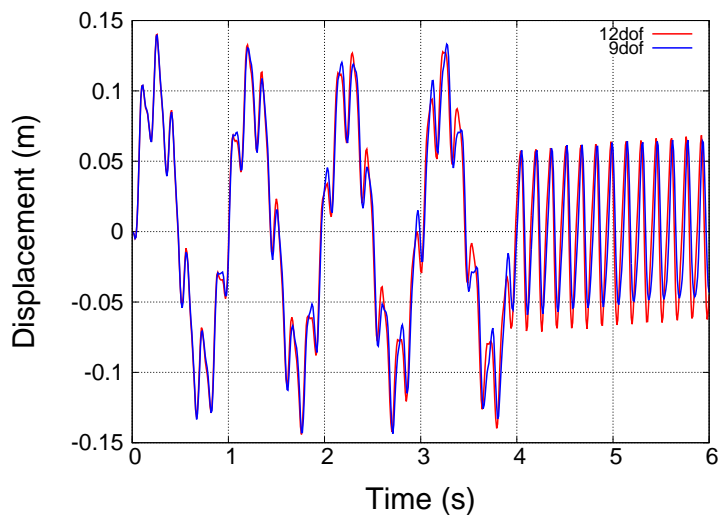


Figure 312.6: Comparison of displacement time histories of top node, Displacement time history applied at the bottom, mass comes only from the lumped mass added to the top

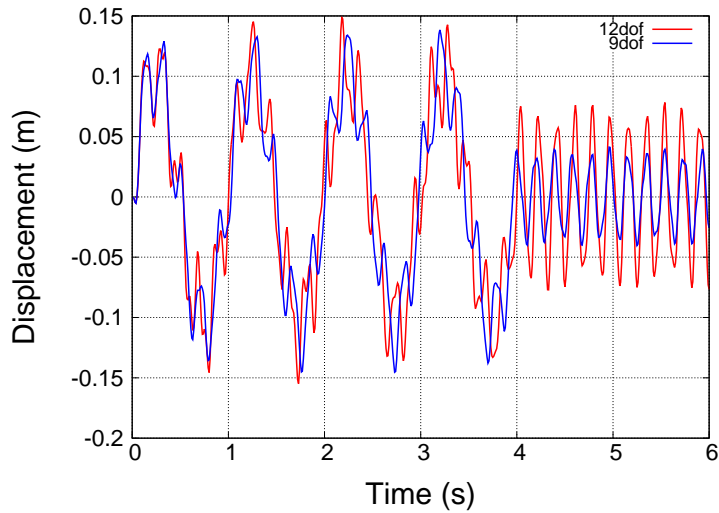


Figure 312.7: Comparison of displacement time histories of top node, Displacement time history applied at the bottom, mass comes from the lumped mass added to the top node as well as the beams density

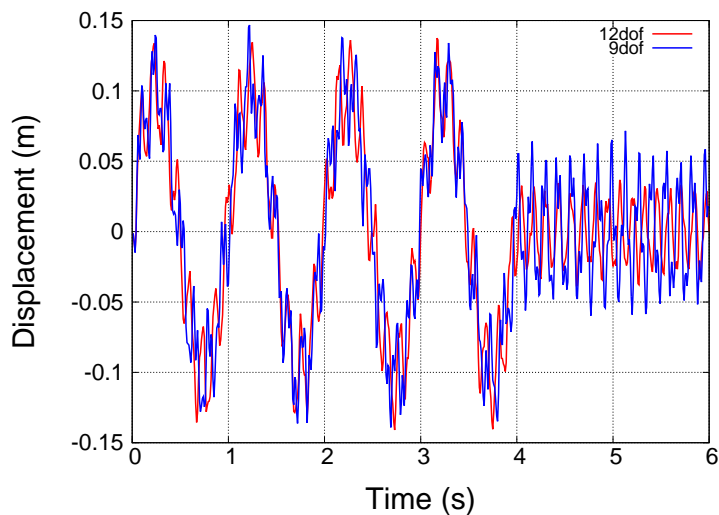


Figure 312.8: Comparison of displacement time histories of top node, Displacement time history applied at the bottom, mass comes only from the beams density

312.3.5 Comparison of eigen frequencies between models of using 9dof beam and 12dof beam

Table 312.2

Table 312.2: Comparison of eigen frequencies

Mode	9dof	12 dof
1	5.253	5.412
2	6.867	7.112
3	9.399	12.570
4	11.60	13.183
5	11.76	13.479
6	12.95	14.605
7	15.97	15.998
8	18.85	19.101
9	25.27	21.378

312.3.6 Eigen modes of model using 12dof beam

Figures 312.9 and 312.10 and 312.11 and 312.12 and 312.13

312.3.7 Eigen Modes of model using 9dof beam

Figures 312.14 and 312.15 and 312.16 and 312.17 and 312.18

## 312.4 Validation Using UNR Soil Box Test Setup

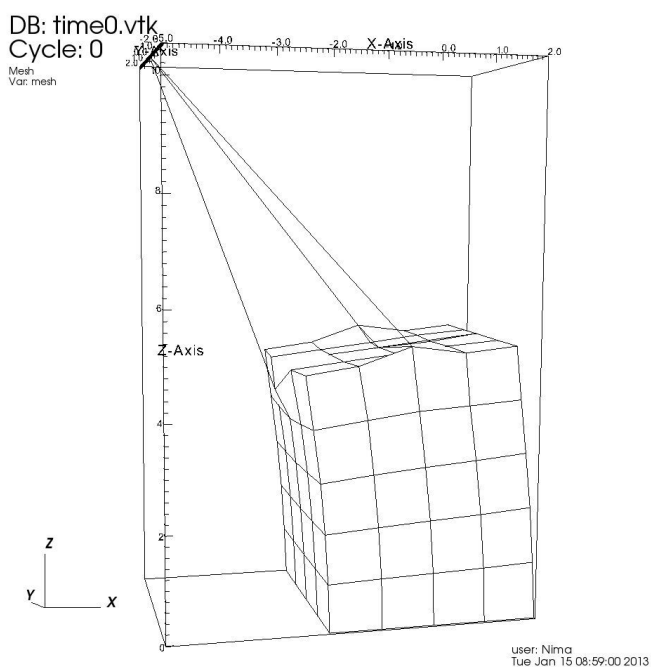


Figure 312.9: Mode 1

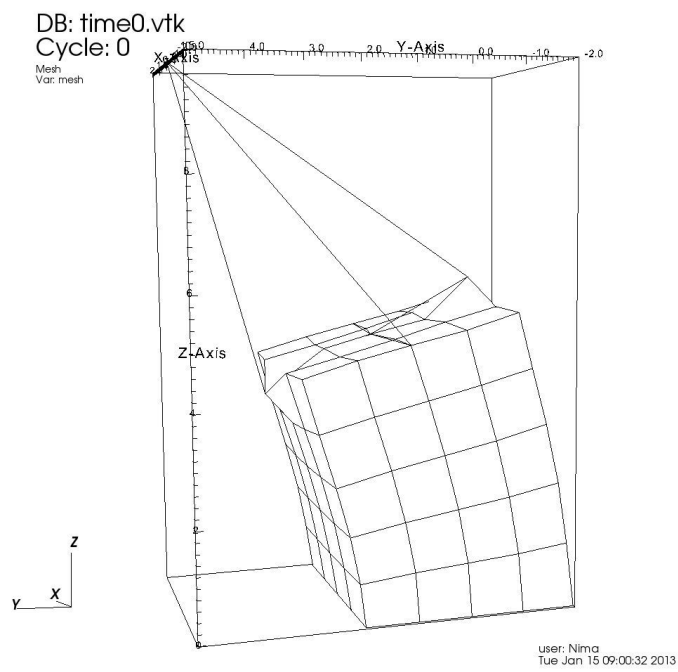


Figure 312.10: Mode 2

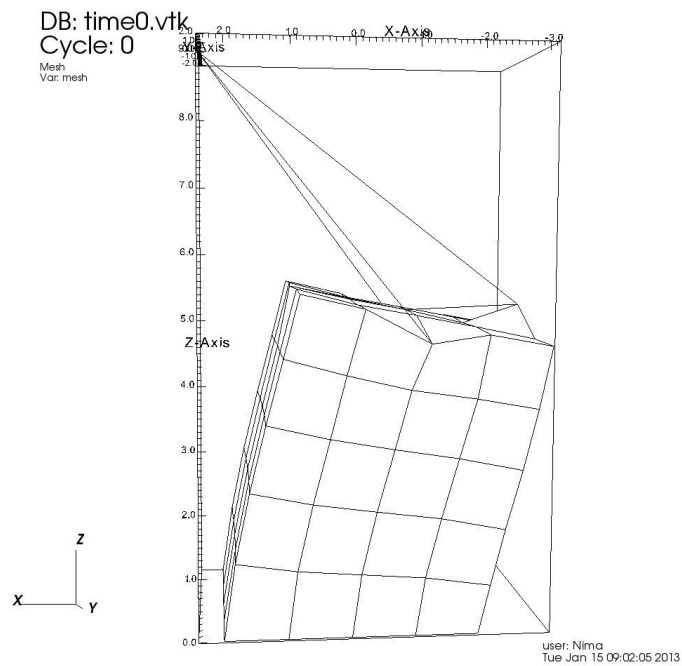


Figure 312.11: Mode 3

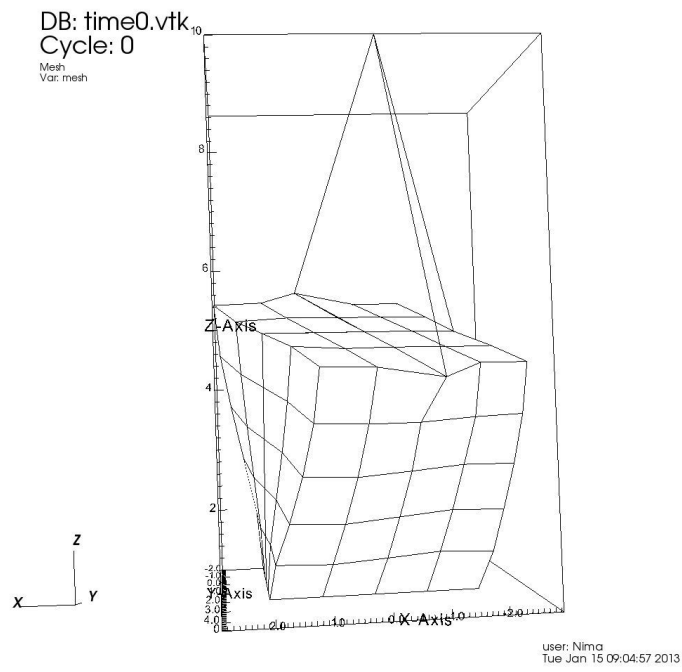


Figure 312.12: Mode 4

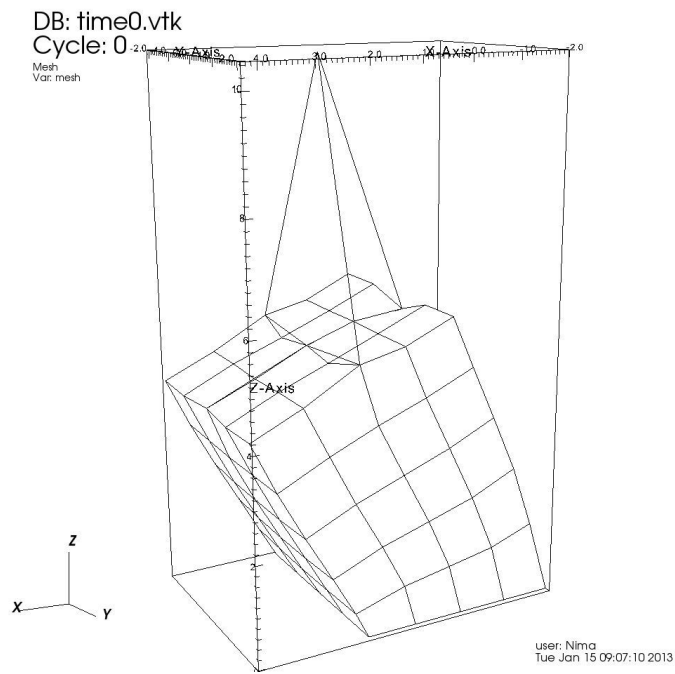


Figure 312.13: Mode 5

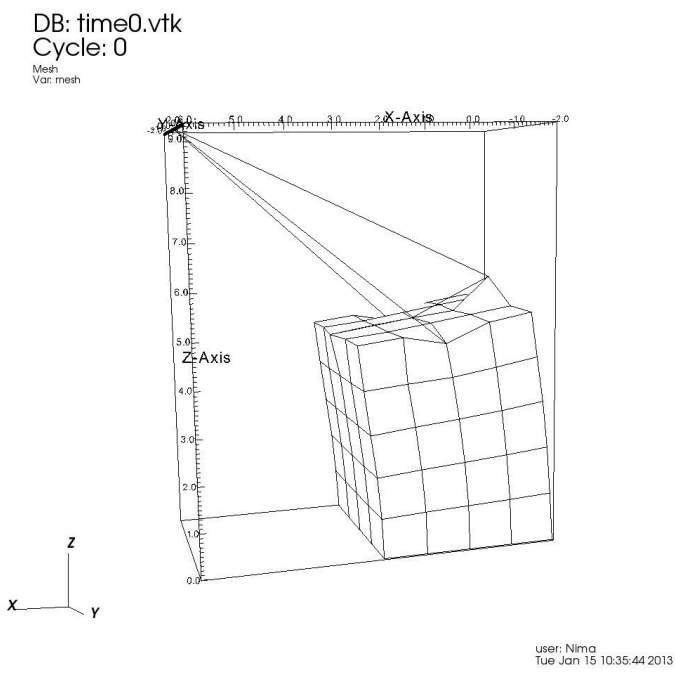


Figure 312.14: Mode 1

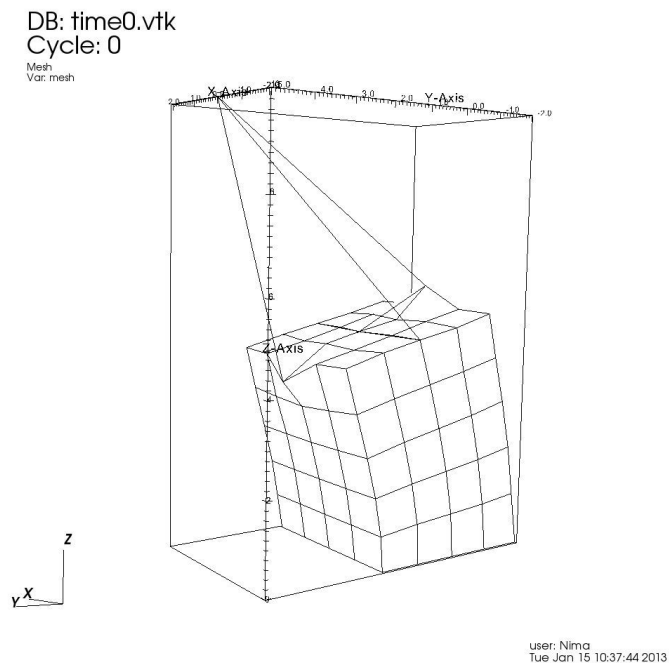


Figure 312.15: Mode 2

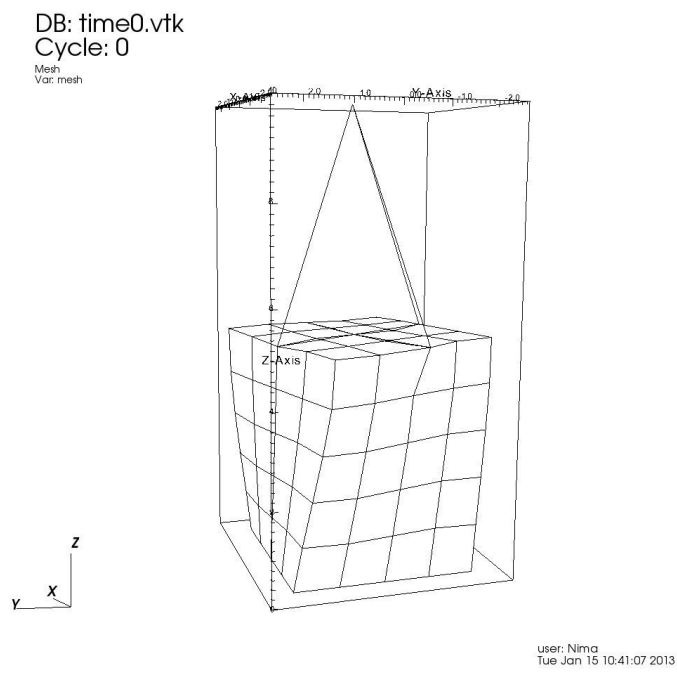


Figure 312.16: Mode 3

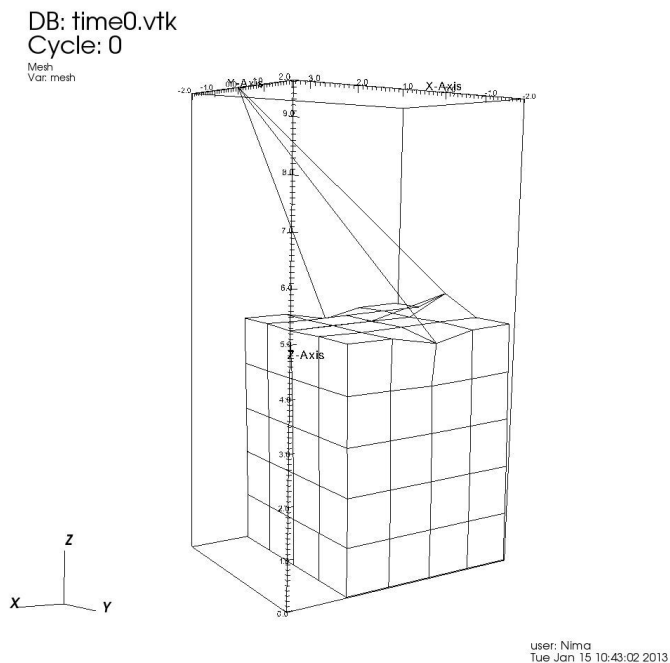


Figure 312.17: Mode 4

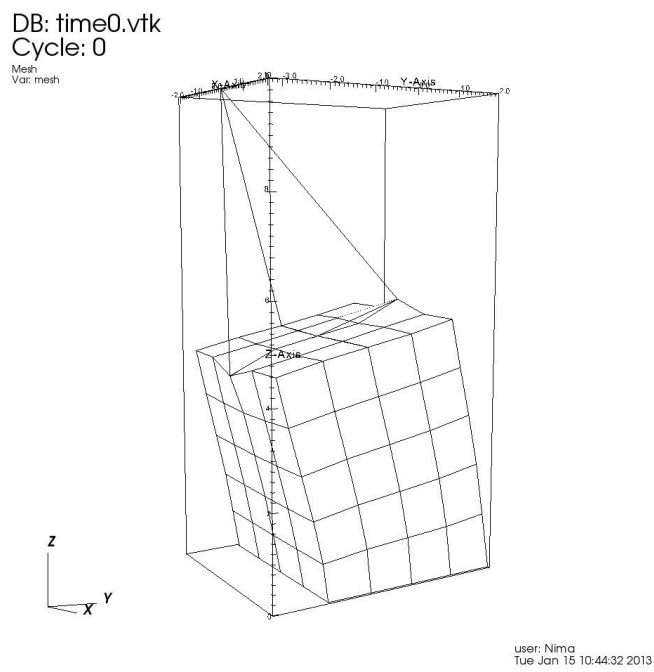


Figure 312.18: Mode 5

Chapter 313

# Verification and Validation for Dynamic Solid-Fluid Interaction

(2017-2018-2019-2020-2021-)

(In collaboration with Dr. Hexiang Wang)

## 313.1 Chapter Summary and Highlights

## 313.2 V&V Examples

### 313.2.1 Box sloshing

A numerical example of earthquake-driven box sloshing is provided here. The initial configuration is shown in figure 313.1. The length of the box is 30 meters and the height is 10 meters. The thickness is 3 meters filled with 8-meter-deep water. The box is shaken by a uniform 1D horizontal excitation plotted in figure 313.2. The box is modeled with elastic material with  $E = 12GPa$ ,  $\mu = 0.2$ .

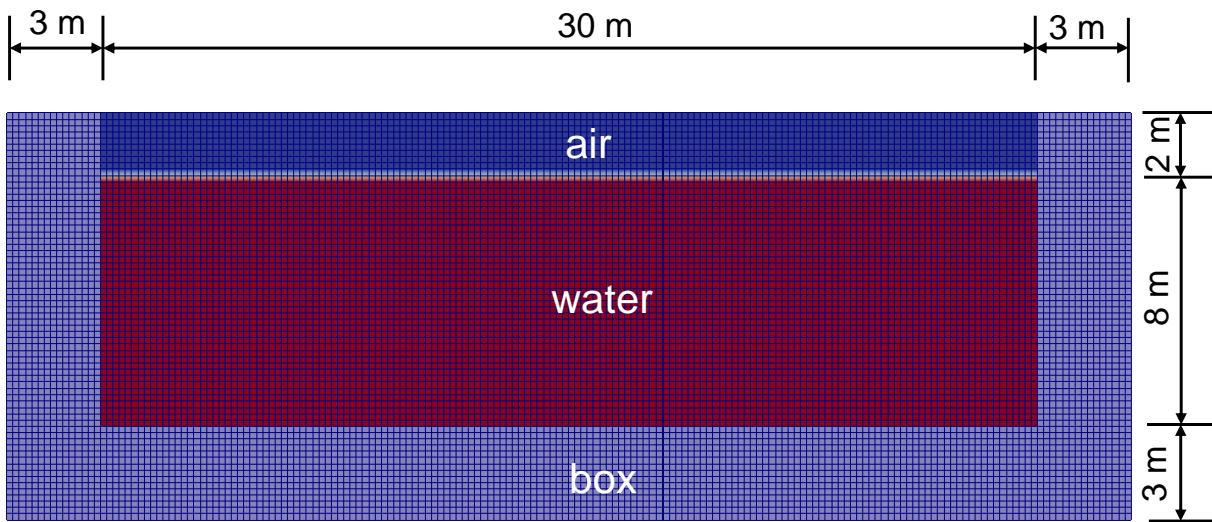


Figure 313.1: Model configuration of 2D sloshing box

The simulation result can be seen in figure 313.3. Clearly, elevations of free water surface can be observed under the excitation.

Another sloshing box example is driven by falling water flow. Figure 313.4(a) shows the result where solid domain and fluid domain has totally compatible mesh size (mesh size ratio 1:1). As mentioned before, VOF method has high requirement for the mesh size. In order to get accurate enough result with limited computation resources, refined mesh in the fluid domain is usually required for soil-structure-fluid interaction analysis. Analysis of model with discontinuous mesh is supported here through generalized interpolation scheme. Figure 313.4(b) shows the result of refined finite volume mesh in fluid domain (mesh size ratio 1:3).

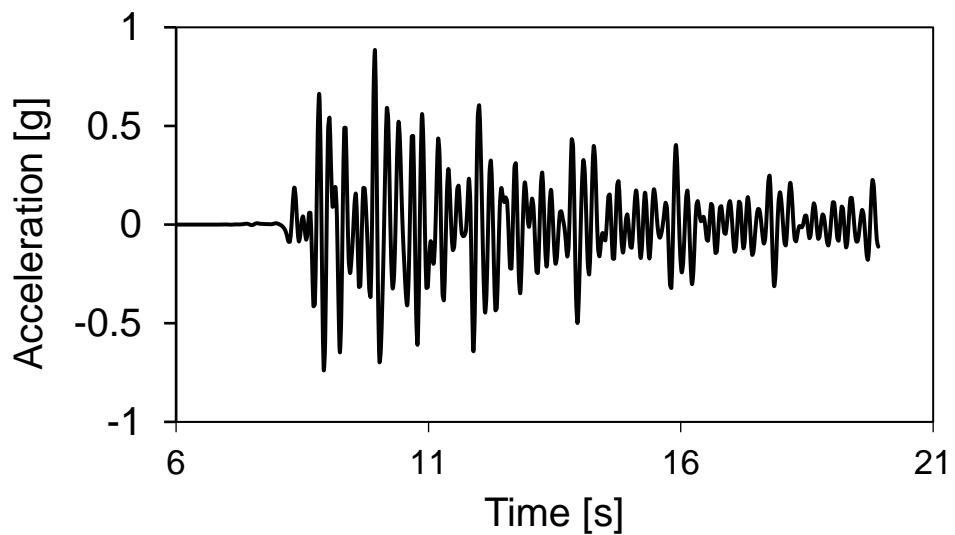


Figure 313.2: Time history of 1D excitation

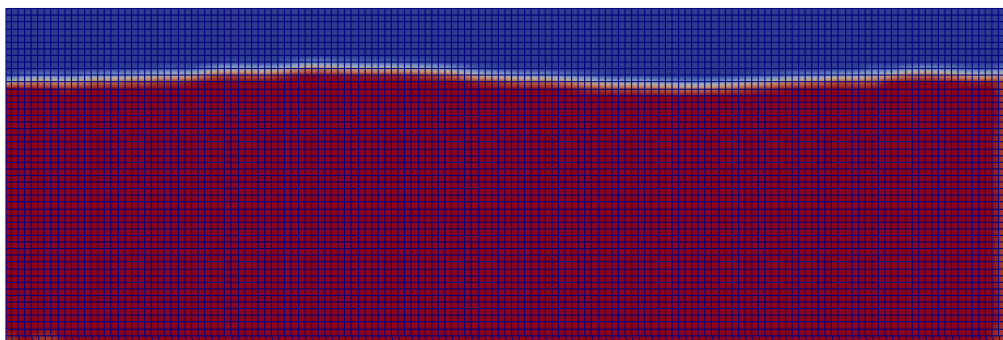


Figure 313.3: Simulation result of 2D sloshing box

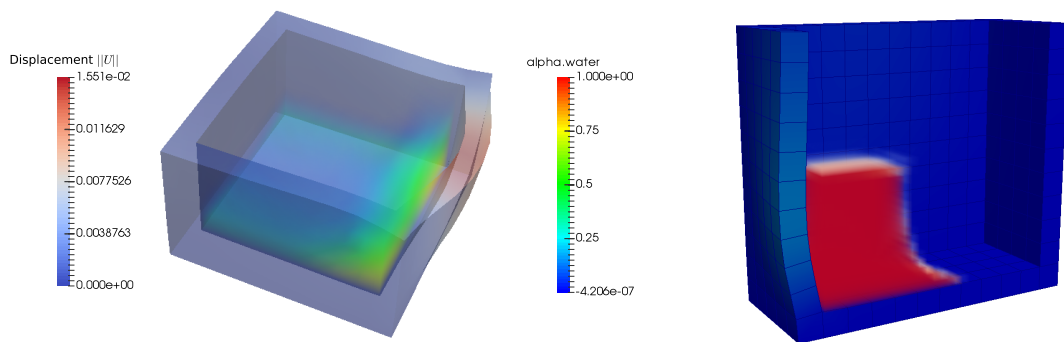


Figure 313.4: Box sloshing under falling water

### 313.2.2 Dam Break

## 313.3 Verification & Validation

Verification and validation is crucially important to guarantee the accuracy of simulation result. Verification and validation (V & V) procedure of SFI problem involve three aspects: V & V for response of solid domain (i.e. V & V for ReaLESSI as a solver for solid mechanics), V & V for response of fluid domain (i.e. V & V for OpenFOAM as a solver for free surface flow) and V & V for SFI (i.e. V & V for interaction between solid domain and fluid domain).

Since ReaLESSI developed by [Jeremić et al. \(1988-2025\)](#) has rigorous V & V procedure, the focus here is on V & V of OpenFOAM and SFI.

### 313.3.1 Free Surface Flow validation

The functionality of OpenFOAM as a solver for free surface flow is validated in this section. A numerical validation test is conducted based on the experiments reported by [Martin and Moyce \(1952\)](#).

A rectangular column of water, in hydrostatic equilibrium, is confined between two vertical walls, as shown in figure 313.5. The water column is 1 unit wide and 2 unit high. At the beginning of the calculation, the right wall (dam) is removed and water is allowed to flow out along a dry horizontal floor.

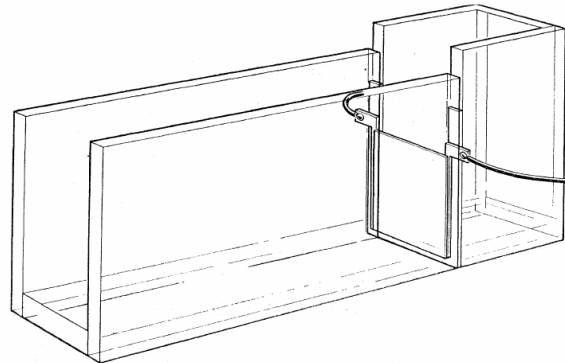


Figure 313.5: Experiment set up by [\]Martin and Moyce \(1952\)](#)

The real-time position of the leading edge of the water is recorded during the experiment. This is a good test problem because it has simple boundary conditions and a simple initial configuration. 2D numerical models with two different types of mesh size ( $\Delta x = 0.1m$  and  $\Delta x = 0.05m$ ) are built (figure 313.6).

The comparison result between numerical solution, experiment result and benchmark solution by [Hirt and Nichols \(1981\)](#) is presented in figure 313.7.

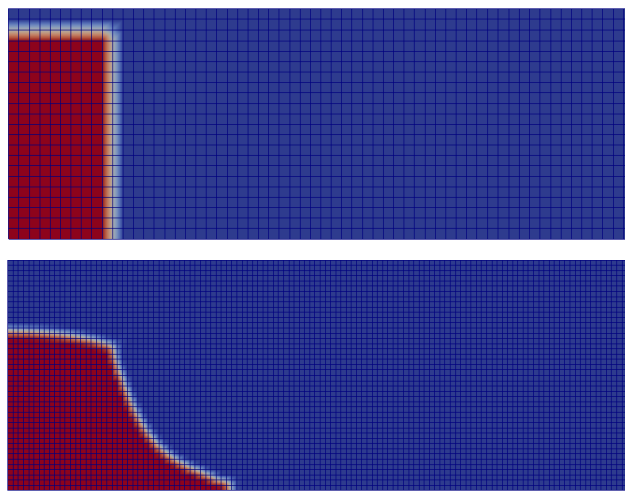


Figure 313.6: Numerical model for validation of free surface flow

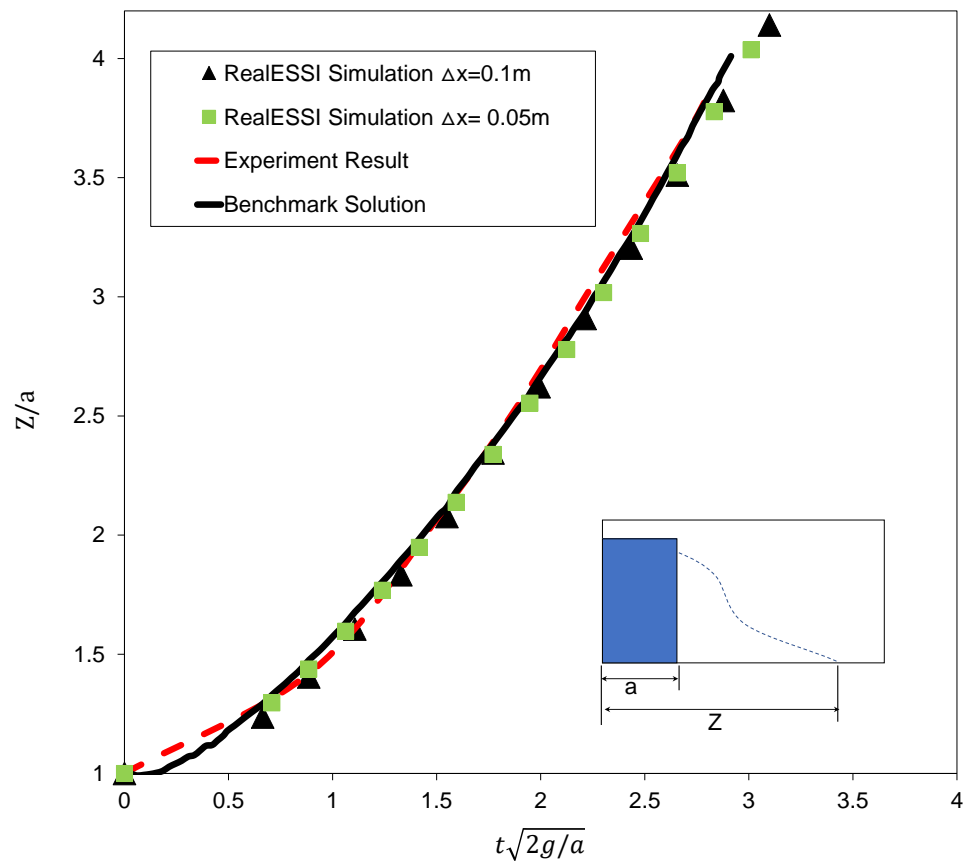


Figure 313.7: Validation result of free surface flow

It can be seen that numerical simulation matches well with both experiment result and benchmark solution. OpenFOAM, as a finite volume solver for free surface flow based on VOF method, is reliable.

### 313.3.2 Mass conservation verification

As mentioned in section 111.4.6, for a closed fluid system, mass conservation should be strictly satisfied. The total volume of fluid in the system can be calculated with equation 313.1.

$$V_{total} = \sum_{i=1}^n \alpha_i V_i \quad (313.1)$$

The time history record of total volume in the numerical example (section 313.2.1) is given in figure 313.8. It can be seen that the total volume remains almost constant during the simulation of SFI. In this example, after 400 time steps, the relative mass change is only 0.25%, which demonstrates that our coupling program has excellent performance regarding mass conservation.

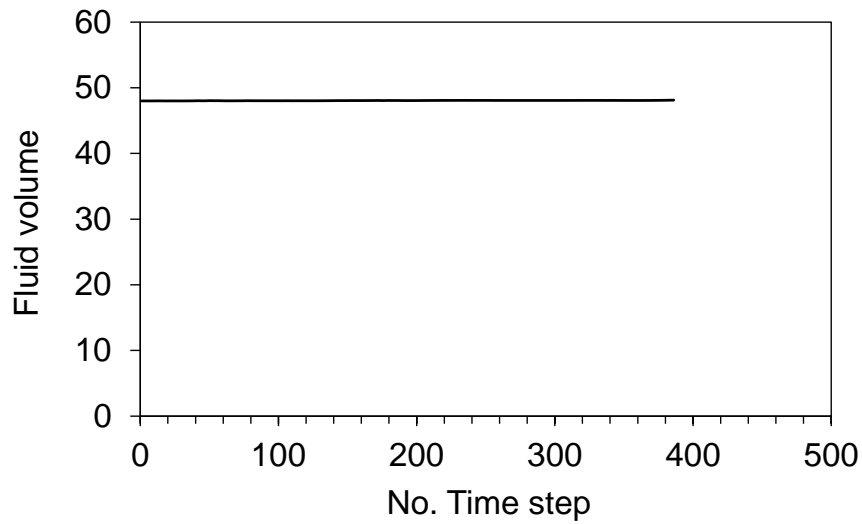


Figure 313.8: Time history record of total fluid volume

### 313.3.3 SFI Verification & Validation

A box sloshing numerical experiment (rectangular tank under sway oscillations  $X(t) = A\sin(\omega t)$ ) is taken as the verification and validation test for solid fluid interaction. The box is 1.0 m long ( $L$ ) and 0.8 m height ( $H$ ). The depth ( $D$ ) of submerged water is 0.5 m. The natural frequency of the tank can be calculated according to Lamb (1932):

$$\omega_i = \sqrt{g \frac{\pi i}{L} \tanh(\frac{\pi i}{L} D)} \quad i = 1, 2, 3, \dots \quad (313.2)$$

where  $\omega_i$  is the natural frequency, and  $g$  is gravitational acceleration. The lowest linear mode  $\omega_1$  is of primary importance for the tank sloshing phenomenon.

Based on the original analytical solution of Linton and McIver (2001), Jin et al. (2014) gives the equation for non-dimensional free surface elevation  $\eta_{max}/A$  as shown in equation 313.3, where  $b = L/2$ ,  $\mu_m = (m + 0.5)\pi/b$ ,  $K_m = \mu_m \tanh \lambda_m D$ ,  $K = \omega^2/g$ .

$$\frac{\eta_{max}}{A} = \frac{\omega}{gA} |A\omega b + \sum_{m=0}^{\infty} \left| \frac{2K}{\mu_m^2 b(K_m - K)} \right| | \quad (313.3)$$

Jin et al. (2014) also conducted a 2D sloshing experiment and report detailed response of free surface elevation under different excitation magnitude  $A$  and frequency  $\omega$ . Here  $A$  is fixed as 2.5 mm and different frequency values ( $\omega/\omega_1 = 0.5 \sim 2$ ) are adopted to implement verification and validation numerical test. The initial setup of numerical experiment can be seen in figure 313.9(a). Figure 313.9(b) and figure 313.9(c) are the sloshing response under excitation of first-mode ( $\omega/\omega_1 = 1$ ) and third-mode ( $\omega/\omega_3 = 1.793$ ) resonance frequency.

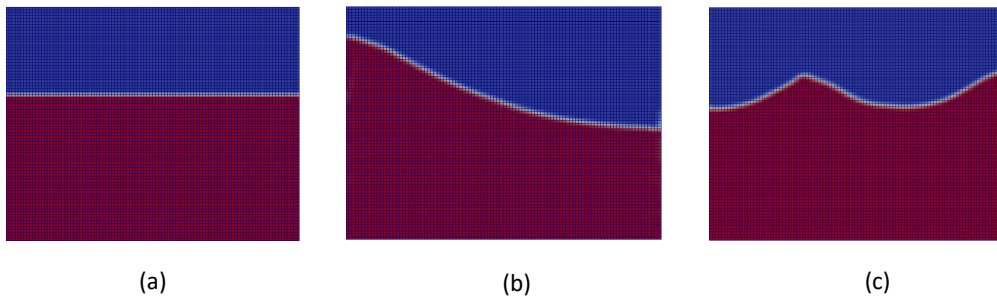


Figure 313.9: Numerical experiment of solid fluid interaction: (a) Initial setup (b) Sloshing response under first-mode resonance excitation (c) Sloshing response under third-mode resonance excitation

Compared with experiment record (figure 313.10) by Jin et al. (2014), it can be seen that the mode shape from our numerical simulation is same as the experimental observations.

The numerical results of  $\eta_{max}/A$  are also plotted into the same figure as theoretical predication and experiment record, as shown in figure 313.11. Very good agreement can be observed, especially between numerical simulation and experiment result. This manifests that suitable mathematical equations about SFI has been numerically solved in a correct way. The SFI coupling implementation in RealESSI is reliable.

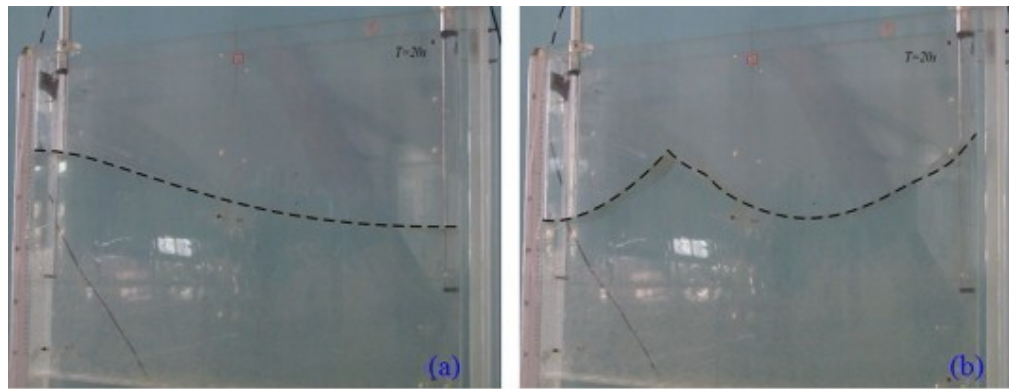


Figure 313.10: Resonant wave shape: (a) First-order mode (b) Third-order mode reproduced from Jin et al. (2014)

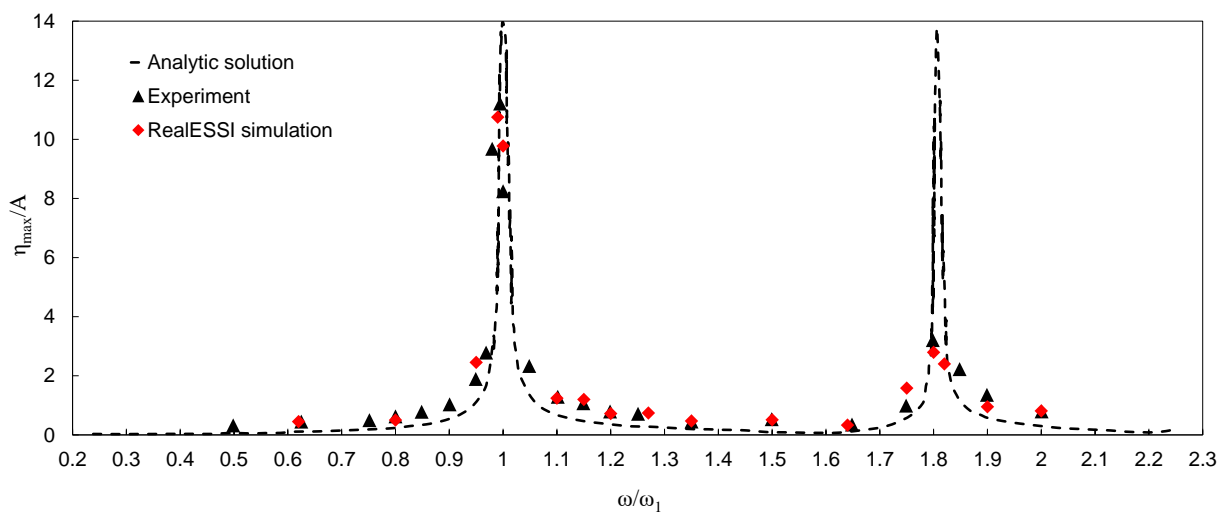


Figure 313.11: Comparison among theoretical prediction, experiment observation and numerical simulation

Chapter 314

# Quality Management System

(2002-2005-2018-2019-2020-2021-)

## 314.1 Chapter Summary and Highlights

## 314.2 Reasoning Behind this Activity

Quality assurance for a numerical modeling system is of highest importance. A good, sound Quality Management System is therefore very important. This section provides details of quality management system used for the development and quality assurance (QA) for the Real-ESSI Simulator system ([Jeremić et al., 1988-2025](#)).

## 314.3 Real-ESSI Simulator System Quality Management System, based on ISO/IEC/IEEE 90003 Standard

This section is based on [ISO/IEC/IEEE 90003 Developers et al. \(2018\)](#). ISO/IEC/IEEE 9003 is a standard developed by the International Organization for Standardization (ISO), International Electrotechnical Commission (IEC), and Institute of Electrical and Electronics Engineers (IEEE), as a guidance for the application of ISO 9001:2015 standard to the acquisition, supply, development, operation and maintenance of computer software and related support services.

### 314.3.1 Real-ESSI Simulator Developer Organization

#### 314.3.1.1 Internal Issues

Internal issues that are relevant to the Real-ESSI Simulator quality management system:

- legal
- Technological
- Competitive
- Market
- Cultural
- Social
- Economic environment, local, national, international

#### 314.3.1.2 Internal Issues

External issues that are relevant to the Real-ESSI Simulator quality management system:

- Values
- Culture
- Knowledge
- Performance

### 314.3.1.3 External and Internal Issues for the Real-ESSI Simulator

External and Internal issues for the Real-ESSI Simulator can include:

- Use of "cloud" services, that is beneficial for ease of access and business continuity, however needs research to ensure lowering all beneficial effects. The Real-ESSI Simulator is fully deployed on Amazon Web Services (AWS), and is tightly managed by development group as well as ESSI Consultants. AWS was chosen after in depth examining other cloud services, namely Google cloud, that actually provided no dedicated tightly parallel computers as of 2018, Microsoft Azure, that was fast but very expensive, and local parallel cloud, Real-ESSI Parallel Computer, that works well for developers, but requires much management for outside users.
- Use of personal computers, laptops, can create a problem in managing safety and security of Real-ESSI Simulator sources. Developers are aware of this issue and have agreed to do tight safety and security and have signed a licensing agreement that commits them to managing such safety and security.
- Risk of external attack on developers computers and network and on Real-ESSI Simulator deployed computers is controlled by regular, up to date Linux and AWS security.
- Delivery of the Real-ESSI Simulator is mostly handled through AWS, while there are a number of examples of remote deployment, whereby remote users commit fully utilizing and following the Real-ESSI Simulator quality management system.
- Legal and operational issues for Real-ESSI Simulator use in context of safety, security and mission assurance.

### 314.3.1.4 Needs and expectations of Interested Parties

Interested parties that are relevant to Quality Management System and their requirements

- Customers, professional practice companies, require working system, that is efficient, easy to use and that can provide more optimal, more economic and more safe designs than what is currently available.
- Partners, collaborators, require in depth knowledge of the system, possibility to influence changes and additions to the Real-ESSI Simulator
- Staff, require stable and nourishing research and development environment

- DOE, not sure anymore?
- NRC, not sure anymore?
- UN-IAEA, ...
- Professional Practice: development of the system that improves design and assessment process, while maintaining practicality, achieving highly efficient, minimally disrupting training for use Real-ESSI
- Research Community: Contributions to modeling and simulations, and use of Real-ESSI to investigate new behavior of ESSI systems.
- Developers form the Real-ESSI Simulator group:
- Competitors:
  - SimCenter ?
  - French project?
  - Linear Elastic community, SASSI,
  - nonlinear FEM programs, LS-Dyna...

### 314.3.2 Scope of the Real-ESSI Simulator Quality Management System

Plan-do-Check-Act (PDCA) cycle

Risk-based thinking

Quality Management Principles

## 314.4 Real-ESSI Simulator System Quality Management System, based on ASME NQA-1 Standard

ASME Nuclear Quality Assurance (NQA-1) is a standard developed by the American Society of Mechanical Engineers (ASME) that provides quality assurance guidance and certification for organizations supplying items and services which provide a safety function for nuclear installations.

### 314.4.1 ASME NQA-1 for the Real-ESSI Simulator System

## Chapter 315

# Comparison with Other Programs

(2016-2017-2020-2021-)

(In collaboration with Dr. Nima Tafazzoli, and Dr. Yuan Feng)

## 315.1 Chapter Summary and Highlights

### 315.1.1 Reasoning Behind this Activity

I personally do not like or approve code to code comparison. If results between two codes are the same, this does not prove that any tested code is right. If results between two codes are different, which code is right?

However, a number of professionals and industry in general feel very comfortable with some usually used codes/programs. In this sense, we provide code comparison with select widely used codes, to satisfy professionals. If results turn out to be the same (impossible to have exactly same results, but say very close) that is good for all codes involved, as we have a full verification suit and guaranty our accuracy to within limits of verification tests we used. If results are different, we still claim accuracy, as we have full verification suit and guaranty our accuracy to within limits of verification tests we used.

## Part 400

# Education, Training and Modeling, Simulation Examples

## Chapter 401

# Ten Section Course on Nonlinear Finite Element Methods for Realistic Modeling and Simulation of Earthquakes, and Soils, and Structures, and their Interaction, Real-ESSI

(1998-2021-)

## 401.1 Delivery

---

Instructor: Boris Jeremić, email: [Jeremic@ucdavis.edu](mailto:Jeremic@ucdavis.edu)

Class meeting: two hour lecture/meetings, twice a week, flipped classroom method

Office hours: two hours, twice a week

Course delivery: live and recorded lectures, and live discussions

Course WWW: <http://sokocalo.engr.ucdavis.edu/~jeremic/Classes/ECI280A/>

---

## 401.2 Objectives

This course will provide students with state of the art finite element methods, numerical analysis tools and models for solving elastic–plastic problems in geotechnical and structural engineering. Focus is on analysis of Soils, Structures and their Interaction (SSI). Presented will be computational formulation, numerical techniques and models for static, nonlinear, elastic-plastic finite element methods that are used in professional practice and research. Both sequential and parallel computational approaches will be presented and used.

During this course students will:

- Learn about linear and nonlinear finite element modeling and simulation
- Select and calibrate nonlinear, elastic-plastic models for soil, rock, concrete, steel and interfaces
- Perform linear elastic and nonlinear, elastic-plastic analysis of solids and structures made of soil, rock, concrete, steel and their interfaces
- Perform elastic and nonlinear, inelastic analysis of soils-structure systems
- Become proficient in performing nonlinear analysis for soils, structures, interfaces, using different levels of sophistication, from simplified models to high fidelity elastic-plastic models of soil structure systems on sequential and parallel computers.

### Who Should Attend?

Students and practicing engineers who want to learn about and expand their knowledge of modeling and simulation for nonlinear/inelastic material behavior, for soils, rock, and structures,

## 401.3 Additional Information

Lecture Notes: <http://sokocalo.engr.ucdavis.edu/~jeremic/LectureNotes/>.

Recorded Lectures: <http://sokocalo.engr.ucdavis.edu/~jeremic/Online-Education/>.

Computers: Most of the problems in this course will require numerical simulations. A finite element modeling system called Real-ESSI Simulator (<http://real-essi.us>) is available for computers running Windows (through WSL), MacOS, Linux. Please refer to <http://real-essi.us> to find out how to use Real-ESSI on local computers or on AWS computers. Other programs can be used as well, as long as they provide modeling and simulation capabilities that are required for assignments, example problems and term project. Both sequential and parallel computers will be used.

Problems: Assigned weekly, students are expected to attempt to develop solutions. You are encouraged to discuss the approach to problem solutions with other students in the course as well as with the instructor.

Examples: Model development, finite element models, finite element mesh, boundary conditions, material models, loads, model verification process, linear and nonlinear elastic FEM with solids and structural elements,

There are a large number of examples available at the Real-ESSI Simulator web site:

<http://real-essi.info/>, or <http://real-essi.us/>, in these documents:

- Real-ESSI Simulator Examples Collection
- Real-ESSI Simulator Short Course Examples Collection

Term Project: Term project will involve work related to developing or using numerical models for numerically simulating elastic–plastic problem of your choice, related to your interests. Term projects will be presented at the end of quarter.

Grading: TBD

Examination: TBD

Literature:

- The Finite Element Method, *Olgierd Cecil Zienkiewicz and Robert L. Taylor*, McGraw-Hill Book Company, Volumes 1 and 2, ISBN 0-07-084175-6
- Non - Linear Finite Element Analysis of Solids and Structures Volume 1: Essentials, *Crisfield, M. A.*, John Wiley and Sons, Inc. New York, 1991 , ISBN 0 471 92956 5 v.1
- Finite Element Procedures in Engineering Analysis, *Klaus-Juergen Bathe*, Prentice Hall, ISBN 0-13-301458-4

- Constitutive Laws for Engineering Materials With Emphasis on Geologic Materials *Chandakant S. Desai and Hema J. Siriwardane*, Prentice-Hall, Inc. Englewood Cliffs, NJ 07632, ISBN 0-13-167940-6
- Plasticity for Structural Engineers *W. F. Chen and D. J. Han*, Springer Verlag, 1988 ISBN 0-387-96711-7
- Boris Jeremić, Zhaojun Yang, Zhao Cheng, Guanzhou Jie, Nima Tafazzoli, Matthias Preisig, Panagiota Tasiopoulou, Federico Pisano, Jose Abell, Kohei Watanabe, Yuan Feng, Sumeet Kumar Sinha, Fatemah Behbehani, Han Yang, and Hexiang Wang. Nonlinear Finite Elements: Modeling and Simulation of Earthquakes, Soils, Structures and their Interaction. University of California, Davis, CA, USA, 1989-2022. ISBN: 978-0-692-19875-9

## 401.4 Teaching Plan, Topics

#### 401.4.1 Section I, Introduction

Introduction: Course objectives, methodology, computer modeling and simulation

Modeling and Simulation System Setup: Introduction to the Real-ESSI Simulator system. Computational Mechanics field of study, kinematics of deformation, strain, stress, linear and nonlinear elasticity, equilibrium relations, finite element method review, nonlinear analysis cycles; Introduction to sequential and parallel computers.

Lectures, recordings and slides:

- Introduction to Modeling and Simulation: [PDF slides](#), [MP4 recording](#)
- Introduction to Modeling Simplifications, Epistemic Uncertainty: [PDF slides](#), [MP4 recording](#)
- Introduction to Parametric, Aleatory Uncertainty: [PDF slides](#), [MP4 recording](#)

Reading: Lecture Notes: 101, 201, 205; Papers/Reports: CM988, CM2714, CM2715, CM3170

Examples: Model development, finite element models, finite element mesh, boundary conditions, material models, loads, model verification process, linear and nonlinear elastic FEM with solids and structural elements. see examples collection at <http://real-essi.info/> or <http://real-essi.us/>,

Problems:

1. Model a  $0.1m \times 0.1m \times 1.0m$  linear elastic cantilever beam, with transversal end forcing, using:
  - Single and ten Bernoulli beam elements
  - Single and ten Timoshenko beam elements
  - 1 ( $1 \times 1 \times 1$ ); 10 ( $1 \times 1 \times 10$ ); 24 node solid brick elements
2. Model a  $0.1m \times 0.1m \times 1.0m$  simple shear linear elastic test using
  - 1 ( $1 \times 1 \times 1$ ) and 32 ( $4 \times 4 \times 4$ ) 8 node solid brick elements
  - 1 ( $1 \times 1 \times 1$ ) and 32 ( $4 \times 4 \times 4$ ) 24 node solid brick elements
3. Model a  $0.1m \times 0.1m \times 1.0m$  pure shear (no rotations) linear elastic test using
  - 1 ( $1 \times 1 \times 1$ ) and 32 ( $4 \times 4 \times 4$ ) 8 node solid brick elements
  - 1 ( $1 \times 1 \times 1$ ) and 32 ( $4 \times 4 \times 4$ ) 24 node solid brick elements

#### 401.4.2 Section II, Inelastic Finite Elements

Theory: Expanding the matrix deformation method, linear elastic truss element, Beams (Bernoulli, Timoshenko), solids, plates, walls (plane stress), shells, stiffness, forces, displacements, interpolating functions for displacements. Local and global equilibrium. Internal and external forces,

Lectures, recordings and slides:

- Introduction to the Finite Element Method (FEM): [PDF slides](#), [MP4 recording](#)
- Derivation of FEM equations of motions for single phase, dry material: [PDF slides](#), [MP4 recording](#)
- Derivation of FEM equations of motions for coupled, two phase, fully and partially saturated material, u-p-U formulation: [PDF slides](#), [MP4 recording](#)

Reading: Lecture Notes: 101, 102; Papers/Reports: CM81, CM125, CM1835, CM2714, CM3155, CM3155

Examples: Truss, beam, solid bricks. external forces. internal forces (sectional forces, stresses). Generalized nodal displacements and internal deformation (curvature, axial, shear, volumetric, general strains), Problems:

1. Develop a set of simple, single element examples using truss, beam and brick finite elements with simple static loads, and extract sectional forces, stress, strain and strain energy from results.

#### 401.4.3 Section III, Micromechanics of Elasto-Plasticity

Theory: Micro-mechanical origins of elasto-plasticity, particles in contact, friction, Hertz, Mindlin-Deresiewicz contact/interface

Lectures, recordings and slides:

- Micromechanical origins of elasto-plasticity:
- Lectures by Prof. Stein Sture (University of Colorado, Boulder) on micromechanical origins of elasto-plasticity are available [HERE](#),

Reading: Lecture Notes: 103; Papers/Reports: CM1000, CM1830, CM1831,

Examples: Particle contact problems.

Problems:

1. Develop a simple, 2D, plane-strain model of two particles in contact and apply normal and then shear forces,
2. For the above model, vary normal and shear forces. Comment on results.

#### 401.4.4 Section IV, Incremental Elastic-Plastic Theory

Theory: Incremental, continuum elasto-plasticity, Material Models, perfectly plastic, hardening and softening. Explicit, forward Euler and Implicit, backward Euler, constitutive integrations,

Lectures, recordings and slides:

- Introduction to the incremental theory of elasto-plasticity: [PDF slides](#), [MP4 recording](#), [YouTube video](#)
- Explicit solution to the constitutive elastic-plastic problem: [PDF slides](#), [MP4 recording](#), [YouTube video](#)
- Implicit solution to the constitutive elastic-plastic problem: [PDF slides](#), [MP4 recording](#), [YouTube video](#)

Reading: Lecture Notes: 104; Papers/Reports: CM3199

Examples: Constitutive integrations, explicit and implicit computations: single element response using select elastic-plastic material models: von Mises, Drucker-Prager, Cam Clay. Perfectly plastic, isotropic hardening, kinematic hardening models and cyclic response. Inelastic, fiber (1D) and 3D structural models for concrete and steel.

Problems:

1. Develop a constitutive only linear elastic example. with monotonic loading and vary elastic modulus and Poisson's ratio. Comment on results
2. Develop a constitutive only elastic-perfectly plastic von-Mises example, for monotonic loading, and vary elastic properties, yield strength. Comment on results.
3. For the above developed example, develop results using explicit and implicit constitutive integrations. Vary step size, integration algorithm, tolerances. Comment on results.
4. For the above developed examples, use two cycles of cyclic loading. Comment on Results.

#### 401.4.5 Section V, Inelastic, Elasto-Plastic Solids Modeling

Theory: Continuation: Incremental elasto-plasticity. Material modeling for practical applications. Advanced topics in constitutive elasto-plasticity, stability and accuracy, errors in constitutive integrations, problematic incremental steps, energy dissipation, sub-incrementation, line search, model calibrations.

Lectures, recordings and slides:

- Choice of elastic-plastic material models for soils and interfaces/contacts/joints: [PDF slides](#), [MP4 recording](#) [YouTube video](#)
- Calibration of elastic-plastic material models for sand: [PDF slides](#), [MP4 recording](#) [YouTube video](#)
- Calibration of elastic-plastic material models for clay: [PDF slides](#), [MP4 recording](#) [YouTube video](#)

Reading: Lecture Notes: 104, 402, 403, 512; Papers/Reports:

Examples: Errors in constitutive modeling, sub-increments. Material model calibration, Constitutive modeling of soil, rock, concrete, steel: von Mises, Drucker-Prager, Cam Clay, SaniSand, rounded Mohr-Coulomb, Pisano. Modeling  $G/G_{max}$  and damping response. Nonlinear, elastic-plastic structural models for concrete and steel (1D, 3D).

Problems:

1. Develop a single element, 8 and 24 node brick, linear elastic example. with monotonic loading and vary elastic modulus and Poisson's ratio. Comment on results
2. Develop a single element elastic-perfectly plastic von-Mises example, for monotonic loading, and vary elastic properties, yield strength. Vary number of integration, Gauss points. Comment on results.
3. For the above developed example, develop results using explicit and implicit constitutive integrations. Vary step size, integration algorithm, tolerances. Comment on results.
4. For the above developed examples, use two cycles of cyclic loading. Comment on Results. Use both axial loading and shear loading.

#### 401.4.6 Section VI, Inelastic, Elastic-Plastic Interfaces, Joints, Contacts Modeling

Theory: Interface/Joint/Contact modeling: Hard contact, Soft contact. Axial contact stiffness, shear contact stiffness. Interface gap opening and closing. Saturated contacts, effective stress and buoyant forces on foundations.

Lectures, recordings and slides:

- Choice of elastic-plastic material models for soils and interfaces/contacts/joints: [PDF slides](#),  
[MP4 recording](#) [YouTube video](#)
- Calibration of elastic-plastic material models for interfaces/contacts/joints: [PDF slides](#), [MP4 recording](#)  
[YouTube video](#)

Reading: Lecture Notes: 104, 403, 512; Papers/Reports:

Examples: Interface: concrete to soil and rock, steel to soil and rock. Gap opening, closing. Shear interface, slip, no slip.

Problems:

1. Develop a two solid element example that are connected using force based interface elements.
2. Develop a two solid element example that are connected using stress based interface elements.
3. For the above developed example, use normal loading and vary load step size. Comment on results.
4. For the above developed example, use normal and then shear loading and vary load step size. Comment on results.
5. For the above developed example, vary interface properties, use interface/contact/joint properties for soil on concrete, soil on steel, concrete on concrete, &c. Comment on results.

#### 401.4.7 Section VII, Inelastic, Elastic-Plastic Structural Modeling

Theory: Inelastic structural models, beams, plates, walls and shells.

Lectures, recordings and slides:

- Choice of elastic-plastic material models for structural elements, beams and walls/plates/shells:  
[PDF slides](#), [MP4 recording](#), [YouTube video](#)
- Calibration of elastic-plastic material models for concrete, in reinforced beams and walls/plates/shells:  
[PDF slides](#), [MP4 recording](#), [YouTube video](#)
- Calibration of elastic-plastic material models for steel, in reinforced beams and walls/beams/shells:  
[PDF slides](#), [MP4 recording](#), [YouTube video](#)

Reading: Lecture Notes: 102, 403, 512; Papers/Reports:

Examples: Nonlinear analysis of structures. Steel Frames. Reinforces concrete frames, walls, plates, shells.

Problems:

1. Develop a nonlinear truss model, and load it using monotonic and cyclic loading up to yielding and past yielding. Comment on results.
2. Develop a nonlinear beam model, and load it in bending using monotonic and cyclic loading up to yielding and past yielding. Comment on results.
3. Develop a two solid element example that are connected using stress based interface elements. Comment on results.

#### 401.4.8 Section VIII, Nonlinear Analysis Progress

Theory: Analysis Progress. Stages, increments, iterations, elastic–plastic stiffness matrix, pure incremental methods, force residuals, Newton iterative algorithm for finite element level iterations, constraints to the global (force residual) system of equations, equilibrium iterations, convergence, load control, displacement control, arc-length, hyper-spherical constraint, convergence criteria, automatic step size control, line search, stability and accuracy. Sequential and parallel computations for inelastic, nonlinear solids and structures.

Lectures, recordings and slides:

- 

Reading: Lecture Notes: 102, 107, 403; Papers/Reports:

Examples: Nonlinear analysis of structures and solids, elastic plastic solids, structures and contacts. Staged analysis steps, incremental only analysis with no equilibrium enforcement, incremental-iterative analysis, with equilibrium enforcement, convergence criteria (force, displacement), convergence tolerances, step size control.

Problems:

1. Develop a nonlinear analysis, using all of previous examples, that will feature explicit, no equilibrium check simulation. Comment on results.
2. Develop a nonlinear analysis, using all of previous examples, that will feature implicit, equilibrium check simulation. Comment on results.

#### 401.4.9 Section IX, Verification and Validation

Theory: Verification, Validation and Prediction, basic theory, solution verification, manufactured solutions, validation experiments, prediction under uncertainty,

Lectures, recordings and slides:

- 

Reading: Lecture Notes: 301, 302, 303..., 313, 314...; Papers/Reports:

Examples: Solution verification examples for elements, material models, constitutive integration algorithms, solution advancement algorithms.

Problems:

1. Choose a model of your interest, and develop a list of verification examples for all components of your model.
2. For the above model, develop a list of validation examples.

#### 401.4.10 Section X, Practical Considerations for Nonlinear Analysis

Theory: Elastic–plastic FEM modeling (practical recommendations for development and analysis of nonlinear (elastic-plastic) finite element models, phased development of general FEM (and ESSI in particular) models. Core Functionality for inelastic/nonlinear modeling, Energy dissipation. Notes on sequential and parallel computing.

Lectures, recordings and slides:

- 

Reading: Lecture Notes: 510, 512; Papers/Reports:

Examples: Illustrations of algorithms and models described above, benefits and detriments of different algorithms and models.

Problems:

1. Develop a realistic nonlinear analysis model of your choice, perhaps the one developed in previous section and experiment with all/most above models and algorithms. Comment on results.

## Chapter 402

# Ten Section Course on Dynamic Finite Element Methods for Realistic Modeling and Simulation of Earthquakes, and Soils, and Structures, and their Interaction, Real-ESSI

(1998-2021-)

## 402.1 Delivery

---

Instructor: Boris Jeremić, email: [Jeremic@ucdavis.edu](mailto:Jeremic@ucdavis.edu)

Class meeting: two hour lecture/meetings, twice a week, flipped classroom approach

Office hours: two hours, twice a week

Course delivery: live and recorded lectures, and live discussions

Course WWW: <http://sokocalo.engr.ucdavis.edu/~jeremic/Classes/ECI280B/>

---

## 402.2 Objectives

This course will provide students with state of the art finite element methods, numerical analysis tools and models for solving dynamic problems in geotechnical and structural engineering. Focus is on analysis of Earthquakes, Soils, Structures and their Interaction (ESSI). Presented will be computational formulation, numerical techniques and models for dynamic, nonlinear, elastic-plastic finite element methods that are used in professional practice and research. In addition, sequential and parallel computing approaches will be explained, and used.

During this course, students will:

- Learn about dynamic finite element modeling and simulation
- Develop dynamic modeling and simulations for linear and nonlinear soils and structures
- Perform dynamic, linear and nonlinear analysis of solids and structures made of soil, rock, concrete, steel and their interfaces, joints and contacts
- Develop and use of one component (1C),  $3 \times 1C$  and 3C seismic motions from given earthquake records and from analytic wave solutions
- Perform dynamic, nonlinear/inelastic earthquake soil structure interaction (ESSI) analysis
- Become proficient in performing nonlinear ESSI analysis using different levels of sophistication, from simplified models to high fidelity elastic-plastic ESSI models on sequential and parallel computers

### Who Should Attend?

Students and practicing engineers who want to learn about and expand their knowledge of modeling and simulation for dynamic, nonlinear/inelastic material behavior, for soils, rock, and structures,

## 402.3 Additional Information

Lecture Notes: <http://sokocalo.engr.ucdavis.edu/~jeremic/LectureNotes/>.

Recorded Lectures: <http://sokocalo.engr.ucdavis.edu/~jeremic/Online-Education/>.

Computers: Most of the problems in this course will require numerical simulations. A finite element modeling system called Real-ESSI Simulator (<http://real-essi.us>) is available for computers running Windows (through WSL), MacOS, Linux. Please refer to <http://real-essi.us> to find out how to use Real-ESSI on local computers or on AWS computers. Other programs can be used as well, as long as they provide modeling and simulation capabilities that are required for assignments, example problems and term project.

Problems: Assigned for each section, students are expected to attempt to develop solutions. You are encouraged to discuss the approach to problem solutions with other students in the course as well as with the instructor.

Term Project: Term project will involve work related to developing or using numerical models for numerically simulating elastic–plastic problem of your choice, related to your interests. Term projects will be presented at the end of quarter.

Grading: TBD

Examination: TBD

Literature:

- The Finite Element Method, *Olgierd Cecil Zienkiewicz and Robert L. Taylor*, McGraw-Hill Book Company, Volumes 1 and 2, ISBN 0-07-084175-6
- Non - Linear Finite Element Analysis of Solids and Structures Volume 1: Essentials, *Crisfield, M. A.*, John Wiley and Sons, Inc. New York, 1991 , ISBN 0 471 92956 5 v.1
- Finite Element Procedures in Engineering Analysis, *Klaus-Juergen Bathe*, Prentice Hall, ISBN 0-13-301458-4
- Constitutive Laws for Engineering Materials With Emphasis on Geologic Materials *Chandakant S. Desai and Hema J. Siriwardane*, Prentice-Hall, Inc. Englewood Cliffs, NJ 07632, ISBN 0-13-167940-6
- Plasticity for Structural Engineers *W. F. Chen and D. J. Han* , Springer Verlag, 1988 ISBN 0-387-96711-7
- Boris Jeremić, Zhaoxi Yang, Zhao Cheng, Guanzhou Jie, Nima Tafazzoli, Matthias Preisig, Panagiota Tasiopoulou, Federico Pisano, Jose Abell, Kohei Watanabe, Yuan Feng, Sumeet Kumar

Sinha, Fatemah Behbehani, Han Yang, and Hexiang Wang. Nonlinear Finite Elements: Modeling and Simulation of Earthquakes, Soils, Structures and their Interaction. University of California, Davis, CA, USA, 1989-2022. ISBN: 978-0-692-19875-9

## 402.4 Teaching Plan, Topics

#### 402.4.1 Section I, Introduction

Introduction: Course objectives, methodology, computer modeling and simulation; Dynamics of nonlinear structures and soils during earthquakes, examples Preliminary theory, terminology, issues to be addressed: Deformation, kinematics of moving systems, elasticity, dynamic equilibrium relations, d'Alembert's principle, forces in dynamic equilibrium, mass, damping, stiffness, external force, single degree of freedom systems,

Modeling and Simulation System Setup: Introduction to the Real-ESSI Simulator system. Computational Mechanics field of study, kinematics of deformation, strain, stress, linear and nonlinear elasticity, equilibrium relations, finite element method review, nonlinear analysis cycles;

Lectures: Recorded lectures covering topics for this section can be found in Section [404.1.1](#) on Page [1937](#) in [Jeremić et al. \(1989-2025\) \(Lecture Notes URL\)](#).

Reading: Lecture notes: 101, 102; Papers/Reports:

Examples: Model Development, simple models vs sophisticated models, pre-processing, post-processing, results visualization.

Problems:

- 1.
- 2.
- 3.

#### 402.4.2 Section II, Dynamic FEM

Dynamic FEM Theory: Dynamic finite element method (FEM) equations, virtual work method in dynamics, nonlinear dynamic equations of motion, consistent and lumped mass, velocity and displacement proportional damping/energy dissipation, Rayleigh and Caughey viscous damping, linear and nonlinear material behavior.

Lectures: Recorded lectures covering topics for this week can be found in Section [404.1.3](#) on Page [1939](#) in Lecture Notes by [Jeremić et al. \(1989-2025\)](#) ([Lecture Notes URL](#)).

Reading: Lecture notes: 102; Papers/Reports:

Examples: Structural and solid elements and models, dynamic excitations, resonance, linear and nonlinear (elastic and inelastic/elastic-plastic) material models, viscous damping, consistent and lumped mass matrix.

Problems:

- 1.
- 2.
- 3.

#### 402.4.3 Section III, Nonlinear FEM

Nonlinear FEM: Elasto-plasticity, material models for dynamics of soils and structures, material parameter calibration, uncertainty in material parameters, explicit and implicit constitutive integrations. Sequential and parallel computations

Lectures: Recorded lectures covering topics for this week can be found in Section 404.1.3 on Page 1939 and Section 404.1.4 on Page 1940 in Lecture Notes by Jeremić et al. (1989-2025) ([Lecture Notes URL](#)).

Reading: Lecture notes: 103, 104; Papers/Reports:

Examples: Elastic plastic solids, beams and shells, material energy dissipation, material damping

Problems:

- 1.
- 2.
- 3.

#### 402.4.4 Section IV, Time Domain Nonlinear Dynamic FEM

Time Domain Nonlinear Dynamic FEM: Direct, time marching solution for dynamics of nonlinear, inelastic systems, general Newmark family of methods, stability and accuracy, nonlinear resonance, numerical damping, explicit and implicit algorithms, unconditionally and conditionally stable Newmark and Hilber–Hughes–Taylor  $\alpha$ -method, stability and accuracy, examples)

Lectures: Recorded lectures covering topics for this week can be found in Section [404.1.3](#) on Page [1939](#) in Lecture Notes by [Jeremić et al. \(1989-2025\)](#) ([Lecture Notes URL](#)).

Reading: Lecture notes: 108; Papers/Reports:

Examples: Nonlinear solid and structural models direct time integration, step size, damping (material, viscous, numerical), stable and unstable computations.

Problems:

- 1.
- 2.
- 3.

#### 402.4.5 Section V, Earthquake Soil Structure Interaction (ESSI)

Earthquake Soil Structure Interaction (ESSI): Background, problem definition, seismic motions, seismic body and surface wave field, seismic energy propagation, free field motions, beneficial and detrimental effects, balancing input and dissipated energy.

Lectures: Recorded lectures covering topics for this week can be found in Section [404.1.8](#) on Page [1946](#) in Lecture Notes by [Jeremić et al. \(1989-2025\)](#) ([Lecture Notes URL](#)).

Reading: Lecture notes: 502; Papers/Reports:

Examples: Analytic development of ground motions, 3D vs 1D motions, seismic energy calculations.

Problems:

- 1.
- 2.
- 3.

#### 402.4.6 Section VI, Seismic Motions

Seismic Motions: Free field vs ESSI motions, incoherent motions, Domain Reduction Method, boundary conditions, radiation damping, 3D inclined wave fields vs 1D vertical motions, nonlinear wave propagation simulations, time step size, element size, earthquake modeling.

Free field motions development, 1D motions, 3D/6D motions, regional scale models, Geophysical models,

Lectures: Recorded lectures covering topics for this week can be found in Section [404.1.7](#) on Page [1945](#) in Lecture Notes by [Jeremić et al. \(1989-2025\)](#) ([Lecture Notes URL](#)).

Reading: Lecture notes: 502, 511, 705, 706; Papers/Reports:

Examples: Real ESSI and analytic wave field models for free field and local (DRM) motions, element and time step size and propagation of (required) frequencies. Vertical and inclined waves development, and input into SSI models

Problems:

- 1.
- 2.
- 3.

#### 402.4.7 Section VII, Coupling with Internal and External Fluids

Dynamics of Coupling with Pore Fluids and External Fluids: Fully coupled, porous solid – pore fluid systems formulation, discretization, basic system of DOFs, coupling damping forces, specialization to slow (consolidation) and fast phenomena (ESSI, liquefaction), boundary conditions, initial conditions, stability and accuracy of various algorithms. Coupling with external fluids, pools, reservoirs.

Lectures: Recorded lectures covering topics for this week can be found in Section [404.1.3](#) on Page [1939](#) in Lecture Notes by [Jeremić et al. \(1989-2025\)](#) ([Lecture Notes URL](#)).

Reading: Lecture notes: 102, 505; Papers/Reports:

Examples: 1D and 3D coupled examples, consolidation, liquefaction and de-liquefaction waves, piles in liquefied soil... Coupling with external fluids, using OpenFOAM...

Problems:

- 1.
- 2.
- 3.

#### 402.4.8 Section VIII, Dynamic Stochastic Elastic-Plastic FEM (SEPFEM)

Stochastic Elastic-Plastic Dynamic FEM:

Lectures: Recorded lectures covering topics for this week can be found in Section [404.1.6](#) on Page [1943](#) in Lecture Notes by [Jeremić et al. \(1989-2025\)](#) ([Lecture Notes URL](#)).

Reading: Lecture notes: Papers/Reports:

Examples:

Problems:

- 1.
- 2.
- 3.

#### 402.4.9 Section IX, Verification and Validation

Verification and Validation: Definition, procedures, code verification, solution verification, validation experiments, model verification

Lectures: Recorded lectures covering topics for this week can be found in Section [404.1.9](#) on Page [1947](#) in Lecture Notes by [Jeremić et al. \(1989-2025\)](#) ([Lecture Notes URL](#)).

Reading: Lecture notes: 301-314; Papers/Reports:

Examples: modeling verification examples, verification for algorithms, elements. Availability of validation data.

Problems:

- 1.
- 2.
- 3.

#### 402.4.10 Section X, ESSI Modeling and Simulation Synthesis

ESSI Modeling and Simulation Synthesis: Example building structure (boundary conditions, initial conditions, nonlinear interface/contact (gap/slip), nonlinear soil/rock, 1D vs 3D seismic motions development, buoyant forces at foundation level, etc.). Use of sequential and parallel computers for analysis.

Lectures: Recorded lectures covering topics for this week can be found in Section [404.1.11](#) on Page [1949](#) in Lecture Notes by [Jeremić et al. \(1989-2025\)](#) ([Lecture Notes URL](#)).

Reading: Lecture notes: 503, 504, 509 510, 512; Papers/Reports:

Examples: Real ESSI illustrative examples

Problems:

- 1.
- 2.
- 3.

Chapter 403

# Nonlinear ESSI for Professional Practice, A Short Course

(2017-2022-)

## 403.1 Short Course Delivery

Instructor: Boris Jeremić, email: [Jeremic00@gmail.com](mailto:Jeremic00@gmail.com); [Jeremic@ucdavis.edu](mailto:Jeremic@ucdavis.edu)

Short Course Meeting: Two hour lectures, twice a week, online, using zoom; live and recorded lectures and discussions.

## 403.2 Objectives

The nonlinear analysis of Earthquakes, Soils, Structures, and their Interaction (ESSI) is crucial in ensuring the safety and efficiency of various structures, such as bridges, dams, buildings, tunnels, nuclear facilities, and other parts of the built environment. This analysis involves a deep understanding of statics and dynamics in soil mechanics, structural mechanics, and numerical modeling in order to accurately analyze ESSI systems' nonlinear behavior under static and dynamic loads.

This online course provides training on nonlinear, inelastic analysis for soil-structure systems, specifically focusing on earthquake soil-structure interaction (ESSI). The course is designed for practicing engineers, consultants, managers, and regulators and covers practical aspects of nonlinear analysis for ESSI systems. The main advantages and disadvantages of using nonlinear analysis for ESSI systems will also be discussed.

Who Should Attend: This short online course is designed for practicing engineers, consultants, managers, and regulators who want to reinforce and expand their knowledge of nonlinear, inelastic analysis for soil-structure systems. If you are looking to improve your understanding of the nonlinear behavior of ESSI systems and become proficient in performing nonlinear ESSI analysis, this course is will help you to achieve your goals.

What will you learn? Upon completion of this course, the participants will be able to:

1. Plan, develop, and verify different levels of sophistication ESSI models,
2. Select and calibrate elastic and elastic-plastic material models for soil, interfaces/contacts, and structural components such as beams and plates/shells,
3. Develop one component (1C), 3×1C, and 3C seismic motions from chosen earthquake records and/or stress test motions,
4. Choose numerical simulation parameters, convergence tolerances, and efficient solvers for high-performance sequential and parallel computing,
5. Identify and explain the limitations of nonlinear, inelastic finite element analysis,

6. Perform nonlinear ESSI analysis with proficiency, ranging from simplified models to high-fidelity elastic-plastic models of soil-structure systems.

Course Delivery: Online course and online office hours will use zoom platform.

Lecture Notes: <http://sokocalo.engr.ucdavis.edu/~jeremic/LectureNotes/>.

Computers: Course will rely on use of analysis system called the Real-ESSI Simulator (<http://real-essi.us>). The Real-ESSI Simulator program is available for computers running Windows (through WSL), MacOS and Linux, Please refer to <http://real-essi.us> to find out how to use Real-ESSI on local computers through Docker. The system is also available in the cloud, on Amazon Web Services (AWS) computers.

Short Course Program:

- Part I: Introduction to Nonlinear Finite Element Analysis
  - Brief overview of static and dynamic finite elements method (FEM)
  - Brief overview of linear and material nonlinear FEM
  - Nonlinear FEM analysis: stages, increments and iterations
  - Quality assurance: verification and validation (V&V) procedures
  - Introduction to the Real ESSI Simulator system, documentation, examples
- Part II: Nonlinear Material Models. Participants will learn about and use nonlinear, inelastic, elastic-plastic models:
  - Nonlinear material models for soil and rock
  - Nonlinear material models for concrete
  - Nonlinear material models for steel
  - Fiber section Nonlinear material models for concrete and steel, for beams and walls,
  - 3D soil-foundation interface/contact nonlinear material models,
- Part III: Nonlinear Finite Element Analysis. Participants will learn about and perform nonlinear finite element analysis:
  - Develop stages-increments-iterations cycles
  - Develop and perform purely incremental nonlinear analysis
  - Develop and perform iterative incremental nonlinear analysis
  - Liquefaction analysis, fully coupled, saturated, porous solid – pore fluid,
  - Energy dissipation during elasto-plastic deformation.
- Part IV: Hands on elasto-plastic example exercise. Participants will develop and use elastic-plastic models for nonlinear material analysis:
  - Calibration of nonlinear/inelastic elastic-plastic models for
    - soil,
    - rock,
    - concrete,
    - steel,
    - interface/contact,
    - base isolators and dissipators
  - Use of best practices for nonlinear, inelastic model development and calibration.

- Part V: Introduction to Seismic Ground Motions. Participants will learn about and develop seismic ground motions from:
  - Ground motions from given surface motions, in 1C, 3×1C, and 3C
  - Analytic, stress test ground motions, in 1C, 3×1C, and 3C
  - Ground motions from small and regional scale models
- Part VI: Ground Motions for ESSI Modeling. Participants will learn about, apply and propagate ground motions through the free field and soil-structure systems:
  - Input ground motion into FEM model
  - Application of free field and ESSI ground motions
  - Ground motions using Domain Reduction Method (DRM)
  - Control ground motion frequency content
- Part VII: Hands on ESSI Ground Motion Exercise. Participants will analyze soil-structure systems using developed ground motions:
  - Develop hierarchy of input ground motions: 1C, 3×1C and 3C.
  - Free field analysis with 1C, 3×1C and 3C motions.
  - ESSI analysis with 1C, 3×1C and 3C motions.
  - Use of best practice for ground motion ESSI modeling
- Part VIII: Hands on nonlinear ESSI examples exercise. Participants will analyze nonlinear ESSI FEM models:
  - Hierarchy of sound engineering judgement ESSI model development steps
  - Nonlinear Finite Element, elastic-plastic examples for: soils, structures, interfaces,
  - Energy dissipation in dynamic ESSI analysis: viscous, plastic, algorithmic...
  - Nonlinear finite element models for ESSI using solids, structural elements, interfaces,
  - Use of best practices for nonlinear/inelastic ESSI modeling

## Chapter 404

# Online Education and Training

(2019-2020-2021-)

(In collaboration with Prof. Han Yang and Dr. Hexiang Wang)

## 404.1 Real-ESSI Simulator Online Education and Training

This chapter was created to present online material for the theory for modeling and simulation of earthquakes, soils, structures and their interaction, as well practical examples using the Real-ESSI Simulator, <http://real-essi.us/>.

It is worth noting that some early recorded material for use of the Real-ESSI Simulator on Amazon Web Services was created in 2019, however, majority of presented, recorded material was created during Corona-Virus (COVID-19) pandemic and quarantine from March through June of 2020, in Zürich Switzerland, where Boris Jeremić was locked-up, and in Davis, California, where Han Yang and Hexiang Wang were locked-up... Internet worked very good across the Atlantic ocean, [zoom.us](#) worked really well as well. Development of online educational material continued with all three contributors now in Davis, California during Summer and Fall 2020, Winter and Spring 2021, still during partial/full lockdown, shelter in place, still using [zoom.us](#), and still keeping physical distance, wearing face masks, etc.

In addition to organizing slides and video lectures through this document, a youtube video channel for the Real-ESSI is available here: [Real-ESSI youtube channel](#).

It is hoped that this material will be helpful to students and engineers that work in the area of modeling and simulation of earthquakes, soils, structures and their interaction.

### 404.1.1 Modeling and Simulations for ESSI

The following recorded lectures modeling and simulation approaches for Earthquakes, Soils, Structures and their Interaction are available:

#### 404.1.1.1 Introduction to Modeling and Simulation

[PDF slides](#), and a direct [MP4 recording](#) and/or alternatively [YouTube video](#)

#### 404.1.1.2 Introduction to Modeling Simplifications, Epistemic Uncertainty

[PDF slides](#), and a direct [MP4 recording](#) and/or alternatively [YouTube video](#)

#### 404.1.1.3 Introduction to Parametric, Aleatory Uncertainty

[PDF slides](#), and a direct [MP4 recording](#) and/or alternatively [YouTube video](#)

#### 404.1.2 Real-ESSI Simulator Modeling and Simulation System

The following recorded lectures about the Real-ESSI Simulator modeling and simulation system are available:

1. The Real-ESSI Simulator, Introduction:

[PDF slides](#), and a direct [MP4 recording](#) and/or alternatively [YouTube video](#)

2. The Real-ESSI Simulator, Modeling Features:

[PDF slides](#), and a direct [MP4 recording](#) and/or alternatively [YouTube video](#)

3. The Real-ESSI Simulator, Domain Specific Language:

[PDF slides](#), and a direct [MP4 recording](#) and/or alternatively [YouTube video](#)

4. The Real-ESSI Simulator, Model Development:

[PDF slides](#), and a direct [MP4 recording](#) and/or alternatively [YouTube video](#)

5. The Real-ESSI Simulator, Results Post Processing:

[PDF slides](#), and a direct [MP4 recording](#) and/or alternatively [YouTube video](#)

6. The Real-ESSI Simulator, Quick Analysis Startup Guide, how to run simple example models:

[PDF slides](#), and a direct [MP4 recording](#) and/or alternatively [YouTube video](#)

### 404.1.3 Finite Element Method

The following recorded lectures on the finite element method are available:

#### 404.1.3.1 Background

1. Introduction to the Finite Element Method (FEM):

[PDF slides](#), [MP4 recording](#)

2. Derivation of FEM equations of motions for single phase, dry material:

[PDF slides](#), [MP4 recording](#)

3. Derivation of FEM equations of motions for coupled, two phase, fully and partially saturated material, u-p-U formulation:

[PDF slides](#), [MP4 recording](#)

#### 404.1.3.2 Nonlinear, Inelastic FEM

4. Nonlinear, Inelastic FEM, residual equations:

[PDF slides](#), and a direct [MP4 recording](#) and/or alternatively [YouTube video](#)

5. Solution of nonlinear, inelastic FEM equations:

[PDF slides](#), and a direct [MP4 recording](#) and/or alternatively [YouTube video](#)

#### 404.1.3.3 Dynamic FEM

6. Dynamic FEM equations:

[PDF slides](#), and a direct [MP4 recording](#) and/or alternatively [YouTube video](#)

7. Time marching algorithms for dynamic FEM equations:

[PDF slides](#), and a direct [MP4 recording](#) and/or alternatively [YouTube video](#)

#### 404.1.4 Deterministic Elasto-Plasticity

##### 404.1.4.1 Introduction to Modeling and Simulation

[PDF slides](#), and a direct [MP4 recording](#) and/or alternatively [YouTube video](#)

The following recorded lectures on deterministic elasto-plasticity are available:

##### 404.1.4.2 Theory Backgound

1. Micromechanical origins of elasto-plasticity:

[PDF slides](#), and a direct [MP4 recording](#) and/or alternatively [YouTube video](#)

2. Introduction to the incremental theory of elasto-plasticity:

[PDF slides](#), and a direct [MP4 recording](#) and/or alternatively [YouTube video](#)

3. Explicit solution to the constitutive elastic-plastic problem:

[PDF slides](#), and a direct [MP4 recording](#) and/or alternatively [YouTube video](#)

4. Implicit solution to the constitutive elastic-plastic problem:

[PDF slides](#), and a direct [MP4 recording](#) and/or alternatively [YouTube video](#)

##### 404.1.4.3 Elastic-Plastic Material Model Choices

5. Choice of elastic-plastic material models for soils and interfaces/contacts/joints:

[PDF slides](#), and a direct [MP4 recording](#) and/or alternatively [YouTube video](#)

6. Choice of elastic-plastic material models for structural elements, beams and walls/plates/shells:

[PDF slides](#), and a direct [MP4 recording](#) and/or alternatively [YouTube video](#)

##### 404.1.4.4 Calibrating Elastic-Plastic Material Models

7. Calibration of elastic-plastic material models for sand:

[PDF slides](#), and a direct [MP4 recording](#) and/or alternatively [YouTube video](#)

8. Calibration of elastic-plastic material models for clay:

[PDF slides](#), and a direct [MP4 recording](#) and/or alternatively [YouTube video](#)

9. Calibration of elastic-plastic material models for interfaces/contacts/joints:

[PDF slides](#), and a direct [MP4 recording](#) and/or alternatively [YouTube video](#)

10. Calibration of elastic-plastic material models for concrete, in reinforced beams and walls/plates/shells:

[PDF slides](#), and a direct [MP4 recording](#) and/or alternatively [YouTube video](#)

11. Calibration of elastic-plastic material models for steel, in reinforced beams and walls/beams/shells:

[PDF slides](#), and a direct [MP4 recording](#) and/or alternatively [YouTube video](#)

#### 404.1.5 Seismic Energy Dissipation

The following recorded lectures on energy dissipation are available:

##### 404.1.5.1 Theory Background

1. Energy dissipation introduction:

[PDF slides](#), and a direct [MP4 recording](#) and/or alternatively [YouTube video](#)

2. Energy dissipation in solids:

[PDF slides](#), and a direct [MP4 recording](#) and/or alternatively [YouTube video](#)

3. Energy dissipation in fiber beams:

[PDF slides](#), and a direct [MP4 recording](#) and/or alternatively [YouTube video](#)

4. Energy dissipation in interfaces/joints/contacts:

[PDF slides](#), and a direct [MP4 recording](#) and/or alternatively [YouTube video](#)

5. Energy dissipation due to viscous effects:

[PDF slides](#), and a direct [MP4 recording](#) and/or alternatively [YouTube video](#)

6. Energy dissipation due to time integration, algorithmic, numerical effects:

[PDF slides](#), and a direct [MP4 recording](#) and/or alternatively [YouTube video](#)

##### 404.1.5.2 Illustrative Examples

7. Energy dissipation examples:

[PDF slides](#), and a direct [MP4 recording](#) and/or alternatively [YouTube video](#)

## 404.1.6 Probabilistic Elasto-Plasticity and Stochastic Elastic-Plastic Finite Element Method

### 404.1.6.1 Theory Background

1. Introduction to the Polynomial Chaos (PC) expansion:

[PDF slides](#), and a direct [MP4 recording](#) and/or alternatively [YouTube video](#)

2. Introduction to the Karhunen-Loëve (KL) expansion:

[PDF slides](#), and a direct [MP4 recording](#) and/or alternatively [YouTube video](#)

3. Introduction to the Stochastic Elastic-Plastic Finite Element Method (SEPFEM)

[PDF slides](#), and a direct [MP4 recording](#) and/or alternatively [YouTube video](#)

4. Introduction to Sensitivity Analysis

[PDF slides](#), and a direct [MP4 recording](#) and/or alternatively [YouTube video](#)

### 404.1.6.2 Choice and Calibration of Probabilistic Material Models and Probabilistic Seismic Loads

5. Choice, analysis and calibration of probabilistic elastic material parameters:

[PDF slides](#), and a direct [MP4 recording](#) and/or alternatively; [YouTube video](#)

6. Choice, analysis and calibration of probabilistic elastic-plastic, nonlinear, inelastic material parameters:

[PDF slides](#), and a direct [MP4 recording](#) and/or alternatively [YouTube video](#)

7. Choice, analysis and calibration of probabilistic seismic motions:

[PDF slides](#), and a direct [MP4 recording](#) and/or alternatively [YouTube video](#)

### 404.1.6.3 Simple Probabilistic Examples

8. SEPFEM, Two Examples:

[PDF slides](#), and a direct [MP4 recording](#) and/or alternatively [YouTube video](#)

9. SEPFEM, Seismic Risk Analysis Example:

[PDF slides](#), and a direct [MP4 recording](#) and/or alternatively [YouTube video](#)

### 404.1.6.4 Probabilistic Wave Propagation Examples

10. Analysis of one component (1C) seismic wave propagation with uncertain motions and uncertain elastic material parameters:

[PDF slides](#), and a direct [MP4 recording](#) and/or alternatively [YouTube video](#)

11. Analysis of one component (1C) seismic wave propagation with uncertain motions and uncertain elastic-plastic, nonlinear, inelastic material parameters:

[PDF slides](#), and a direct [MP4 recording](#) and/or alternatively [YouTube video](#)

12. Sensitivity analysis for uncertain motions and uncertain elastic material parameters:

[PDF slides](#), and a direct [MP4 recording](#) and/or alternatively [YouTube video](#)

13. Sensitivity analysis for uncertain motions and uncertain elastic-plastic, nonlinear, inelastic material parameters:

[PDF slides](#), and a direct [MP4 recording](#) and/or alternatively [YouTube video](#)

#### 404.1.7 Seismic Motions

The following recorded lectures on seismic motions are available:

1. On earthquakes:

[PDF slides](#), and a direct [MP4 recording](#) and/or alternatively [YouTube video](#)

2. On six component (6C) seismic motions:

[PDF slides](#), and a direct [MP4 recording](#) and/or alternatively [YouTube video](#)

3. On the Domain Reduction Method (DRM):

[PDF slides](#), and a direct [MP4 recording](#) and/or alternatively [YouTube video](#)

4. Development of DRM motions from surface records, 1C, 2×1C, and 3×1C:

[PDF slides](#), and a direct [MP4 recording](#) and/or alternatively [YouTube video](#)

5. Development of DRM motions from inclined, 3C seismic waves:

[PDF slides](#), and a direct [MP4 recording](#) and/or alternatively [YouTube video](#)

#### 404.1.8 Earthquake Soil Structure Interaction

The following recorded lectures on Earthquake Soil Structure Interaction (ESSI) are available:

1. On ESSI:

[PDF slides](#), and a direct [MP4 recording](#) and/or alternatively [YouTube video](#)

#### 404.1.9 Verification and Validation

Basic theory of Verification and Validation (V&V), as well as V&V examples for the Real ESSI Simulator are shown in recorded lectures below:

1. Verification and Validation introduction:

[PDF slides](#), and a direct [MP4 recording](#) and/or alternatively [YouTube video](#)

2. Real ESSI Simulator Verification and Validation system:

[PDF slides](#), and a direct [MP4 recording](#) and/or alternatively [YouTube video](#)

3. Real ESSI Simulator Verification examples:

[PDF slides](#), and a direct [MP4 recording](#) and/or alternatively [YouTube video](#)

4. Real ESSI Simulator Validation examples:

[PDF slides](#), and a direct [MP4 recording](#) and/or alternatively [YouTube video](#)

#### 404.1.10 High Performance Computing

High Performance Computing (HPC) is helping with analysis of sophisticated models efficiently on sequential and parallel computers.

##### 404.1.10.1 HPC Introduction

1. HPC, an Introduction:

[PDF slides](#), and a direct [MP4 recording](#) and/or alternatively [YouTube video](#)

2. Fine grained HPC:

[PDF slides](#), and a direct [MP4 recording](#) and/or alternatively [YouTube video](#)

3. Coarse grained HPC, a Distributed Memory Parallel (DMP) Introduction:

[PDF slides](#), and a direct [MP4 recording](#) and/or alternatively [YouTube video](#)

##### 404.1.10.2 HPC and Real-ESSI

1. Real-ESSI Simulator HPC Approach:

[PDF slides](#), and a direct [MP4 recording](#) and/or alternatively [YouTube video](#)

##### 404.1.10.3 Real-ESSI Parallel Computing Examples

1. Real-ESSI Simulator Parallel Examples:

[PDF slides](#), and a direct [MP4 recording](#) and/or alternatively [YouTube video](#)

#### 404.1.11 Real-ESSI Simulator Examples

Select Real-ESSI examples are shown in recorded lectures below:

1. How to run already installed Real-ESSI program on a simple example:

[MP4 recording](#) and/or alternatively [YouTube video](#)

2. Running Real-ESSI program for a frame model:

[MP4 recording](#) and/or alternatively [YouTube video](#)

3. Running Real-ESSI program for a elastic-plastic solids model:

[MP4 recording](#) and/or alternatively [YouTube video](#)

4. Running Real-ESSI program for a solids, beams and shells model:

[MP4 recording](#) and/or alternatively [YouTube video](#)

5. Post-processing Real-ESSI results using Paraview for frame model:

[MP4 recording](#) and/or alternatively [YouTube video](#)

6. Post-processing Real-ESSI results using Paraview for a solids, beams and shells model:

[MP4 recording](#) and/or alternatively [YouTube video](#)

7. Developing a DRM SSI model, solids and beams:

[PDF slides](#), and a direct [MP4 recording](#) and/or alternatively [YouTube video](#)

8. Running a DRM SSI model, solids and beams:

[PDF slides](#), and a direct [MP4 recording](#) and/or alternatively [YouTube video](#)

## Chapter 405

# Constitutive, Material Behaviour Examples

(2016-2017-2019-2023-)

(In collaboration with Dr. Yuan Feng and Dr. Han Yang)

## 405.1 Chapter Summary and Highlights

In this Chapter constitutive behavior of elastic-plastic material is illustrated through a number of examples.

All the examples described here, and many more, organized in sub-directories, for constitutive behavior, static and dynamic behavior can be directly downloaded from a repository at: [http://sokocalo.engr.ucdavis.edu/~jeremic/lecture\\_notes\\_online\\_material/Real-ESSI\\_Examples/education\\_examples](http://sokocalo.engr.ucdavis.edu/~jeremic/lecture_notes_online_material/Real-ESSI_Examples/education_examples). These examples can then be tried, analyzed using Real-ESSI Simulator that is available on Amazon Web Services (AWS) computers around the word. Login to AWS market place and search for Real-ESSI...

## 405.2 Elastic Solid Constitutive Examples

### 405.2.1 Linear Elastic Constitutive Examples

#### 405.2.1.1 Pure Shear, Monotonic Loading

The Real-ESSI input files for this example are available [HERE](#). The compressed package of Real-ESSI input files and postprocessing results for this example is available [HERE](#).

Material properties in Real-ESSI input:

```
1 model name "test";
2 add material # 1 type linear_elastic_isotropic_3d
3   mass_density = 2E3 * kg/m^3
4   elastic_modulus = 2E7 * Pa
5   poisson_ratio= 0.0 ;
6 simulate constitutive testing strain control pure shear monotonic loading use ←
    material # 1
7   confinement_strain = 0.001
8   strain_increment_size = 0.0001
9   number_of_increment = 100;
10 bye;
```

Material Response:

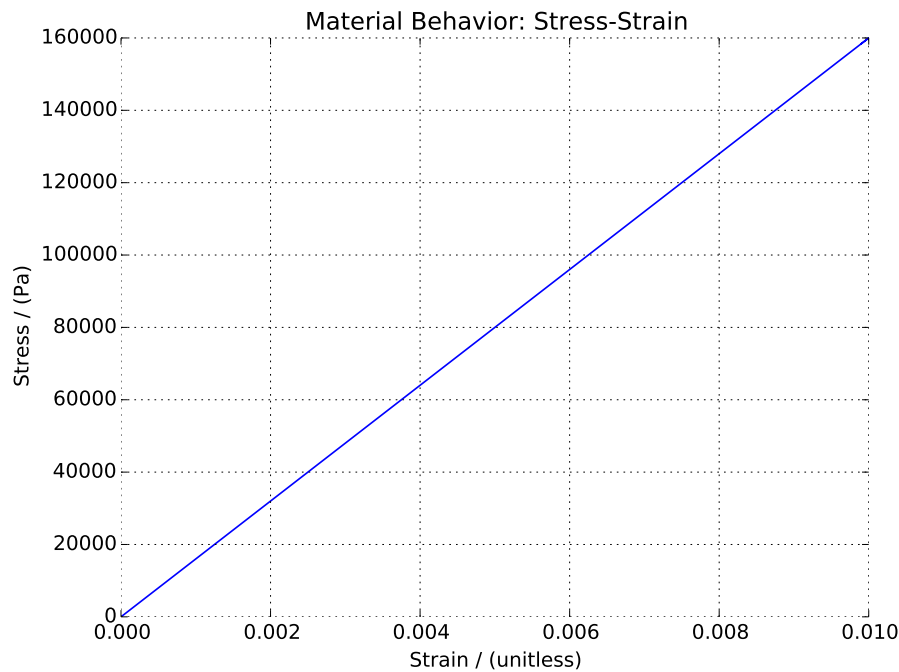


Figure 405.1: Linear Elastic Pure Shear Monotonic Loading

#### 405.2.1.2 Pure Shear, Cyclic Loading

The Real-ESSI input files for this example are available [HERE](#). The compressed package of Real-ESSI input files and postprocessing results for this example is available [HERE](#).

Material properties in Real-ESSI input:

```
1 model name "test";
2 add material # 1 type linear_elastic_isotropic_3d
3   mass_density = 2E3 * kg/m^3
4   elastic_modulus = 2E7 * Pa
5   poisson_ratio= 0.25 ;
6 simulate constitutive testing strain control pure shear cyclic loading use ←
    material # 1
7   confinement_strain = 0.001
8   strain_increment_size = 0.0001
9   maximum_strain = 0.01
10  number_of_cycles = 1;
11 bye;
```

Material Response:

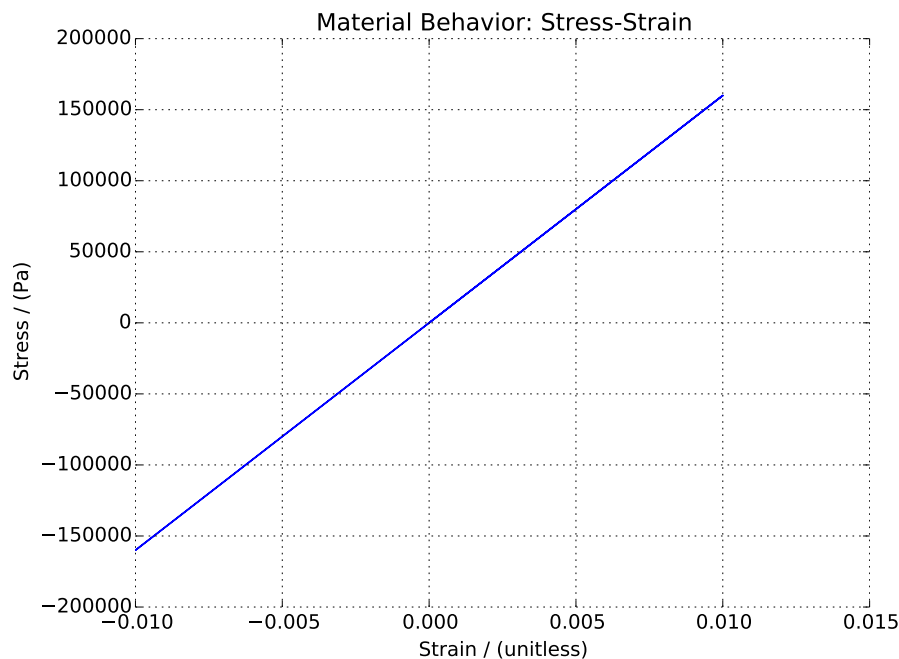


Figure 405.2: Linear Elastic Pure Shear Cyclic Loading.

#### 405.2.1.3 Uniaxial Strain, Monotonic Loading

The Real-ESSI input files for this example are available [HERE](#). The compressed package of Real-ESSI input files and postprocessing results for this example is available [HERE](#).

Material properties in Real-ESSI input:

```
1 model name "test";
2 add material # 1 type linear_elastic_isotropic_3d
3   mass_density = 2E3 * kg/m^3
4   elastic_modulus = 2E7 * Pa
5   poisson_ratio= 0.0 ;
6 simulate constitutive testing strain control uniaxial monotonic loading use ←
    material # 1
7   confinement_strain = 0.001
8   strain_increment_size = 0.0001
9   number_of_increment = 100;
10 bye;
```

Material Response:

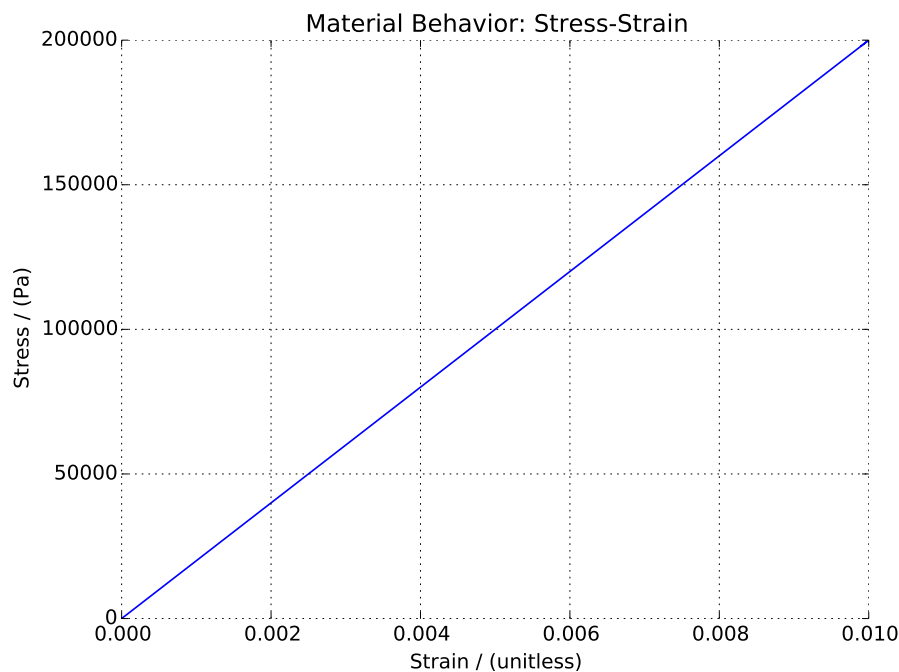


Figure 405.3: Linear Elastic Uniaxial Monotonic Loading

#### 405.2.1.4 Uniaxial Strain, Cyclic Loading

The Real-ESSI input files for this example are available [HERE](#). The compressed package of Real-ESSI input files and postprocessing results for this example is available [HERE](#).

Material properties in Real-ESSI input:

```
1 model name "test";
2 add material # 1 type linear_elastic_isotropic_3d
3   mass_density = 2E3 * kg/m^3
4   elastic_modulus = 2E7 * Pa
5   poisson_ratio= 0.25 ;
6 simulate constitutive testing strain control pure shear cyclic loading use ←
    material # 1
7   confinement_strain = 0.001
8   strain_increment_size = 0.0001
9   maximum_strain = 0.01
10  number_of_cycles = 1;
11 bye;
```

Material Response:

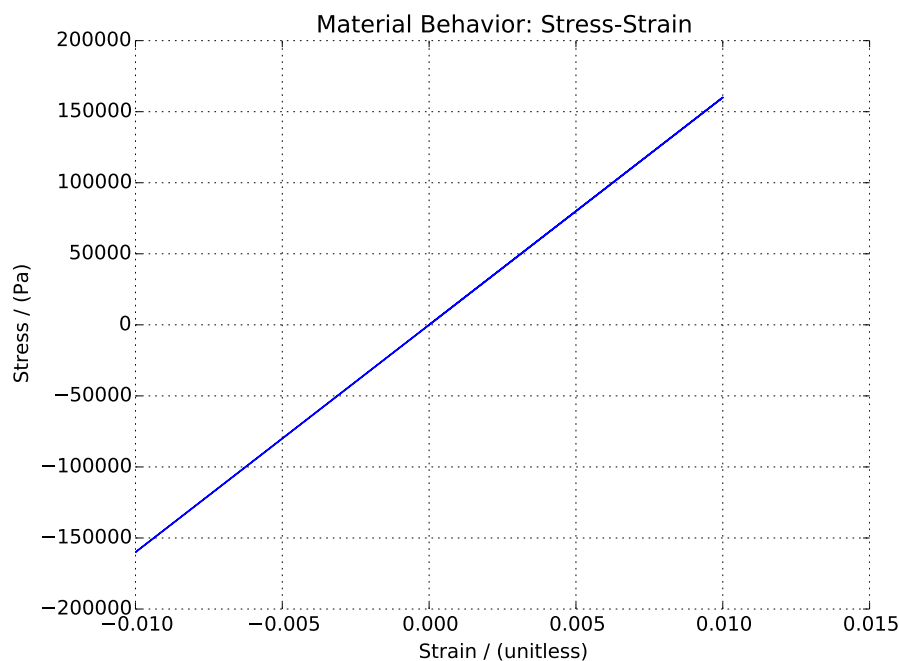


Figure 405.4: Linear Elastic Uniaxial Cyclic Loading

## 405.2.2 Nonlinear Elastic Constitutive Examples

### 405.2.2.1 Triaxial Uniform Pressure, Monotonic Loading

The Real-ESSI input files for this example are available [HERE](#). The compressed package of Real-ESSI input files and postprocessing results for this example is available [HERE](#).

The Duncan-Chang nonlinear elastic materials:

$$E = K p_a \left( \frac{\sigma_3}{p_a} \right)^n \quad (405.1)$$

where  $K$  and  $n$  are material constants. And pressure  $p_a$  is atmospheric pressure. And stress  $\sigma_3$  is the minor principal stress.

Material properties in Real-ESSI input:

```

1 model name "test";
2 add material # 1 type Duncan_Chang_nonlinear_elastic_isotropic_3d_LT
3   mass_density = 2E3 * kg/m^3
4   initial_elastic_modulus = 3E5 * Pa
5   poisson_ratio= 0.15
6   DuncanChang_K = 1E3
7   DuncanChang_pa = 1E5 * Pa
8   DuncanChang_n = 0.5 ;
9 simulate constitutive testing strain control triaxial confinement loading use ←
  material # 1
10  strain_increment_size = 0.00001
11  maximum_strain = 0.01
12  number_of_increment = 2000;
13 bye;
```

Material Response:

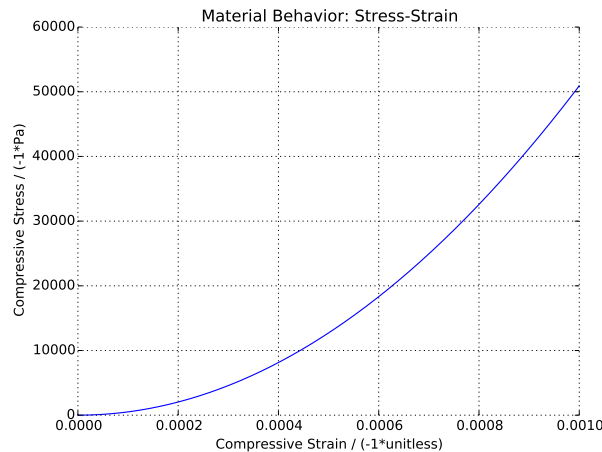


Figure 405.5: Results of Duncan-Chang Nonlinear Elastic Monotonic Loading

## 405.3 Elastic Plastic Solid Constitutive Examples

### 405.3.1 Elastic Perfectly Plastic Constitutive Examples

#### 405.3.1.1 Pure Shear

The Real-ESSI input files for this example are available [HERE](#). The compressed package of Real-ESSI input files and postprocessing results for this example is available [HERE](#).

Material properties in Real-ESSI input:

```

1 model name "test";
2 add material # 1 type VonMises
3   mass_density = 2E3*kg/m^3
4   elastic_modulus = 2E7 * Pa
5   poisson_ratio=0.25
6   von_mises_radius = 1E5*Pa
7   kinematic_hardening_rate = 0.0 *Pa
8   isotropic_hardening_rate = 0.0*Pa ;
9 define NDMaterial constitutive integration algorithm Backward_Euler
10  yield_function_relative_tolerance = 1E-2
11  stress_relative_tolerance = 1E-3
12  maximum_iterations = 30;
13 simulate constitutive testing strain control pure shear cyclic loading use ↵
    material # 1
14  confinement_strain = 0.001
15  strain_increment_size = 0.0001
16  maximum_strain = 0.01
17  number_of_cycles = 1;
18 bye;
```

Material Response:

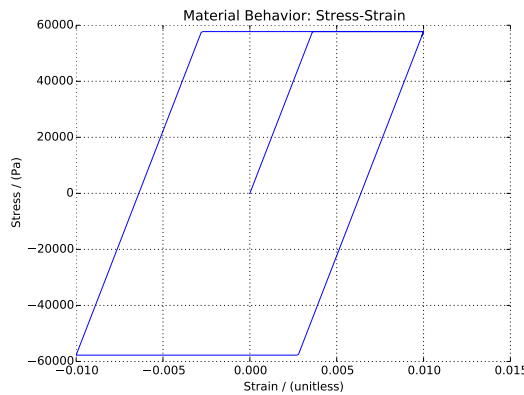


Figure 405.6: Perfectly Plastic Pure Shear Cyclic Loading.

#### 405.3.1.2 Uniaxial Strain

The Real-ESSI input files for this example are available [HERE](#). The compressed package of Real-ESSI input files and postprocessing results for this example is available [HERE](#).

Material properties in Real-ESSI input:

```

1 model name "test";
2 add material # 1 type VonMises
3   mass_density = 2E3*kg/m^3
4   elastic_modulus = 2E7 * Pa
5   poisson_ratio=0.25
6   von_mises_radius = 1E5*Pa
7   kinematic_hardening_rate = 0.0 *Pa
8   isotropic_hardening_rate = 0.0*Pa ;
9 define NDMaterial constitutive integration algorithm Backward_Euler
10  yield_function_relative_tolerance = 1E-2
11  stress_relative_tolerance = 1E-3
12  maximum_iterations = 30;
13 simulate constitutive testing strain control uniaxial cyclic loading use ↵
    material # 1
14  confinement_strain = 0.001
15  strain_increment_size = 0.0001
16  maximum_strain = 0.01
17  number_of_cycles = 1;
18 bye;
```

Material Response:

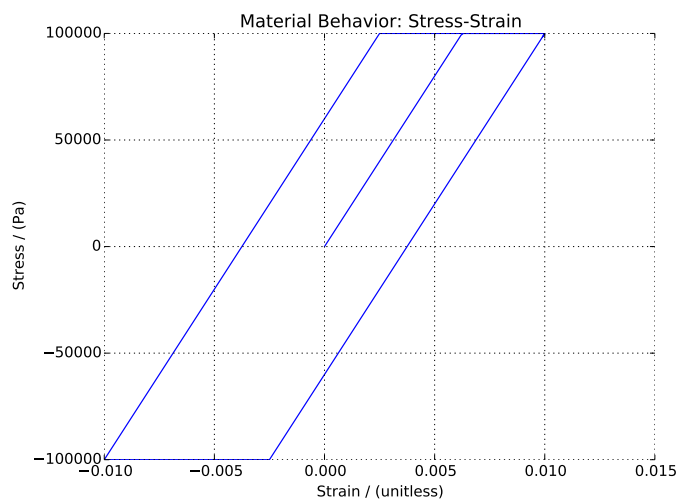


Figure 405.7: Perfectly Plastic Uniaxial Cyclic Loading

## 405.3.2 Elastic Plastic, Isotropic Hardening, Constitutive Examples

### 405.3.2.1 Pure Shear, Monotonic Loading

The Real-ESSI input files for this example are available [HERE](#). The compressed package of Real-ESSI input files and postprocessing results for this example is available [HERE](#).

Material properties in Real-ESSI input:

```

1 model name "test";
2 add material # 1 type VonMises
3   mass_density = 2E3*kg/m^3
4   elastic_modulus = 2E7 * Pa
5   poisson_ratio=0.25
6   von_mises_radius = 1E5*Pa
7   kinematic_hardening_rate = 0.0*Pa
8   isotropic_hardening_rate = 2E6 *Pa ;
9 define NDMaterial constitutive integration algorithm Backward_Euler
10  yield_function_relative_tolerance = 1E-2
11  stress_relative_tolerance = 1E-3
12  maximum_iterations = 30;
13 simulate constitutive testing strain control pure shear monotonic loading use ←
    material # 1
14  confinement_strain = 0.001
15  strain_increment_size = 0.0001
16  number_of_increment = 99;
17 bye;
```

Material Response:

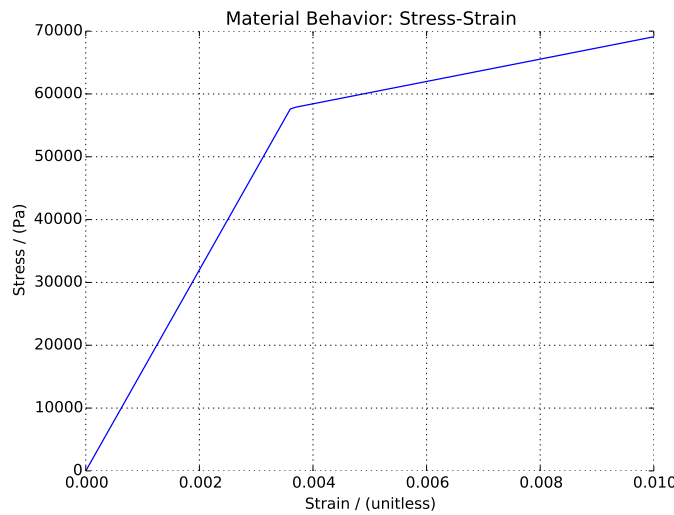


Figure 405.8: Isotropic Hardening Pure Shear Monotonic Loading

#### 405.3.2.2 Pure Shear, Cyclic Loading

The Real-ESSI input files for this example are available [HERE](#). The compressed package of Real-ESSI input files and postprocessing results for this example is available [HERE](#).

Material properties in Real-ESSI input:

```

1 model name "test";
2 add material # 1 type VonMises
3   mass_density = 2E3*kg/m^3
4   elastic_modulus = 2E7 * Pa
5   poisson_ratio=0.25
6   von_mises_radius = 1E5*Pa
7   kinematic_hardening_rate = 0.0*Pa
8   isotropic_hardening_rate = 2E6 *Pa ;
9 define NDMaterial constitutive integration algorithm Backward_Euler
10  yield_function_relative_tolerance = 1E-2
11  stress_relative_tolerance = 1E-3
12  maximum_iterations = 30;
13 simulate constitutive testing strain control pure shear cyclic loading use ←
    material # 1
14  confinement_strain = 0.001
15  strain_increment_size = 0.0001
16  maximum_strain = 0.01
17  number_of_cycles = 1;
18 bye;
```

Material Response:

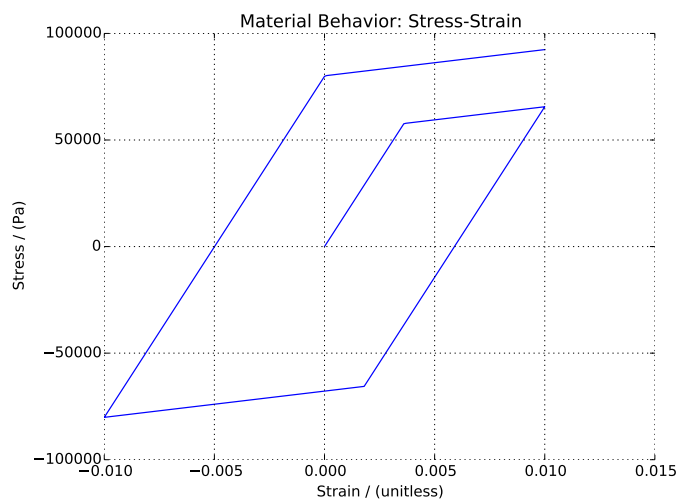


Figure 405.9: Isotropic Hardening Pure Shear Cyclic Loading.

#### 405.3.2.3 Uniaxial Strain, Monotonic Loading

The Real-ESSI input files for this example are available [HERE](#). The compressed package of Real-ESSI input files and postprocessing results for this example is available [HERE](#).

Material properties in Real-ESSI input:

```
1 model name "test";
2 add material # 1 type VonMises
3   mass_density = 2E3*kg/m^3
4   elastic_modulus = 2E7 * Pa
5   poisson_ratio=0.25
6   von_mises_radius = 5E4*Pa
7   kinematic_hardening_rate = 0.0*Pa
8   isotropic_hardening_rate = 2E6 *Pa ;
9 define NDMaterial constitutive integration algorithm Backward_Euler
10  yield_function_relative_tolerance = 1E-2
11  stress_relative_tolerance = 1E-3
12  maximum_iterations = 30;
13 simulate constitutive testing strain control uniaxial monotonic loading use ↵
    material # 1
14  confinement_strain = 0.001
15  strain_increment_size = 0.0001
16  number_of_increment = 99;
17 bye;
```

Material Response:

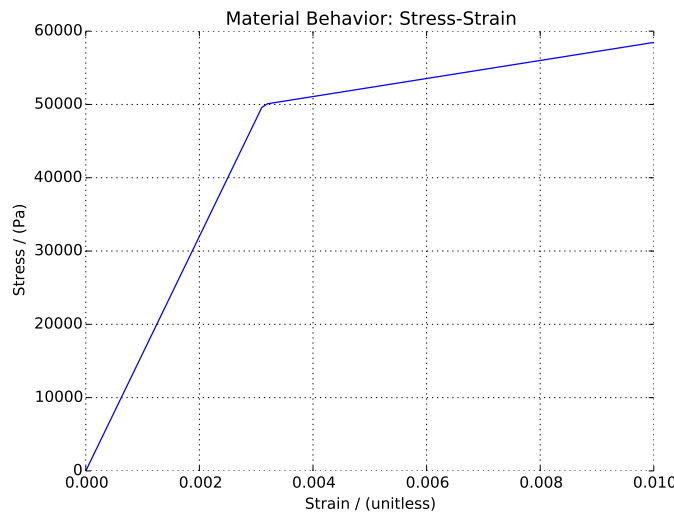


Figure 405.10: Isotropic Hardening Uniaxial Monotonic Loading

#### 405.3.2.4 Uniaxial Strain, Cyclic Loading

The Real-ESSI input files for this example are available [HERE](#). The compressed package of Real-ESSI input files and postprocessing results for this example is available [HERE](#).

Material properties in Real-ESSI input:

```

1 model name "test";
2 add material # 1 type VonMises
3   mass_density = 2E3*kg/m^3
4   elastic_modulus = 2E7 * Pa
5   poisson_ratio=0.25
6   von_mises_radius = 5E4*Pa
7   kinematic_hardening_rate = 0.0*Pa
8   isotropic_hardening_rate = 2E6 *Pa ;
9 define NDMaterial constitutive integration algorithm Backward_Euler
10  yield_function_relative_tolerance = 1E-2
11  stress_relative_tolerance = 1E-3
12  maximum_iterations = 30;
13 simulate constitutive testing strain control uniaxial cyclic loading use ↵
    material # 1
14  confinement_strain = 0.001
15  strain_increment_size = 0.0001
16  maximum_strain = 0.01
17  number_of_cycles = 1;
18 bye;
```

Material Response:

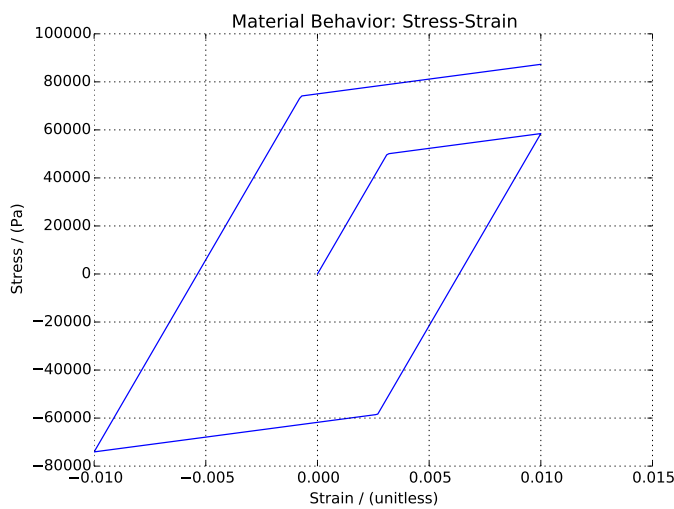


Figure 405.11: Isotropic Hardening Uniaxial Cyclic Loading

### 405.3.3 Elastic Plastic, Kinematic Hardening, Constitutive Examples

#### 405.3.3.1 Pure Shear, Monotonic Loading

The Real-ESSI input files for this example are available [HERE](#). The compressed package of Real-ESSI input files and postprocessing results for this example is available [HERE](#).

Material properties in Real-ESSI input:

```

1 model name "test";
2 add material # 1 type VonMises
3   mass_density = 2E3*kg/m^3
4   elastic_modulus = 2E7 * Pa
5   poisson_ratio=0.25
6   von_mises_radius = 1E5*Pa
7   kinematic_hardening_rate = 2E6*Pa
8   isotropic_hardening_rate = 0.0*Pa ;
9 define NDMaterial constitutive integration algorithm Backward_Euler
10  yield_function_relative_tolerance = 1E-2
11  stress_relative_tolerance = 1E-3
12  maximum_iterations = 30;
13 simulate constitutive testing strain control pure shear monotonic loading use ←
    material # 1
14  confinement_strain = 0.001
15  strain_increment_size = 0.0001
16  number_of_increment = 99;
17 bye;
```

Material Response:

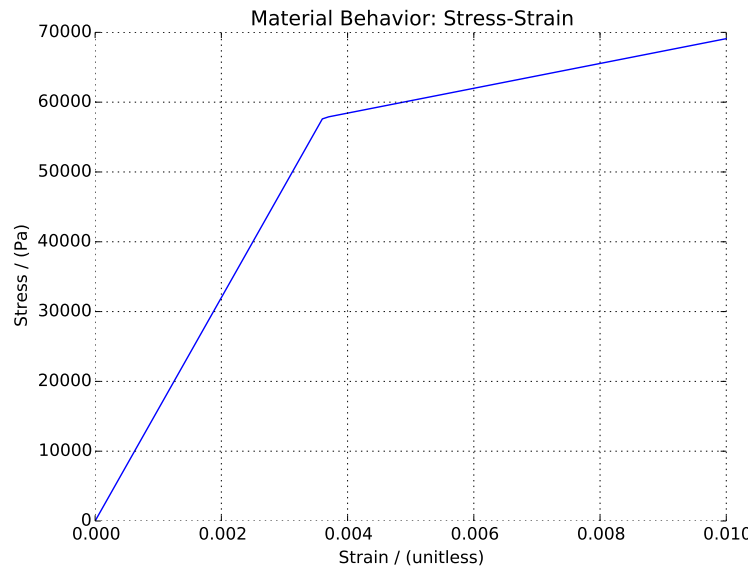


Figure 405.12: Kinematic Hardening Monotonic Cyclic Loading

#### 405.3.3.2 Pure Shear, Cyclic Loading

The Real-ESSI input files for this example are available [HERE](#). The compressed package of Real-ESSI input files and postprocessing results for this example is available [HERE](#).

Material properties in Real-ESSI input:

```

1 model name "test";
2 add material # 1 type VonMises
3   mass_density = 2E3*kg/m^3
4   elastic_modulus = 2E7 * Pa
5   poisson_ratio=0.25
6   von_mises_radius = 1E5*Pa
7   kinematic_hardening_rate = 2E6*Pa
8   isotropic_hardening_rate = 0.0*Pa ;
9 define NDMaterial constitutive integration algorithm Backward_Euler
10  yield_function_relative_tolerance = 1E-2
11  stress_relative_tolerance = 1E-3
12  maximum_iterations = 30;
13 simulate constitutive testing strain control pure shear cyclic loading use ←
    material # 1
14  confinement_strain = 0.001
15  strain_increment_size = 0.0001
16  maximum_strain = 0.01
17  number_of_cycles = 1;
18 bye;
```

Material Response:

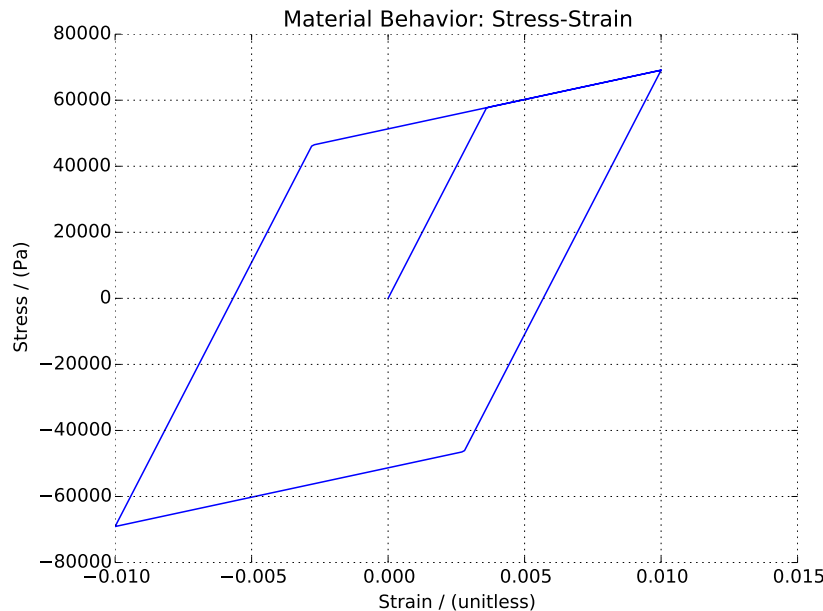


Figure 405.13: Kinematic Hardening Pure Shear Cyclic Loading.

#### 405.3.3.3 Uniaxial Strain, Monotonic Loading

The Real-ESSI input files for this example are available [HERE](#). The compressed package of Real-ESSI input files and postprocessing results for this example is available [HERE](#).

Material properties in Real-ESSI input:

```
1 model name "test";
2 add material # 1 type VonMises
3   mass_density = 2E3*kg/m^3
4   elastic_modulus = 2E7 * Pa
5   poisson_ratio=0.25
6   von_mises_radius = 5E4*Pa
7   kinematic_hardening_rate = 2E6*Pa
8   isotropic_hardening_rate = 0.0*Pa ;
9 define NDMaterial constitutive integration algorithm Backward_Euler
10  yield_function_relative_tolerance = 1E-2
11  stress_relative_tolerance = 1E-3
12  maximum_iterations = 30;
13 simulate constitutive testing strain control uniaxial monotonic loading use ↵
    material # 1
14  confinement_strain = 0.001
15  strain_increment_size = 0.0001
16  number_of_increment = 99;
17 bye;
```

Material Response:

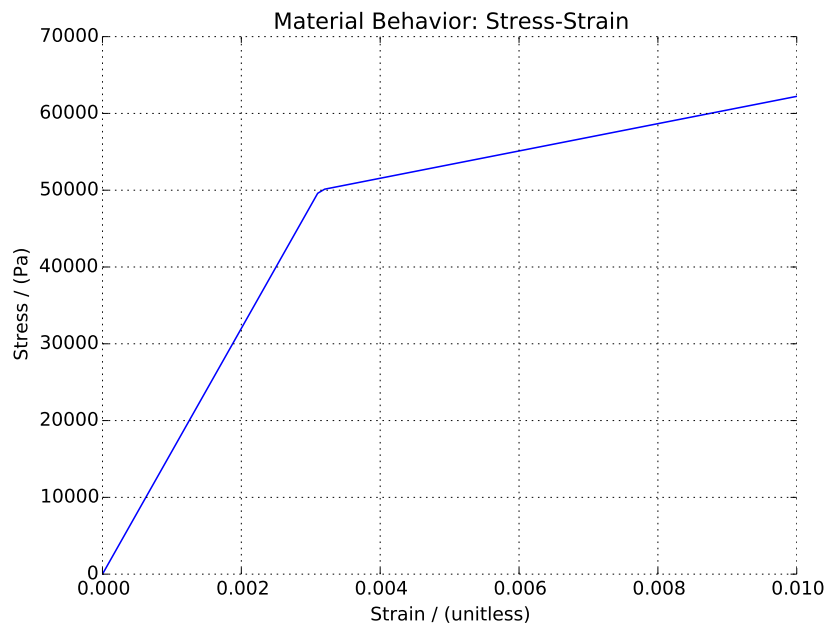


Figure 405.14: Kinematic Hardening Uniaxial Monotonic Loading

#### 405.3.3.4 Uniaxial Strain, Cyclic Loading

The Real-ESSI input files for this example are available [HERE](#). The compressed package of Real-ESSI input files and postprocessing results for this example is available [HERE](#).

Material properties in Real-ESSI input:

```

1 model name "test";
2 add material # 1 type VonMises
3   mass_density = 2E3*kg/m^3
4   elastic_modulus = 2E7 * Pa
5   poisson_ratio=0.25
6   von_mises_radius = 5E4*Pa
7   kinematic_hardening_rate = 2E6*Pa
8   isotropic_hardening_rate = 0.0*Pa ;
9 define NDMaterial constitutive integration algorithm Backward_Euler
10  yield_function_relative_tolerance = 1E-2
11  stress_relative_tolerance = 1E-3
12  maximum_iterations = 30;
13 simulate constitutive testing strain control uniaxial cyclic loading use ↵
    material # 1
14  confinement_strain = 0.001
15  strain_increment_size = 0.0001
16  maximum_strain = 0.01
17  number_of_cycles = 1;
18 bye;
```

Material Response:

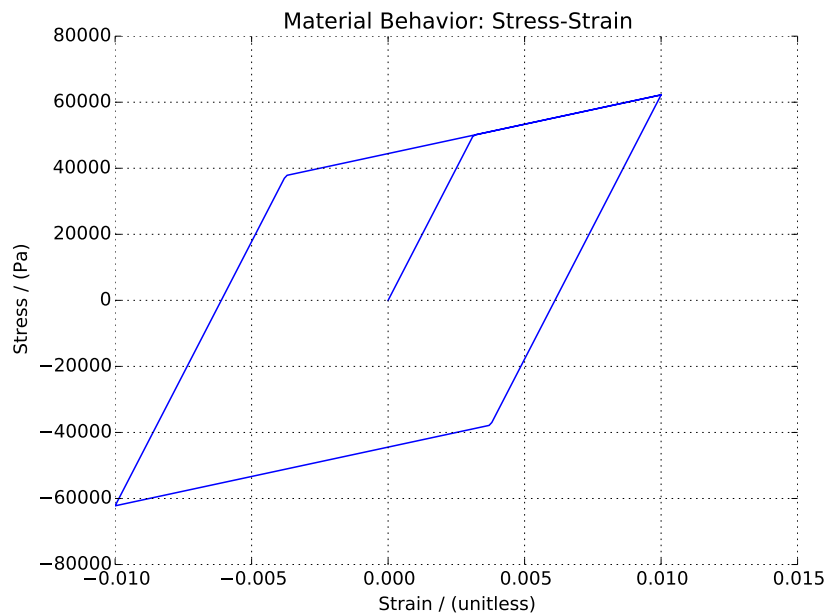


Figure 405.15: Kinematic Hardening Uniaxial Cyclic Loading

#### 405.3.4 Elastic Plastic, Armstrong-Frederick, von-Mises, Constitutive Examples

##### 405.3.4.1 Pure Shear, Cyclic Loading

The Real-ESSI input files for this example are available [HERE](#). The compressed package of Real-ESSI input files and postprocessing results for this example is available [HERE](#).

Material properties in Real-ESSI input:

```

1 model name "vmaf";
2 add material # 1 type vonMisesArmstrongFrederick
3   mass_density = 0.0*kg/m^3
4   elastic_modulus = 2E7*N/m^2
5   poisson_ratio = 0.0
6   von_mises_radius = 100 * Pa
7   armstrong_frederick_ha = 2E7*N/m^2
8   armstrong_frederick_cr = 1000
9   isotropic_hardening_rate = 0*Pa ;
10 define NDMaterial constitutive integration algorithm Backward_Euler
11   yield_function_relative_tolerance = 1E-6
12   stress_relative_tolerance = 1E-6
13   maximum_iterations = 30;
14 simulate constitutive testing strain control pure shear cyclic loading use ←
    material # 1
15   confinement_strain = 0.001
16   strain_increment_size = 0.0001
17   maximum_strain = 0.01
18   number_of_cycles = 1;
19 bye;
```

Material Response:

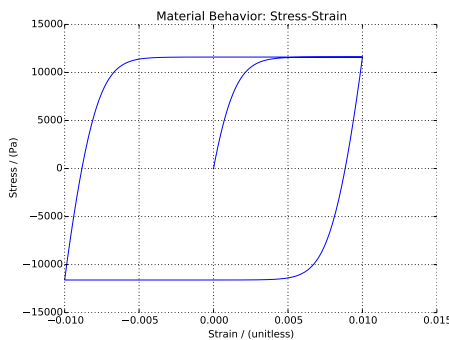


Figure 405.16: Material von-Mises Armstrong-Frederick under Pure Shear Cyclic Loading.

### 405.3.5 Elastic Plastic, Armstrong-Frederick, Drucker-Prager, Constitutive Examples

#### 405.3.5.1 Pure Shear, Cyclic Loading

The Real-ESSI input files for this example are available [HERE](#). The compressed package of Real-ESSI input files and postprocessing results for this example is available [HERE](#).

Material properties in Real-ESSI input:

```
1 model name "test";
2 phi = 5;
3 phirad = pi*phi/180;
4 eta = 6*sin(phirad)/(3-sin(phirad));
5 add material # 1 type DruckerPragerNonAssociateArmstrongFrederick
6     mass_density = 0.0*kg/m^3
7     elastic_modulus = 2E7*N/m^2
8     poisson_ratio = 0.0
9     druckerprager_k = eta
10    armstrong_frederick_ha = 2E7*N/m^2
11    armstrong_frederick_cr = 100
12    isotropic_hardening_rate = 0*Pa
13    initial_confining_stress = 1*Pa
14    plastic_flow_xi = 0.0
15    plastic_flow_kd = 0.0 ;
16 define NDMaterial constitutive integration algorithm Backward_Euler
17     yield_function_relative_tolerance = 1E-6
18     stress_relative_tolerance = 1E-6
19     maximum_iterations = 30;
20 simulate constitutive testing strain control pure shear cyclic loading use ←
21     material # 1
22     confinement_strain = 0.001
23     strain_increment_size = 0.0001
24     maximum_strain = 0.01
25     number_of_cycles = 1;
26 bye;
```

Material Response:

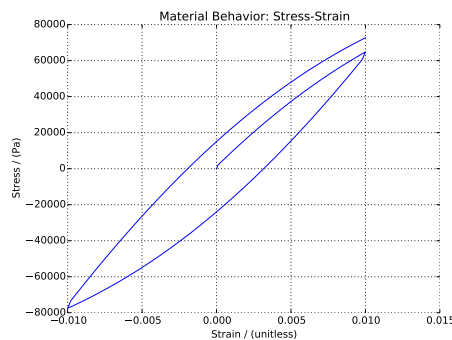


Figure 405.17: Drucker-Prager Armstrong-Frederick under Pure Shear Cyclic Loading.

### 405.3.6 Elastic Plastic, SaniSAND, Constitutive Examples

#### 405.3.6.1 Bardet Constraint Examples

The compressed package of Real-ESSI input files and postprocessing scripts and results for this example is available [HERE](#). Material Response is shown in Figure 405.18

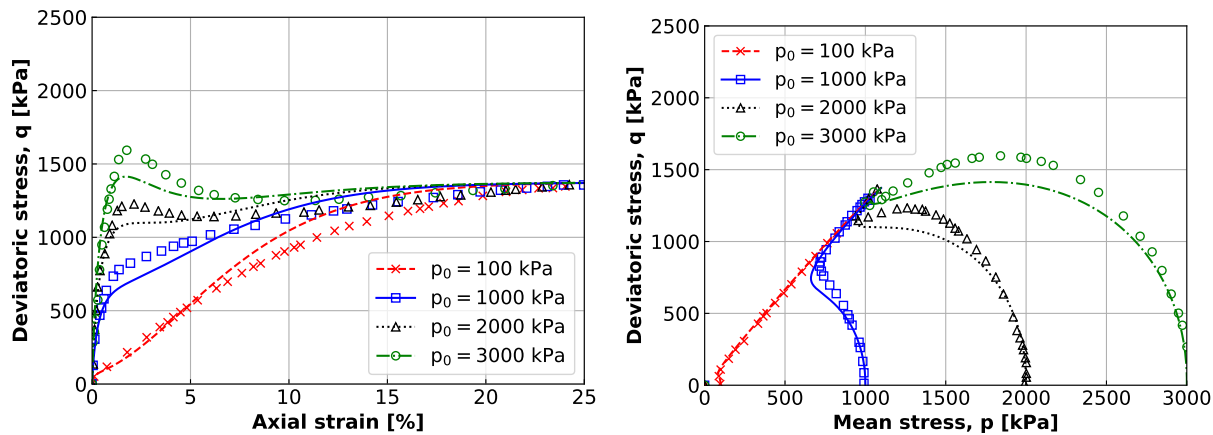


Figure 405.18: SaniSAND response.

## 405.4 Stiffness Reduction and Damping Curves Modeling

### 405.4.1 Multi-yield-surface von-Mises

The Real-ESSI input files for this example are available [HERE](#). The compressed package of Real-ESSI input files and postprocessing results for this example is available [HERE](#).

#### 405.4.1.1 Model description

This model illustrates the G/Gmax input to multi-yield-surface von-Mises material. This example is based on one Gauss-point with multi-yield-surface von-Mises material. The G/Gmax is converted to material modeling parameters (yield-surface size and hardening parameter) inside the DSL.

#### 405.4.1.2 Real-ESSI input file

```

1 model name "test";
2 add material # 1 type vonMisesMultipleYieldSurfaceGoverGmax
3   mass_density = 0.0*kg/m^3
4   initial_shear_modulus = 3E8 * Pa
5   poisson_ratio = 0.0
6   total_number_of_shear_modulus = 9
7   GoverGmax =
8     "1,0.995,0.966,0.873,0.787,0.467,0.320,0.109,0.063"
9   ShearStrainGamma =
10    "0,1E-6,1E-5,5E-5,1E-4, 0.0005, 0.001, 0.005, 0.01"
11    ;
12 define NDMaterial constitutive integration algorithm Backward_Euler
13   yield_function_relative_tolerance = 1E-6
14   stress_relative_tolerance = 1E-6
15   maximum_iterations = 30
16   ;
17 incr_size = 0.000001 ;
18 max_strain= 0.005 ;
19 num_of_increm = max_strain/incr_size -1 ;
20 simulate constitutive testing strain control pure shear use material # 1
21   confinement_strain = 0.0
22   strain_increment_size = incr_size
23   maximum_strain = max_strain
24   number_of_increment = num_of_increm;
25 bye;
```

Material Response at Gauss Point:

Computed G/Gmax curve exactly matches the one used for input at control points.

The difference in G/Gmax between control points can be reduced by using more than just 9 control points as in this example.

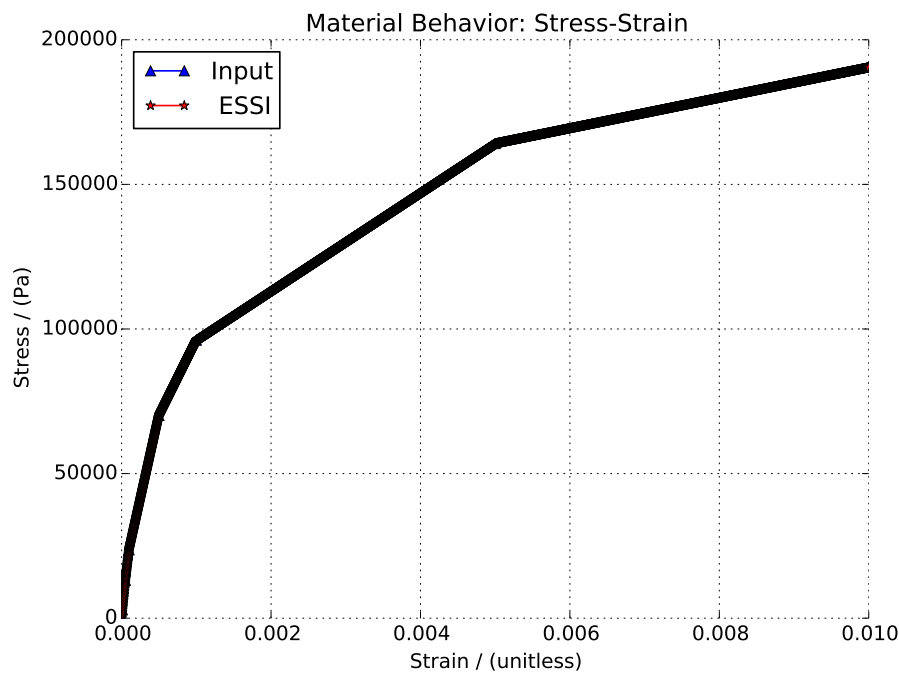


Figure 405.19: Stress-Strain Relationship

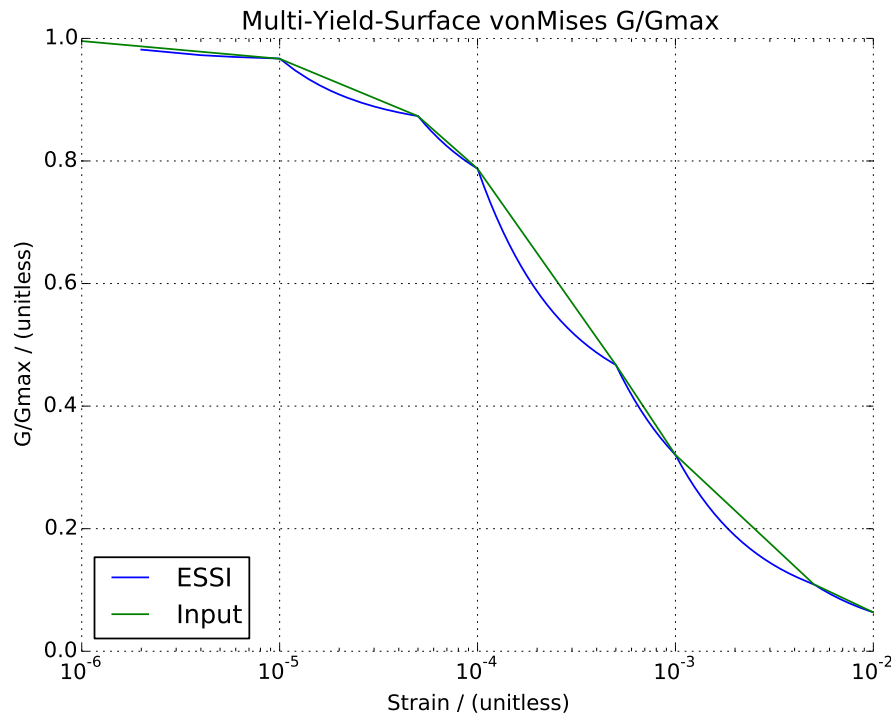


Figure 405.20: The G/Gmax results.

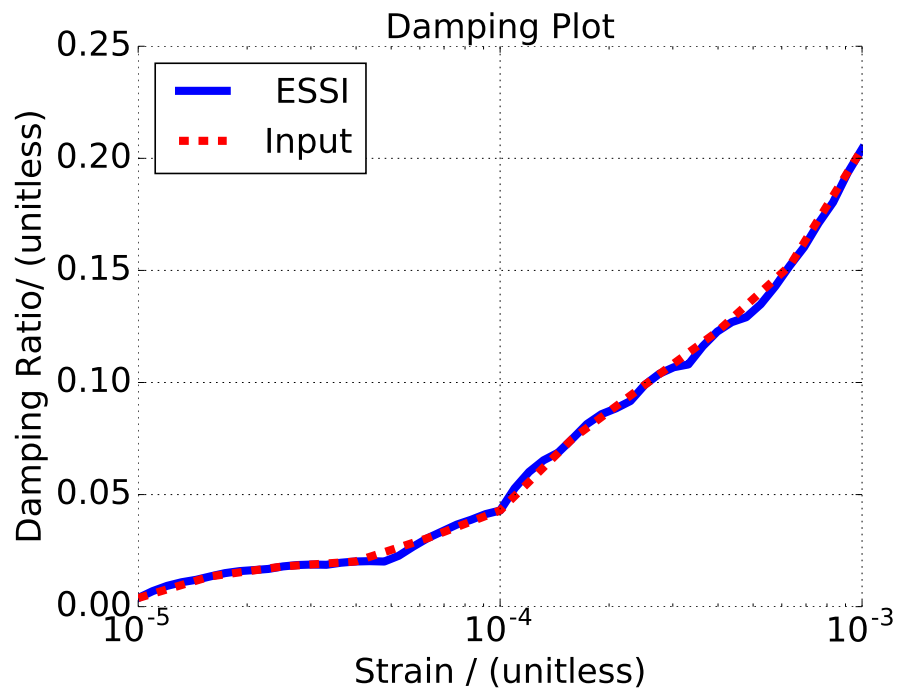


Figure 405.21: Damping Ratio Plot

## 405.4.2 Multi-yield-surface Drucker-Prager

The Real-ESSI input files for this example are available [HERE](#). The compressed package of Real-ESSI input files and postprocessing results for this example is available [HERE](#).

### 405.4.2.1 Problem description

This model illustrates the G/Gmax input to multi-yield-surface Drucker-Prager material. Purely deviatoric plastic flow is used in this material, which means that the parameter dilation\_scale is set to zero. If user wants to model change of volume (dilation or compression) for this material, then G/Gmax curve need to be iterated upon manually by changing yield surface size directly, which is done using different DruckerPragerMultipleYieldSurface command. This example is based on one Gauss-point which use multi-yield-surface Drucker-Prager material. The G/Gmax is converted to the yield-surface size and hardening parameter inside the DSL.

### 405.4.2.2 Real-ESSI input file:

```

1 model name "test";
2
3 add material # 1 type DruckerPragerMultipleYieldSurfaceGoverGmax
4     mass_density = 0.0*kg/m^3
5     initial_shear_modulus = 3E8 * Pa
6     poisson_ratio = 0.0
7     initial_confining_stress = 1E5 * Pa
8     reference_pressure = 1E5 * Pa
9     pressure_exponential_n = 0.5
10    cohesion = 0. * Pa
11    dilation_angle_eta =1.0
12    dilation_scale = 0.0
13    total_number_of_shear_modulus = 9
14    GoverGmax =
15    "1,0.995,0.966,0.873,0.787,0.467,0.320,0.109,0.063"
16    ShearStrainGamma =
17    "0,1E-6,1E-5,5E-5,1E-4, 0.0005, 0.001, 0.005, 0.01"
18    ;
19 define NDMaterial constitutive integration algorithm Backward_Euler
20     yield_function_relative_tolerance = 1E-6
21     stress_relative_tolerance = 1E-6
22     maximum_iterations = 30;
23 simulate constitutive testing strain control pure shear use material # 1
24     confinement_strain = 0.0
25     strain_increment_size = 0.000001
26     maximum_strain = 0.005
27     number_of_increment = 0.005 / 0.000001 -1 ;
28 bye;
```

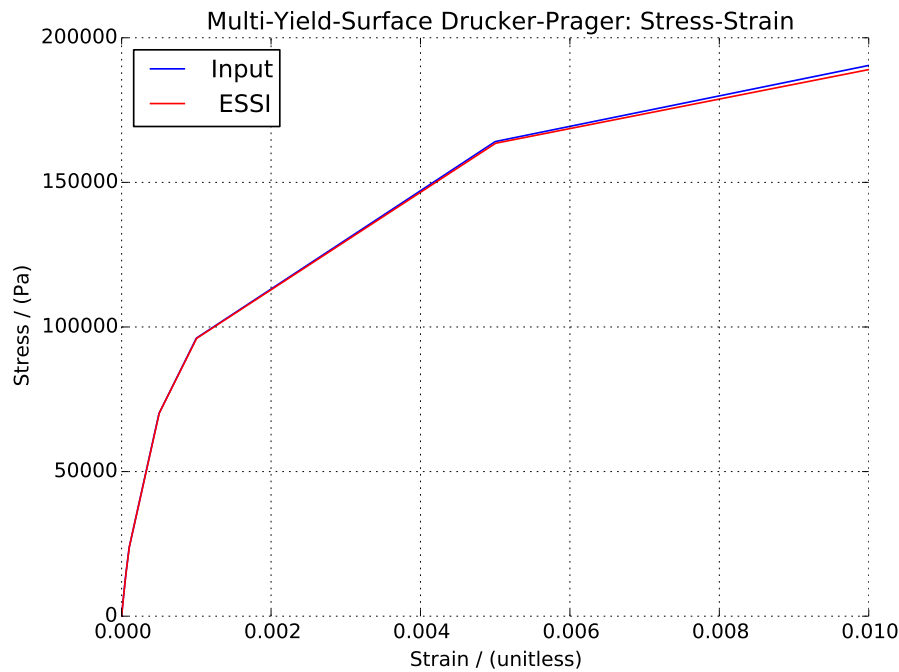


Figure 405.22: Nested-Yield-Surface Drucker-Prager Stress-Strain Relationship

Inside the DSL, the yield surface radius is calculated as  $\sqrt{3}\sigma_y$ , where  $\sigma_y$  is the yield stress of the corresponding yield surface. Then, the radius is divided by the confinement to obtain the slope (opening angle).

The hardening parameter is calculated as

$$\frac{1}{H'_i} = \frac{1}{H_i} - \frac{1}{2G} \quad (405.2)$$

where  $H'_i$  is the current hardening parameter corresponding to yield surface  $i$ .  $H_i$  is the current tangent shear modulus to surface  $i$ , namely,  $H_i = 2(\tau_{i+1} - \tau_i)/(\gamma_{i+1} - \gamma_i)$ . And  $G$  is the initial shear modulus.

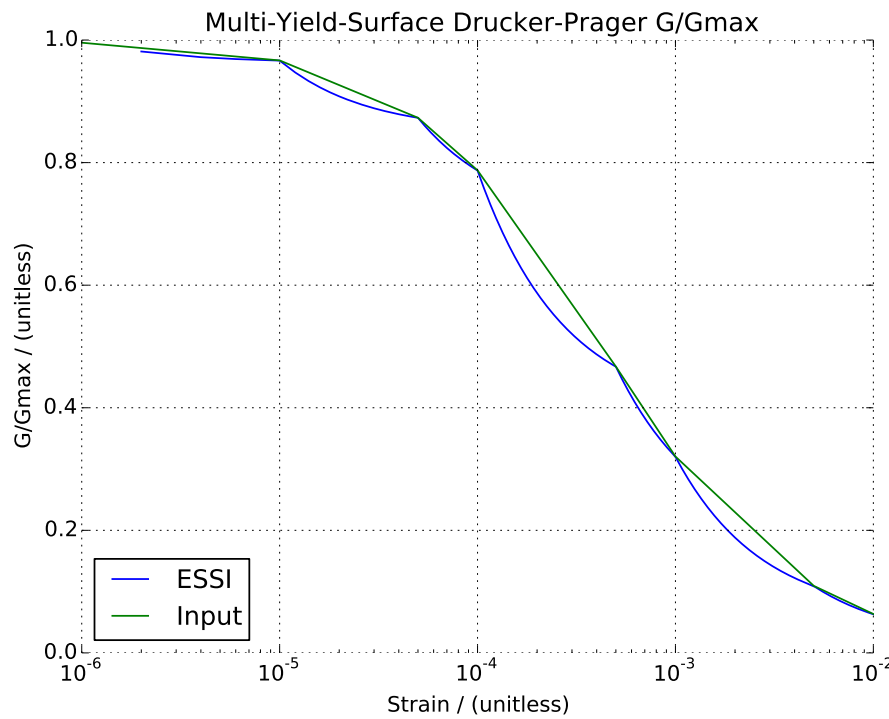


Figure 405.23: Nested-Yield-Surface Drucker-Prager G/Gmax results

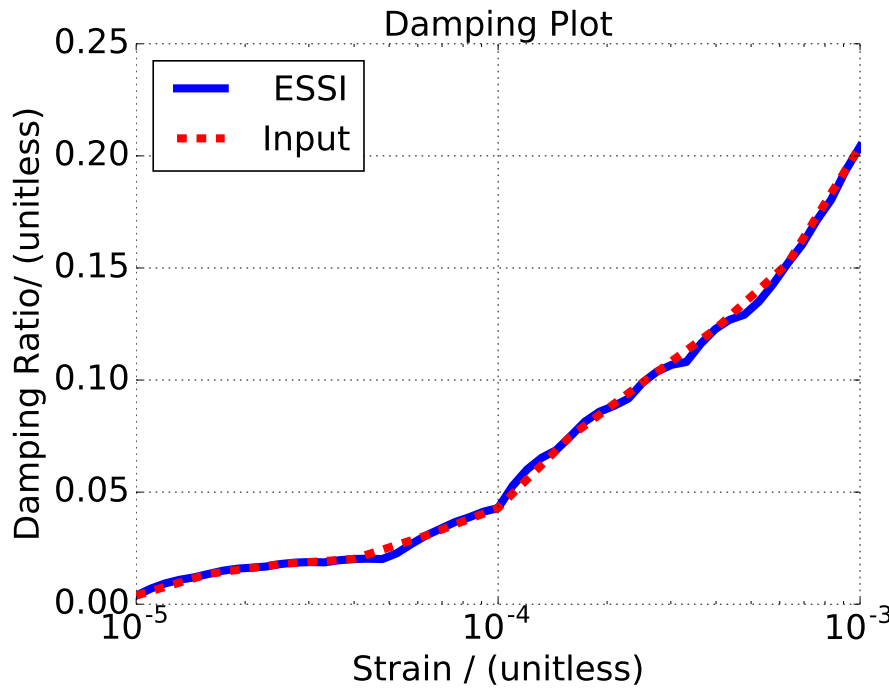


Figure 405.24: Damping Ratio Plot

### 405.4.3 Simulate Stiffness Reduction using von-Mises Armstrong-Frederick

The Real-ESSI input files for this example are available [HERE](#). The compressed package of Real-ESSI input files and postprocessing results for this example is available [HERE](#).

#### 405.4.3.1 Model description

This model illustrates the simulation of stiffness reduction using von-Mises Armstrong-Frederick. This example is based on one Gauss-point.

#### 405.4.3.2 Real-ESSI input file:

```

1 model name "test";
2
3 add material # 1 type vonMisesArmstrongFrederick
4   mass_density = 2500.0*kg/m^3
5   elastic_modulus = 3E7*N/m^2
6   poisson_ratio = 0.2
7   von_mises_radius = 300 * Pa
8   armstrong_frederick_ha = 5*3E7*N/m^2
9   armstrong_frederick_cr = 25000
10  isotropic_hardening_rate = 0*Pa
11  ;
12 define NDMaterial constitutive integration algorithm Backward_Euler
13   yield_function_relative_tolerance = 1E-6
14   stress_relative_tolerance = 1E-6
15   maximum_iterations = 30
16   ;
17 incr_size = 0.000001 ;
18 max_strain= 0.005 ;
19 num_of_increm = max_strain/incr_size -1 ;
20 simulate constitutive testing strain control pure shear use material # 1
21 confinement_strain = 0.0
22 strain_increment_size = incr_size
23 maximum_strain = max_strain
24 number_of_increment = num_of_increm;
25 bye;
```

The von-Mises Armstrong-Frederick material behavior matches the stiffness reduction curve.

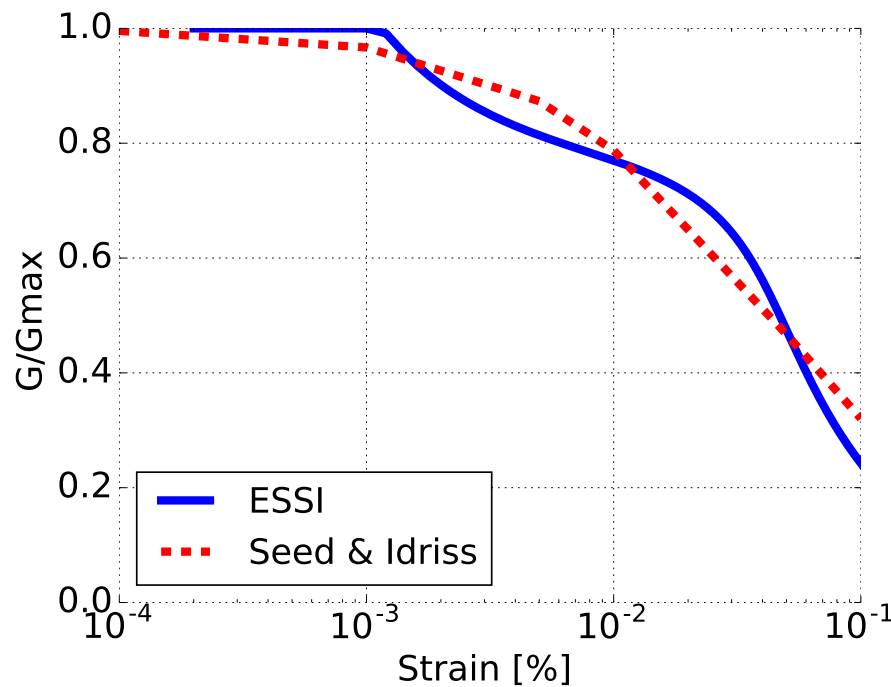


Figure 405.25: The stiffness reduction results.

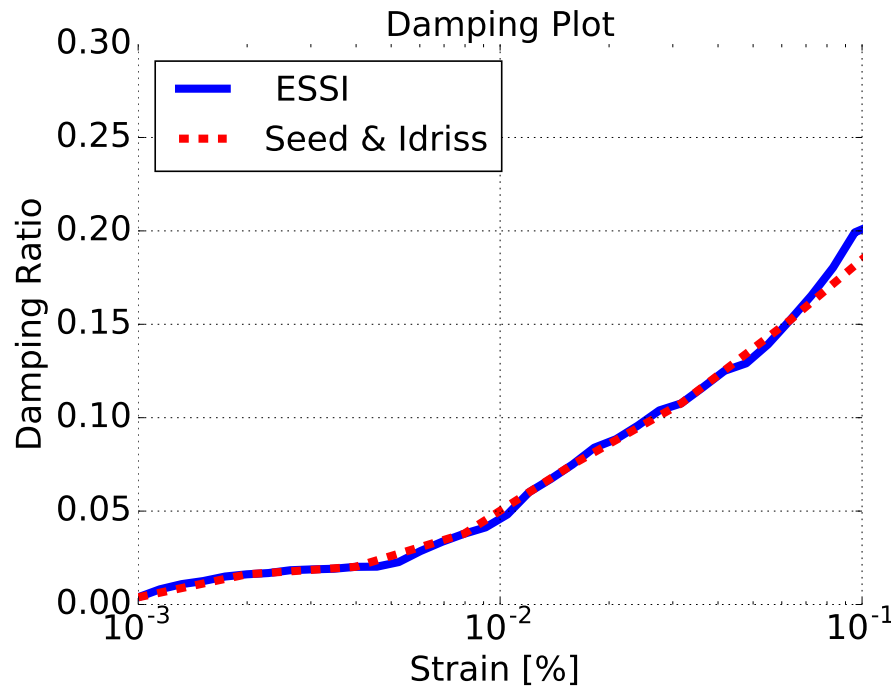


Figure 405.26: Damping Ratio Plot

## 405.5 Cosserat, Micropolar Material Modeling

#### 405.5.1 Cosserat, Micropolar Elastic Material Model (example in development)

### 405.5.2 Cosserat, Micropolar Elastic-Plastic von Mises Material Model (example in development)

405.5.3 Cosserat, Micropolar Elastic-Plastic Druekcr Prager Material Model (example in development)

# Chapter 406

## Static Examples

(2016-2017-2019-2021-)

(In collaboration with Prof. José Abell, Dr. Yuan Feng, Mr. Sumeet Kumar Sinha, and Dr. Han Yang)

### 406.1 Chapter Summary and Highlights

In this Chapter static modeling and simulation of solids and structures is illustrated through a number of examples.

All the examples described here, and many more, organized in sub-directories, for constitutive behavior, static and dynamic behavior can be directly downloaded from a repository at: [http://sokocalo.engr.ucdavis.edu/~jeremic/lecture\\_notes\\_online\\_material/Real-ESSI\\_Examples/education\\_examples](http://sokocalo.engr.ucdavis.edu/~jeremic/lecture_notes_online_material/Real-ESSI_Examples/education_examples). These examples can then be tried, analyzed using Real-ESSI Simulator that is available on Amazon Web Services (AWS) computers around the word. Login to AWS market place and search for Real-ESSI...

### 406.2 Static Elastic Solid Examples

#### 406.2.1 Statics, Bricks, with Nodal Forces

##### 406.2.1.1 Statics, 8 Node Brick, with Nodal Forces

The Real-ESSI input files for this example are available [HERE](#). The compressed package of Real-ESSI input files and postprocessing results for this example is available [HERE](#).

Problem description: a cantilever with a nodal force at the tip. Length=6m, Width=1m, Height=1m, Force=100N, E=1E8Pa,  $\nu = 0.0$ . The force direction was shown in Figure (406.1).

The mesh is generated with elastic 8 node brick.

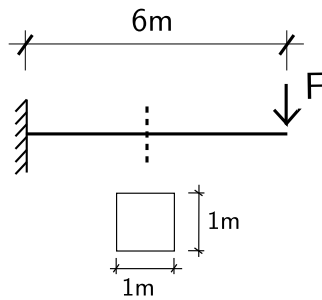


Figure 406.1: Problem description for cantilever beams.

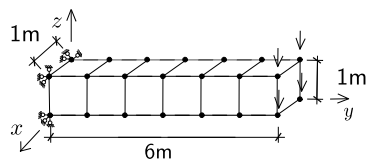


Figure 406.2: Six 8NodeBrick elements.

#### 406.2.1.2 Statics, 27 Node Brick, with Nodal Forces

The Real-ESSI input files for this example are available [HERE](#). The compressed package of Real-ESSI input files and postprocessing results for this example is available [HERE](#).

Problem description: a cantilever with a nodal force at the tip. Length=6m, Width=1m, Height=1m, Force=100N, E=1E8Pa,  $\nu = 0.0$ . The force direction was shown in Figure (406.3).

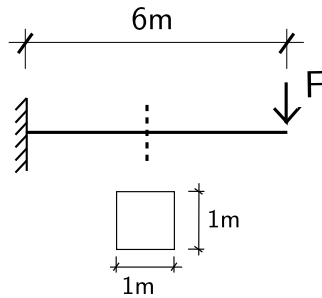


Figure 406.3: Problem description for cantilever beams.

The mesh is generated with elastic 27 node brick.

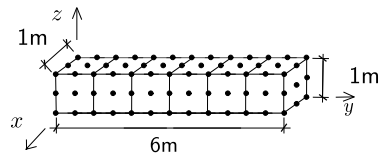


Figure 406.4: Six 27NodeBrick elements.

#### 406.2.1.3 Statics, 8-27 Node Brick, with Nodal Forces

The Real-ESSI input files for this example are available [HERE](#). The compressed package of Real-ESSI input files and postprocessing results for this example is available [HERE](#).

Problem description: a cantilever with a nodal force at the tip. Length=2m, Width=2m, Height=2m,  $\nu = 0.0$ . The force direction was shown in Figure (406.5).

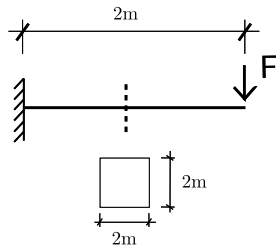


Figure 406.5: Problem description for cantilever beams.

The mesh is generated with an elastic 8-27 node brick. As shown in the Figure 406.16, some of the nodes are missing on purpose. The variable node brick element is usually used as the transition mesh between 8 node brick and 27 node brick.

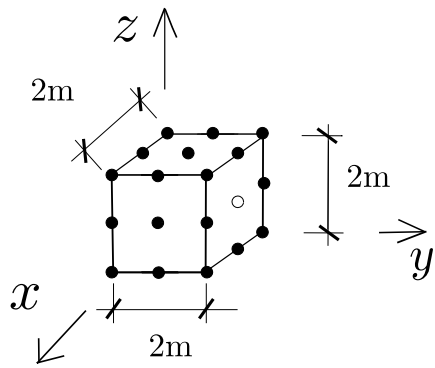


Figure 406.6: One 8-27 Node elements.

## 406.2.2 Statics, Bricks, with Surface Loads

### 406.2.2.1 Statics, 8 Node Brick, with Surface Forces

The Real-ESSI input files for this example are available [HERE](#). The compressed package of Real-ESSI input files and postprocessing results for this example is available [HERE](#).

Problem description: a cantilever with the load on one surface. Length=2m, Width=2m, Height=2m,  $\nu = 0.0$ . The force distribution was shown in Figure (406.7).

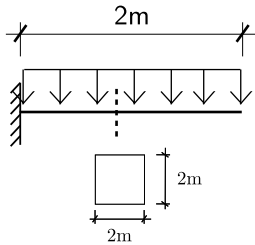


Figure 406.7: Problem description for cantilever beams.

The mesh is generated with an elastic 8 node brick.

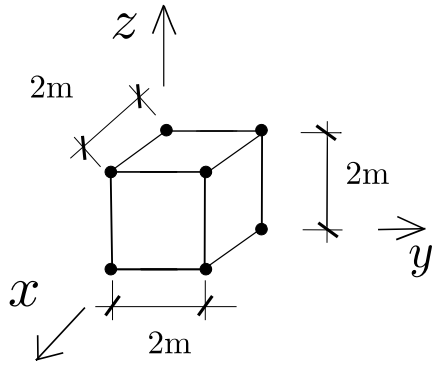


Figure 406.8: One element with surface load.

### 406.2.2.2 Statics, 27 Node Brick, with Surface Forces

The Real-ESSI input files for this example are available [HERE](#). The compressed package of Real-ESSI input files and postprocessing results for this example is available [HERE](#).

Problem description: a cantilever with the load on one surface. Length=2m, Width=2m, Height=2m.

The force distribution was shown in Figure (406.9).

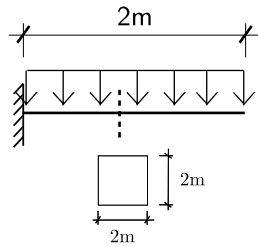


Figure 406.9: Problem description for cantilever beams.

The mesh is generated with an elastic 27 node brick.

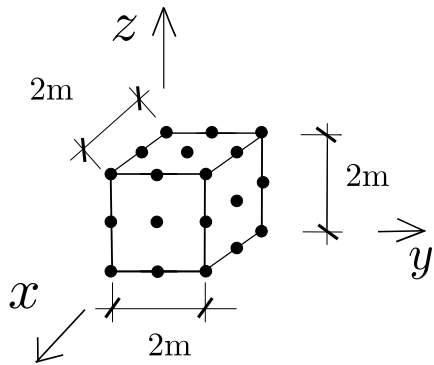


Figure 406.10: One element with surface load.

### 406.2.3 Statics, Bricks, with Body Forces

#### 406.2.3.1 Statics, 8 Node Brick, with Body Forces

The Real-ESSI input files for this example are available [HERE](#). The compressed package of Real-ESSI input files and postprocessing results for this example is available [HERE](#).

Problem description: a cantilever with self weight on the whole element. Length=6m, Width=1m, Height=1m,  $\nu = 0.3$ . The force direction was shown in Figure (406.11).

The mesh is generated with an elastic 8 node brick.

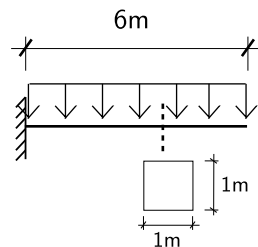


Figure 406.11: Problem description for cantilever beams.

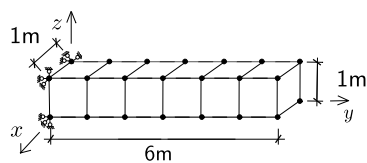


Figure 406.12: Six 8NodeBrick elements.

#### 406.2.3.2 Statics, 27 Node Brick, with Body Forces

The Real-ESSI input files for this example are available [HERE](#). The compressed package of Real-ESSI input files and postprocessing results for this example is available [HERE](#).

Problem description: a cantilever with self weight on the whole element. Length=6m, Width=1m, Height=1m,  $\nu = 0.3$ . The force direction was shown in Figure (406.13).

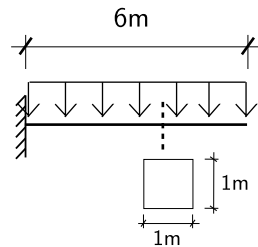


Figure 406.13: Problem description for cantilever beams.

The mesh is generated with an elastic 27 node brick.

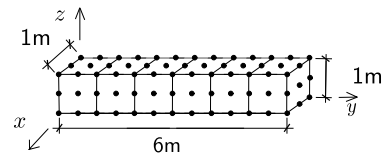


Figure 406.14: Six 27NodeBrick elements.

### 406.2.3.3 Statics, 8-27 Node Brick, with Body Forces

The Real-ESSI input files for this example are available [HERE](#). The compressed package of Real-ESSI input files and postprocessing results for this example is available [HERE](#).

Problem description: a cantilever with self weight on the whole element. Length=2m, Width=2m, Height=2m,  $\nu = 0.3$ . The force direction was shown in Figure (406.15).

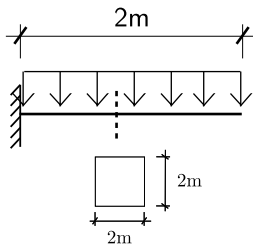


Figure 406.15: Problem description for cantilever beams.

The mesh is generated with an elastic 8-27 node brick. As shown in the Figure 406.16, some of the nodes are missing on purpose. The variable node brick element is usually used as the transition mesh between 8 node brick and 27 node brick.

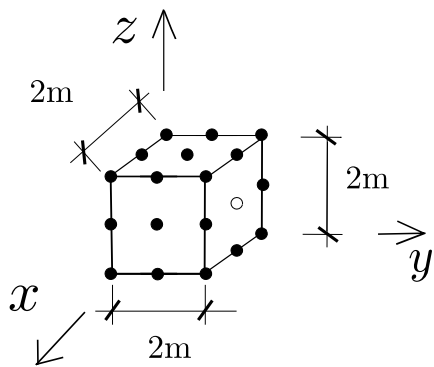


Figure 406.16: One variable Node Brick elements.

## 406.3 Static Elastic Structural Examples

### 406.3.1 Statics, Truss, with Nodal Forces

The Real-ESSI input files for this example are available [HERE](#). The compressed package of Real-ESSI input files and postprocessing results for this example is available [HERE](#).

Problem description: a cantilever with the nodal load on the tip. Length=1m, Cross Section= $1\text{m}^2$ . The cross section shape is not necessarily a square. The force direction was shown in Figure (406.17). Truss only takes axial force.

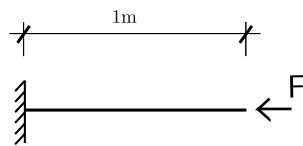


Figure 406.17: Problem description for a cantilever.

### 406.3.2 Statics, Elastic Beam, with Nodal Forces

The Real-ESSI input files for this example are available [HERE](#). The compressed package of Real-ESSI input files and postprocessing results for this example is available [HERE](#).

Problem description: a cantilever with nodal load on the tip. Length=1m, Width=1m, Height=1m,  $E=1Pa$ . The force direction was shown in Figure (406.18).

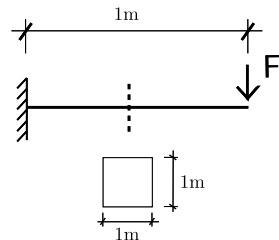


Figure 406.18: Problem description for cantilever beams.

### 406.3.3 Statics, Elastic Beam, with Body Forces

The Real-ESSI input files for this example are available [HERE](#). The compressed package of Real-ESSI input files and postprocessing results for this example is available [HERE](#).

Problem description: a cantilever with self weight. Length=1m, Width=1m, and Height=1m. The force direction was shown in Figure ([406.19](#)).

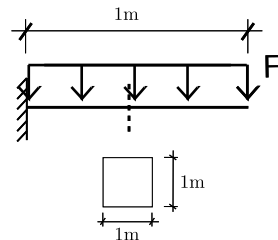


Figure 406.19: Problem description for cantilever beams.

#### 406.3.4 Statics, ShearBeam Element

##### 406.3.4.1 Problem description

The Real-ESSI input files for this example are available [HERE](#). The compressed package of Real-ESSI input files and postprocessing results for this example is available [HERE](#).

In the element type "ShearBeam", only one Gauss point exists. ShearBeam element was used here to test the von Mises Armstrong-Frederickó material model. Vertical force  $F_z$  was used to apply confinement to the element. Then, cyclic force  $F_x$  is used to load. Usually, pressure-dependent materials, like Drucker-Prager, require the confinement. The pressure-independent materials, like von Mises, do not require the confinement.

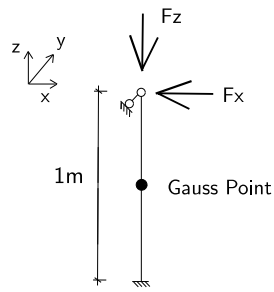


Figure 406.20: ShearBeam element.

##### 406.3.4.2 Results

Resulting stress-strain relationship is shown in Fig.([707.51](#)).

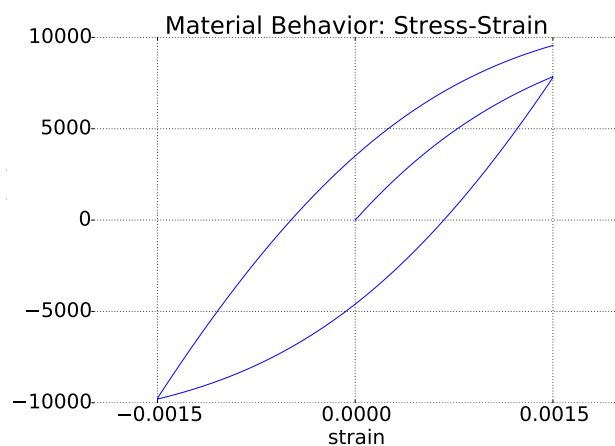


Figure 406.21: Shear stress-strain response.

### 406.3.5 Statics, Elastic Shell, with Nodal Forces

#### 406.3.5.1 ANDES Shell, out of Plane Force

The Real-ESSI input files for this example are available [HERE](#). The compressed package of Real-ESSI input files and postprocessing results for this example is available [HERE](#).

Problem description: Length=6m, Width=1m, Height=1m, Force=100N, E=1E8Pa,  $\nu = 0.0$ .

The force direction was shown in Figure (406.22).

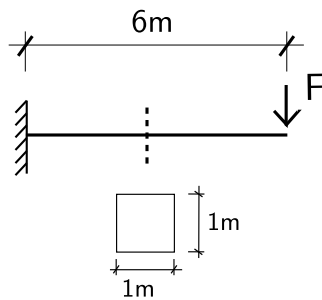


Figure 406.22: Problem description for cantilever beams.

#### 406.3.5.2 ANDES Shell, Perpendicular to Plane, bending

The mesh and the out-of-plane force is shown in Fig. 406.23.

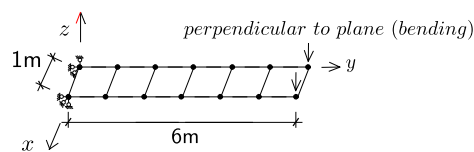


Figure 406.23: Six 4NodeANDES elements.

#### 406.3.5.3 ANDES Shell, In-plane Force

The Real-ESSI input files for this example are available [HERE](#). The compressed package of Real-ESSI input files and postprocessing results for this example is available [HERE](#).

Problem description: a cantilever with a nodal force at the tip. Length=6m, Width=1m, Height=1m, Force=100N, E=1E8Pa,  $\nu = 0.0$ . The force direction was shown in Figure (406.24).

The mesh and the inplane force is shown in Fig. 406.25.

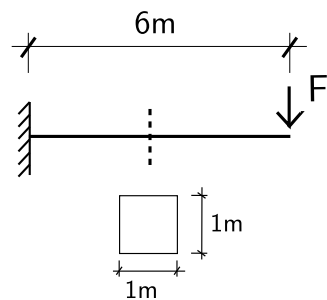


Figure 406.24: Problem description for cantilever beams.

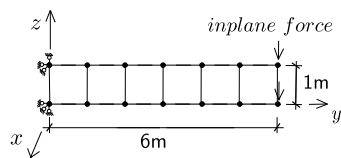


Figure 406.25: Six 4NodeANDES elements.

### 406.3.6 Statics, Elastic Shell, with Body Forces

#### 406.3.6.1 ANDES shell under the out-of-Plane Body Force

The Real-ESSI input files for this example are available [HERE](#). The compressed package of Real-ESSI input files and postprocessing results for this example is available [HERE](#).

Problem description: Length=6m, Width=1m, Height=1m, Force=100N, E=1E8Pa,  $\nu = 0.0$ . The force direction was shown in Figure (406.26).

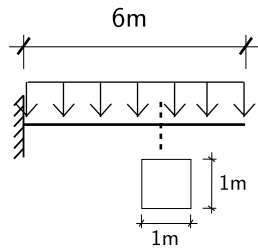


Figure 406.26: Problem description for cantilever beams.

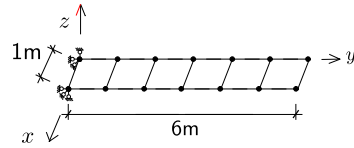


Figure 406.27: Six 4NodeANDES elements.

#### 406.3.6.2 ANDES Shell, In-plane Body Force

The Real-ESSI input files for this example are available [HERE](#). The compressed package of Real-ESSI input files and postprocessing results for this example is available [HERE](#).

Problem description: a cantilever with a nodal force at the tip. Length=6m, Width=1m, Height=1m, Force=100N, E=1E8Pa,  $\nu = 0.0$ . The force direction was shown in Figure (406.28).

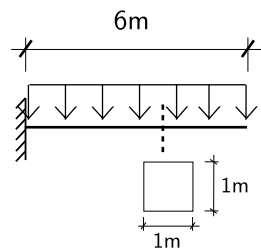


Figure 406.28: Problem description for cantilever beams.

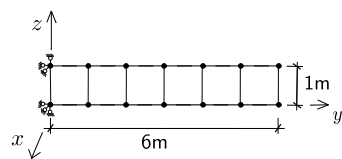


Figure 406.29: Six 4NodeANDES elements.

## 406.4 Statics, Interface/Contact Elements

### 406.4.1 Statics, Two Bar Normal Interface/Contact Problem Under Monotonic Loading.

The Real-ESSI input files for this example are available [HERE](#). The compressed package of Real-ESSI input files and postprocessing results for this example is available [HERE](#).

This is an example of normal monotonic loading on a 1-D contact/interface between two bars separated by an initial gap of 0.1 unit. An illustrative diagram of the problem statement is shown below.

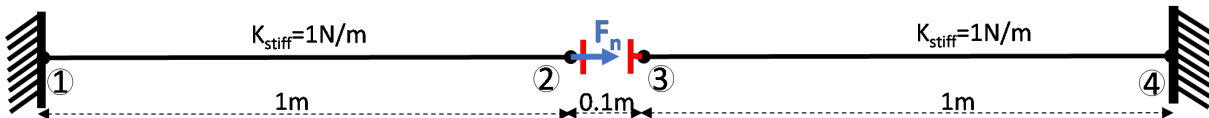


Figure 406.30: Illustration of Two Bar Normal Interface/Contact Problem under monotonic loading with initial gap.

The displacement output of *Node 2* and *Node 3* are shown below.

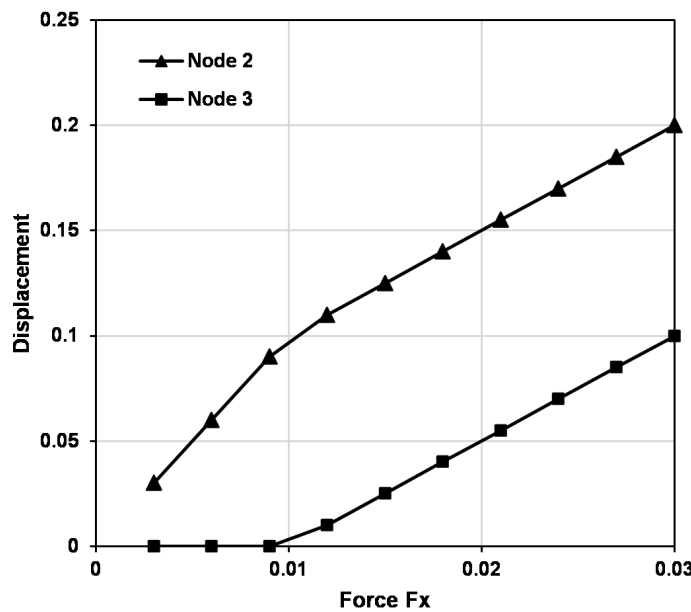


Figure 406.31: Displacement of Nodes 2 and 3.

#### 406.4.2 Statics, Four Bar Interface/Contact Problem With Normal and Shear Force Under Monotonic Loading

The Real-ESSI input files for this example are available [HERE](#). The compressed package of Real-ESSI input files and postprocessing results for this example is available [HERE](#).

This is an example to show the normal and tangential behavior (stick and slip case) of contacts using four bars in 2-D plane. The bars in x-directions are in contact/interface (initial gap=0).

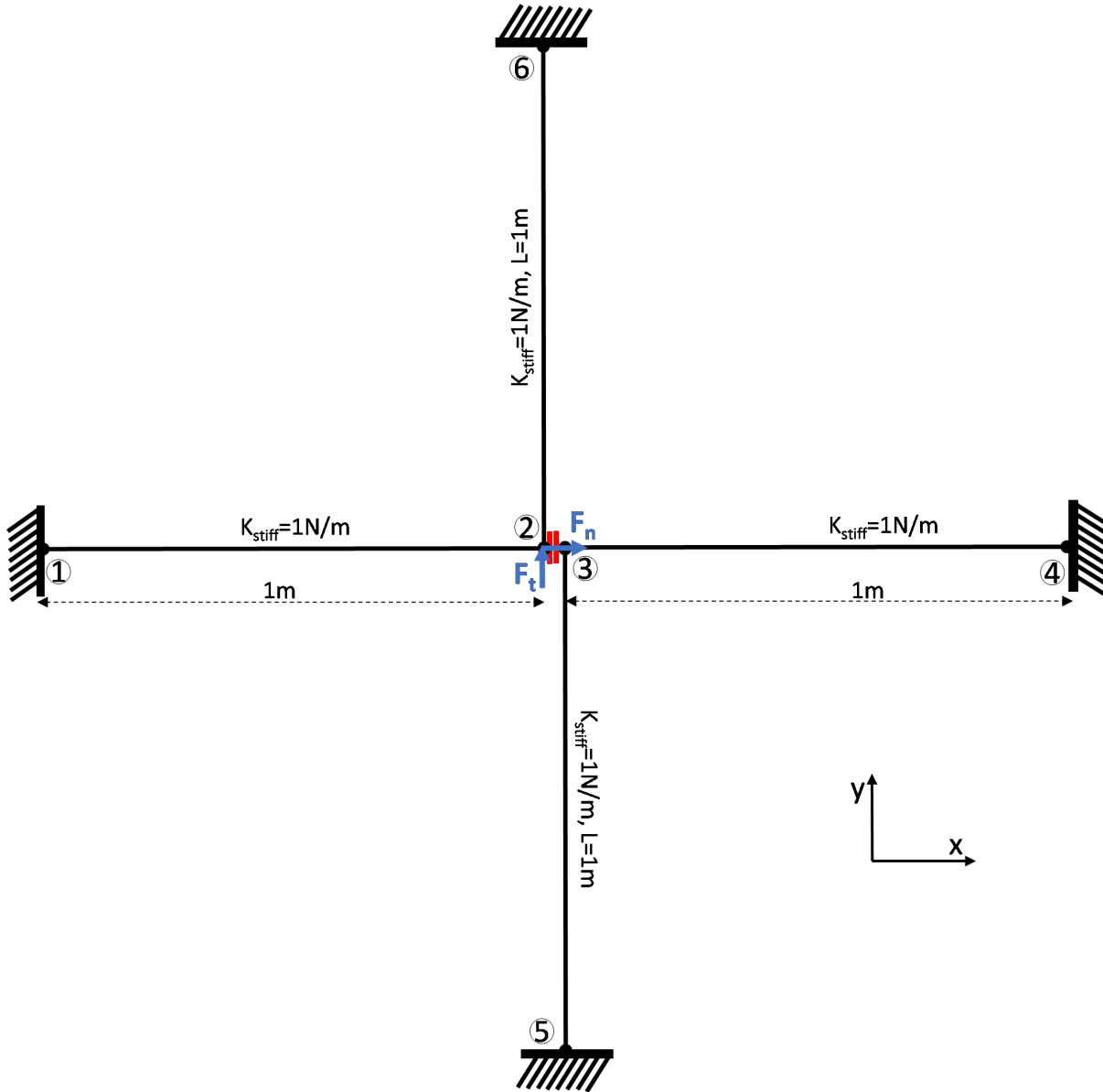


Figure 406.32: Illustration of Four Bar Normal Interface/Contact Problem With Normal and Shear Force Under Monotonic Loading with no initial gap.

The displacement output of *Node 2* and *Node 3* are shown below.

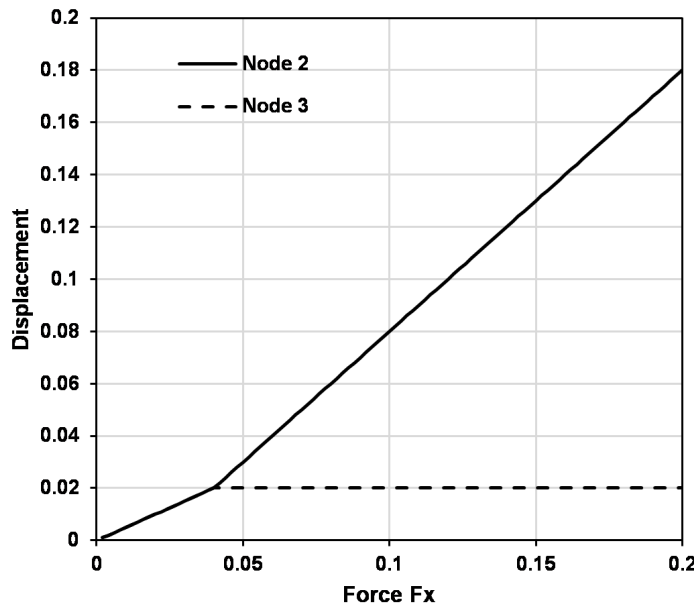


Figure 406.33: Displacement of Nodes 2 and 3 along y direction.

#### 406.4.3 Statics, 3-D Truss example with normal confinement and Shear Loading

The Real-ESSI input files for this example are available [HERE](#). The compressed package of Real-ESSI input files and postprocessing results for this example is available [HERE](#).

A simple 3-D truss example with Normal confinement in z-direction of  $F_N = 0.5N$ , friction coefficient  $\mu = 0.2$  and shear loading of magnitude  $F_s = 0.5N$ . Figure 707.57 below, shows the description of the problem.

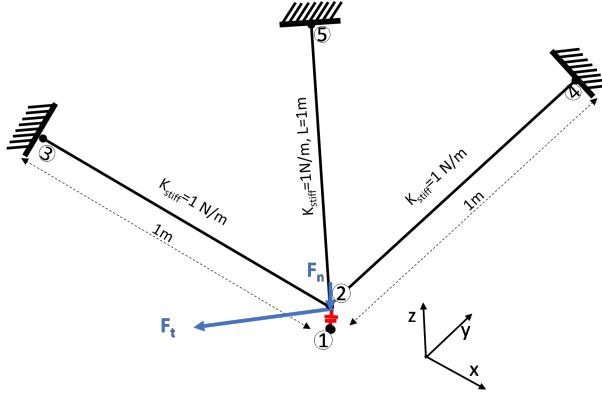


Figure 406.34: Illustration of 3-D Truss Problem with confinement loading in z-direction of 0.5N and then shear loading of 0.5N in x-y plane.

The generalized displacement response of the tangential loading stage is shown below.

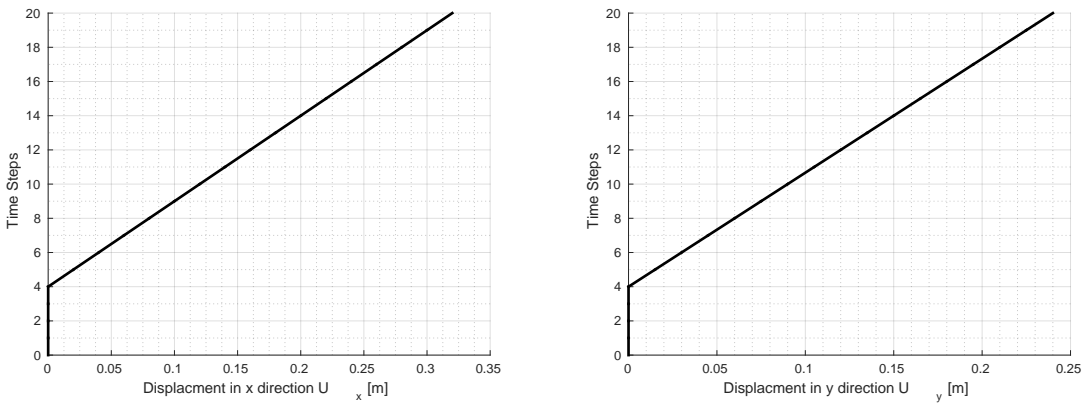


Figure 406.35: Displacements of Node 2 with applied shear tangential load step.

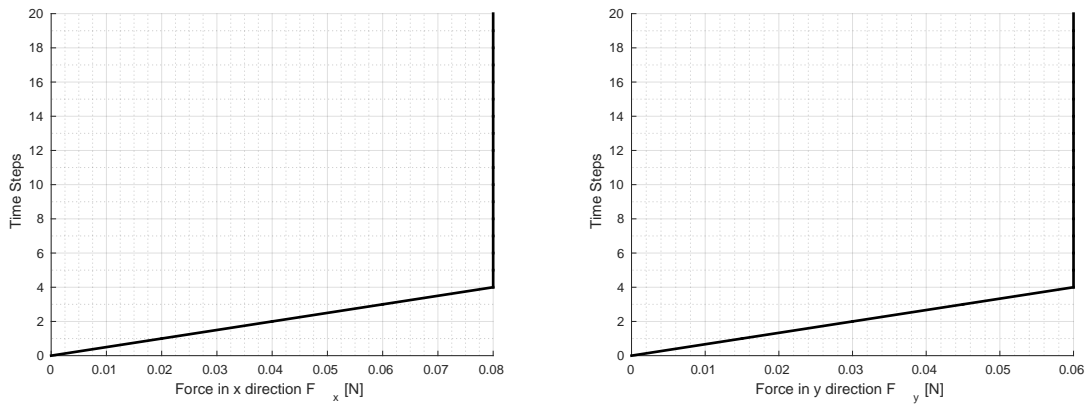


Figure 406.36: Resisting force by the contact/interface element with applied shear tangential load step.

#### 406.4.4 Statics, Six Solid Blocks Example With Interface/Contact

The Real-ESSI input files for this example are available [HERE](#). The compressed package of Real-ESSI input files and postprocessing results for this example is available [HERE](#).

This is a 3-D solid block example with initial normal and then tangential load on different surfaces as shown below.

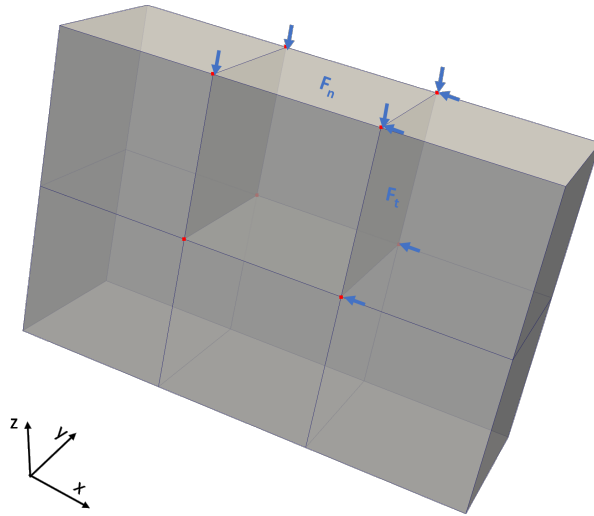


Figure 406.37: Illustration of Six Solid Blocks Example with Interface/Contact with first normal and then tangential loading stages.

The generalized displacement field of the two loading stages *normal loading* and *tangential loading* is shown below..

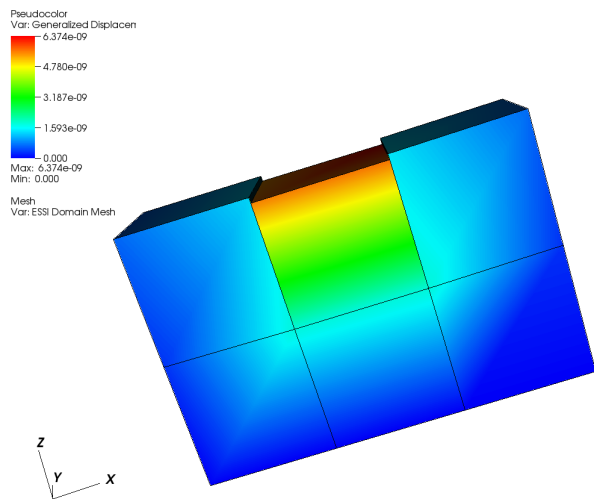


Figure 406.38: Generalized displacement magnitude visualization of normal loading.

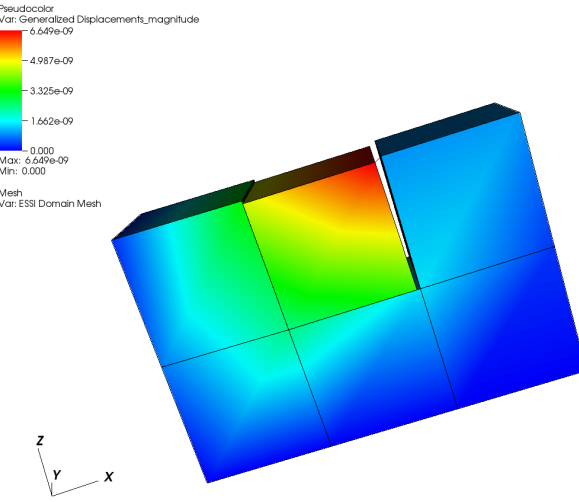


Figure 406.39: Generalized displacement magnitude visualization of tangential loading.

## 406.5 Static Inelastic Solid Examples

### 406.5.1 Statics, Bricks, Elastic-Plastic, von Mises, with Nodal Forces

The Real-ESSI input files for this example are available [HERE](#). The compressed package of Real-ESSI input files and postprocessing results for this example is available [HERE](#).

Model Description:

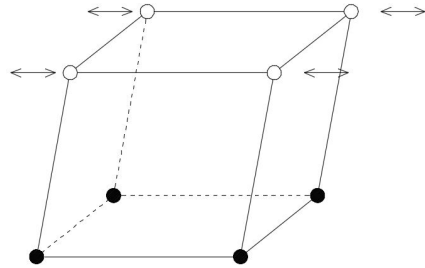


Figure 406.40: Perfectly Plastic Pure Shear Cyclic Loading.

Material Response at Gauss Point:

### 406.5.2 Statics, Bricks, Elastic-Plastic, Drucker Prager, with Nodal Forces

The Real-ESSI input files for this example are available [HERE](#). The compressed package of Real-ESSI input files and postprocessing results for this example is available [HERE](#).

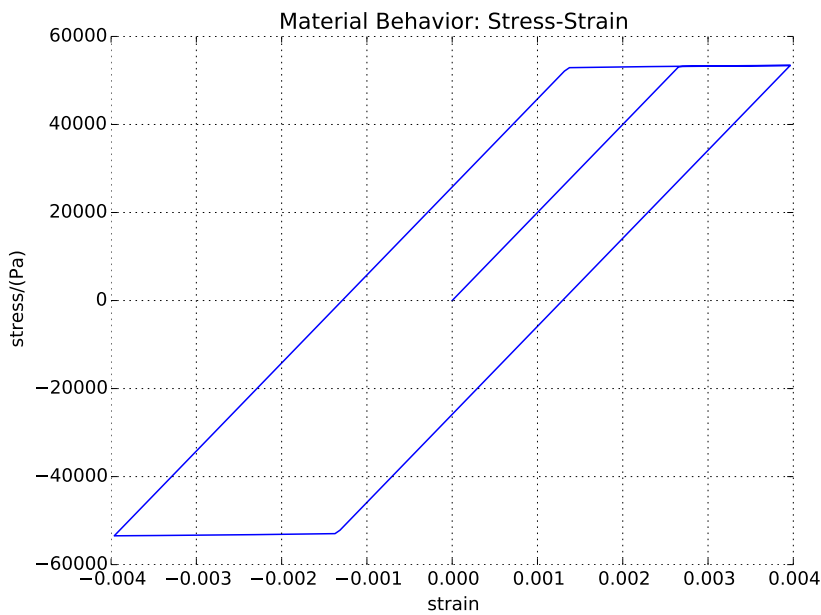


Figure 406.41: Results of Perfectly Plastic Pure Shear Cyclic Loading.

Model Description:

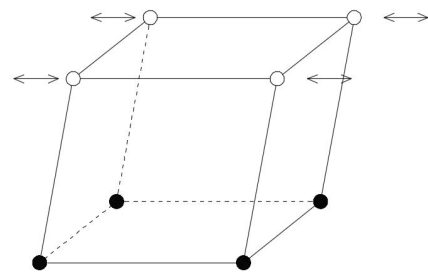


Figure 406.42: Diagram of Drucker-Prager Armstrong-Frederick Pure Shear Cyclic Loading.

Material Response at Gauss Point:

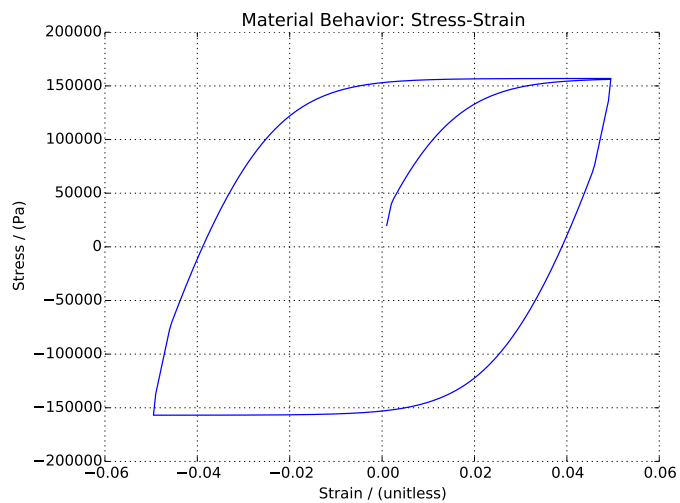


Figure 406.43: Result of Drucker-Prager Armstrong-Frederick Pure Shear Cyclic Loading.

## 406.6 Static Inelastic Shell Examples (example in development)

## 406.7 Statics, Elastic Single Solid Finite Element Examples

### 406.7.1 Statics, Linear Elastic, Solid Examples

#### 406.7.1.1 Statics, Pure Shear, Monotonic Loading

The Real-ESSI input files for this example are available [HERE](#). The compressed package of Real-ESSI input files and postprocessing results for this example is available [HERE](#).

Model Description:

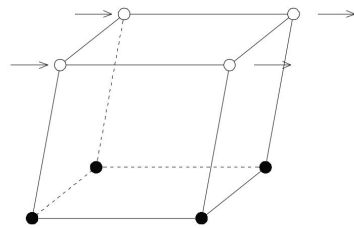


Figure 406.44: Diagram Linear Elastic Solid Pure Shear Monotonic Loading.

Material Response at Gauss Point:

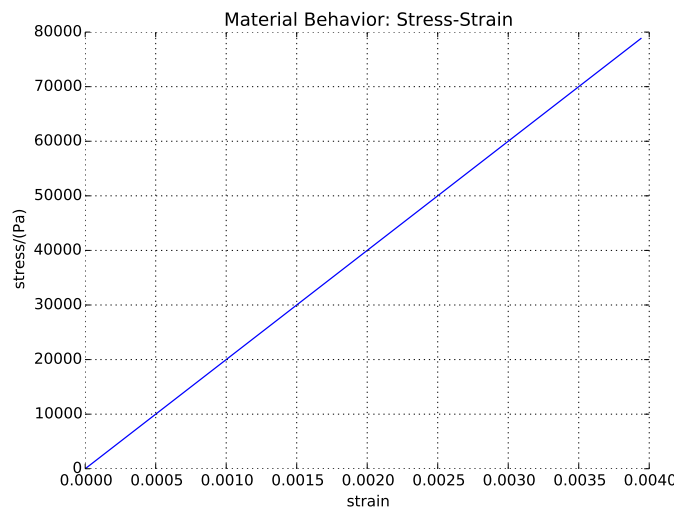


Figure 406.45: Results of Linear Elastic Solid Pure Shear Monotonic Loading.

### 406.7.1.2 Pure Shear, Cyclic Loading

The Real-ESSI input files for this example are available [HERE](#). The compressed package of Real-ESSI input files and postprocessing results for this example is available [HERE](#).

Model Description:

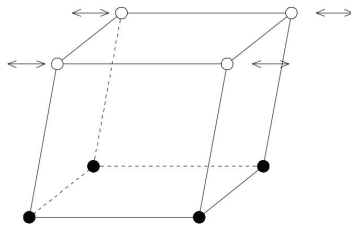


Figure 406.46: Diagram Linear Elastic Solid Pure Shear Cyclic Loading.

Material Response at Gauss Point:

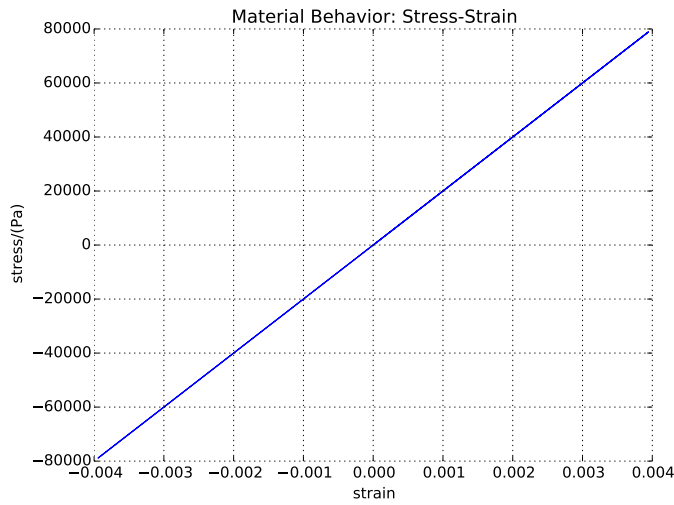


Figure 406.47: Results of Linear Elastic Solid Pure Shear Cyclic Loading.

### 406.7.1.3 Uniaxial Strain, Monotonic Loading

The Real-ESSI input files for this example are available [HERE](#). The compressed package of Real-ESSI input files and postprocessing results for this example is available [HERE](#).

Model Description:

Material Response at Gauss Point:

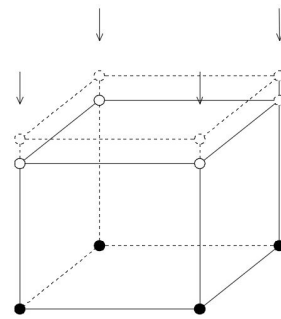


Figure 406.48: Diagram Linear Elastic Uniaxial Strain Solid Monotonic Loading.

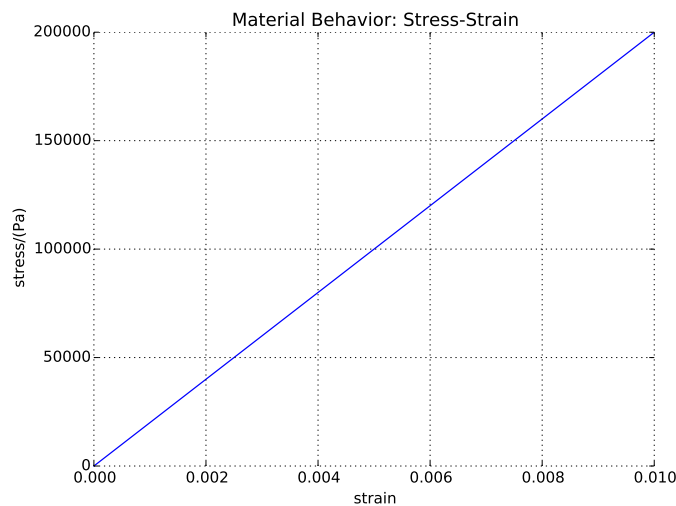


Figure 406.49: Results of Linear Elastic Pure Shear Monotonic Loading.

#### 406.7.1.4 Uniaxial Strain, Cyclic Loading

The Real-ESSI input files for this example are available [HERE](#). The compressed package of Real-ESSI input files and postprocessing results for this example is available [HERE](#).

Model Description:

Material Response at Gauss Point:

#### 406.7.2 Statics, Nonlinear Elastic, Duncan-Chang, Pure Shear, Solid Examples

##### 406.7.2.1 Pure Shear, Monotonic Loading

The Real-ESSI input files for this example are available [HERE](#). The compressed package of Real-ESSI input files and postprocessing results for this example is available [HERE](#).

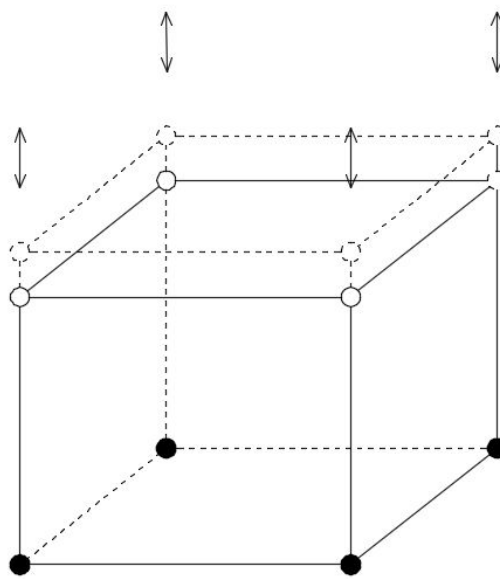


Figure 406.50: Linear Elastic Uniaxial Strain Cyclic Loading.

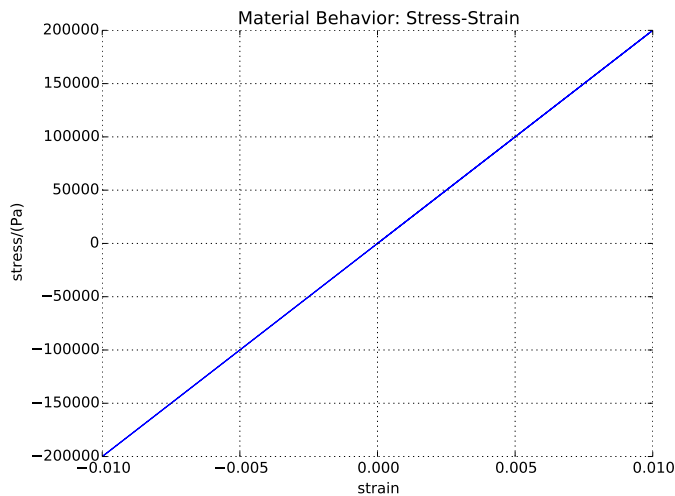


Figure 406.51: Results of Linear Elastic Pure Shear Cyclic Loading.

Model Description:

Material Response at Gauss Point:

#### 406.7.2.2 Pure Shear, Cyclic Loading

The Real-ESSI input files for this example are available [HERE](#). The compressed package of Real-ESSI input files and postprocessing results for this example is available [HERE](#).

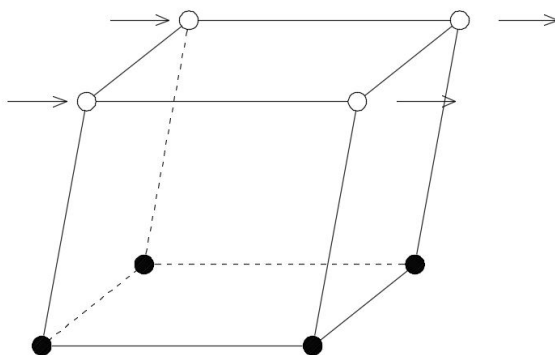


Figure 406.52: Nonlinear Elastic Uniaxial Strain Monotonic Loading.

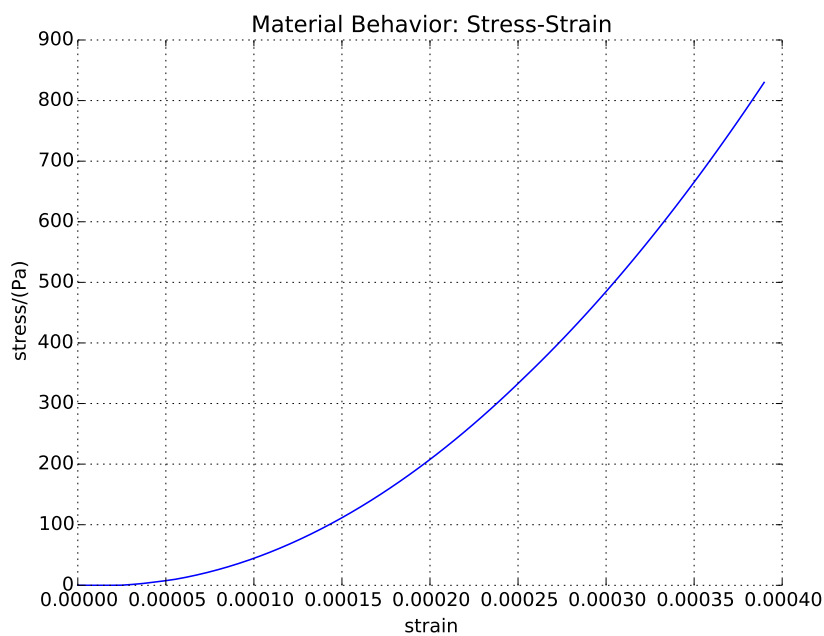


Figure 406.53: Results of Nonlinear Elastic Pure Shear Monotonic Loading.

Model Description:

Material Response at Gauss Point:

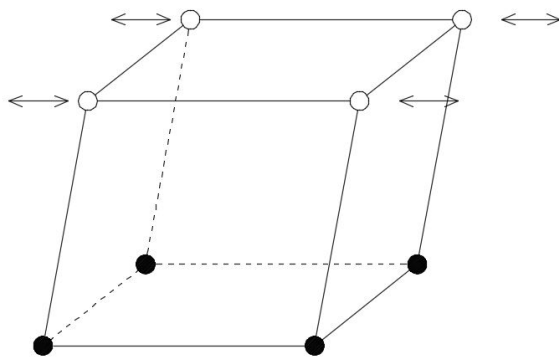


Figure 406.54: Nonlinear Elastic Uniaxial Strain Cyclic Loading.

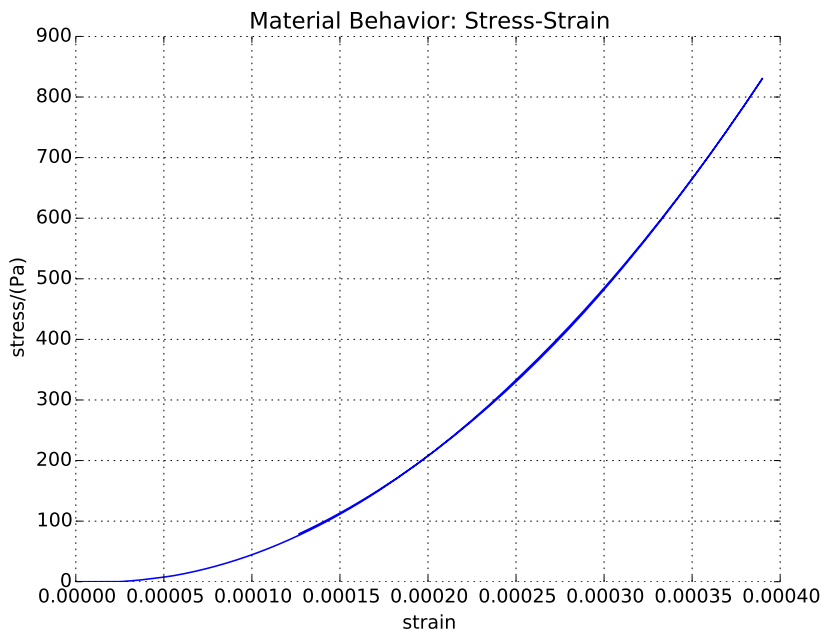


Figure 406.55: Results of Nonlinear Elastic Pure Shear Cyclic Loading.

## 406.8 Statics, Elastic-Plastic Single Solid Finite Element Examples

### 406.8.1 Statics, Elastic Perfectly Plastic, Cyclic Loading, Pure Shear Solid Examples

The Real-ESSI input files for this example are available [HERE](#). The compressed package of Real-ESSI input files and postprocessing results for this example is available [HERE](#).

Model Description:

Material Response at Gauss Point:

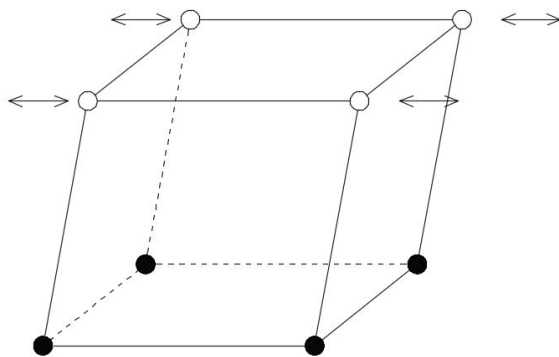


Figure 406.56: Perfectly Plastic Pure Shear Cyclic Loading.

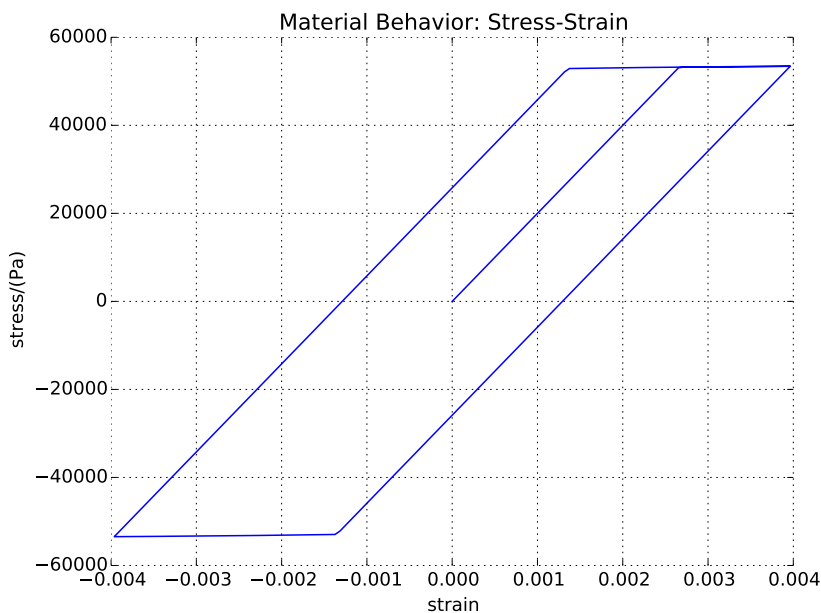


Figure 406.57: Results of Perfectly Plastic Pure Shear Cyclic Loading.

#### 406.8.1.1 Statics, von-Mises Yield Function, Isotropic Hardening

The Real-ESSI input files for this example are available [HERE](#). The compressed package of Real-ESSI input files and postprocessing results for this example is available [HERE](#).

Model Description:

Material Response at Gauss Point:

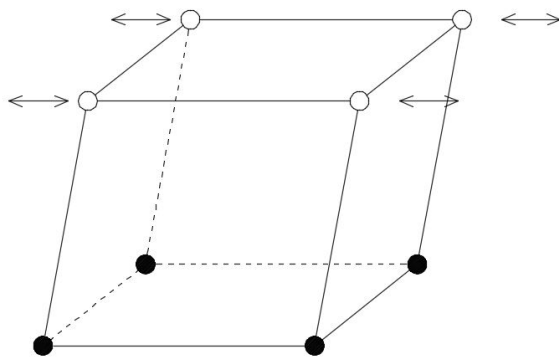


Figure 406.58: Pure Shear Cyclic Loading.

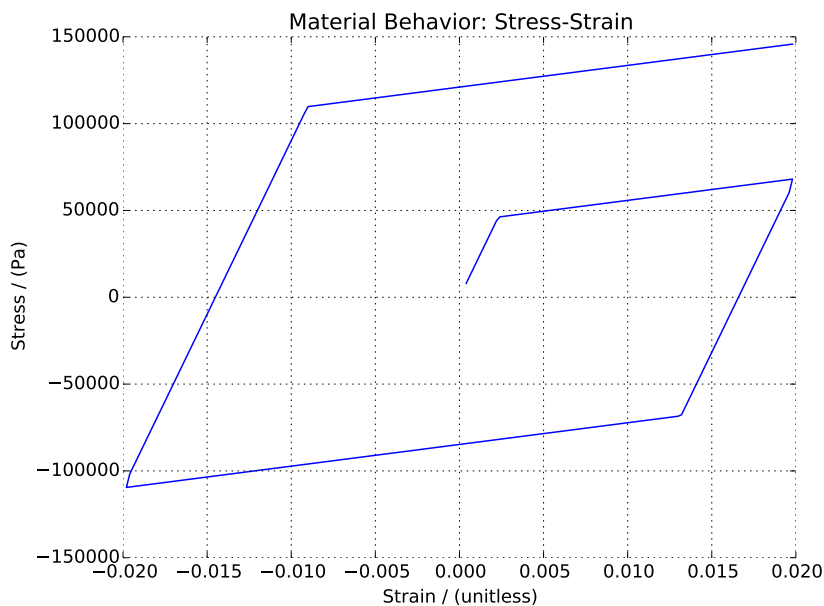


Figure 406.59: Material von-Mises Isotropic Hardening under Pure Shear Cyclic Loading.

#### 406.8.1.2 Statics, von Mises Yield Function, Kinematic Hardening

The Real-ESSI input files for this example are available [HERE](#). The compressed package of Real-ESSI input files and postprocessing results for this example is available [HERE](#).

Model Description:

Material Response at Gauss Point:

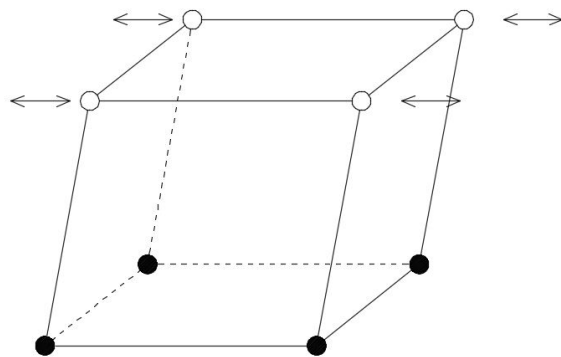


Figure 406.60: Pure Shear Cyclic Loading.

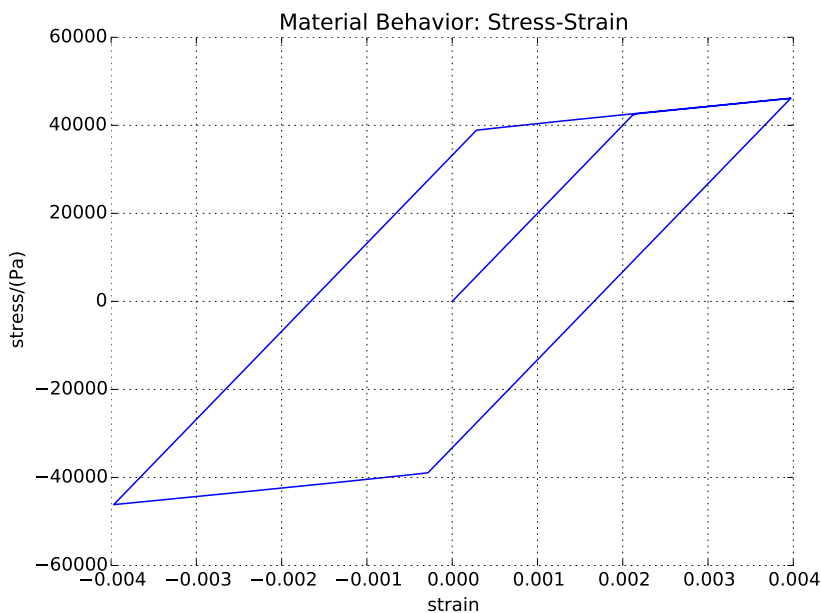


Figure 406.61: Results of von-Mises Kinematic Hardening Pure Shear Cyclic Loading.

#### 406.8.1.3 Statics, Drucker Prager Yield Function, von-Mises Plastic Potential Function, Perfectly Plastic Hardening Rule

The Real-ESSI input files for this example are available [HERE](#). The compressed package of Real-ESSI input files and postprocessing results for this example is available [HERE](#).

Model Description:

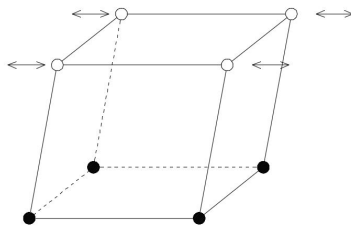


Figure 406.62: Pure Shear Cyclic Loading.

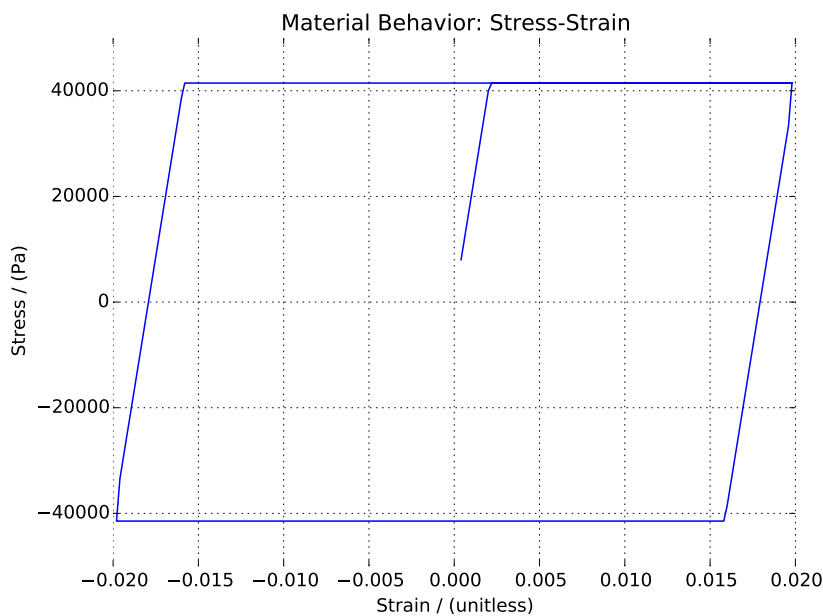


Figure 406.63: Results of Drucker Prager Yield Surface with Purely Deviatoric Plastic Flow under Pure Shear Cyclic Loading.

#### 406.8.1.4 Statics, Drucker Prager Yield Function, Drucker Prager Plastic Potential Function, Perfectly Plastic Hardening Rule

The Real-ESSI input files for this example are available [HERE](#). The compressed package of Real-ESSI input files and postprocessing results for this example is available [HERE](#).

Model Description:

Material Response at Gauss Point:

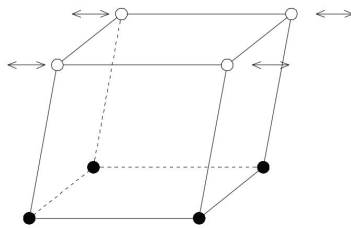


Figure 406.64: Pure Shear Cyclic Loading.



Figure 406.65: Results of Associative Drucker Prager Pure Shear Cyclic Loading.

#### 406.8.2 Statics, Drucker Prager with Armstrong Frederick Nonlinear Kinematic Hardening Material Model

The Real-ESSI input files for this example are available [HERE](#). The compressed package of Real-ESSI input files and postprocessing results for this example is available [HERE](#).

Model Description:

Material Response at Gauss Point:

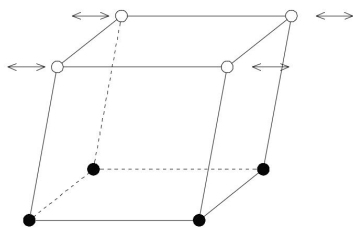


Figure 406.66: Pure Shear Cyclic Loading.

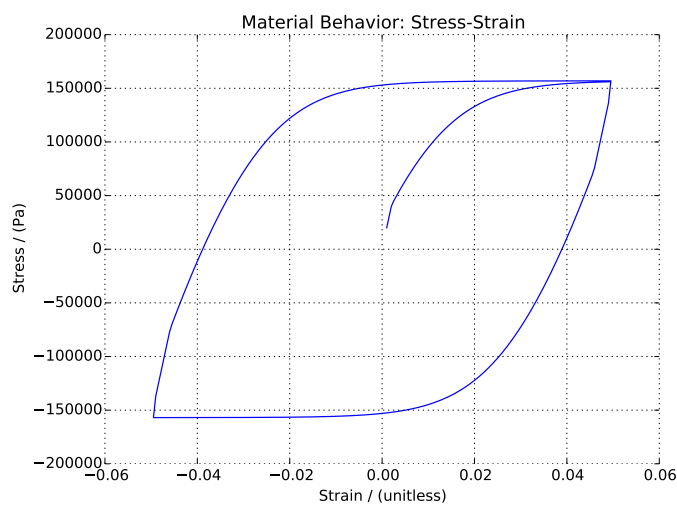


Figure 406.67: Result of Drucker-Prager Armstrong-Frederick Pure Shear Cyclic Loading.

## 406.9 Statics, Elastic, Fiber Cross Section Beam Finite Element Examples

### 406.9.1 Statics, Linear Elastic, Normal Loading and Pure Bending Fiber Cross Section Beam Finite Element Examples

#### 406.9.1.1 Linear Elastic Normal Loading, Fiber Cross Section Beam Finite Element Examples

The Real-ESSI input files for this example are available [HERE](#). The compressed package of Real-ESSI input files and postprocessing results for this example is available [HERE](#).

The linear elastic beam is represented by the elastic section. This example is under the load of normal loading.

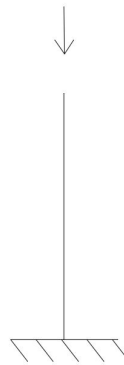


Figure 406.68: Normal Loading on the Fiber Beam with Elastic Section.

The elastic section represents the cross section properties of the beam.

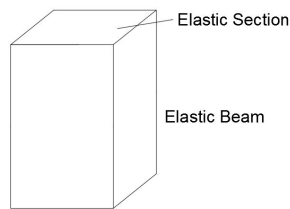


Figure 406.69: Diagram of the Fiber Beam with Elastic Section.

#### 406.9.1.2 Linear Elastic Pure Bending, Fiber Cross Section Beam Finite Element Examples

The Real-ESSI input files for this example are available [HERE](#). The compressed package of Real-ESSI input files and postprocessing results for this example is available [HERE](#).

The linear elastic beam is represented by the elastic section. This example is under the bending load.

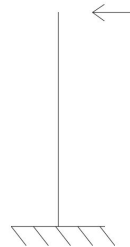


Figure 406.70: Bending on the Fiber Beam with Elastic Section.

The elastic section represents the cross section properties of the beam.

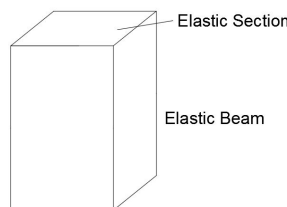


Figure 406.71: Diagram of the Fiber Beam with Elastic Section.

## 406.10 Statics, Elastic-Plastic, Fiber Cross Section Beam Finite Element Examples

### 406.10.1 Statics, Elastic-Plastic, Normal Loading and Pure Bending Fiber Cross Section Beam Finite Element

#### 406.10.1.1 Elastic-Plastic Normal Loading, (Fiber Cross Section) Beam Finite Element Examples

The Real-ESSI input files for this example are available [HERE](#). The compressed package of Real-ESSI input files and postprocessing results for this example is available [HERE](#).

The Elastic-Plastic beam is represented by the fiber section. This example is under the load of normal loading.

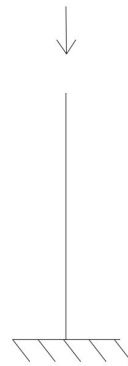


Figure 406.72: Normal Loading on the Fiber Beam with Elastic-Plastic Section.

The fiber represents the rebar. The section of all fibers represents the cross section properties of the inelastic beam.

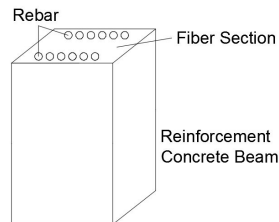


Figure 406.73: Diagram of the Fiber Beam with Elastic-Plastic Section.

#### 406.10.1.2 Elastic-Plastic Pure Bending, (Fiber Cross Section) Beam Finite Element Examples

The Real-ESSI input files for this example are available [HERE](#). The compressed package of Real-ESSI input files and postprocessing results for this example is available [HERE](#).

The Elastic-Plastic beam is represented by the fiber section. This example is under the load of normal loading.

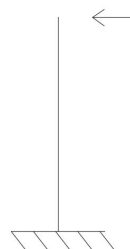


Figure 406.74: Bending on the Fiber Beam with Elastic-Plastic Section.

The fiber represents the rebar. The section of all fibers represents the cross section properties of the inelastic beam.

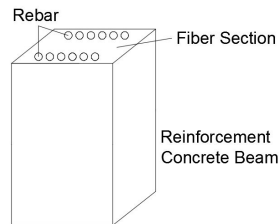


Figure 406.75: Diagram of the Fiber Beam with Elastic-Plastic Section.

## 406.11 Statics, Elastic, Inelastic Wall Finite Element Examples

### 406.11.1 Statics, Linear Elastic, Wall Finite Element Examples

#### 406.11.1.1 Statics, Linear Elastic, Wall Finite Element Examples

## 406.11.1.2 Linear Elastic, Bi-Axial, Wall Finite Element Examples

#### 406.11.1.3 Linear Elastic, Shear, (Fiber Cross Section) Wall Finite Element Examples

## 406.12 Statics, Elastic-Plastic Wall Finite Element Examples

### 406.12.1 Statics, Elastic-Plastic, in Plane, Wall Finite Element Examples

#### 406.12.1.1 Elastic-Plastic, Uni-Axial, Wall Finite Element Examples

## 406.12.1.2 Elastic-Plastic, Bi-Axial, Wall Finite Element Examples

#### 406.12.1.3 Elastic-Plastic, Shear, Wall Finite Element Examples

## 406.13 Statics, Solution Advancement Control

### 406.13.1 Increments: Load Control

When load-control is used as the solution advancement method, perfectly plastic model will fail immediately after the yield point. Load-control works with isotropic hardening and kinematic hardening.

#### 406.13.1.1 Solids Example, Elastic Plastic Isotropic Hardening

The Real-ESSI input files for this example are available [HERE](#). The compressed package of Real-ESSI input files and postprocessing results for this example is available [HERE](#).

Model Description:

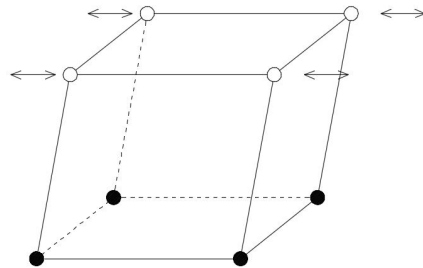


Figure 406.76: Pure Shear Cyclic Loading.

Material Response at Gauss Point:

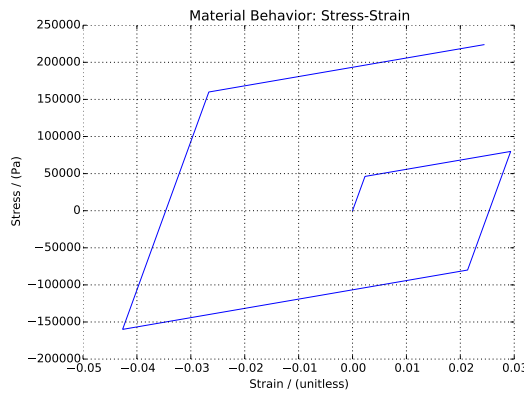


Figure 406.77: Material von-Mises Isotropic Hardening under Pure Shear Cyclic Loading.

#### 406.13.1.2 Solids Example, Elastic Plastic Kinematic Hardening

The Real-ESSI input files for this example are available [HERE](#). The compressed package of Real-ESSI input files and postprocessing results for this example is available [HERE](#).

Model Description:

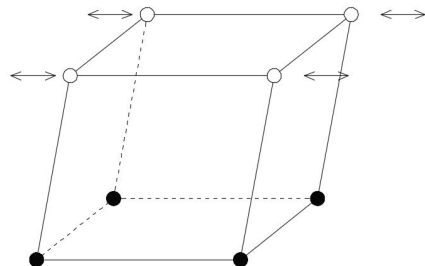


Figure 406.78: Pure Shear Cyclic Loading.

Material Response at Gauss Point:

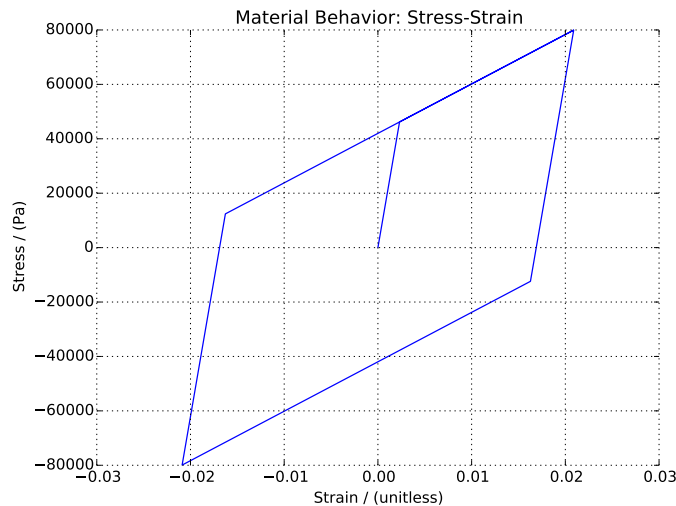


Figure 406.79: Material von-Mises Kinematic Hardening under Pure Shear Cyclic Loading.

#### 406.13.1.3 Inelastic Beam Example, Steel and Reinforced Concrete

The Real-ESSI input files for this example are available [HERE](#).

The compressed package of Real-ESSI input files and postprocessing results for this example is available [HERE](#).

The Elastic-Plastic beam is represented by the fiber section. This example is under the load of normal loading.

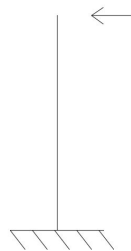


Figure 406.80: Normal Loading on the Beam with Fiber Section.

The fiber represents the rebar. The section of all fibers represents the cross section properties of the inelastic beam.

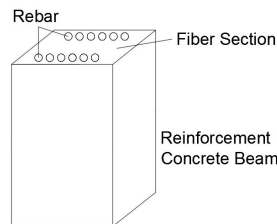


Figure 406.81: Diagram of the Beam with Fiber Section.

#### 406.13.2 Statics, Increments: Displacement Control

##### 406.13.2.1 Statics, Single Displacement Control

##### 406.13.2.2 Solids Example, Elastic-Perfectly Plastic

The Real-ESSI input files for this example are available [HERE](#). The compressed package of Real-ESSI input files and postprocessing results for this example is available [HERE](#).

Model Description:

Material Response at Gauss Point:

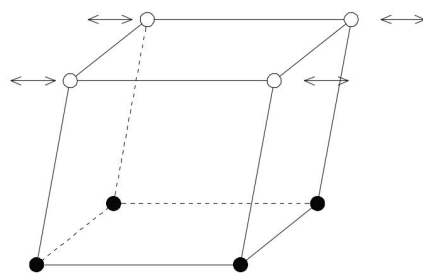


Figure 406.82: Pure Shear Cyclic Loading.

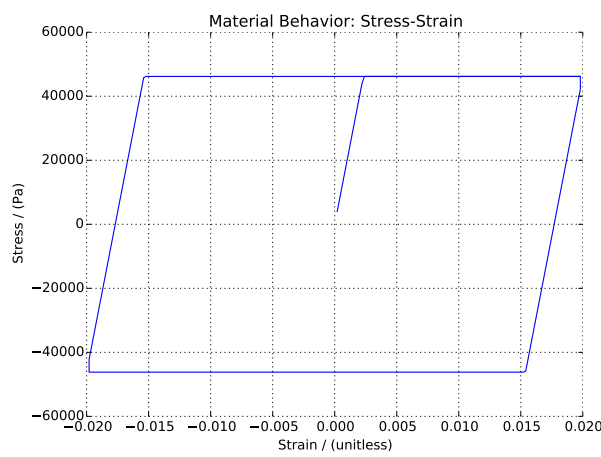


Figure 406.83: Displacement-Control of Perfectly Plastic Material under Pure Shear Cyclic Loading.

#### 406.13.2.3 Solids Example, Elastic Plastic Isotropic Hardening

The Real-ESSI input files for this example are available [HERE](#). The compressed package of Real-ESSI input files and postprocessing results for this example is available [HERE](#).

Model Description:

Material Response at Gauss Point:

#### 406.13.2.4 Solids Example, Elastic Plastic Kinematic Hardening

The Real-ESSI input files for this example are available [HERE](#). The compressed package of Real-ESSI input files and postprocessing results for this example is available [HERE](#).

Model Description:

Material Response at Gauss Point:

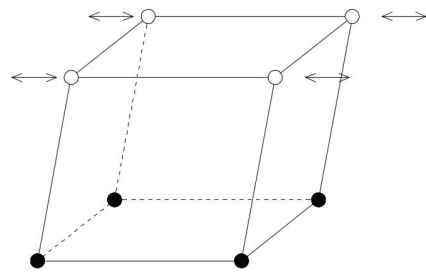


Figure 406.84: Pure Shear Cyclic Loading.

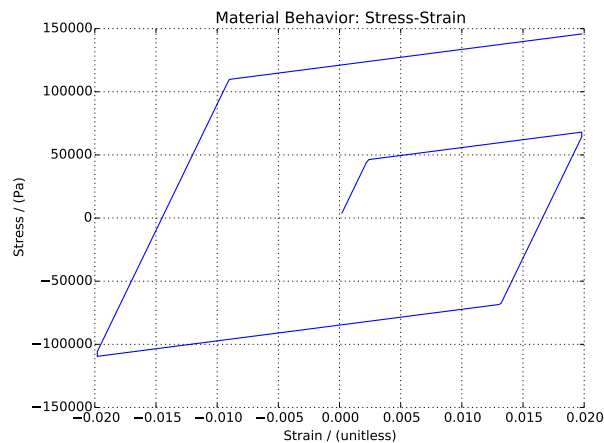


Figure 406.85: Displacement-Control of Isotropic Hardening Material under Pure Shear Cyclic Loading.

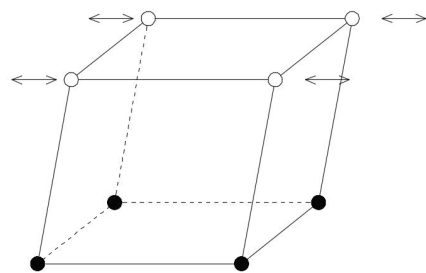


Figure 406.86: Pure Shear Cyclic Loading.

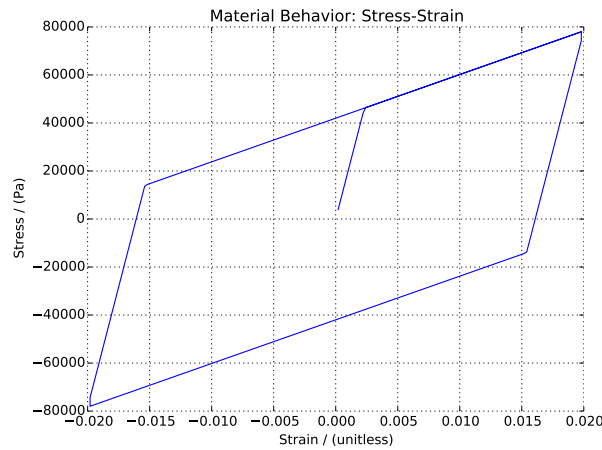


Figure 406.87: Displacement-Control of Kinematic Hardening Material under Pure Shear Cyclic Loading.

#### 406.13.2.5 Inelastic Beam Example, Steel and Reinforced Concrete

The Real-ESSI input files for this example are available [HERE](#). The compressed package of Real-ESSI input files and postprocessing results for this example is available [HERE](#).

The Elastic-Plastic beam is represented by the fiber section. This example is under the load of normal loading.

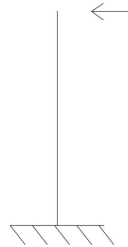


Figure 406.88: Bending on the Fiber Beam with Elastic-Plastic Section

The fiber represents the rebar. The section of all fibers represents the cross section properties of the inelastic beam.

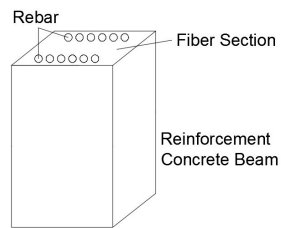


Figure 406.89: Diagram of the Fiber Beam with Elastic-Plastic Section.

### 406.13.3 Statics, Solution Algorithms

#### 406.13.3.1 Statics, Solution Algorithm: No Convergence Check

The Real-ESSI input files for this example are available [HERE](#). The compressed package of Real-ESSI input files and postprocessing results for this example is available [HERE](#).

When no convergence check is used, the stress-strain curves drift away a little. The stress-strain curve did not close, as shown in Figure 406.57.

Model Description:

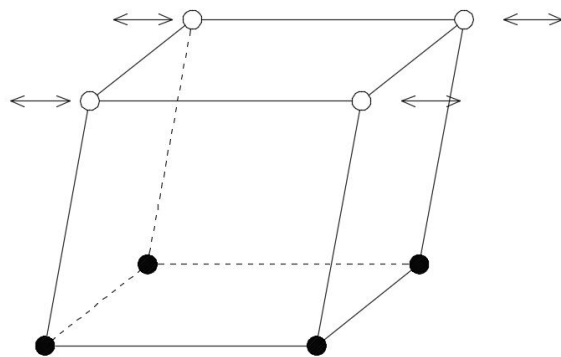


Figure 406.90: Pure Shear Cyclic Loading.

Material Response at Gauss Point:

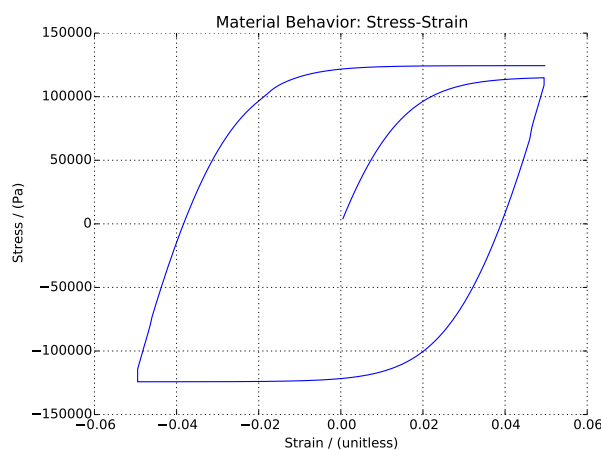


Figure 406.91: Results of No-Convergence-Check Pure Shear Cyclic Loading.

#### 406.13.3.2 Statics, Solution Algorithm: Newton Algorithm

The Real-ESSI input files for this example are available [HERE](#). The compressed package of Real-ESSI input files and postprocessing results for this example is available [HERE](#).

Model Description:

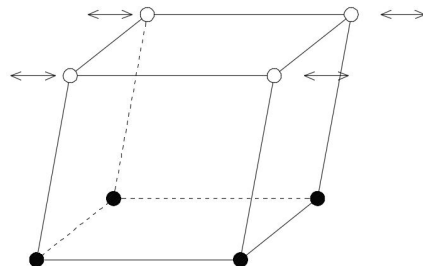


Figure 406.92: Pure Shear Cyclic Loading.

Material Response at Gauss Point:

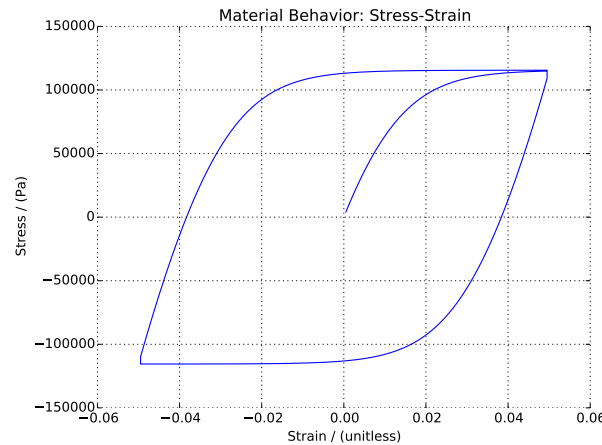


Figure 406.93: Results of Convergence Check with Newton-Raphson Iteration under Pure Shear Cyclic Loading.

#### 406.13.3.3 Statics, Solution Algorithm: Newton Algorithm with Line Search

The Real-ESSI input files for this example are available [HERE](#). The compressed package of Real-ESSI input files and postprocessing results for this example is available [HERE](#).

Model Description:

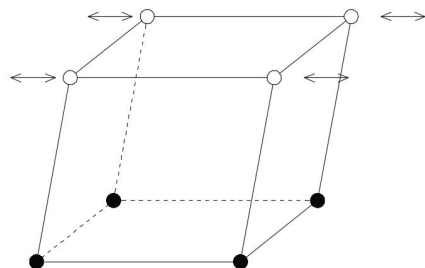


Figure 406.94: Pure Shear Cyclic Loading.

Material Response at Gauss Point:

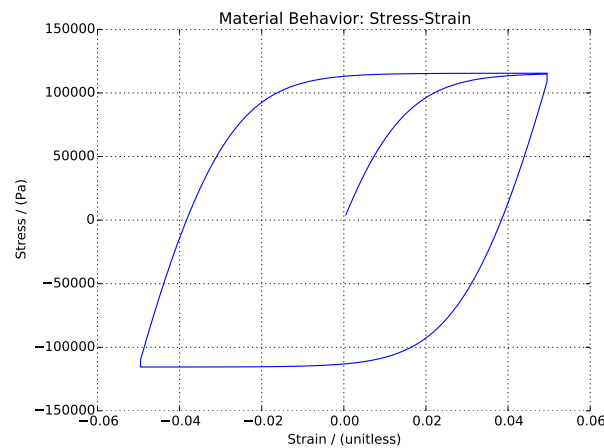


Figure 406.95: Results of Convergence Check with Newton-Raphson Iterations and Line Search under Pure Shear Cyclic Loading.

#### 406.13.4 Statics, Solution Advancement Control, Iterations: Convergence Criteria

##### 406.13.4.1 Statics, Solution Advancement Control, Convergence Criteria: Unbalanced Force

The Real-ESSI input files for this example are available [HERE](#). The compressed package of Real-ESSI input files and postprocessing results for this example is available [HERE](#).

Model Description:

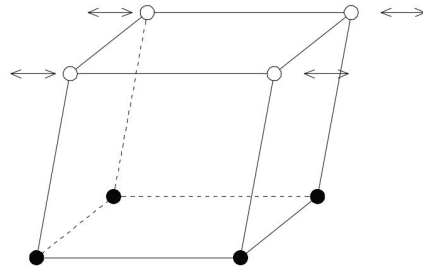


Figure 406.96: Pure Shear Cyclic Loading.

Material Response at Gauss Point:

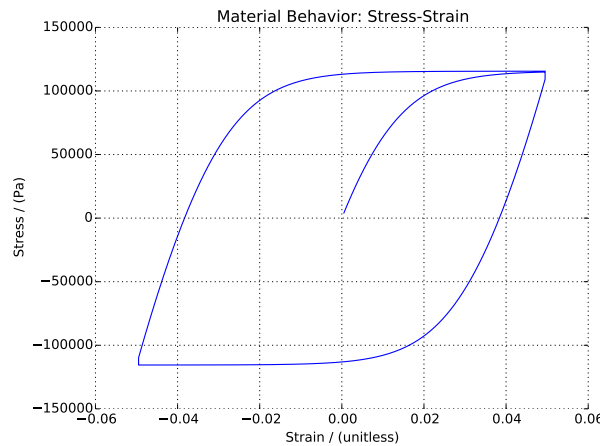


Figure 406.97: Results of Convergence Check with Unbalanced Force Criteria under Pure Shear Cyclic Loading.

#### 406.13.4.2 Statics, Solution Advancement Control, Convergence Criteria: Displacement Increment

The Real-ESSI input files for this example are available [HERE](#). The compressed package of Real-ESSI input files and postprocessing results for this example is available [HERE](#).

Model Description:

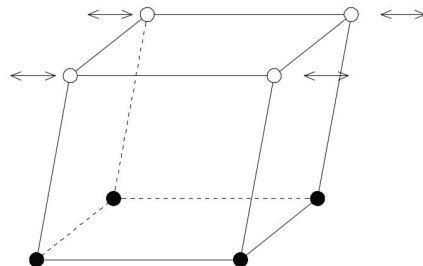


Figure 406.98: Pure Shear Cyclic Loading.

Material Response at Gauss Point:

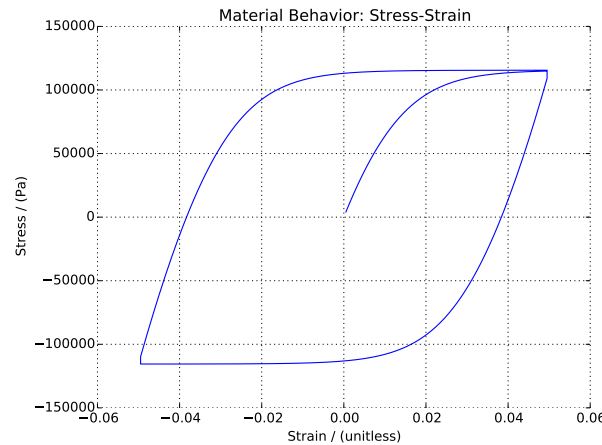


Figure 406.99: Results of Convergence Check with Displacement Increment under Pure Shear Cyclic Loading.

#### 406.13.5 Statics, Solution Advancement Control, Different Convergence Tolerances (Examples in preparation)

## 406.14 Statics, Small Practical Examples

### 406.14.1 Statics, Elastic Beam Element for a Simple Frame Structure

The Real-ESSI input files for this example are available [HERE](#). The compressed package of Real-ESSI input files and postprocessing results for this example is available [HERE](#).

#### 406.14.1.1 Problem Description

- Dimensions: width=6m, height=6m, force=100N
- Element dimensions: length=6m, cross section width=1m, cross section height=1m, mass density  $\rho = 0.0\text{kN/m}^3$ , Young's modulus  $E = 1E8 \text{ Pa}$ , Poisson's ratio  $\nu = 0.0$ .

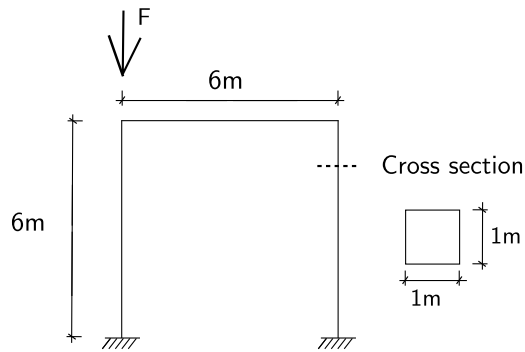


Figure 406.100: Elastic frame with beam\_elastic elements.

#### 406.14.2 Statics, 4NodeANDES Square Plate, Four Edges Clamped

The Real-ESSI input files for this example are available [HERE](#). The compressed package of Real-ESSI input files and postprocessing results for this example is available [HERE](#).

##### 406.14.2.1 Problem description

Length=20m, Width=20m, Height=1m, Force=100N, E=1E8Pa,  $\nu = 0.3$ .

The four edges are clamped.

The load is a self weight.

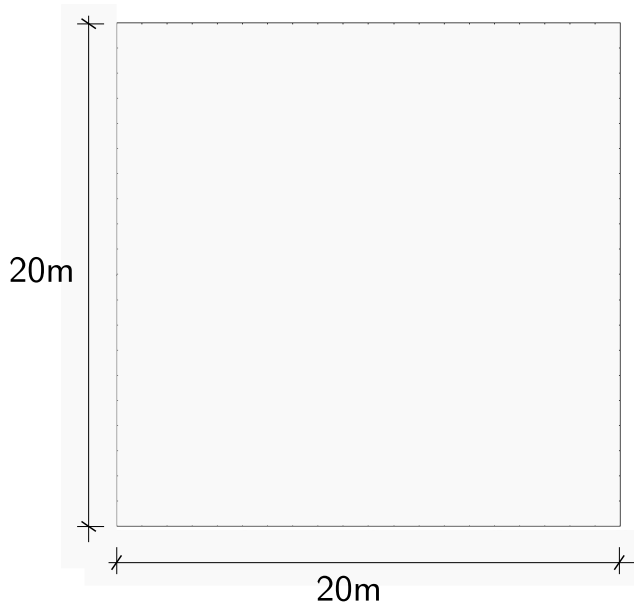


Figure 406.101: Square plate with four edges clamped.

##### 406.14.2.2 Numerical model

The element side length is 1 meter.

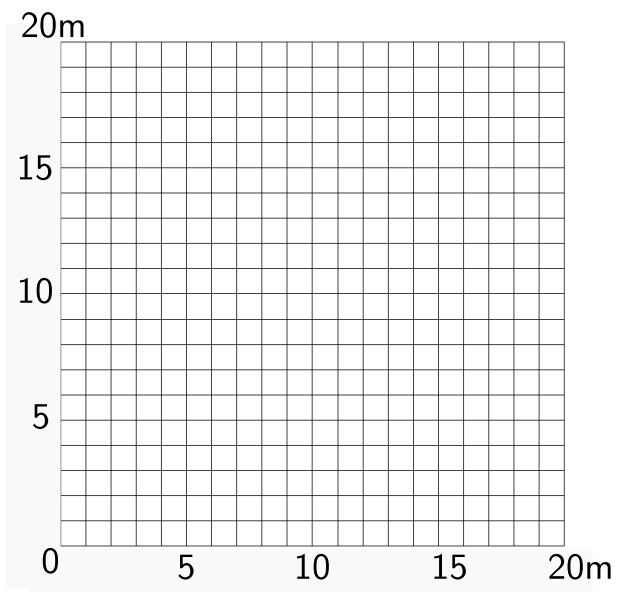


Figure 406.102: 4NodeANDES edge clamped square plate with element side length 1m.

#### 406.14.3 Statics, Six Solid Blocks Example With Interface/Contact

The Real-ESSI input files for this example are available [HERE](#). The compressed package of Real-ESSI input files and postprocessing results for this example is available [HERE](#).

This is a 3-D solid block example with initial normal and then tangential load on different surfaces as shown below.

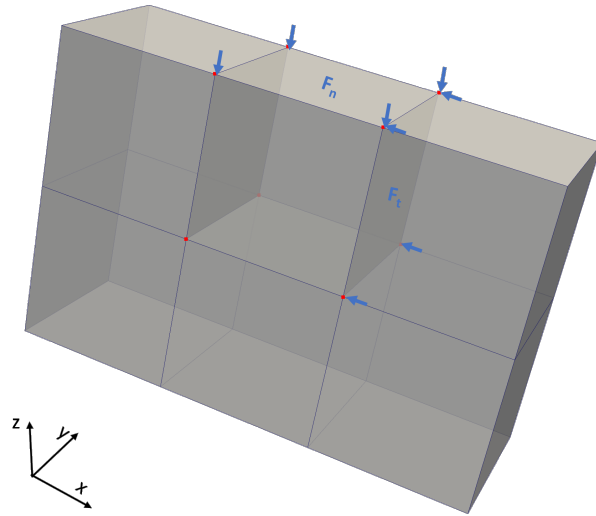


Figure 406.103: Illustration of Six Solid Blocks Example with Interface/Contact with first normal and then tangential loading stages.

The generalized displacement field of the two loading stages normal loading and tangential loading is shown below..

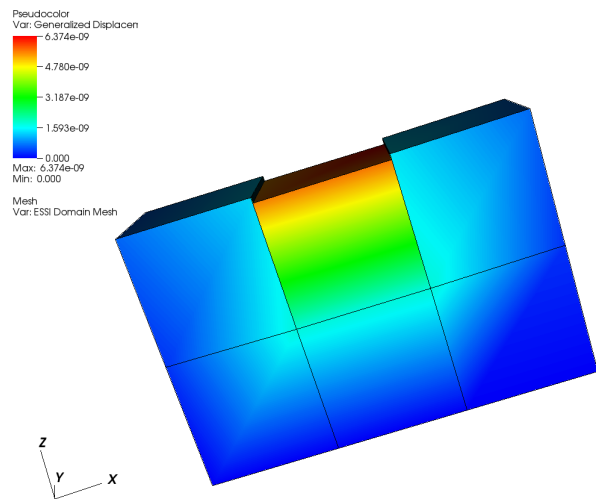


Figure 406.104: Generalized displacement magnitude visualization of normal loading.

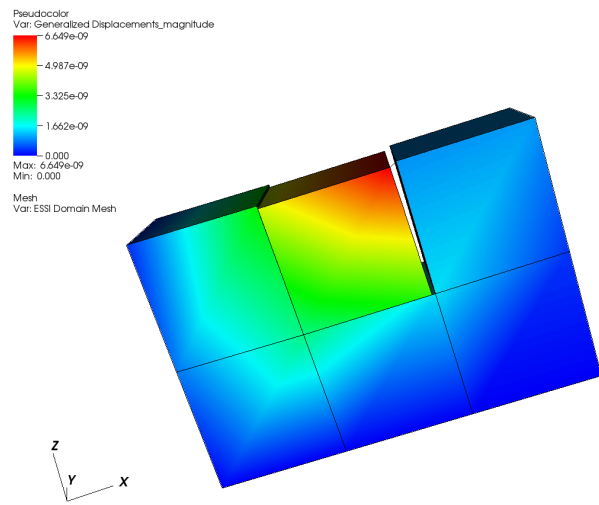


Figure 406.105: Generalized displacement magnitude visualization of tangential loading.

# Chapter 407

## Dynamic Examples

(2016-2017-2018-2019-2021-)

(In collaboration with Prof. José Abell, Dr. Yuan Feng, Mr. Sumeet Kumar Sinha, Dr. Hexiang Wang, and Dr. Han Yang)

### 407.1 Chapter Summary and Highlights

In this Chapter dynamic/transient modeling and simulation of solids and structures is illustrated through a number of examples.

All the examples described here, and many more, organized in sub-directories, for constitutive behavior, static and dynamic behavior can be directly downloaded from a repository at: [http://sokocalo.engr.ucdavis.edu/~jeremic/lecture\\_notes\\_online\\_material/Real-ESSI\\_Examples/education\\_examples](http://sokocalo.engr.ucdavis.edu/~jeremic/lecture_notes_online_material/Real-ESSI_Examples/education_examples). These examples can then be tried, analyzed using Real-ESSI Simulator that is available on Amazon Web Services (AWS) computers around the word. Login to AWS market place and search for Real-ESSI...

### 407.2 Dynamic Solution Advancement (in Time)

#### 407.2.1 Dynamics: Newmark Method

##### 407.2.1.1 Newmark Model Description

The Real-ESSI input files for this example are available [HERE](#). The compressed package of Real-ESSI input files and postprocessing results for this example is available [HERE](#).

Firstly, the model is given an initial displacement at one side. Second, the model starts free vibration.

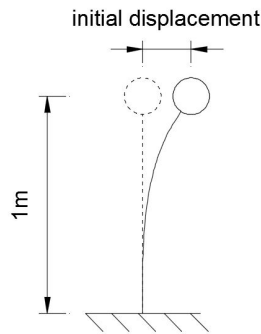


Figure 407.1: Problem Description for Newmark Method

#### 407.2.1.2 Newmark Results

With damping, the displacement peak is smaller and smaller. The displacement at the top is

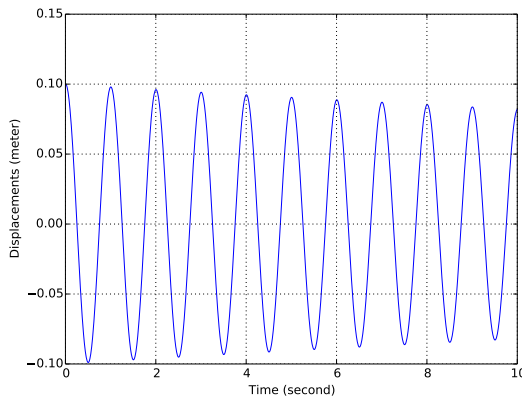


Figure 407.2: Results for Newmark Method

#### 407.2.2 Dynamics: Hilber-Hughes-Taylor ( $\alpha$ ) Method

##### 407.2.2.1 HHT Model Description

The Real-ESSI input files for this example are available [HERE](#). The compressed package of Real-ESSI input files and postprocessing results for this example is available [HERE](#).

Firstly, the model is given an initial displacement at one side. Second, the model starts free vibration.

##### 407.2.2.2 HHT Results

With NO damping, the displacement peak keeps the same. The displacement at the top is

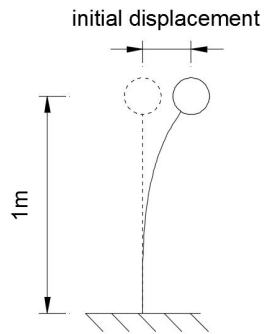


Figure 407.3: Problem Description for HHT Method

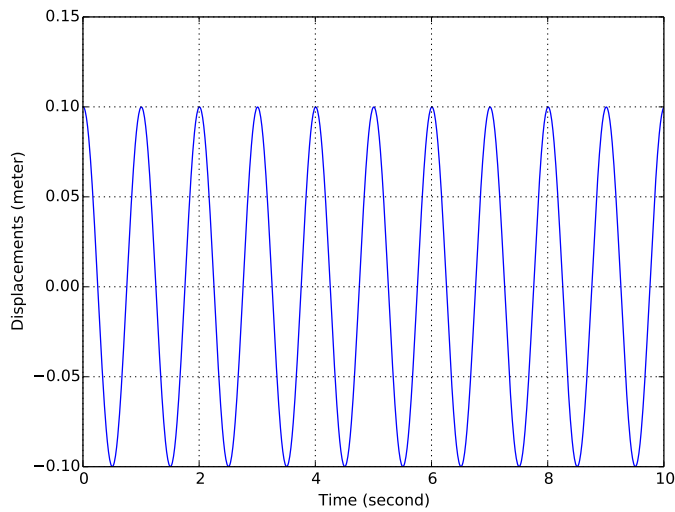


Figure 407.4: Results for HHT Method

## 407.3 Dynamics: Solution Advancement: Time Step Size

### 407.3.1 Dynamics: Solution Advancement: Equal Time Step

#### 407.3.1.1 Model Description

The Real-ESSI input files for this example are available [HERE](#). The compressed package of Real-ESSI input files and postprocessing results for this example is available [HERE](#).

The model is given an earthquake input motion at the bottom with equal time step. After the wave propagation, the motion at the top is recorded.

#### 407.3.1.2 Results

The input motion is on the left, while the output motion is on the right.

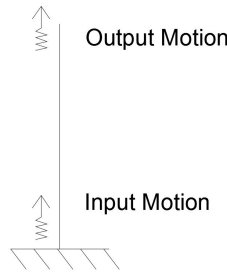


Figure 407.5: Problem Description for Solution Advancement

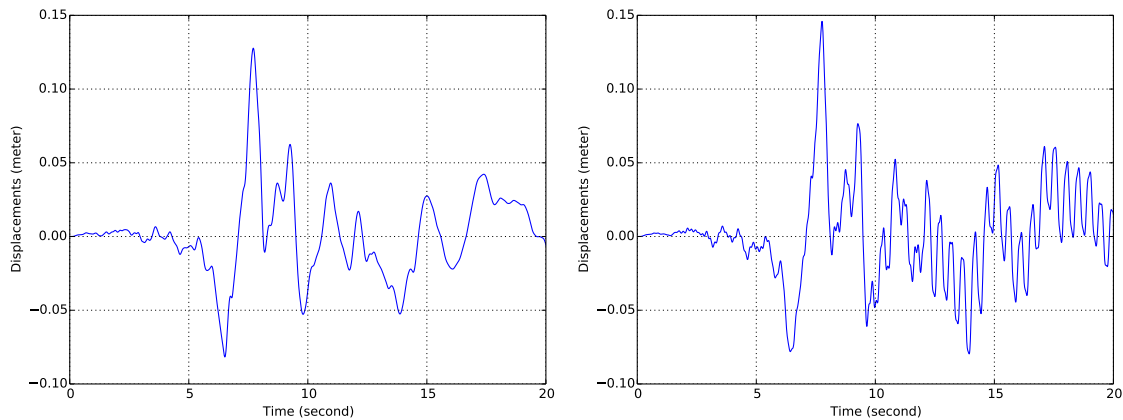


Figure 407.6: Input Motion (Left) And Output Motion (Right)

## 407.3.2 Dynamics Solution Advancement: Variable Time Step

### 407.3.2.1 Model Description

The Real-ESSI input files for this example are available [HERE](#). The compressed package of Real-ESSI input files and postprocessing results for this example is available [HERE](#).

The model is given an earthquake input motion at the bottom with variable time step. After the wave propagation, the motion at the top is recorded.

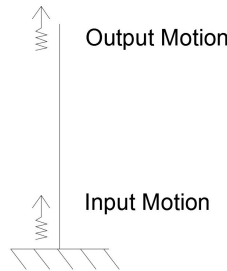


Figure 407.7: Problem Description for Newmark Method

### 407.3.2.2 Results

The input motion is on the left, while the output motion is on the right. The input motion is in variable time step. As shown in Fig 407.8, from time 10-11 second, the input motion is a straight line (a big time step) without the small time steps.

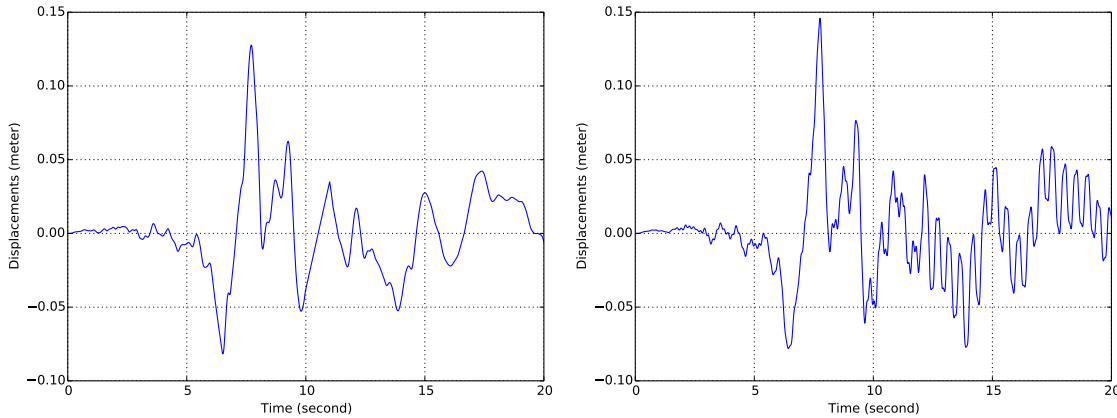


Figure 407.8: Input Motion (Left) And Output Motion (Right)

## 407.4 Dynamics: Energy Dissipation, Damping

### 407.4.1 Dynamics: Energy Dissipation: Viscous Damping

#### 407.4.1.1 Dynamics: Energy Dissipation, Viscous Damping: Rayleigh Damping

**Model Description** The Real-ESSI input files for this example are available [HERE](#). The compressed package of Real-ESSI input files and postprocessing results for this example is available [HERE](#).

Firstly, the model is given an initial displacement at the top from 0 to 1 second. Second, after the time 1 second, the model starts free vibration.

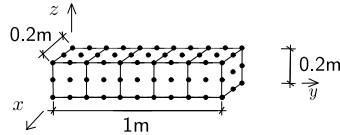


Figure 407.9: Problem Description for Newmark Method

**Results** This model employs Rayleigh damping. The displacement at the top is

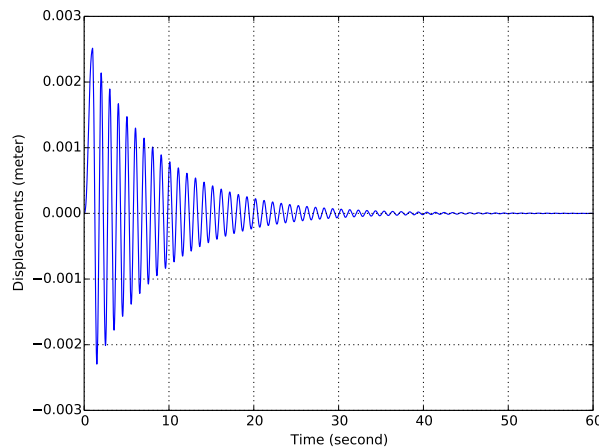


Figure 407.10: Results for Newmark Method

#### 407.4.1.2 Dynamics: Energy Dissipation, Viscous Damping: Caughey Damping

**Model Description** The Real-ESSI input files for this example are available [HERE](#). The compressed package of Real-ESSI input files and postprocessing results for this example is available [HERE](#).

Firstly, the model is given an initial displacement at the top from 0 to 1 second. Second, after the time 1 second, the model starts free vibration.

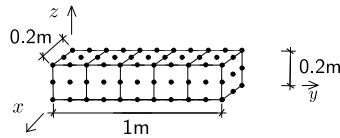


Figure 407.11: Problem Description for Newmark Method

**Results** This model employs Caughey damping. The displacement at the top is

#### 407.4.2 Dynamics: Energy Dissipation: Material (Elastic-Plastic, Hysteretic) Damping

##### 407.4.2.1 Dynamics: Energy Dissipation, Material Damping: Elastic Perfectly Plastic Models

**Model Description** The Real-ESSI input files for this example are available [HERE](#). The compressed package of Real-ESSI input files and postprocessing results for this example is available [HERE](#).

The model is a one-element solid brick example with perfectly plastic materials.

**Results** The Hysteretic loop at the Gauss point is

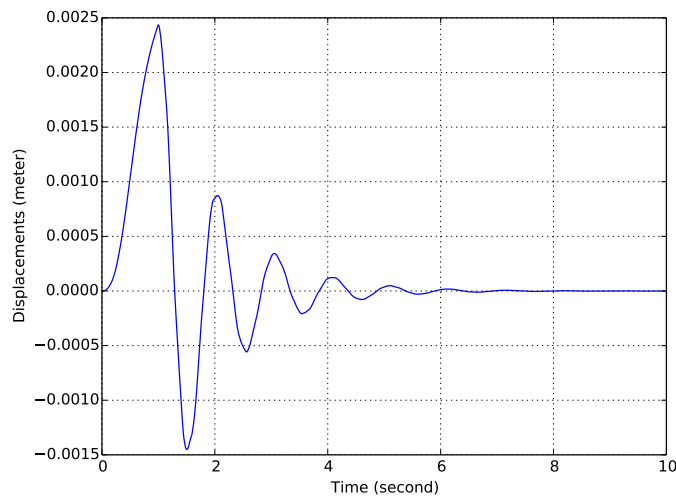


Figure 407.12: Results for Newmark Method

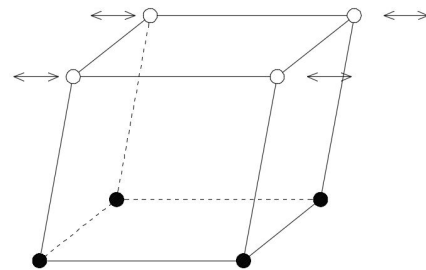


Figure 407.13: Problem Description for Newmark Method

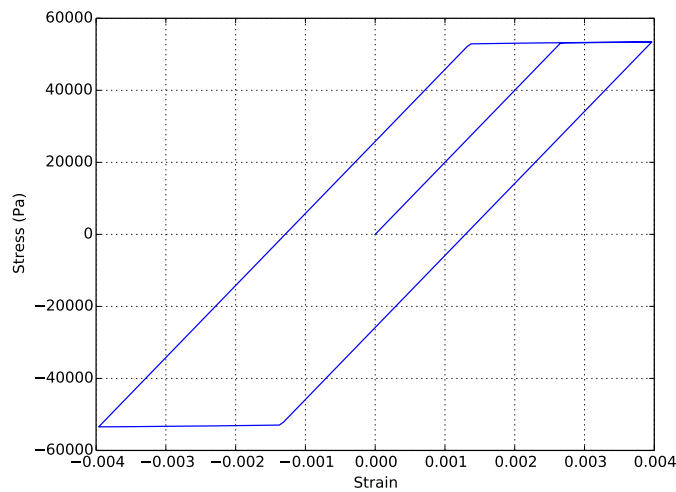


Figure 407.14: Results for Newmark Method

#### 407.4.2.2 Dynamics: Energy Dissipation, Material/Hysteretic Damping: Elastic Plastic Isotropic Hardening Models

**Model Description** The Real-ESSI input files for this example are available [HERE](#). The compressed package of Real-ESSI input files and postprocessing results for this example is available [HERE](#).

The model is a one-element solid brick example with isotropic hardening materials.

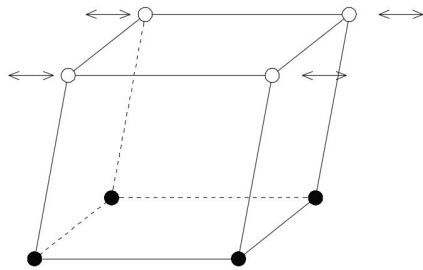


Figure 407.15: Problem Description for Newmark Method

**Results** The Hysteretic loop at the Gauss point is

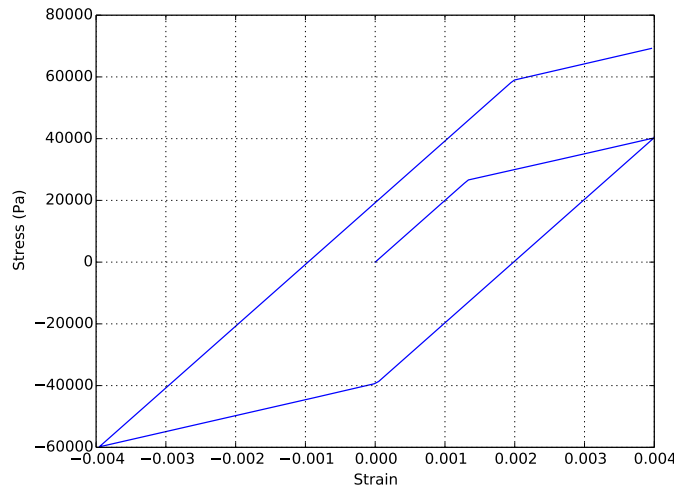


Figure 407.16: Results for Newmark Method

#### 407.4.2.3 Dynamics: Energy Dissipation, Material/Hysteretic Damping: Elastic Plastic Kinematic Hardening Models

**Model Description** The Real-ESSI input files for this example are available [HERE](#). The compressed package of Real-ESSI input files and postprocessing results for this example is available [HERE](#).

The model is a one-element solid brick example with kinematic hardening materials.

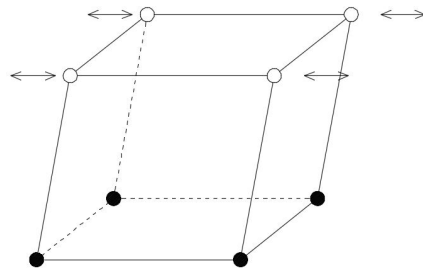


Figure 407.17: Problem Description for Newmark Method

**Results** The Hysteretic loop at the Gauss point is

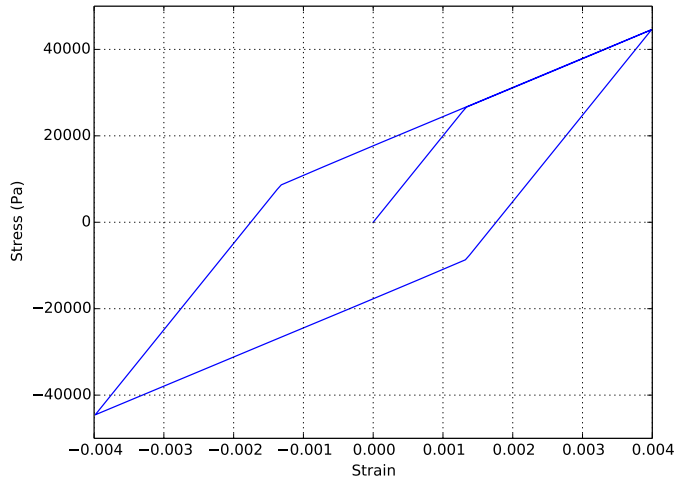


Figure 407.18: Results for Newmark Method

#### 407.4.2.4 Dynamics: Energy Dissipation, Material/Hysteretic Damping: Elastic Plastic Armstrong-Frederick Models

**Model Description** The Real-ESSI input files for this example are available [HERE](#). The compressed package of Real-ESSI input files and postprocessing results for this example is available [HERE](#).

The model is a one-element solid brick example with materials with nonlinear hardening Armstrong-Frederick.

**Results** The Hysteretic loop at the Gauss point is

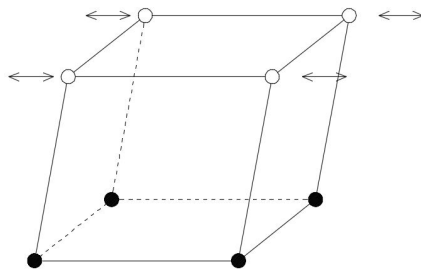


Figure 407.19: Problem Description for Newmark Method

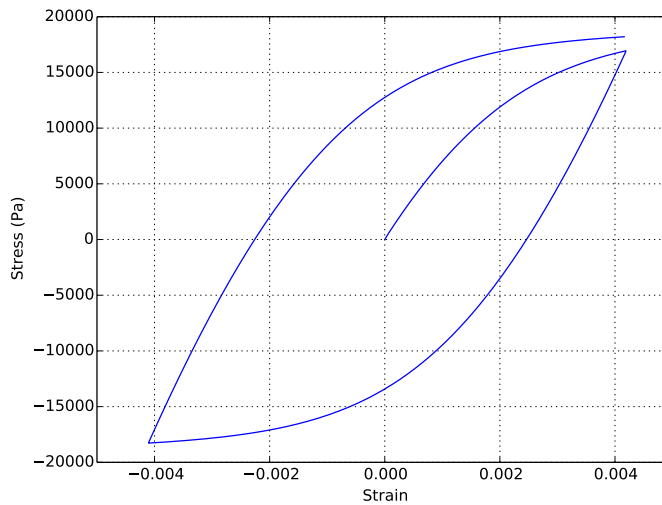


Figure 407.20: Results for Material Armstrong-Frederick

### 407.4.3 Dynamics: Energy Dissipation: Numerical Damping

#### 407.4.3.1 Energy Dissipation, Numerical Damping: Newmark Method

**Model Description** The Real-ESSI input files for this example are available [HERE](#). The compressed package of Real-ESSI input files and postprocessing results for this example is available [HERE](#).

Firstly, the model is given an initial displacement in the first loading stage. In the second loading stage, the model starts free vibration.

**Results** This model employs Newmark numerical damping. The displacement at the top in the second loading stage is

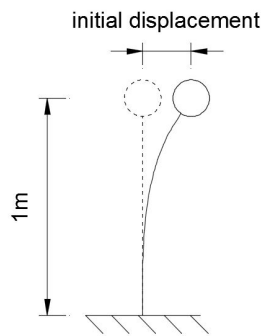


Figure 407.21: Problem Description for Newmark Method

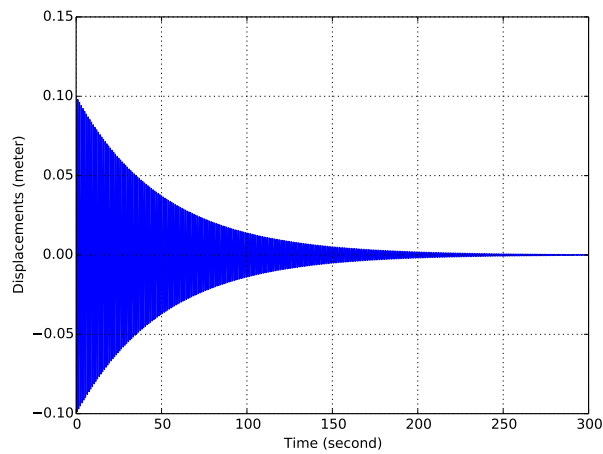


Figure 407.22: Results for Newmark Method

#### 407.4.3.2 Dynamics: Energy Dissipation, Numerical Damping: Hilber-Hughes-Taylor ( $\alpha$ ) Method

**Model Description** The Real-ESSI input files for this example are available [HERE](#). The compressed package of Real-ESSI input files and postprocessing results for this example is available [HERE](#).

Firstly, the model is given an initial displacement in the first loading stage. In the second loading stage, the model starts free vibration.

**Results** This model employs HHT numerical damping. The displacement at the top in the second loading stage is

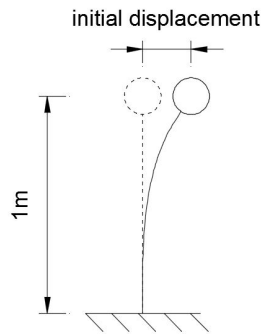


Figure 407.23: Problem Description

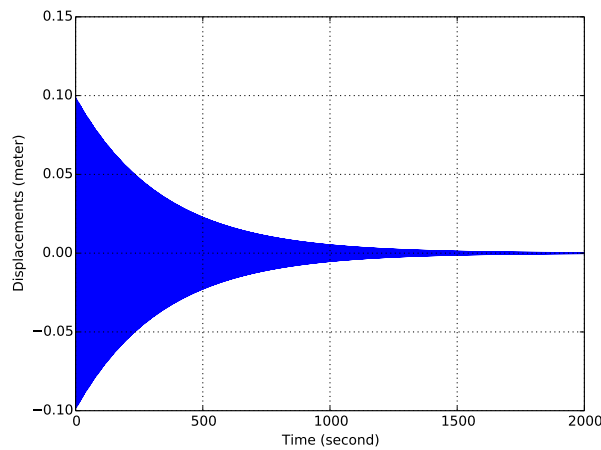


Figure 407.24: Results for HHT Method

## 407.5 Dynamics: Elastic Solid Dynamic Examples

### 407.5.1 Model Description

The Real-ESSI input files for this example are available [HERE](#). The compressed package of Real-ESSI input files and postprocessing results for this example is available [HERE](#).

Firstly, the model is given an initial displacement at the top from 0 to 1 second. Second, after the time 1 second, the model starts free vibration.

### 407.5.2 Results

This model employs Caughey damping. The displacement at the top is

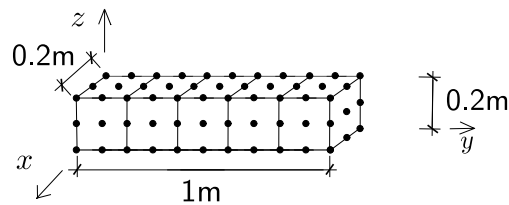


Figure 407.25: Problem Description for Newmark Method

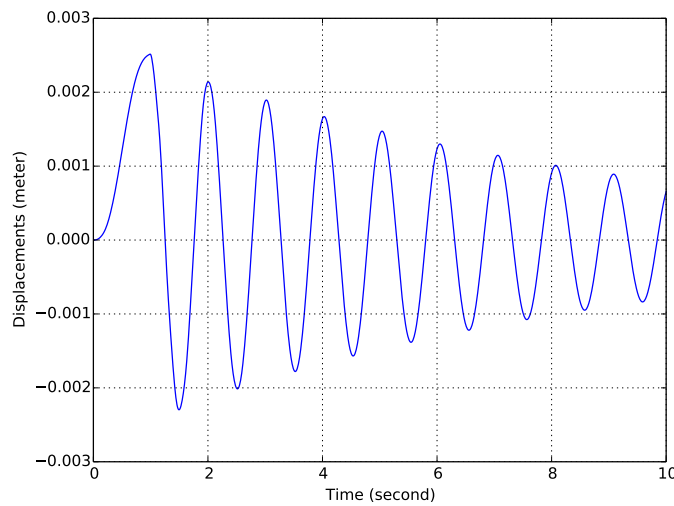


Figure 407.26: Results for Newmark Method

## 407.6 Dynamics: Elastic Structural Dynamic Examples

### 407.6.1 Model Description

The Real-ESSI input files for this example are available [HERE](#). The compressed package of Real-ESSI input files and postprocessing results for this example is available [HERE](#).

Firstly, the model is given an initial displacement in the first loading stage. In the second loading stage, the model starts free vibration.

### 407.6.2 Results

With NO damping, the displacement peak keeps the same. The displacement at the top is

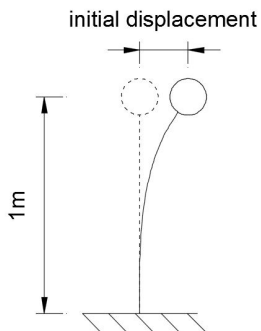


Figure 407.27: Problem Description for Newmark Method

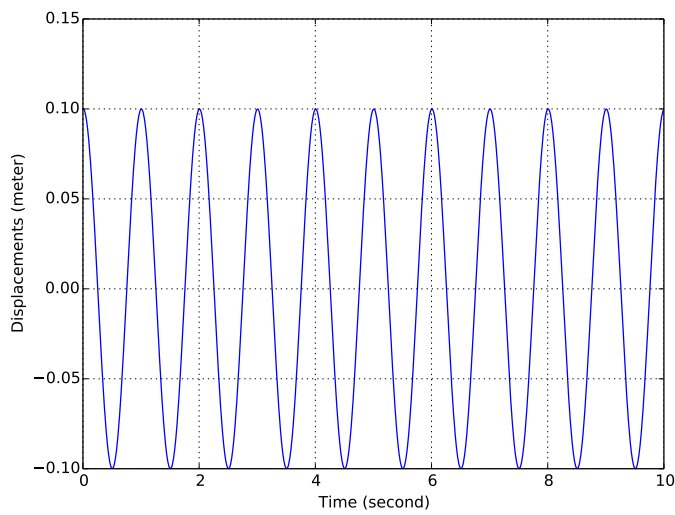


Figure 407.28: Results for Newmark Method

## 407.7 Dynamics: Interface/Contact Elements

### 407.7.1 Dynamics: Hard Interface/Contact: One Bar Normal Interface/Contact Dynamics

#### 407.7.1.1 Model Description

This is an example of a ball, bouncing on a solid flat surface. There is only normal contact/interface between the ball and the floor. An upward force is first applied to the concentrated mass lifting it up by  $0.1m$  and then the force is removed, resulting in free vibration of the ball. An illustrative diagram of the problem is shown below.

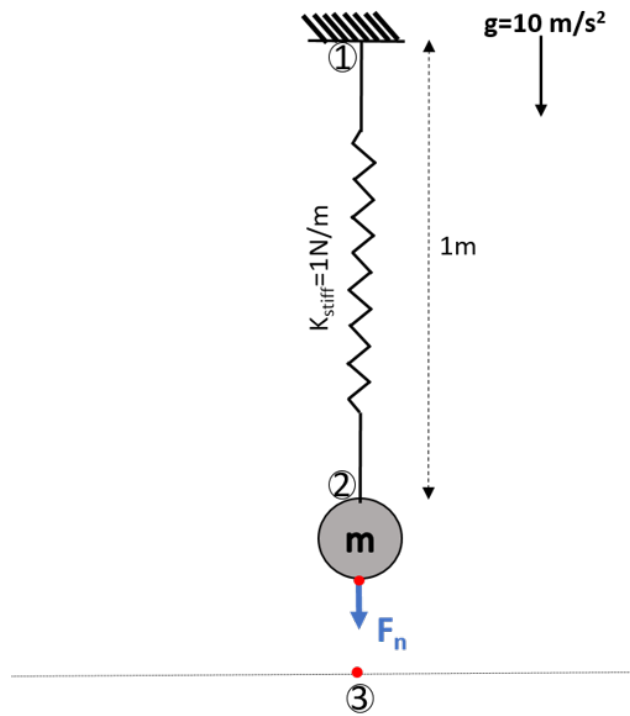


Figure 407.29: Illustration of one bar normal contact/interface dynamics.

The same example can be modeled with different contact/interface and simulation parameters as shown below. For all the different cases shown below, no numerical damping is applied. Only the contact parameters are changed to expose their functionality. The response of node 2 is plotted for all the cases.

#### 407.7.1.2 Dynamics: No Viscous Damping

The Real-ESSI input files for this example are available [HERE](#). The compressed package of Real-ESSI input files and postprocessing results for this example is available [HERE](#).

**Results** Here, no viscous damping between the contact/interface pair nodes is applied. The displacement output of *Node 2* is shown below.

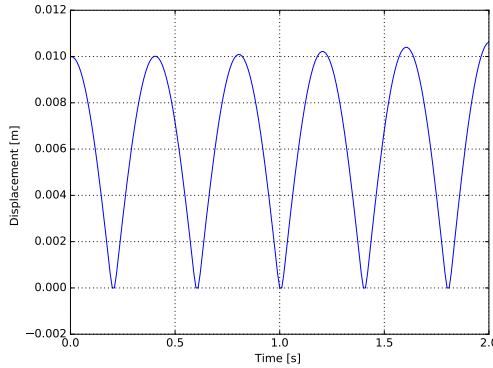


Figure 407.30: Displacement of Node 2

#### 407.7.1.3 Dynamics: Normal Viscous Damping Between Interface/Contact Node Pairs

The Real-ESSI input files for this example are available [HERE](#). The compressed package of Real-ESSI input files and postprocessing results for this example is available [HERE](#).

**Results** Viscous damping between the contact/interface pair nodes is applied in normal contact/interface direction. The displacement output of *Node 2* is shown below.

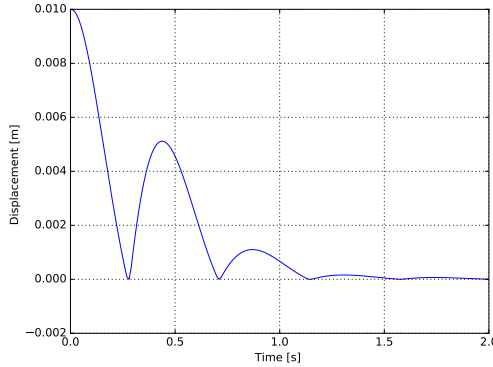


Figure 407.31: Displacement of Node 2

#### 407.7.1.4 Dynamics: Explicit Simulation

The Real-ESSI input files for this example are available [HERE](#). The compressed package of Real-ESSI input files and postprocessing results for this example is available [HERE](#).

**Results** With no viscous damping, the analysis is run explicitly without any convergence check. The displacement output of *Node 2* is shown below.

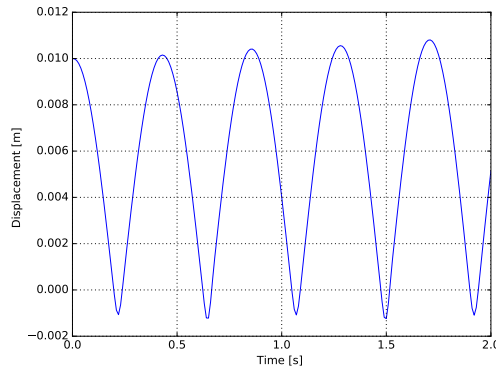


Figure 407.32: Displacement of Node 2

#### 407.7.2 Dynamics: Hard Interface/Contact: Frictional Single Degree of Freedom Problem

**Model Description** This is an example of a block on a rough surface under gravity. It has been attached to a spring at one end. At the other end a tangential load is applied greater than the coulomb friction and is then removed. The block oscillates back and forth with continuously loosing energy because of frictional force and then stops, with some permanent deformation. This kind of damping is called frictional damping which is linear as compared to exponential in case of viscous damping. An illustrative diagram of the problem is shown below.

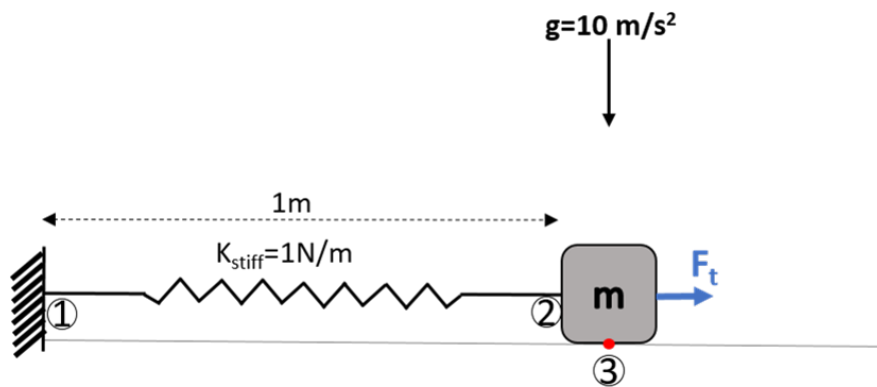


Figure 407.33: Illustration of frictional single degree of freedom problem

The same example can be modeled with different contact/interface and simulation parameters as shown below. For all the different cases shown below, no numerical damping is applied. Only the contact/interface parameters are changed to expose their functionality. The response of node 2 is plotted for all the cases.

#### 407.7.2.1 Dynamics: No Viscous Damping

The Real-ESSI input files for this example are available [HERE](#). The compressed package of Real-ESSI input files and postprocessing results for this example is available [HERE](#).

**Results** In this examples, no viscous damping between the contact/interface pair nodes is applied. The displacement output of *Node 2* is shown below.

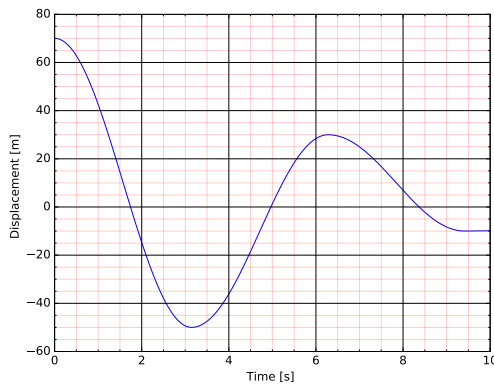


Figure 407.34: Displacement of Node 2

#### 407.7.2.2 Dynamics: Tangential Viscous Damping Between Interface/Contact Node Pairs

The Real-ESSI input files for this example are available [HERE](#). The compressed package of Real-ESSI input files and postprocessing results for this example is available [HERE](#).

**Results** Viscous damping between the contact/interface pair nodes is applied in tangential contact/interface direction. The displacement output of *Node 2* is shown below.

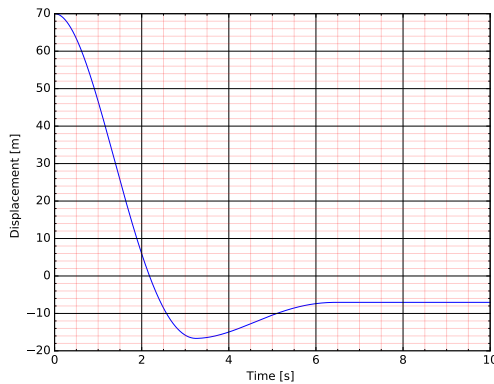


Figure 407.35: Displacement of Node 2

#### 407.7.2.3 Dynamics: Explicit Simulation

The Real-ESSI input files for this example are available [HERE](#). The compressed package of Real-ESSI input files and postprocessing results for this example is available [HERE](#).

**Results** With no viscous damping, the analysis is run explicitly without any convergence check. The displacement output of *Node 2* is shown below.

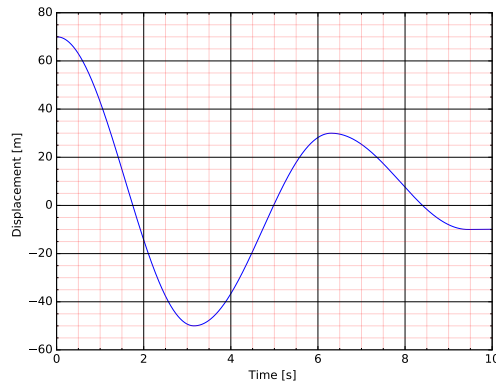


Figure 407.36: Displacement of Node 2

### 407.7.3 Dynamics: Soft Interface/Contact: One Bar Normal Interface/Contact Dynamics

**Model Description** This is an example of a ball, bouncing on a solid flat surface. There is only normal contact/interface between the ball and the floor. An upward force is first applied to the concentrated mass lifting it up by  $0.1m$  and then the force is removed, resulting in free vibration of the ball. An illustrative diagram of the problem is shown below.

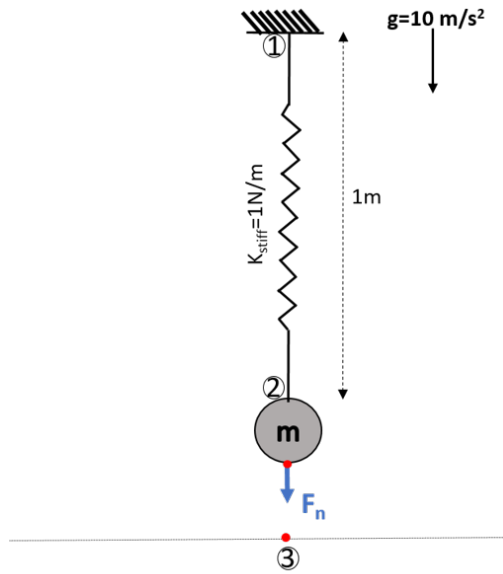


Figure 407.37: Illustration of one bar normal contact/interface dynamics

The same example can be modeled with different contact/interface and simulation parameters as shown below. For all the different cases shown below, no numerical damping is applied. Only the contact/interface parameters are changed to expose their functionality. The response of node 2 is plotted for all the cases.

#### 407.7.3.1 Dynamics: No Viscous Damping

The Real-ESSI input files for this example are available [HERE](#). The compressed package of Real-ESSI input files and postprocessing results for this example is available [HERE](#).

**Results** In this example, no viscous damping between the contact/interface pair nodes is applied. The displacement output of *Node 2* is shown below.

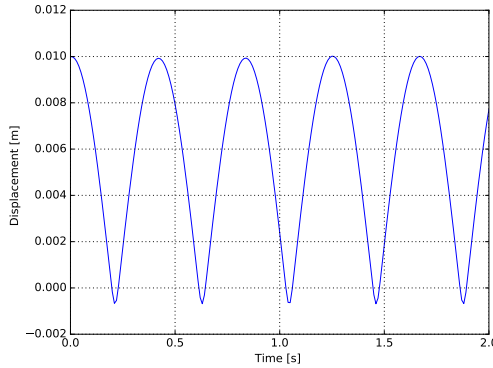


Figure 407.38: Displacement of Node 2

#### 407.7.3.2 Dynamics: With Normal Viscous Damping Between Interface/Contact Node Pairs

The Real-ESSI input files for this example are available [HERE](#). The compressed package of Real-ESSI input files and postprocessing results for this example is available [HERE](#).

**Results** Viscous damping between the contact/interface pair nodes is applied in normal contact/interface direction. The displacement output of *Node 2* is shown below.

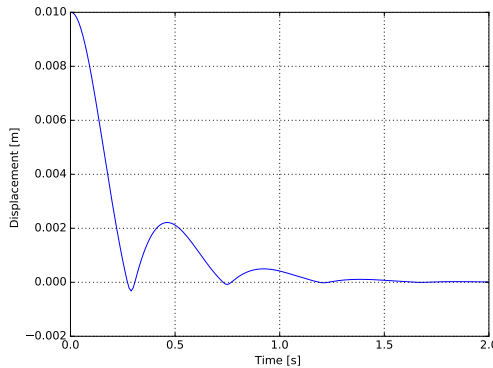


Figure 407.39: Displacement of Node 2

#### 407.7.3.3 Dynamics: Explicit Simulation

The Real-ESSI input files for this example are available [HERE](#). The compressed package of Real-ESSI input files and postprocessing results for this example is available [HERE](#).

**Results** With no viscous damping, the analysis is run explicitly without any convergence check. The displacement output of *Node 2* is shown below.

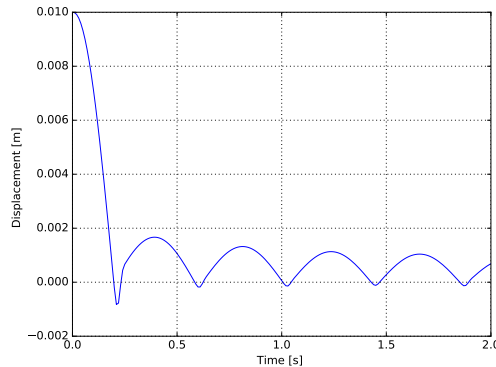


Figure 407.40: Displacement of Node 2

#### 407.7.4 Dynamics: Soft Interface/Contact: Frictional Single Degree of Freedom Problem

**Model Description** This is an example of a block on a rough surface under gravity. It has been attached to a spring at one end. At the other end a tangential load is applied greater than the coulomb friction and is then removed. The block oscillates back and forth with continuously loosing energy because of frictional force and then stops, with some permanent deformation. This kind of damping is called frictional damping which is linear as compared to exponential in case of viscous damping. An illustrative diagram of the problem is shown below.

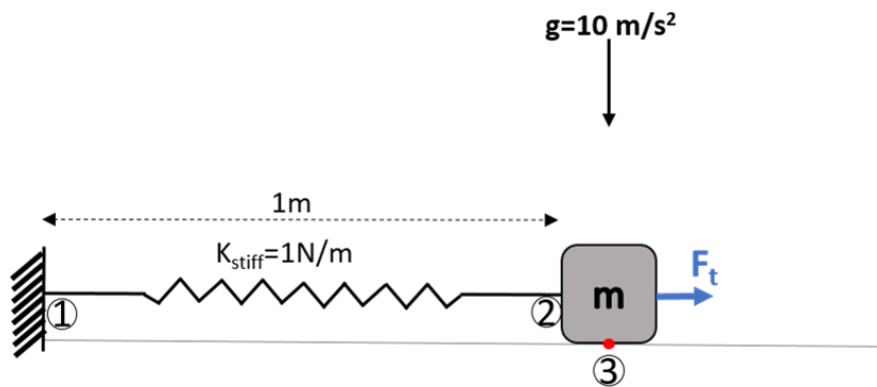


Figure 407.41: Illustration of frictional single degree of freedom problem

The same example can be modeled with different contact/interface and simulation parameters as shown below. For all the different cases shown below, no numerical damping is applied. Only the contact/interface parameters are changed to expose their functionality. The response of node 2 is plotted for all the cases.

#### 407.7.4.1 Dynamics: No Viscous Damping

The Real-ESSI input files for this example are available [HERE](#). The compressed package of Real-ESSI input files and postprocessing results for this example is available [HERE](#).

**Results** In this example, no viscous damping between the contact/interface pair nodes is applied. The displacement output of *Node 2* is shown below.

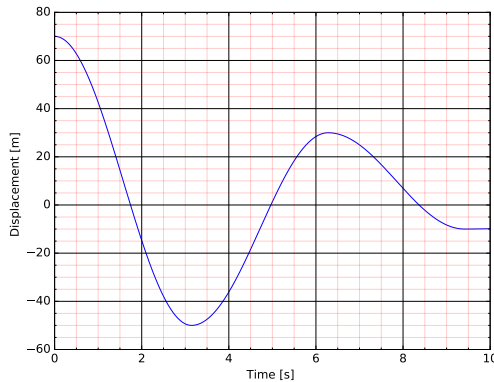


Figure 407.42: Displacement of Node 2

#### 407.7.4.2 Dynamics: Tangential Viscous Damping Between Interface/Contact Node Pairs

The Real-ESSI input files for this example are available [HERE](#). The compressed package of Real-ESSI input files and postprocessing results for this example is available [HERE](#).

**Results** Viscous damping between the contact/interface pair nodes is applied in tangential contact/interface direction. The displacement output of *Node 2* is shown below.

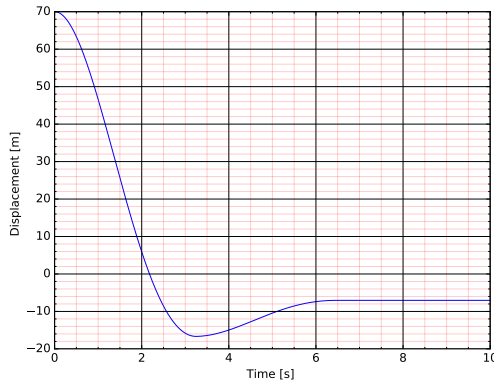


Figure 407.43: Displacement of Node 2

#### 407.7.4.3 Dynamics: Explicit Simulation

The Real-ESSI input files for this example are available [HERE](#). The compressed package of Real-ESSI input files and postprocessing results for this example is available [HERE](#).

**Results** With no viscous damping, the analysis is run explicitly without any convergence check. The displacement output of *Node 2* is shown below.

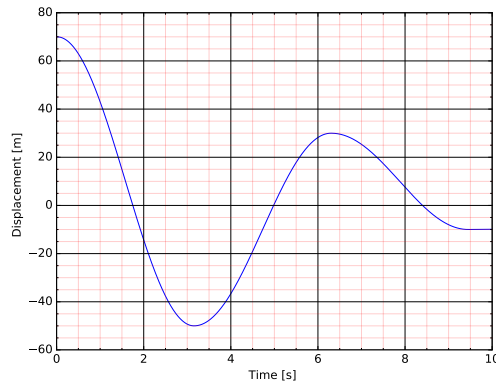


Figure 407.44: Displacement of Node 2

### 407.7.5 Dynamics: Split Beam

#### 407.7.5.1 Model Description

In this example, a normal beam is split into two halves along its depth. A uniform surface load of 50 Pa is applied to the top half of the beam, pulling it away from its lower part. Then, the load is removed, to allow free vibration between the split beams. An illustrative diagram of the problem is shown below.

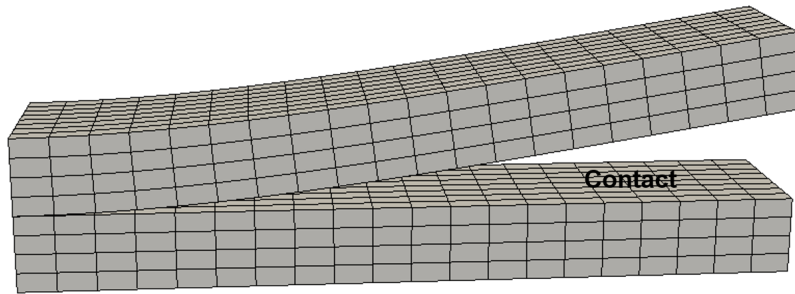


Figure 407.45: Illustration of Split Beam Analysis

The same example was modelled with soft and hard contact/interface. Numerical as well as viscous damping between contact/interface pair nodes was applied. The displacement response of the extreme right mid node of top half beam is plotted.

#### 407.7.5.2 Dynamics: Split Beam With Hard Interface/Contact

The Real-ESSI input files for this example are available [HERE](#). The compressed package of Real-ESSI input files and postprocessing results for this example is available [HERE](#).

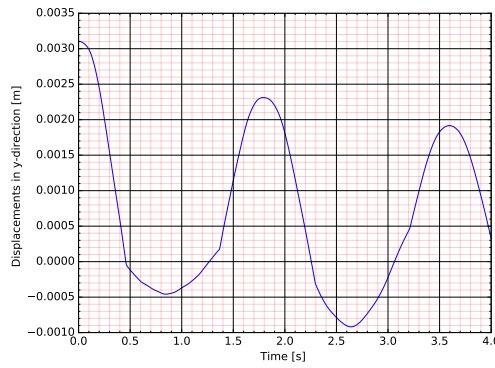


Figure 407.46: Displacement response of extreme mid node of top half beam

#### 407.7.5.3 Dynamics: Split Beam With Soft Interface/Contact

The Real-ESSI input files for this example are available [HERE](#). The compressed package of Real-ESSI input files and postprocessing results for this example is available [HERE](#).

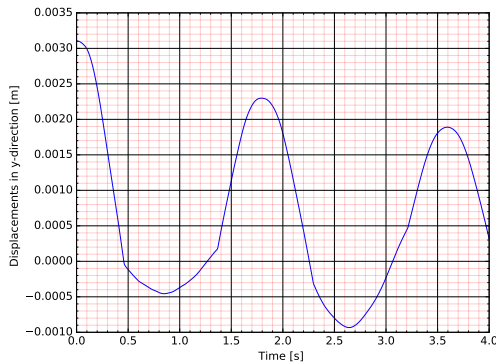


Figure 407.47: Displacement response of extreme mid node of top half beam

#### 407.7.6 Dynamics: Block on Soil ESSI

**Model Description** The Real-ESSI input files for this example are available [HERE](#). The compressed package of Real-ESSI input files and postprocessing results for this example is available [HERE](#).

A solid block is placed in the soil. There is contact/interface between the interface of solid and the soil. First, self-weight and then a uniform acceleration in x-direction is applied to the whole model. This analysis would provide relative displacement, velocity and acceleration response for the given shaking. An illustrative diagram of the problem is shown below.

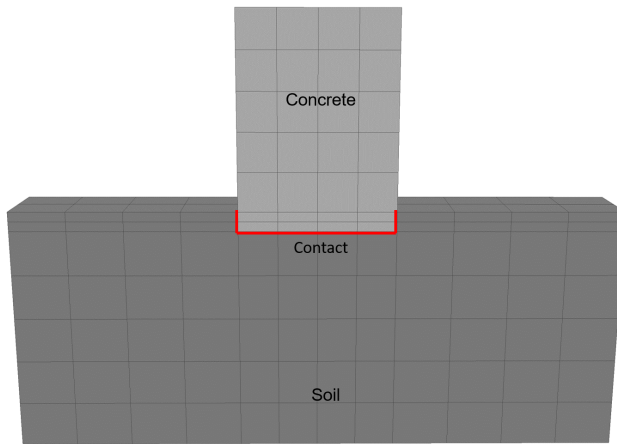


Figure 407.48: Illustration of frictional single degree of freedom problem

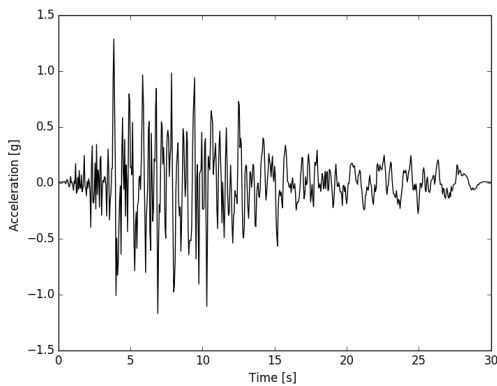


Figure 407.49: Applied Motion

**Results** Displacement response of the top of the solid block is shown below. Numerical Damping, Raleigh damping and viscous damping between contact/interface node pairs are applied.

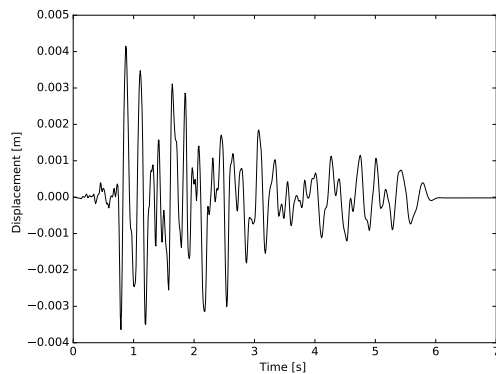


Figure 407.50: Displacement response at the top of the block

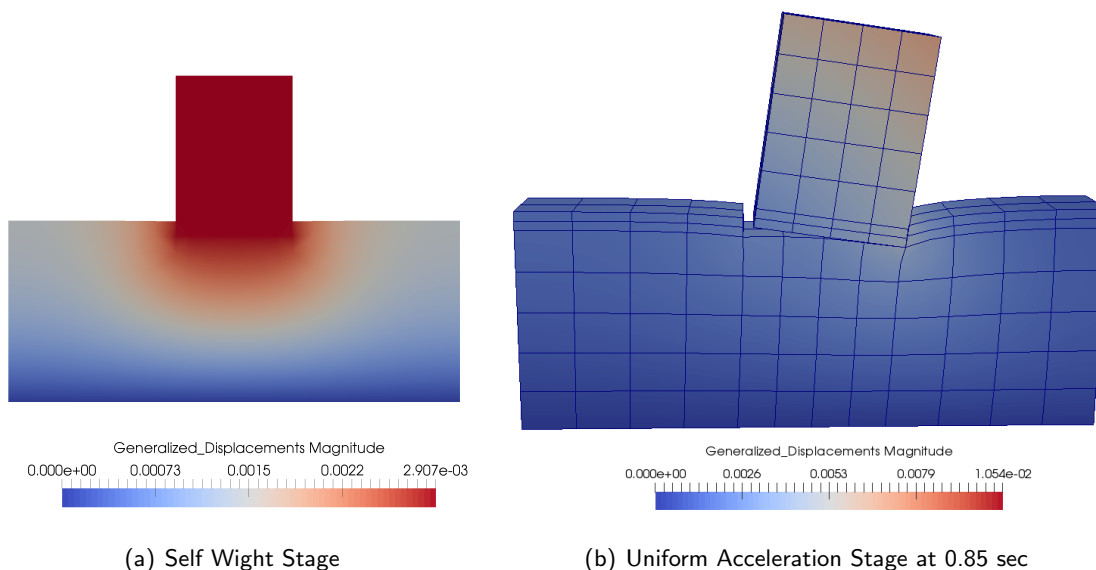


Figure 407.51: Simulation results visualization

## 407.8 Dynamics: Inelastic Solid Examples

The Real-ESSI input files for this example are available [HERE](#). The compressed package of Real-ESSI input files and postprocessing results for this example is available [HERE](#).

Firstly, the model is given an initial displacement at the top from 0 to 1 second. Second, after the time 1 second, the model starts free vibration.

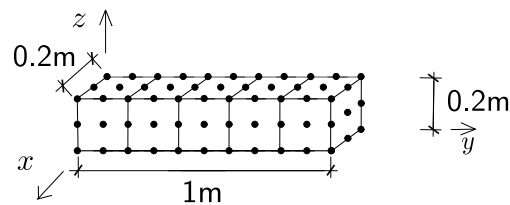


Figure 407.52: Problem Description for Newmark Method

**Results** This model has material damping. The displacement at the top is

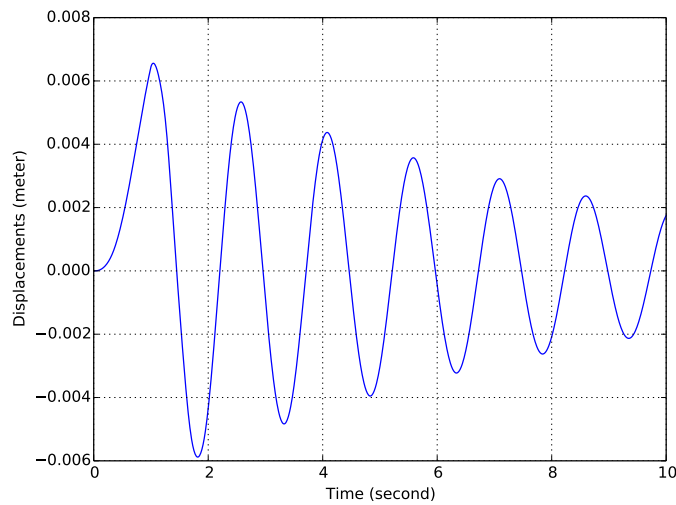


Figure 407.53: Results for Newmark Method

## 407.9 Dynamics: Inelastic Structural Examples

The Real-ESSI input files for this example are available [HERE](#). The compressed package of Real-ESSI input files and postprocessing results for this example is available [HERE](#).

The column beam is represented by the fiber section. This example is under the dynamic load of ground motion.

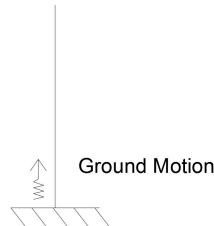


Figure 407.54: Ground motion on the Fiber Beam with Column Section

The fiber represents the rebar. The section of all fibers represents the cross section properties of the inelastic beam.

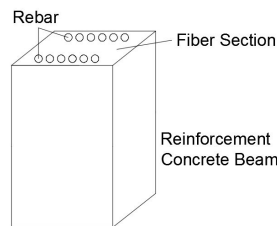


Figure 407.55: Diagram of the Fiber Beam with Column Section

## 407.10 Dynamics: Domain Reduction Method (DRM)

### 407.10.1 Dynamics: DRM One Dimensional (1D) Model

The Real-ESSI input files with 8NodeBrick for this example are available [HERE](#).

The same model for this example with 27NodeBrick is available [HERE](#).

A simple 1D DRM model is shown in Fig.([707.44](#)). The "DRM element", "Exterior node" and "Boundary node" are required to be designated in the DRM HDF5 input. The format and script for the HDF5 input is available in DSL/input manual.

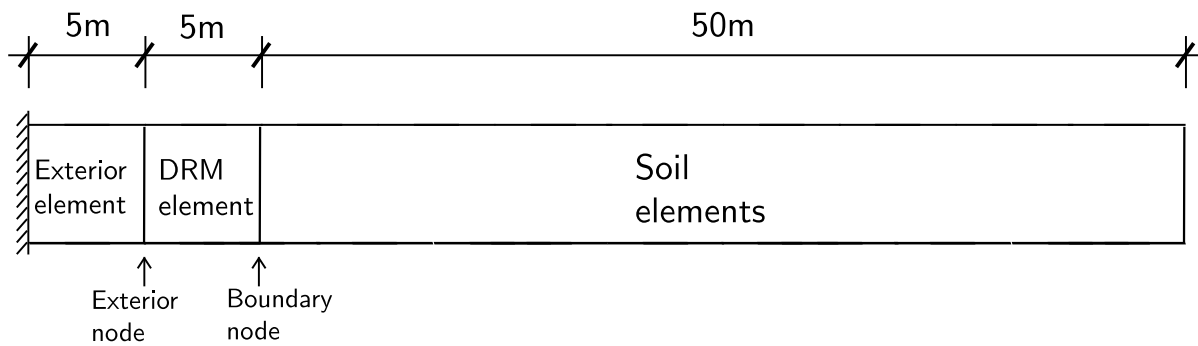


Figure 407.56: 1D DRM model.

#### Numerical model

Long 1D DRM model 1000:1 The Real-ESSI input files for this example are available [HERE](#).

The results can also be seen from this [ANIMATION](#).

To show the wave propagation explicitly, a long 1D model (1000:1) similar to the 1D DRM model above was made in this section.

The model description is same to Fig.([707.44](#)) except this model use far more soil elements.

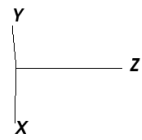
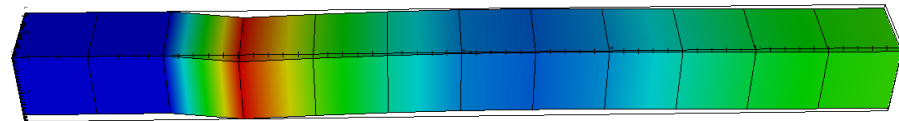
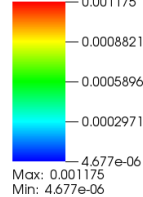
The general view is shown in Fig.([707.46](#)) below.

There is still now outgoing waves at the exterior layers, which is shown in Fig([707.47](#)).

DB: DRM\_1D.h5.feiooutput  
Time: 2.87

Mesh  
Var: ESSI Domain Mesh

Pseudocolor  
Var: Generalized Displacements\_magnitude



user: yuan  
Sat Nov 7 11:34:02 2015

Figure 407.57: 1D DRM model.

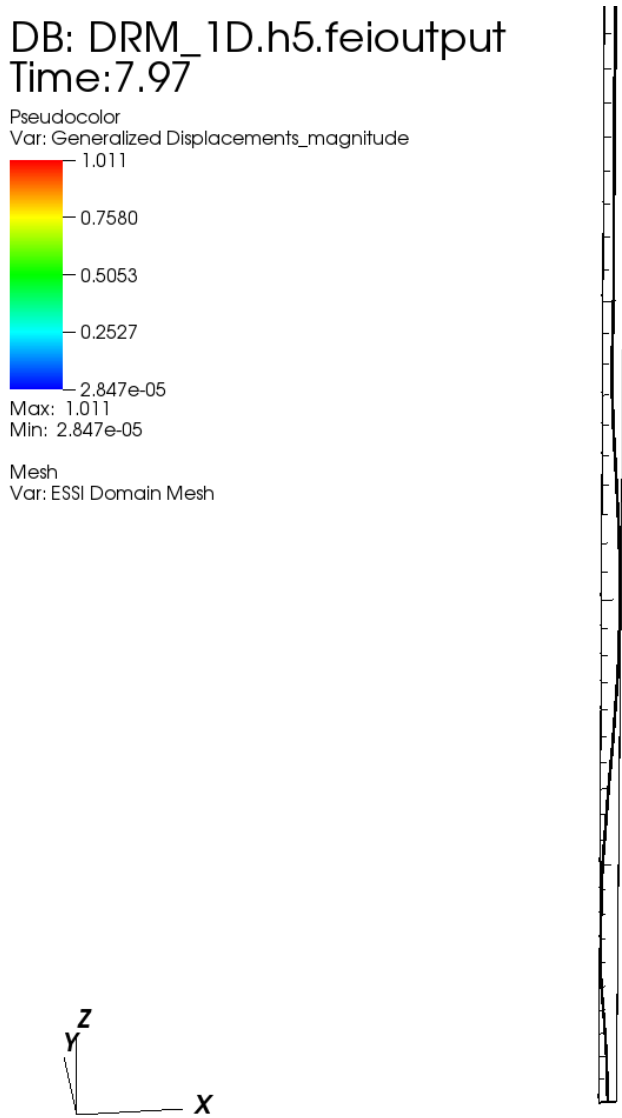


Figure 407.58: Long 1D DRM model

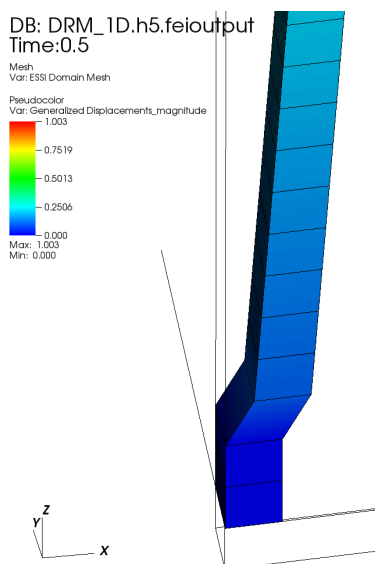


Figure 407.59: Long 1D DRM model: exterior layer

#### 407.10.2 Dynamics: Three Dimensional (3D) DRM Model

The Real-ESSI input files with 8NodeBrick for this example are available [HERE](#).

The same model for this example with 27NodeBrick is available [HERE](#).

As shown in Fig.(707.48), the DRM layer is used to add the earthquake motion.

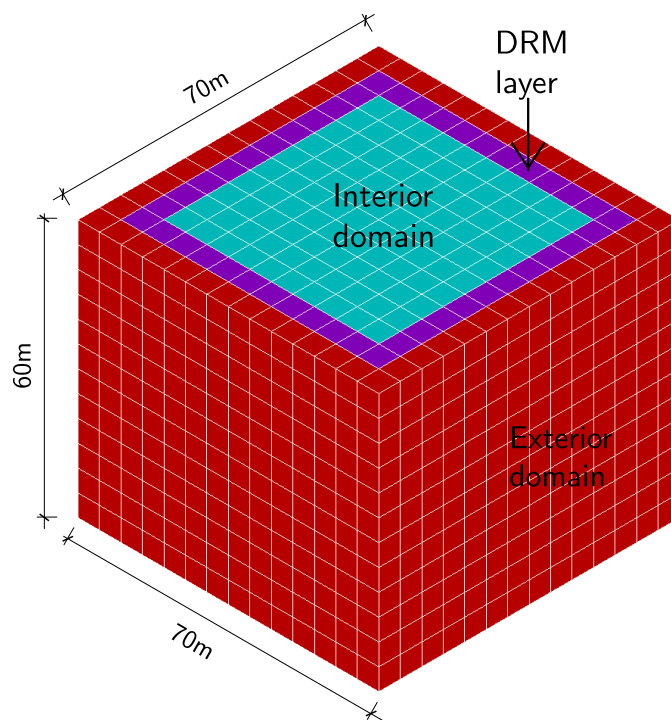


Figure 407.60: The diagram for 3D Domain Reduction Method example.

Numerical result

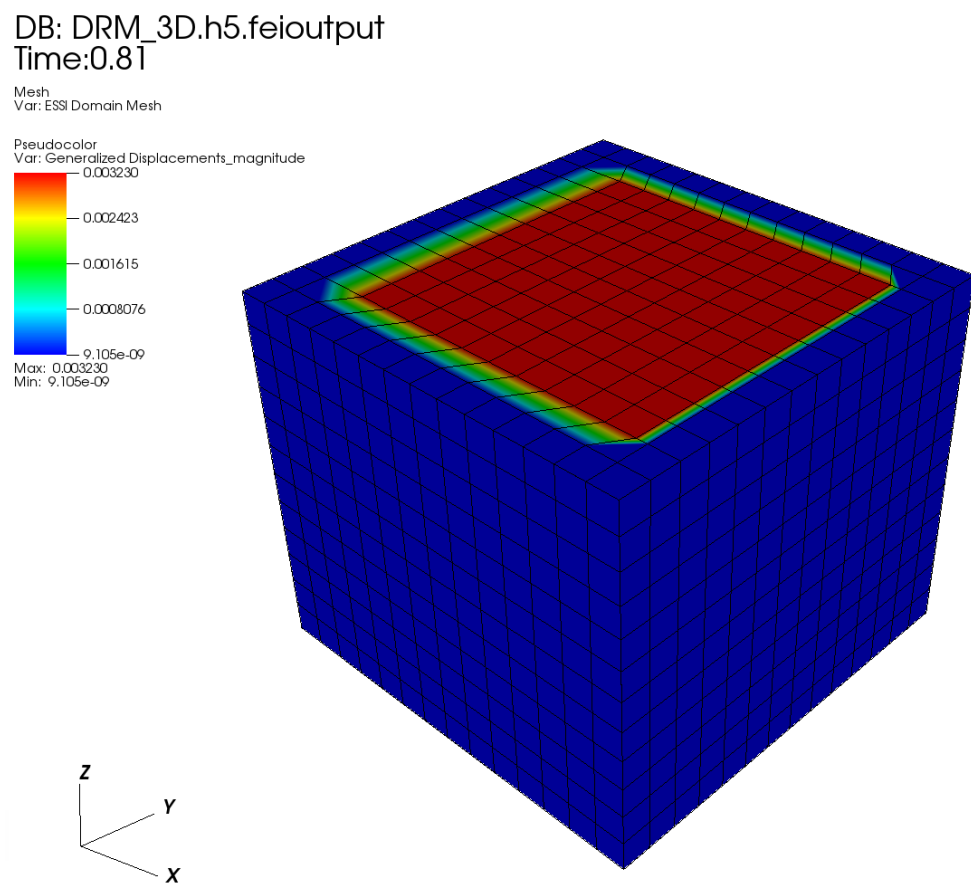


Figure 407.61: Diagram for the 3D DRM model.

### 407.10.3 Dynamics: DRM Model with Structure

Problem description The Real-ESSI input files for this example are available [HERE](#).

The compressed package of Real-ESSI input files and postprocessing results for this example is available [HERE](#).

As shown in Fig.(407.62), the structure is placed in the middle. Five different materials are assigned to structure, contact/interface zones, soil, DRM layer, and damping layers, respectively.

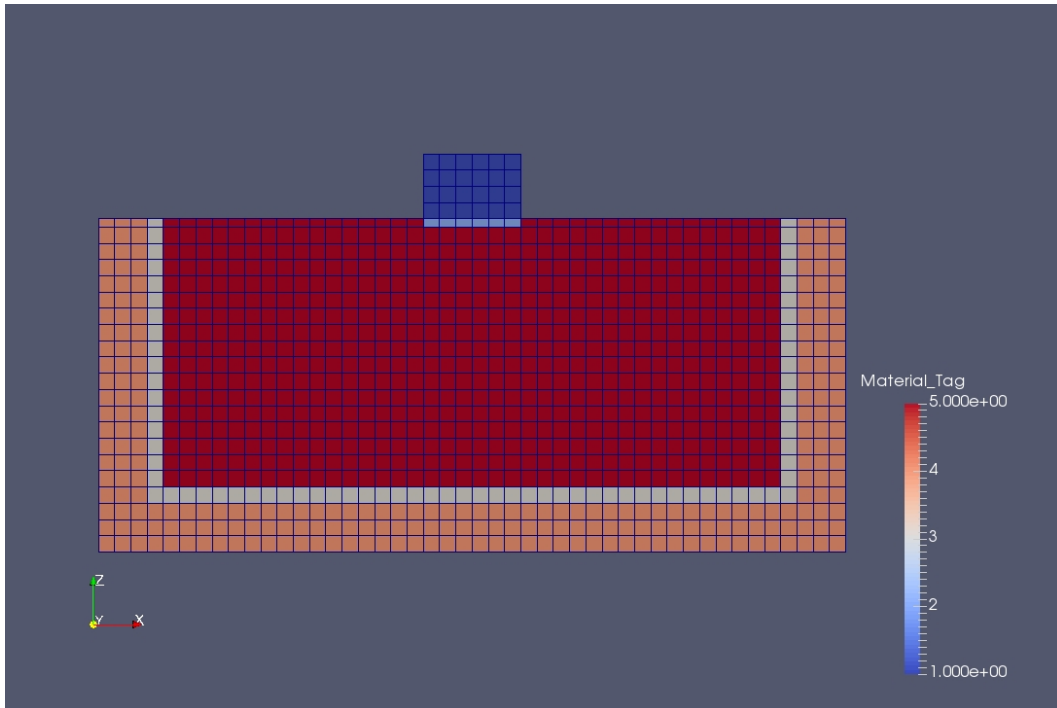


Figure 407.62: A Domain Reduction Method example with a Simple Structure.

## 407.11 Dynamics: Eigen Analysis

The Real-ESSI input files for this example are available [HERE](#). The compressed package of Real-ESSI input files and postprocessing results for this example is available [HERE](#).

Model is a brick beam with distributed mass.

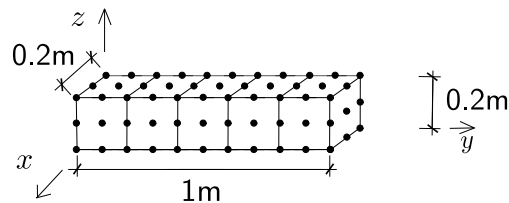


Figure 407.63: Problem Description for Newmark Method

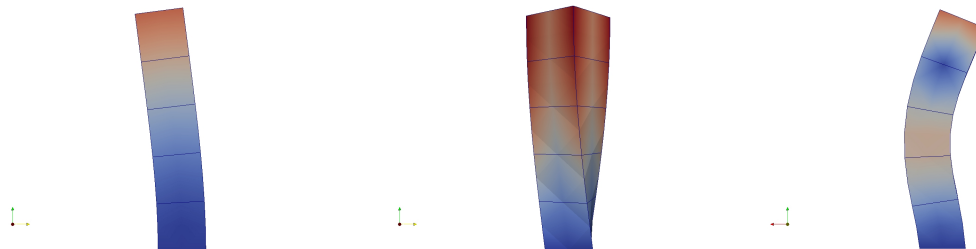


Figure 407.64: Solid Brick Cantilever Eigen Mode 1, 3, 4(From left to Right)

Results

## 407.12 Dynamics: Fully Coupled u-p-U and u-p Elements

The Real-ESSI input files for coupled example are available [HERE](#).

## 407.13 Dynamics: Partially Saturated / Unsaturated u-p-U Element (example in development)

## 407.14 Dynamics: Coupled Interface/Contact Element (example in development)

## 407.15 Dynamics: Buoyant Forces (example in development)

## 407.16 Chapter Summary and Highlights

In this Chapter stochastic/probabilistic modeling and simulation is illustrated through a number of examples. These examples can then be analyzed using Real-ESSI Simulator that is available for Linux, Windows (through ESL) or MacOS, and on Amazon Web Services (AWS) computers. Please refer to the Real-ESSI web site [real-essi.us](http://real-essi.us), for more information on how to install Real-ESSI on your computer (Linux, Windows, MacOS...).

# Chapter 408

## Stochastic Examples

(2018-2019-2020-2021-)

(In collaboration with Dr. Hexiang Wang)

### 408.1 Probabilistic Constitutive Modeling

#### 408.1.1 Probabilistic Constitutive Modeling: Linear Elastic

The model description:

The Real-ESSI input files for this example are available in a zip archive [HERE](#).

A stochastic uniaxial elastic material with lognormal distributed random elastic modulus, mean 155 MPa and coefficient of variation 30%.

Results:

The probabilistic stress strain response of the stochastic uniaxial elastic material is shown in Figure 408.1.

#### 408.1.2 Probabilistic Constitutive Modeling: Elasto-Plastic

The model description:

The Real-ESSI input files for this example are available in a zip archive [HERE](#).

A stochastic uniaxial elastoplastic material with vanishing elastic region and nonlinear Armstrong-Frederick kinematic hardening rule is modeled. The model parameters are: Armstrong-Frederick pa-

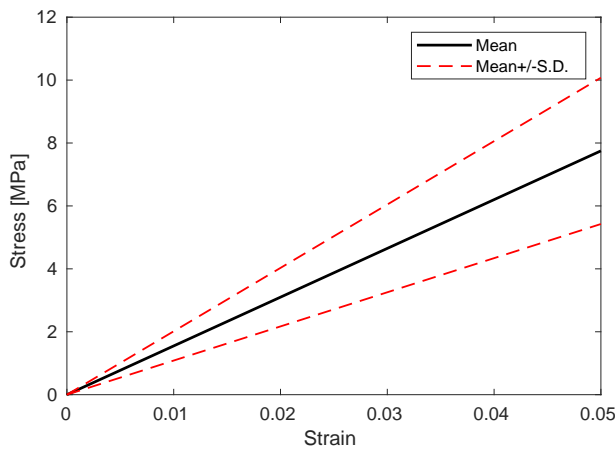


Figure 408.1: Constitutive behavior of stochastic uniaxial elastic material.

parameter  $H_a$  follows lognormal distribution with marginal mean 12 MPa and coefficient of variation 20%. Armstrong-Frederick parameter  $C_r$  follows lognormal distribution with marginal mean 200 and coefficient of variation (CV) 20%.

Results:

The probabilistic stress strain response of the stochastic uniaxial elastic material is shown in Figure 408.2.

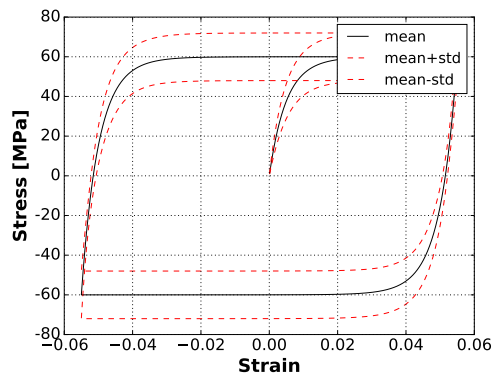


Figure 408.2: Constitutive behavior of stochastic uniaxial elastoplastic material.

## 408.2 Probabilistic Characterization of Seismic Motions

The model description:

The Real-ESSI input files for this example are available in a zip archive [HERE](#).

For stochastic analysis with uncertain seismic excitations, it is important to characterize input uncertain motions as a non-stationary random process. The random process can be quantified through marginal mean, marginal standard deviation and correlation structure, and can be represented as Hermite polynomial chaos (PC). This example presents such a random process of seismic motions with marginal mean, marginal standard deviation and correlation structure defined through plain text files. It is noted that this random process is used as input bedrock excitations in the subsequent stochastic wave propagation analysis.

Results:

It is important to check that the statistics synthesized from PC representation matches well with the input. Figures 408.3 and 408.2 compare the marginal statistics and correlation structure synthesized from PC representation with the target input.

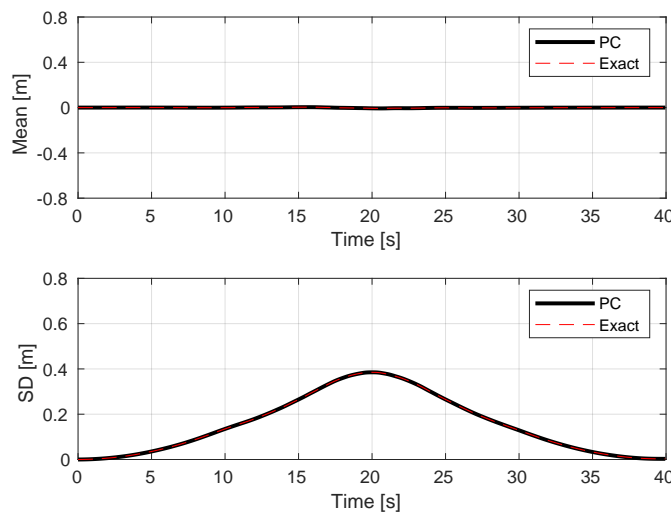


Figure 408.3: Verification of marginal statistics of random process motions.

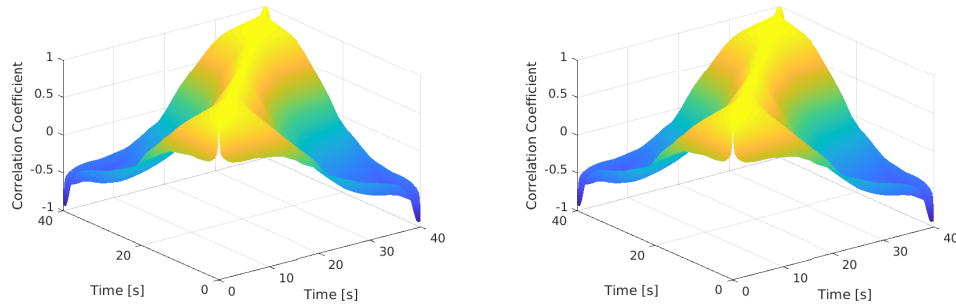


Figure 408.4: Input correlation structure (Left) and PC-synthesized correlation structure (Right).

## 408.3 1D Stochastic Seismic Wave Propagation

### 408.3.1 1D Stochastic Seismic Wave Propagation: Linear Elastic

The model description:

The Real-ESSI input files for this example are available in a zip archive [HERE](#).

Presented is 1D stochastic seismic wave propagation through uncertain linear elastic, layered ground. The uncertain motions characterized in section 408.2 is adopted as bedrock input. The ground is 10m thick with three layers and discretized with 10 stochastic shear beam elements as shown in Figure 408.5.

- Layer #1: Thickness 3m, uncertain elastic modulus follows lognormal distribution with marginal mean 120 MPa and 20% coefficient of variation.
- Layer #2: Thickness 3m, uncertain elastic modulus follows lognormal distribution with marginal mean 150 MPa and 25% coefficient of variation.
- Layer #3: Thickness 4m, uncertain elastic modulus follows lognormal distribution with marginal mean 180 MPa and 25% coefficient of variation.

The correlation structure of the uncertain elastic modulus random field follows exponential correlation with correlation length as 10m.

Results:

Time evolving marginal mean and marginal standard deviation of surface probabilistic displacement and acceleration response are shown in Figure 408.6 and 408.7.

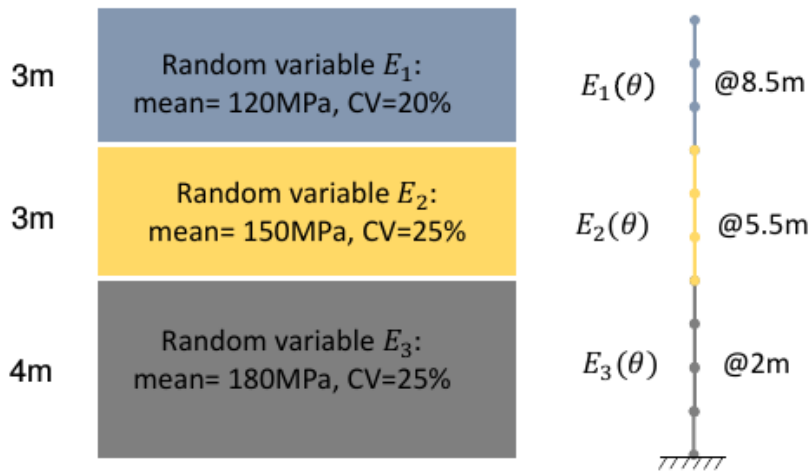


Figure 408.5: 1D layered ground and stochastic shear beam FEM model.

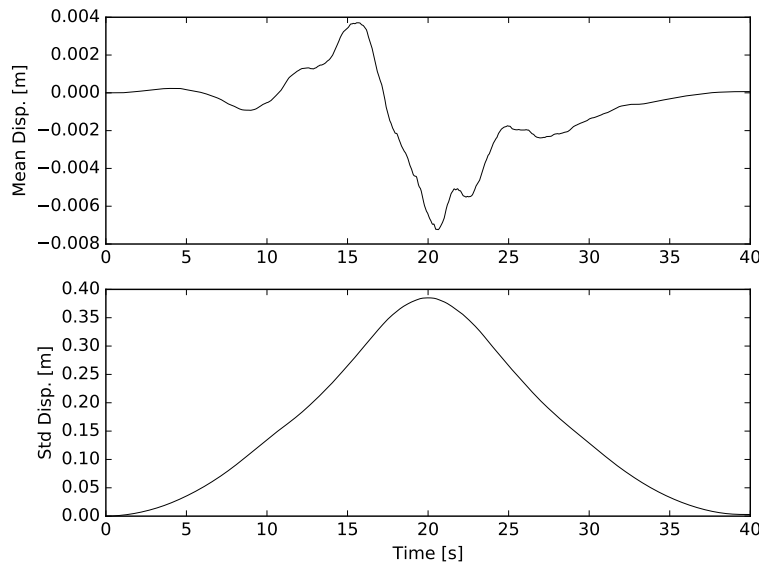


Figure 408.6: Probabilistic displacement response of ground surface.

#### 408.3.2 1D Stochastic Seismic Wave Propagation: Elasto-Plastic

The model description:

The Real-ESSI input files for this example are available in a zip archive [HERE](#).

The model geometry and input seismic excitations are identical to the example in section 408.3.1. The only difference is the constitutive model of soil. In this example, probabilistic elasto-plastic soil model with vanishing elastic region and Armstrong-Frederick kinematic hardening is adopted.

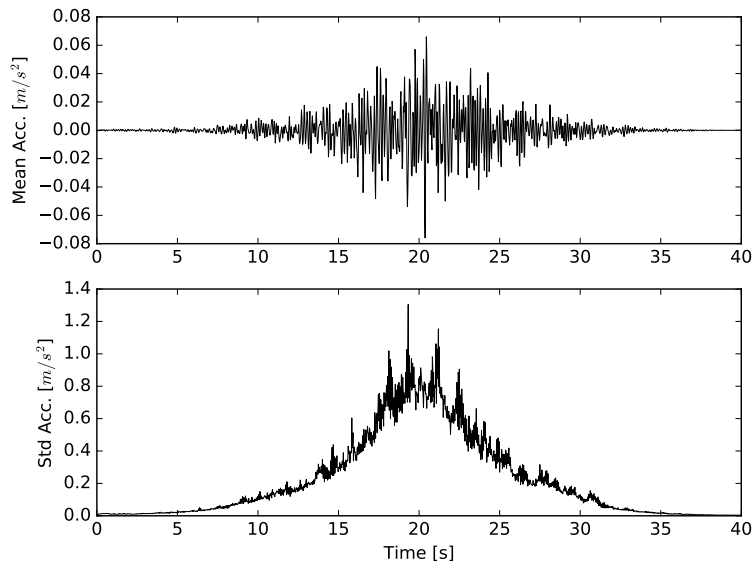


Figure 408.7: Probabilistic acceleration response of ground surface.

Results:

Time evolving marginal mean and marginal standard deviation of surface probabilistic displacement and acceleration response are shown in Figure 408.8 and 408.9.

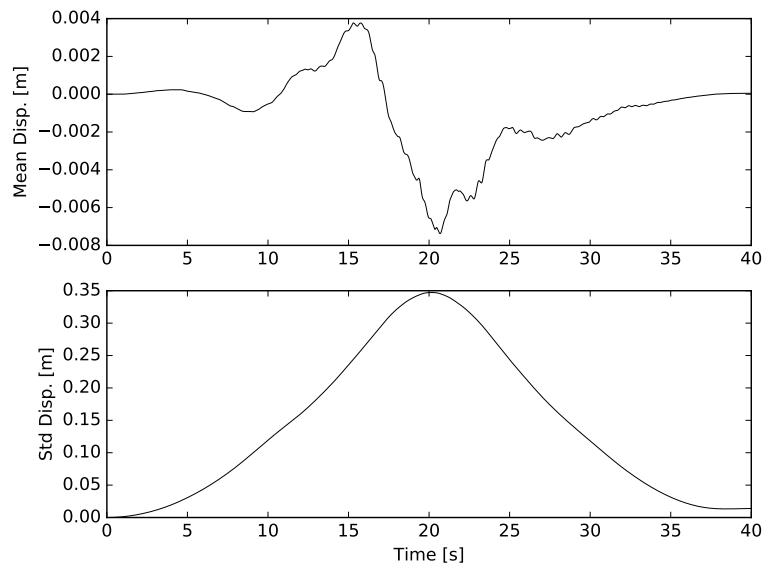


Figure 408.8: Probabilistic displacement response of ground surface.

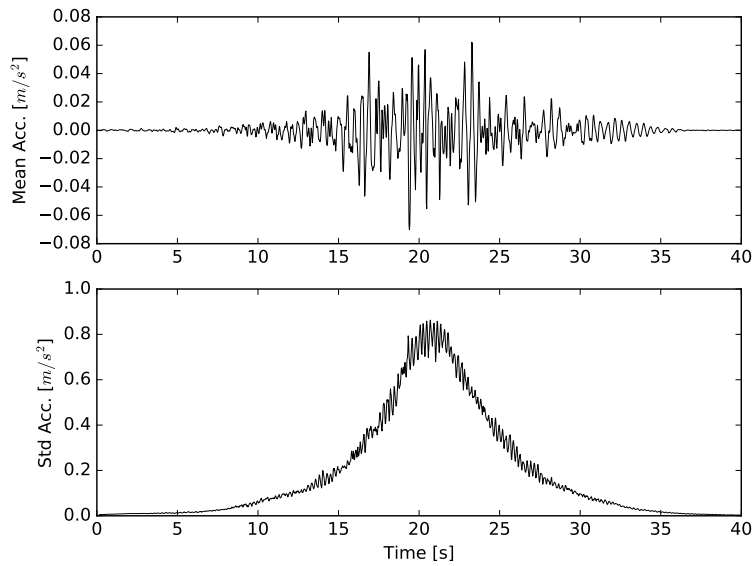


Figure 408.9: Probabilistic acceleration response of ground surface.

## 408.4 1D Stochastic Seismic Wave Propagation: Sobol Sensitivity Analysis

The Real-ESSI input files for this example are available in a zip archive [HERE](#).

Sobol sensitivity analysis is performed for the stochastic wave propagation example in section 408.3.1. From the sensitivity analysis results for probabilistic response at ground surface, it is shown that for this specific case most of the variance comes from the uncertain input motions.

## Chapter 409

# Large Scale, Realistic Examples

(2016-2018-)

(In collaboration with Dr. Yuan Feng, Mr. Sumeet Kumar Sinha, Dr. Han Yang, and Dr. Hexiang Wang)

Full scale, realistic examples of statics and dynamics of bridges, dams, buildings and nuclear power plants are presented in part 500 on page 2189 in Jeremić et al. (1989-2025).